OSLO METROPOLITAN UNIVERSITY
OsloMet – storbyuniversitetet

Department of Civil Engineering and Energy Technology
Mailing address: P.O.Box 4 St. Olavs plass, NO-0130 Oslo, Norway
Visiting adress: Pilestredet 35, Oslo

Telephon: 67 23 50 00
www.oslomet.no

GROUP NUMBER
7

ACCESS
RESTRICTED

MASTER THESIS

TITLE OF THE PROJECT REPORT	**DATE**
Structural Analysis of Reinforced Concrete Beams Affected by Alkali-Silica Reaction *with Focus on Material Models for Concrete*	15.05.2020
	NO. OF PAGES : 146 **NO. OF ATTACHMENT:** Appendix A and B
AUTHORS: Albian Tairi & Leonard-Johan Nesheim	**SUPERVISOR:** Professor Gro Markeset, Oslo Metropolitan University PhD Candidate Simen Sørgaard Kongshaug, Oslo Metropolitan University

SUMMARY
Alkali-silica reaction (ASR) is a chemical reaction that occurs in concrete between the alkalized cement and silica within the aggregates. ASR produces a gel around the aggregates which absorbs water, expands, results in local stresses, and causes the concrete to crack internally and externally. Research on this chemical reaction and development of concrete models including this reaction has been extensive. However, limited research about the structural effects of ASR and load actions due to ASR has been carried out. Due to lack of applicable constitutive models including the effect of ASR in finite element softwares, simplified methods for the assessment of ASR damaged reinforced concrete structures are used.

In this master thesis structural analyses of reinforced concrete beams affected by ASR have been carried out. Analyses on one span- and three span beams have been carried out to study the effect of using more complex concrete material models which includes the stress dependency of the ASR expansion and the stiffness reduction due to ASR. The load actions due to ASR with different concrete material models are computed and compared. From the case studies it was found that the non-unifrom ASR expansion and the stress dependency of the ASR expansion had significant impact on the load actions.

3 KEYWORDS
Reinforced Concrete Structure
Alkali-Silica Reaction
Structural Analysis

Oslo Metropolitan University
Oslo, Spring 2020

Structural Analysis of Reinforced Concrete Beams Affected by Alkali-Silica Reaction

with focus on Load Actions due to ASR

Albian Tairi and Leonard-Johan Nesheim

Supervisors: Professor Gro Markeset and PhD Candidate Simen Sørgaard Kongshaug

Master thesis, Structural Engineering and Building Technology

Major: Structural Engineering Specializations

OSLO METROPOLITAN UNIVERSITY

This master thesis is written as a part of the Master's Degree program "Structural Engineering and Building Technology" at Oslo Metropolitan University, Department of Civil Engineering and Energy Technology. Please note that neither the institution nor the examiners are responsible – through the approval of this thesis – for the theories and methods used, or results and conclusions drawn in this work.

Acknowledgements

This master thesis represents the end of the Master's Degree program in Structural Engineering and Building Technology at Oslo Metropolitan University, Department of Civil Engineering and Energy Technology. We would like to thank Professor Gro Markeset, PhD candidate Simen Sørgaard Kongshaug and Dr. Ing. A. Aas-Jakobsen AS for their excellent help, making this master thesis possible.

The thesis has been led by Professor Gro Markeset. As our supervisor, Gro Markeset has provided us with great help, guidance and her expertise to this topic. She has played an important role regards content and composition of the master thesis. With her many years of experience in concrete structures, has she guided us into a new and interesting topic which is relevant when it comes to structural analysis of reinforced concrete structures.

PhD candidate Simen Sørgaard Kongshaug has provided us with great guidance about ASR in which he specializes in. He has been a key factor in the structural analyses were he has provided great help with the theory of ASR and the FEM modelling in Abaqus. He has supported the structural analyses greatly by providing customized subroutines for the various material models used in this master thesis.

The master's thesis is written in partnership with Dr. Ing. A. Aas-Jakobsen AS, a leading building and construction consultancy, specializing in civil engineering. Dr. Ing. A. Aas-Jakobsen AS has provided us with their experience, expertise and informative reports regarding Elgeseter Bridge. They have had an important role in the making of the second case study were they have provided us with a three span beam model which represents the actual behaviour of a three span beam part of Elgeseter Bridge.

Structural Engineering and Building Technology

Oslo, 15th June 2020

Albian Tairi

Albian Tairi

Leonard-Johan Nesheim

Leonard-Johan Nesheim

Abstract

Alkali-silica reaction (ASR) is a chemical reaction that occurs in concrete between the alkalized cement and silica within the aggregates. ASR produces a gel around the aggregates which absorbs water, expands, results in local stresses, and causes the concrete to crack internally and externally. Research on this chemical reaction and development of concrete models including this reaction has been extensive. However, limited research about the structural effects of ASR and load actions due to ASR has been carried out. Due to lack of applicable constitutive models including the effect of ASR in finite element softwares, simplified methods for the assessment of ASR damaged reinforced concrete structures are used.

In this master thesis structural analyses of reinforced concrete beams affected by ASR have been carried out. Analyses on one span- and three span beams have been carried out to study the effect of using more complex concrete material models which includes the stress dependency of the ASR expansion and the stiffness reduction due to ASR. The load actions due to ASR with different concrete material models are computed and compared.

The concrete material models have been incorporated into the finite element software Abaqus. Approaches in Abaqus such as kinematic coupling and rebar has been used in the modeling of the case studies for the structural analysis which were too complex to solve analytically. The kinematic coupling method has proven to be a great approach for the structural analysis of reinforced concrete beams affect by ASR.

From the case studies it was found that the non-unifrom ASR expansion and the stress dependency of the ASR expansion had significant impact on the load actions.

Keywords – Reinforced Concrete, Alkali-Silica Reaction, Elgeseter Bridge, Material Models, Finite Element Method, Abaqus

Contents

List of Figures

List of Tables

Structural Analysis of Reinforced Concrete Beams Affected by Alkali-Silica Reaction

Chapter 1

Introduction

Oslo Metropolitan University

Engineering and Building Technology

15th of June 2020, Oslo, Norway

1 Introduction

1.1 Background and Motivation

Alkali-silica reaction (ASR) is a chemical reaction that occurs in concrete between the alkalized cement and silica within the aggregates. ASR produces a gel around the aggregates which absorbs water, expands, results in local stresses, and causes the concrete to crack internally and externally.

Alkali-silica reaction was first discovered in United States of America in the 1930's, as a result of cracking and expansion in several Californian concrete structures. The interest in the ASR problem grew in the 1970's where the problem was given a lot of media coverage. In United Kingdom ASR damages was identified in over 200 structures. In the 1980's, a survey was carried out in south of Norway including more than 400 dams, hydropower plant and road bridges, where it was identified that 31 of the structures had ASR problems. In New Zealand same survey was carried out for 400 bridges in 1989, where they found that 33 of the bridges had ASR problems. In the last three decades, ASR was found in many countries all over the world [27].

Alkali Silica reaction is a slow processes that develop over decades. The first regulations to prevent ASR damage in Norwegian concrete structures were introduced in the 1990's, meaning that structures designed before 1990's may contain ASR reactive aggregates that over time can lead to ASR damage to the structure. It is therefore assumed that a considerable amount of reinforced concrete (RC) structures constructed before this time, will develop damage related to ASR. As many of today's concrete structures are from the 60s and 70s, one can expect that problems related to ASR will increase over the next years. Norwegian structures such as Elgester bridge [22], Tjeldsund bridge [13], Tromsø bridge [17] and several more has been exposed to ASR damage.

ASR is a geographic problem that tend to occur in larger scale in some countries than others. This has to do with differences in countries concrete practice and environmental differences, e.g. larger alkali levels consequent on the change in cement chemistry, the rise in cement contents in concrete, the use of new aggregate sources (such as sea-dredged aggregate), more extensive use of de-icing salt etc. Guidelines for minimizing the risk

of ASR have been progressively introduced and updated in most countries in the 1980s and 1990s [27]. The Norwegian Public Road Administration have developed guideline for structural analysis of a ASR affected structure [29].

ASR induced stresses leads to additional load actions, thus changing the total loads on the structure. The induces stresses also causes deformations on the structure. If the stress state can be known on a ASR affected structure, the current structural capacity can be found. However, ASR is a complex phenomenon which makes it difficult to analyse its exact influence on existing reinforced concrete structures. Numerical ASR models are present today. These models describe the development of ASR by implementing ASR's influencing parameter into the model. The accuracy of these numerical models varies by the number of influencing parameters included in the model and by the degree these parameters are described.

Normally, finite element (FEM) softwares are used in structural analysis. Commercial FEM softwares do not contain material models that can be used to simulate the concrete affected by ASR. The only way to model ASR using commercial FEM software today is by converting the ASR expansion into a thermal expansion. This is a simplified method as it neglects many of the influencing ASR parameters, that may result in inaccurate assessments. By implementing more complex ASR material models into a FEM program, calculations and assessments of an ASR affected structure should become more accurate and precise, giving a realistic result of the load actions.

1.2 Objective and Research Questions

In this thesis different material models for the ASR expansion are going to be implemented in the FEM software Abaqus. The objectives are to study the effect of ASR by including the stress dependency and/or the stiffness reduction due to ASR in the material model. Structural analyses will be conducted on part of an entire construction. We will use a simplified beam of a real construction, that is comparable.

In this thesis, we have the following research questions:

- How to model reinforced concrete beams in Abaqus using beam finite elements?
- How to model the effect of ASR using existing material models in Abaqus and what are the limitations with this approach?
- How to model ASR affected concrete based on experimental observed behaviour, and how to apply such models to Abaqus?
- What is the effect of ASR expansion on the load actions on reinforced concrete beams?
- How does the material model that incorporates a stress dependent ASR expansion affect the load actions due to ASR?
- How does the material model that incorporates stiffness reduction due to ASR expansion affect the load actions due to ASR?
- How does applied ASR gradient on the height of the beam cross section affect the load actions due to ASR?
- How does the applied axial tension- and compression force on the beam affect the load actions due to ASR?

1.3 Thesis Content

Chapter 2 present a literature study on the alkali-silica reaction, expansion of concrete due to ASR and the mechanical changes of concrete. Constitutive ASR models will then be introduced. In the end of the chapter the effect of ASR on a structural level will be presented.

In Chapter 3 Euler-Bernoulli beam theory will be introduced as this is used in the structural analysis. Then the material models for concrete which are included in the structural analyses for reinforced concrete beams affect by ASR are presented. Analytical solution and numerical solutions are then described since they are used for the computation of the load actions.

In Chapter 4 and 5 structural analysis on two case studies are performed. First case study a one span reinforced concrete beam is used. The structural analyses shall be done using the solution procedures described in chapter 3. The case studies shall be analysed by including:

- Uniform or non-uniform ASR expansion
- Similar or non-similar end deformations
- Axial tension- or compression force

Discussion of the structural analyses for two case studies will be presented in chapter 6. In this chapter discussion regarding the modeling of the case studies, the effect of material models to the load actions, the use of uniform or non-uniform ASR expansion, the use of similar or non-similar end deformations and the use of axial tension or compression force will be presented.

Chapter 7 will clarify the most important findings from the structural analyses. Further work will be presented in chapter 8.

1.4 Limitations

Due to the complexity of structural analysis of a ASR affected reinforced concrete structures, the case studies will have some limitations in this thesis.

The structural analyses will be performed on simple beams and not the whole structure. The modeling of the beams will be done in 1D with beam elements.

In the structural analysis has focused on the ASR expansion, all other mechanisms, apart from creep, that lead to strains are not considered. This is because we want to look exclusively at what the effect of ASR is on the beams.

The structural analyses are limited to linear elastic material behaviour, the effect of a cracked concrete cross section and yielding of the reinforcement is therefore not taken into account.

Chapter 2

Alkali-Silica Reaction in Reinforced Concrete

Oslo Metropolitan University

Engineering and Building Technology

15th of June 2020, Oslo, Norway

2 Alkali-Silica Reaction in Reinforced Concrete

2.1 The Alkali-Silica Reaction

Concrete structures can be affected by chemical degradation processes during their service lifetime. One harmful degradation mechanism a structure can be exposed to is Alkali-aggregate reaction(AAR). AAR is a chemical process were alkaline cement reacts with reactive aggregates. The most common AAR is Alkali-Silica-Reaction (ASR), a chemical reaction between the alkalized cement and silica within the aggregates. Hydroxyl ions ($OH-$) in the alkaline pore solution in the cement react with silica (SiO_2) in the aggregates. ASR is a major degrading component to a concrete structure leading to a higher need of maintenance and/or repairs [28].

ASR and it affect can be seen in two steps, micro and macro. The ASR development starts on a micro level affecting on a chemical level which then develops and affects mechanical properties on a macro level. In the micro level the reactive silica in the aggregates form a chemical reaction with the alkali in the cement to produce alkali-silica gel [28]:

Reactive silica in aggregate + alkali in cement → alkali-silica gel

$$[xSiO_2] + [yNa(K)OH] \rightarrow [Na(K)_ySixO_zaq] \tag{2.1}$$

In the macro level the alkali-silica gel expands from the moisture absorption [28]:

Alkali-silica gel + moisture → expanded alkali-silica gel

$$[Na(K)_ySi_xO_zaq] + [H_2O] \rightarrow [Na(K)_ySi_xO_zwH_2O] \tag{2.2}$$

The gel that form around the reactive aggregate applies stresses locally which lead to the cement having tensile stresses. The effects will lead to micro-cracking, as seen in figure 2.1. The micro-cracks inside the mass of the concrete is unrestrained which makes for an randomly orientation. The micro-cracking can be examined petrographically and is

influenced by the aggregate size, spacing and porosity. Micro-cracks reduces the concrete stiffness and strength [31].

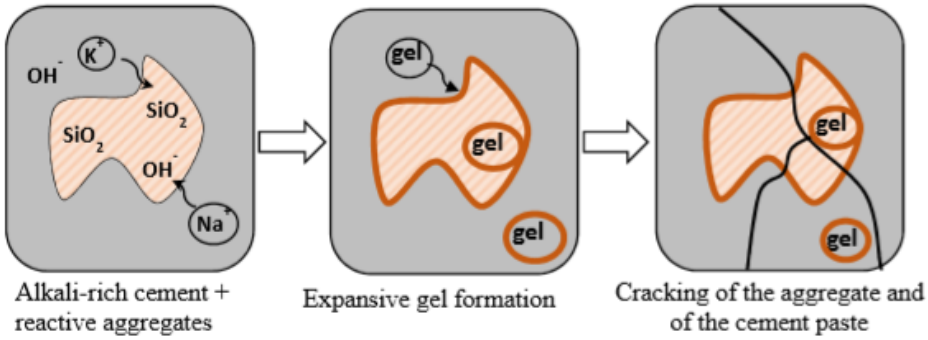

Figure 2.1: ASR development [16]

The micro-cracking tends to concentrate on the surface layer of reinforcement. These micro-cracks on can develop into more severe cracks from high expansions which can lead to debonding and stepped cracks along the reinforcement. This is due to the expansion of the concrete while the reinforcement remain the same. Since the ASR expansion only occurs in the concrete part of the structure and not in the reinforcement.

A lot of research has been done to understand and to find solutions for the ASR that appear in concrete structures. The deterioration of the concrete due to the ASR is a complex long-term reaction, the initiation of ASR may take many years and the damages normally appear 15-30 years after the concrete is cast. It all depends on the amount of reactive aggregates, content of alkali in the cement, relative humidity and the temperature [30]. Three preconditions must be met at the same time for the ASR swelling and damage to occur, as illustrated in figure 2.2. There are three main ways to minimize the risk of ASR. By choosing aggregates that are non-reactive, through tests to see if the aggregates have alkali content. By decreasing the amount of cement in the concrete mixture, since cement contains alkali. By using additives in the binders (fly ash, silica, slag etc.) the cement mix which will contain less cement, thus less alkali. The last measure that can be done is to decrease the permeability of the concrete. The permeability can be decreased by using low cement-water ratio, good curing of the concrete, good consolidation and the use of porosity-decreasing additives. This will help to reduce the water penetrating in the concrete which will further reduce the water being absorbed by the ASR gel around the aggregates. Concrete must contain moisture over a curtain level for ASR to initiate. In

Norway the level is set to $\leq 80\%$ relative humidity [26].

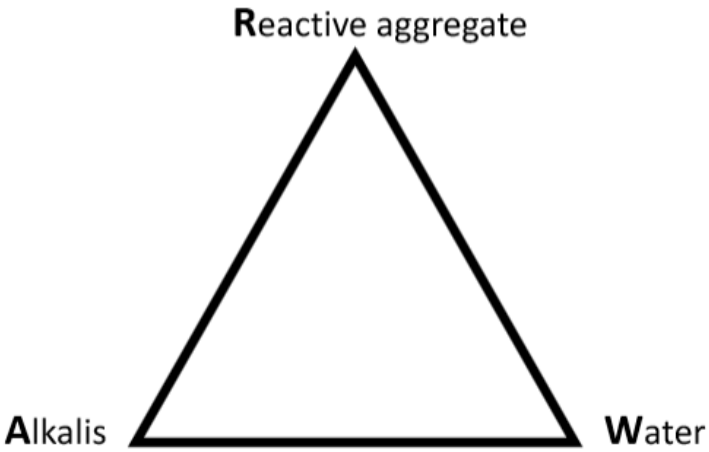

Figure 2.2: RAW - triangle illustrating the three conditions that must take place for ASR to occur

2.2 Expansion of Concrete due to ASR

There are variations that influence the expansion of the ASR. The variations are [31]:

- The type and quantity of reactive aggregate in the concrete structures may be different
- Concrete structures can be exposed to different type of moisture, drying and heating dependent of the environment its in
- The concrete structure may be exposed to different level of leaching from the surface due to moisture and alkali migration
- The reinforcement, structural loading and external restraint which influence the expansion direction and growth
- The concrete permeability, more pours in the concrete gives more room for expansion without giving internal pressure

The alkali in the cement and silica in the aggregate are available in the concrete, so the concrete expansion is dependent of the water absorption into the alkali silica gel. ASR damage is usually found in concrete exposed to the weather, in contact with or buried under ground, in splashing zones or under the water and concrete exposed to

heavy condensation. But the water availability can also come from withing the concrete structure, were expansion occurs due to high water-cement ratio with high alkali cement is used [31].

Multon et al [24] did experiments on the aggregate size and its effect on the ASR expansion. What they found was that the small reactive particles under about 160 µm do not cause expansion. ASR-expansion appears for particles having diameters greater than 160 µm. ASR expansion decreased with the amount of small reactive particles in the mortars. The more small reactive particles the mortar contained, the smaller was the ASR-expansion. The concrete having particles the size between 0.63-1.25 mm causes the biggest expansion of 33%. The researchers found out that having only large aggregate in the concrete will slow the ASR expansion compared to having concrete with different size of aggregate size. This is due to the difficulty of the alkali solution to enter the aggregates. The larger aggregates also gives the concrete larger porous zone which decreases the expansion because the gel has more space to expand in the porous before giving the concrete internal pressure.

The researchers Esposito and Hendriks [11] showed an overview of researches done on the expansion rate of the ASR effected concrete. It was found that the expansion rate very on the design mix. The figure 2.3 shows the ASR expansion after 1000 days for the different design mix types.

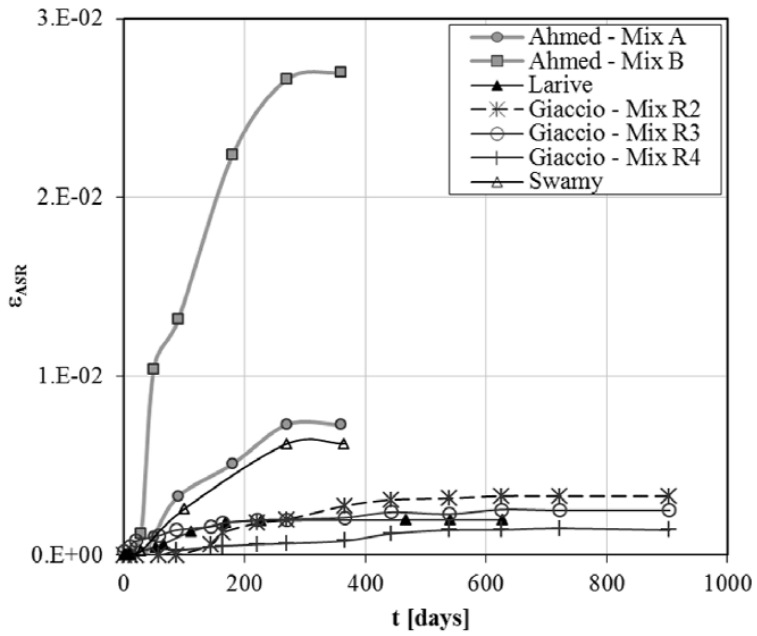

Figure 2.3: ASR expansion curves of different concrete design mixes [11]

2.2.1 Anisotropic Expansion of Concrete

It was shown by Larive [20] that the swelling process of concrete affected by ASR appears to be anisotropic. Trough her experiments she tested specimens in free expansion condition and found out that concrete prefers to swell in the direction parallel to the casting direction. The expansion in the parallel direction ranges from 1.3 to 2.8 times the expansion in the perpendicular direction. Tensile tests on concrete with the same aggregate size has shown that the tensile strength is lower along the casting direction. This means that distribution of pores with various shapes and orientations determines both the direction of the expansion.

The anisotropric behaviour of concrete has been shown by Barbosa et al [4]. In their study the researchers investigated the compressive strength of concrete cores which was drilled out from three severely damaged ASR slab in a bridge which is in service. The researchers also investigated the influence the ASR induced crack orientation had on the compressive strength and the Young's modulus. Uniaxial compression test, visual observations and thin section examinations were performed on more than 100 cores drilled from the three ASR-damaged slabs. The tested cores were vertically and horizontally drilled.

The figure 2.4 shows white arrows that indicates the horizontal AS induced cracks. During compression loading of the core several vertical splitting cracks, showed by the black arrows, are formed between the perpendicular ASR induced cracks. The vertical cracks results in significant lateral deformation of the core during loading [4].

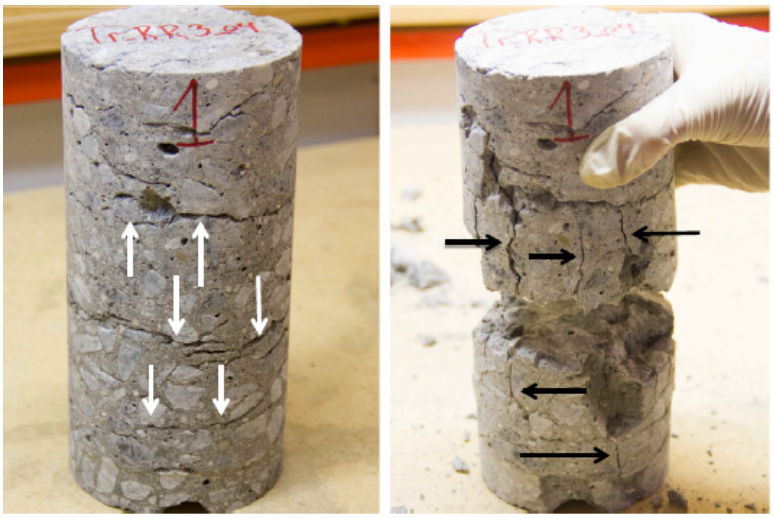

Figure 2.4: Core having perpendicular ASR-induced cracks (white arrows), (a) before loading and (b) after reaching the ultimate load, where vertical splitting cracks were formed (black arrows) during loading [4]

The figure 2.5 shows a core having ASR cracks parallel to the load direction, before the loading and after reaching the ultimate load. The arrows in the figure shows the ASR induced cracks. The core was split into small columns during loading [4].

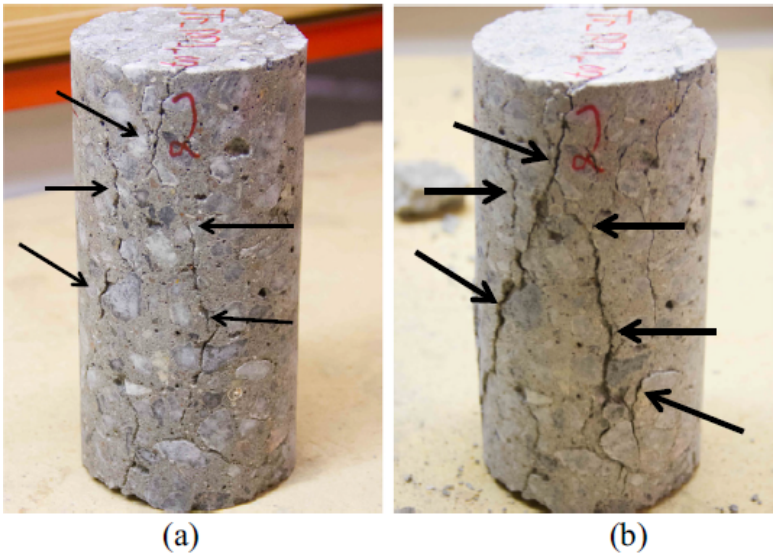

Figure 2.5: Core having parallel ASR-induced cracks (indicated by arrows), (a) before loading and (b) after reaching the ultimate load [4]

The researchers found out that the compressive strength in the vertical drilled cores which are in the direction perpendicular to the ASR cracks can be much lower than the compressive strength in the horizontal drilled cores which are in the direction parallel to

the ASR cracks. The experiments showed also that the Young's modulus depends on the cracks orientation. The Young's modulus is much lower on cores having perpendicular cracks than on cores having parallel cracks [4].

2.2.2 Influence of Stresses on ASR Expansion

There have been done numerous researches to understand the influence the stresses has on the ASR expansion. Jones and Clark [15] have presented a comparison of results which were developed by the Building Research Establishment(BRE) for the Science and Engineering Research Council (SERC). These results was derived by uni-axial loading tests which were performed on different types of samples. The samples were exposed to loading in the range of $0 - 8N/mm^2$. Tthey observed that the free expansion percentage decreased with increased restraint, as shown in 2.6.

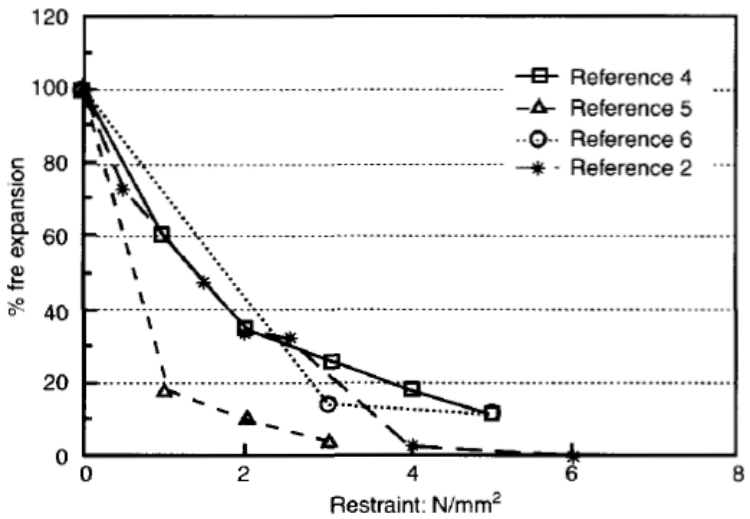

Figure 2.6: Relation of restraint and expansion for SERC/BRE bridge mix expressed as percentage of free expansion: 100 mm diameter samples[2,4]; 70 mm diameter samples[5]; 150 x 150 columns 1.4% reinforced[6] [15]

Jones and Clark [15] carried out their own experiment were they tested 180 cylindrical specimens with 100 mm diameter which had a length of 200 mm. The test specimens were applied constant stresses ranging from $4N/mm^2$ tension to $7N/mm^2$ compression and had reinforcement ranging from 0,125 to 2%. The stresses were applied after the concrete specimens had cured for 28 days. The concrete specimens had constant stresses for 250 days. They presented a final expansion comparison were the non-ASR strains that occured before 50 days, strains such as creep, were excluded as seen in figure 2.7.

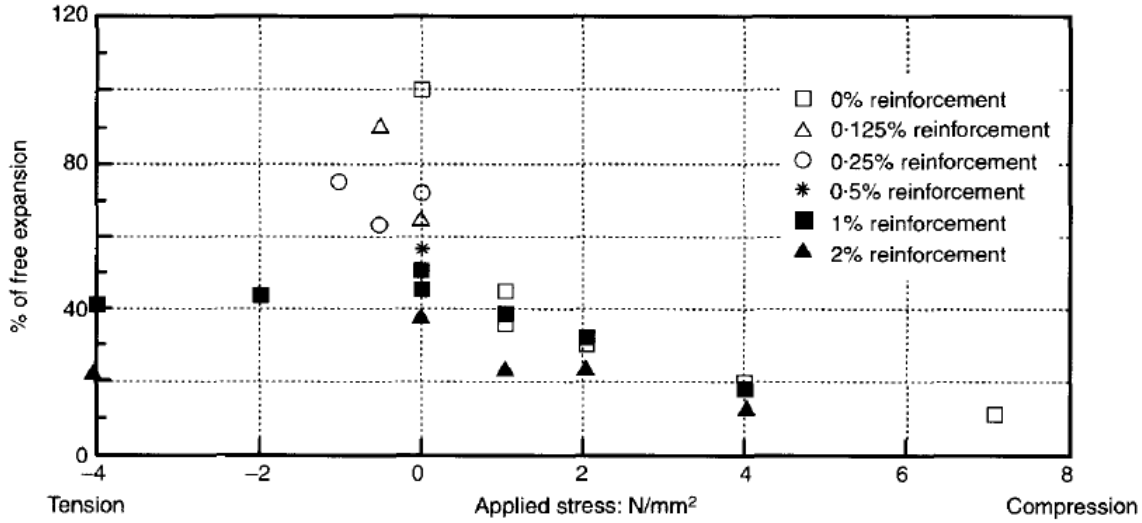

Figure 2.7: ASR expansion of cylindrical samples under various stress/reinforcement combinations: each point represents the average final expansion of four cylinders expressed as a percentage of cylinder free expansion [15]

It can be observed from the results that compressive stresses reduce the ASR expansion. The tensile stresses increased the ASR expansion for specimens with $0 - 0,25\%$ reinforcement and the tensile stresses reduced the ASR expansion for specimens with 2% reinforcement. They concluded that the ASR expansion is stress dependent.

Liaudat et al [23] did experiments with concrete specimens under multi-axial loading test. The testing was done on $150x150x150mm$ cubical specimens which were applied tri-axial loading with an "Alkali-Aggregate Reaction Triaxial Machine" (AARTM). AARTM had plates that covers most of the surface of the specimens, as seen in 2.8

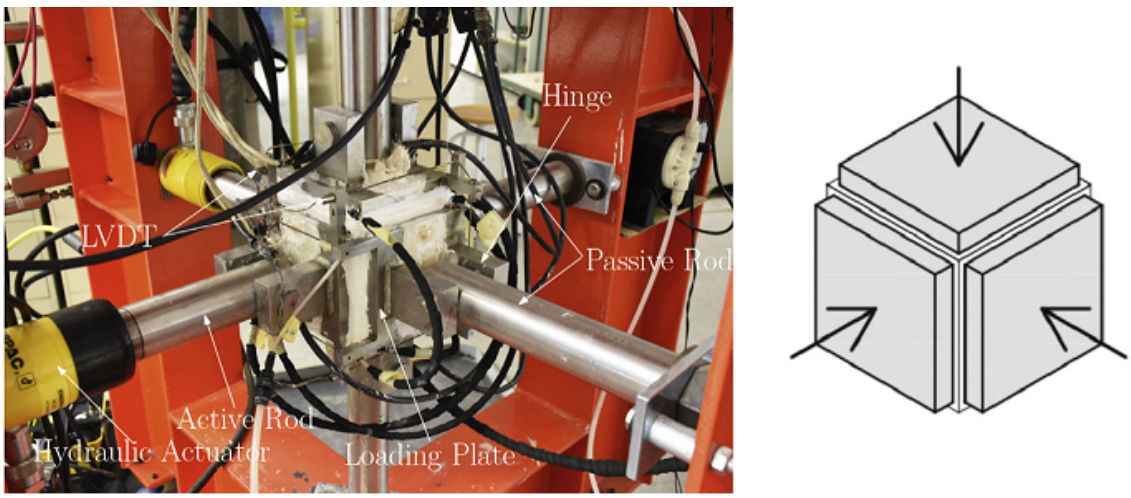

Figure 2.8: Alkali-Aggregate Reaction Triaxial Machine" (AARTM)[23]

The experiment had two types of concrete specimens, "control concrete" which was non-reactive and "reactive concrete" which was reactive. The non-reactive specimens was exposed to same condition under testing as reactive specimens. This was done to assess creep and/or shrinkage. In the experiments they studied three normal load cases with the AARTM:

- “Case 1-1-1”, $\sigma_x = \sigma_y = \sigma_z = -1MPa$
- "Case 9-9-9”, $\sigma_x = \sigma_y = \sigma_z = -9MPa$
- “Case 9-9-1”, $\sigma_x = \sigma_y = -9MPa,\ \sigma_z = -1MPa$

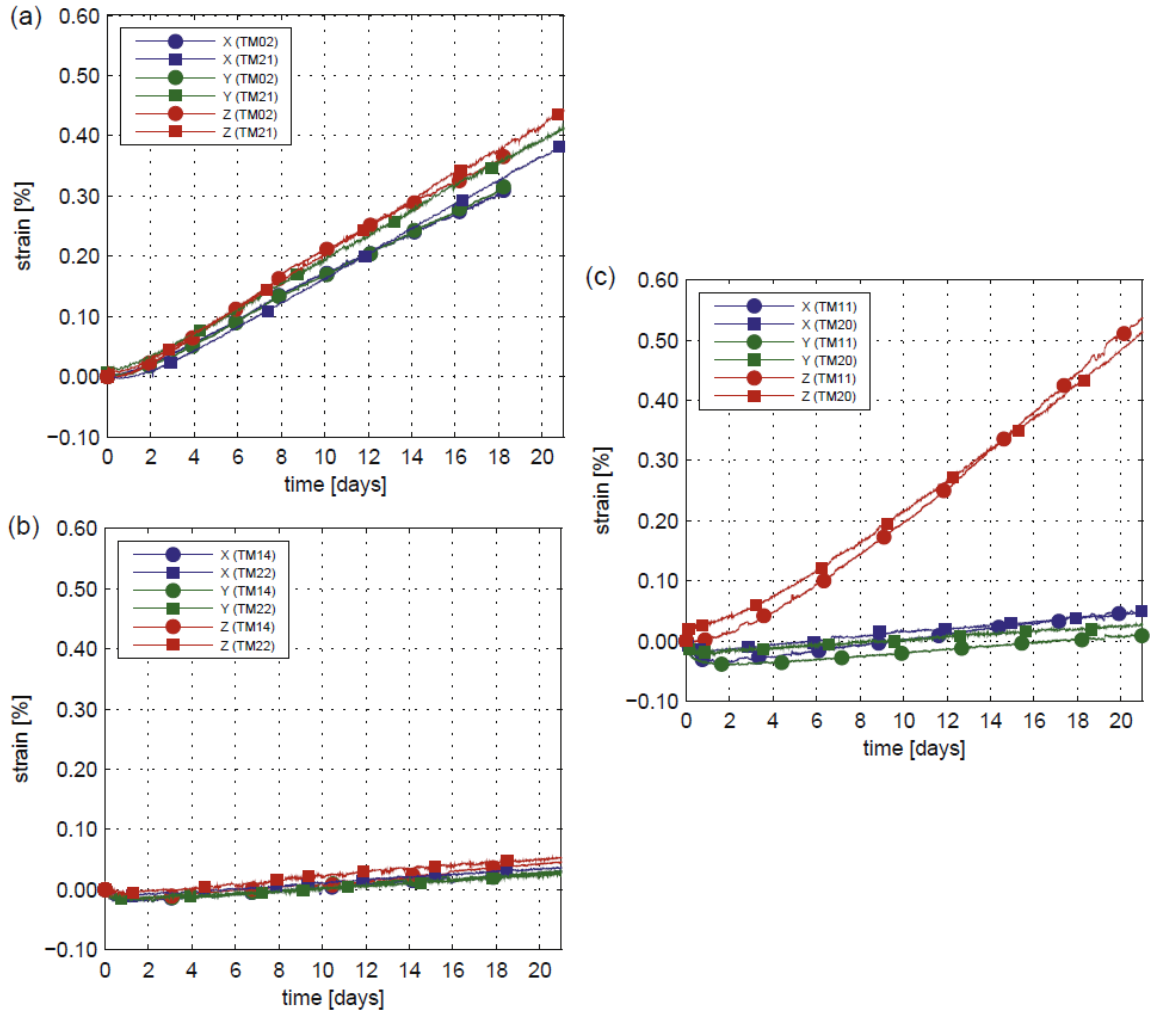

Figure 2.9: Axial strain curves, after deducting creep, of reactive specimens under (a) 1-1-1, (b) 9-9-9, and (c) 9-9-1 load cases [23]

The researches presented results with deducted creep strains by subtracting the strains measured in the control specimens from those in the reactive specimens. As the result shows in 2.9 is the ASR expansion is stress dependent. The ASR expansion decreases as the applied load stresses increases, this can be observed from “Case 1-1-1” to "Case 9-9-9”. Further can it be observed that the stress state of the specimens influence the ASR expansion as “Case 9-9-1” showed. The axial expansion in the z-direction (TM11, TM20) was greater than the other two directions(TM14, TM22, TM14,TM22) of the same specimen [23].

The ASR expansion can be influenced by restrains such as surrounding non-reactive concrete, stresses applied or reinforcements. The restrains prevent the expansion from growing the direction of the restrain and will further influence cracks so they appear parallel to the direction of the restrain. Figure 2.10 illustrates how the reinforcement can influence the ASR cracks on a beam from the expansion. First beam has only bottom reinforcement which exposes the top part of the beam for the known map cracking. This is due to the unrestrained top section which allows for free expansion. While in the second beam had reinforcement in the top and bottom of the beam which restrains the beam and doesn’t allow for free expansion. In this case cracks will occur parallel to the reinforcements direction and the ASR expansion will occur perpendicular to the restrains direction [31].

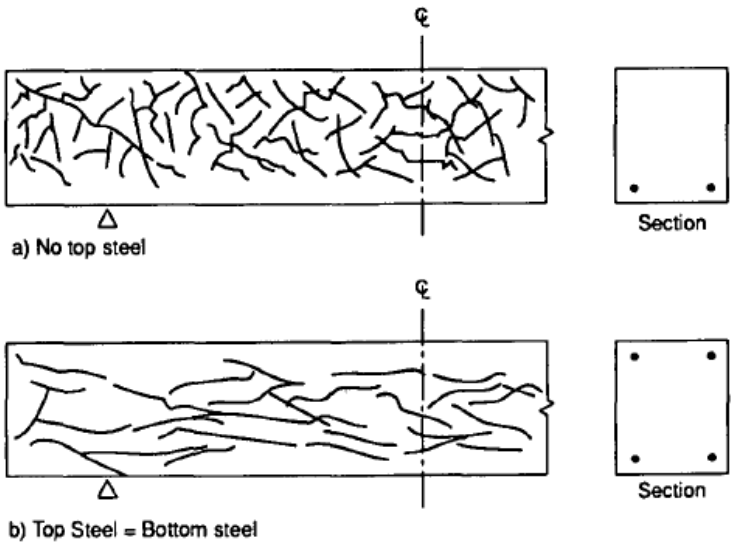

Figure 2.10: Influence of reinforcement on ASR cracking [31]

The reinforcement restrains will reduce the total ASR expansion compered to the free unrestrained ASR expansion. This is show by the graph in the left in figure 2.11. Beams with different amount of reinforcement is exposed to ASR expansion. It can be observed that the restraint delays the start and slows the expansion rate. Interesting observation from the test is that small amount of reinforcement significantly restrains the expansion. The increase of expansion rate in the concrete increases the compressive stresses as seen in the right graph in figure 2.11. Since the graph show laboratory test where the expansion rate is increased to a level which not represents the expansion rate on actual ASR affected concrete structures, the compressive stresses are likely to be lower then what the graph shows [31].

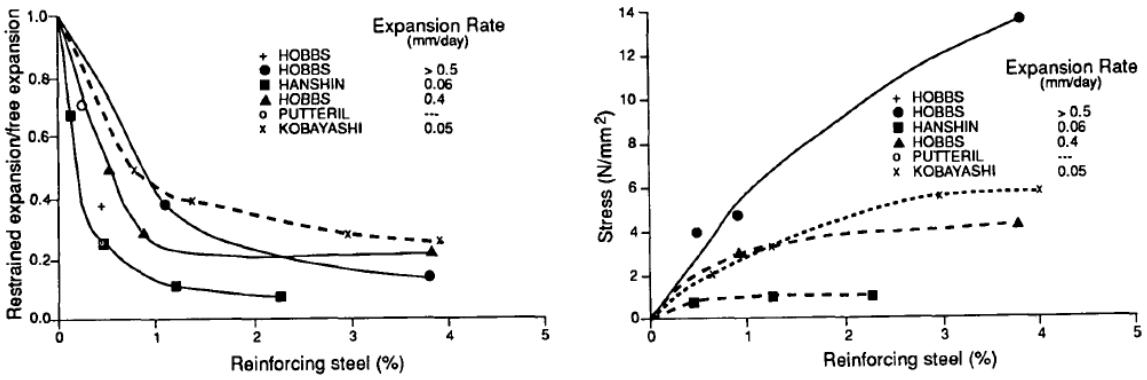

Figure 2.11: Left graph showing restrained expansion and right graph showing compressive stress due to increased reinforcing steel and expansion rate [31]

The ASR expansion in concrete will also result in tensile stresses in the reinforcement to occur. The tensile stresses from the ASR expansion are greater at the reinforcements with smaller cross section area or in section with less reinforcements. This means that longitudinal reinforcement will experience less strains then shear reinforcements. The ASR expansion alone can give local yield of the reinforcement. These local yields are not harmful for the ultimate capacity of the steel if the reinforcement are anchored by hooks and bends. The compressive stress reduces the expansion in the direction of the stress while the tensile stresses increases the expansion in the direction of the stress [31].

The external retrains from applied stresses has same effect on ASR expansion as the internal restrains from the reinforcement. As the two types of restrains effects the expansion direction and crack direction. This is observed on example bridge columns were the main transverse reinforcement(internal retrains) and axial stresses from dead-load(external

restrains) resulted in vertical cracks and horizontal expansion [31].

2.3 Changes in Mechanical Properties of Concrete due to ASR

2.3.1 Material Behaviour of Unreacted Concrete

From uniaxial tests is it proven that concrete behaves in a non-linear manner as show in figure 2.12. The material behaves linear elastic when the stresses is lower than approximately 30% of the maximum compressive strength. After the linear elastic part the concrete enters a plastic hardening state until it reaches maximum compressive stress. After reaching its maximum stress value, the stresses decreases. This part is called softening. Softening will continue until the concrete reaches its ultimate strain where failure occurs [6].

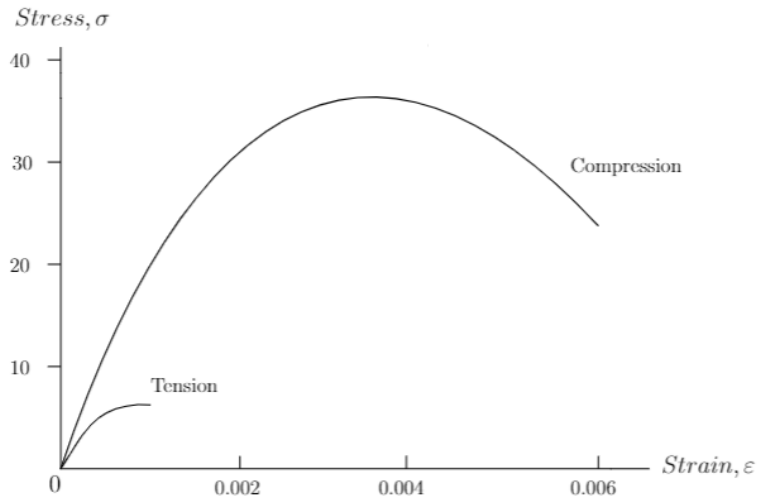

Figure 2.12: General compression and tension stress-strain curve for concrete [6]

Reinforced concrete consists of two materials, concrete and steel, where the concrete itself is a mixture of different materials. Due to concrete's limited tensile strength, reinforcement is embedded in the concrete to make up for the lack of tensile capacity. Concrete and steel act together by resisting the forces. The materials have approximately the same expansion rate which is important for the materials to work together. The different stages of reinforced concrete is shown in figure 2.13 and is as follows:

- **Stadium I:** Stadium I contains the linear elastic uncracked concrete stage. The occurring tensile forces is less than the concrete tensile strength capacity. In stadium I the effect and contribution of both the concrete and rebars are included. In stadium I the concrete has a linear elastic behavior in the entire cross section. The rebars does also have a linear elastic behavior.

- **Stadium II:** Stadium II contains linear elastic cracked concrete stage. The tension zone is cracked, and the concrete does not absorb/carry any forces in the tension zone. The occurring tensile forces is greater than the concrete tensile strength capacity. In stadium II only the compression zone has a linear elastic behavior. The rebars still have a linear elastic behavior like in stadium I in both compression and tension. The stiffness is reduced as cracks occur.

- **Non-linear analysis:** The non-linear stage includes the non-linear behavior of both concrete and reinforcement. A non-linear behavior can be described using different material models with varying complexity. There are two types of non-linear behavior, time dependent and time independent non-linearity. Time independent non-linearity include: The bond-slip between concrete and steel, dowel action of reinforcement, cracking and crushing of concrete and yielding of reinforcement. The time dependent non-linearities include: creep, shrinkage and temperature effects.

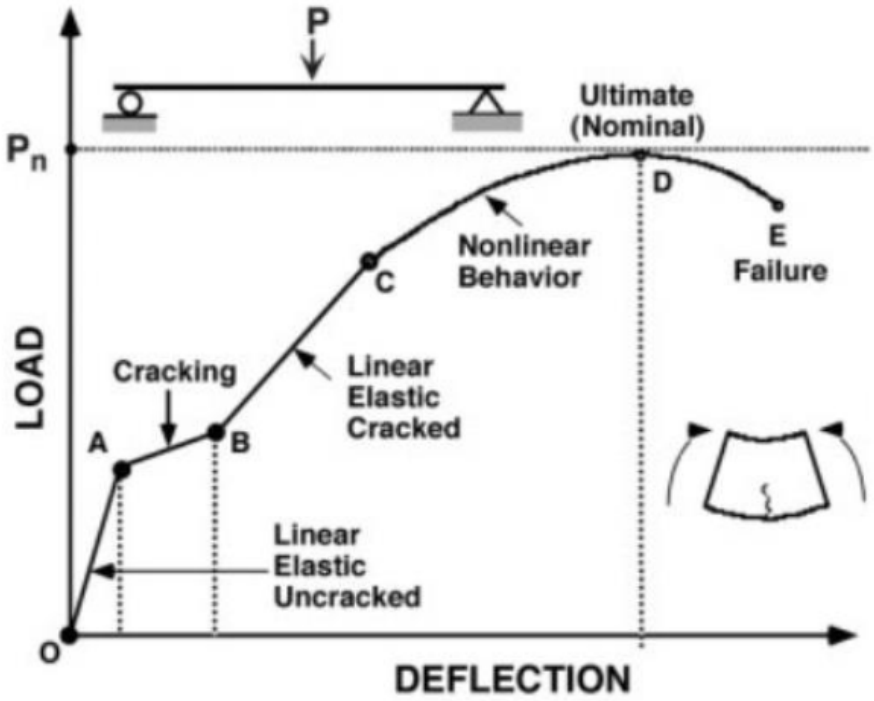

Figure 2.13: Illustration showing the different stages of the behaviour of reinforced concrete [25]

2.3.2 Material Behaviour of Reacted Concrete

The researchers Esposito and Hendriks [11] showed an overview of researches done on the changes in mechanical properties of ASR affected concrete. The researches studied the evolution of the Young's modulus, the tensile strength and the compressive strength in concrete specimen's. The researchers mostly concluded that the compressive strength is not a reliable parameter to detect ASR-swelling since the results was questionable and is some cases even increased compressive strength was observed. Therefore was the Young's modulus and tensile strength observed further. Even though the paper goes in more detail on how the degradation of Young's modulus and tensile strength is dependent of the design mix, what is observed in general is that the ASR expansion weakens the concretes mechanical properties.

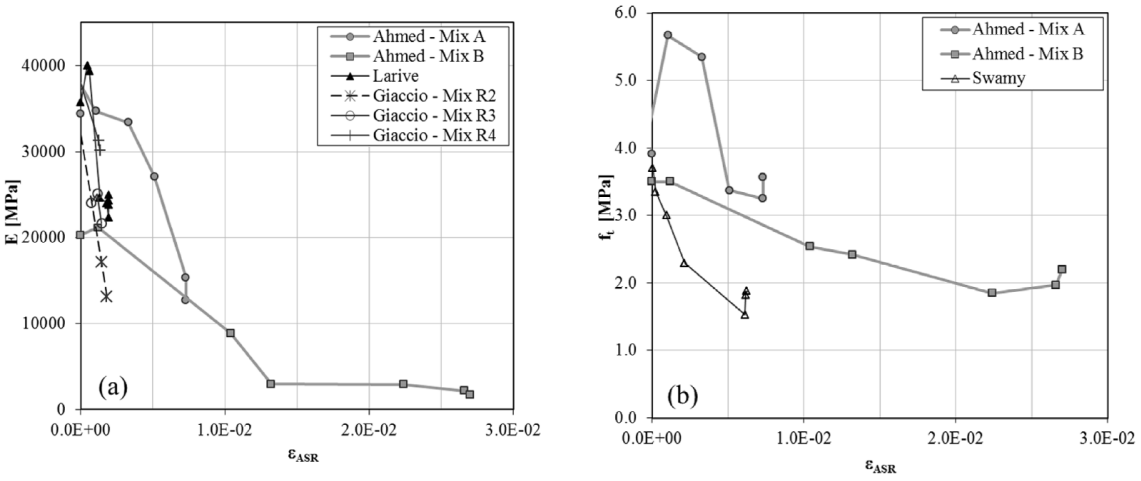

Figure 2.14: Degradation of Young's modulus (a) and tensile strength (b) for different design mixes [11]

In the following chapters the degradation on the mechanical properties such as compressive strength, tensile strength and Young's modulus of ASR affected concrete will be investigated in more detail.

Effect on Compressive Strength

In Larive's [20] experimental study for cylindrical standard specimens, she showed that there is no decreased compressive strength caused by ASR. The negative effects on compressive strength was concluded to be caused by the hydration processes. However, in the experimental study carried out by Swamy and Al-Asli [30] showed that in fact the compressive strength was weakened after the induction period of ASR is finished. In their study they tested the effect compressive strength for ASR affected specimens containing opal and fused silica. They observed that the concrete had increased in strength followed by gradually decrease in strength, as shown in figure 2.15.

Linear expansion ($x10^{-3}$)	4.5% opal		15% fused silica	
	Age (days)	Loss (%)	Age (days)	Loss (%)
0.5	6	9	40	12
1.0	8	11	60	11
2.0	17	20	87	15
4.0	36	27	140	30
6.0	60	30	200	40
10.0	117	38	-	-
16.0	270	62	-	-

Figure 2.15: Percentage loss in compressive strength of ASR-affected concrete [30]

Effect on Tensile Strength

Swamy and Al-Asli [30] showed that the tensile strength is the most effected mechanical property of the concrete due to ASR. The cracking that occurs when the ASR-swelling takes place specifically reduces the tensile strength. The experiments was performed with on specimens containing fused silica. The experiments showed that the tensile strength is more sensitive then compressive strength, even at early ages. The experiment was performed using modulus of rapture and tensile splitting test. The figure 2.16 shows the loss in tensile strength as the specimens expands.

Linear expansion ($x10^{-3}$)	Age (days)	Loss of tensile strength (%)	
		Modulus of rupture	Indirect tensile[1]
0.2	27	11	11
0.4	36	20	19
0.5	40	30	27
0.6	45	29	23
0.8	54	40	26
1.0	60	48	29
1.5	75	56	38
3.0	110	67	55
6.0	200	78	64

[1]from split cylinder test

Figure 2.16: Percentage loss in tensile strength of ASR-affected concrete [30]

Effect on Modulus of Elasticity

The reduction in modulus of elasticity for the concrete affected by ASR is significant. The loss in stiffness increases as the ASR expansion increases. The experimental study performed by Swamy and Al-Asli [30] showed that the loss in stiffness is different from the specimens with opal compared to the specimens with fused silica. The loss in stiffens in the opal specimens was observed to have significantly decreased from 0 to 28 days, with a loss of 51%. While the fused silica specimen had significantly decreased from 28 to 100 days, with a loss of $45,7\%$. In general it's been observed that ASR expansion can give a stiffness reduction of $58.4 - 77.1\%$ compered to the initial stiffness.

Linear expansion ($x10^{-3}$)	Age (days)	Loss of tensile strength (%)	
		Modulus of rupture	Indirect tensile[1]
0.2	27	11	11
0.4	36	20	19
0.5	40	30	27
0.6	45	29	23
0.8	54	40	26
1.0	60	48	29
1.5	75	56	38
3.0	110	67	55
6.0	200	78	64

[1]from split cylinder test

Figure 2.17: Percentage loss in elastic modulus of ASR affected concrete [30]

The stiffness reduction has also been shown by Kongshaug et al. [19] where they performed stiffness damage tests (STD) on drilled core specimens at different age of testing, see figure 2.18.

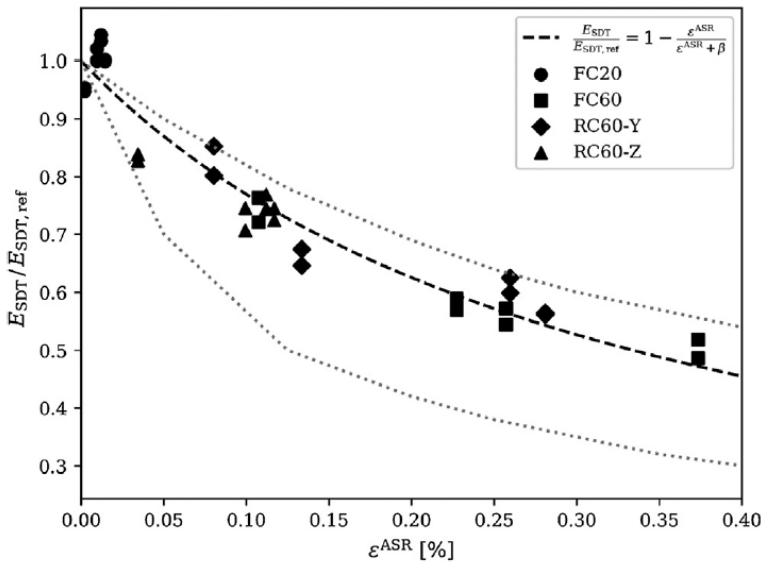

Figure 2.18: Evolution of relative modulus of elasticity [19]

2.4 Constitutive Models for ASR

The following basic aspects should be addressed in a comprehensive model: the kinetics of the reaction and the diffusion process, the mechanical damage caused by the expansion due to ASR, and the evaluation of ASR-induced strains. It is difficult to formulate a model which encompasses all the variables since ASR is influenced by many factors. Modeling of ASR expansion has been undertaken by various researchers which has resulted in several models being developed to reproduce the ASR effect at a chemical, material or structural scale. The models falls into one of three categories: micro-models, meso-models and macro-models depended on the level at which ASR is described. These models will be introduced in more detail in the furthering chapters [28].

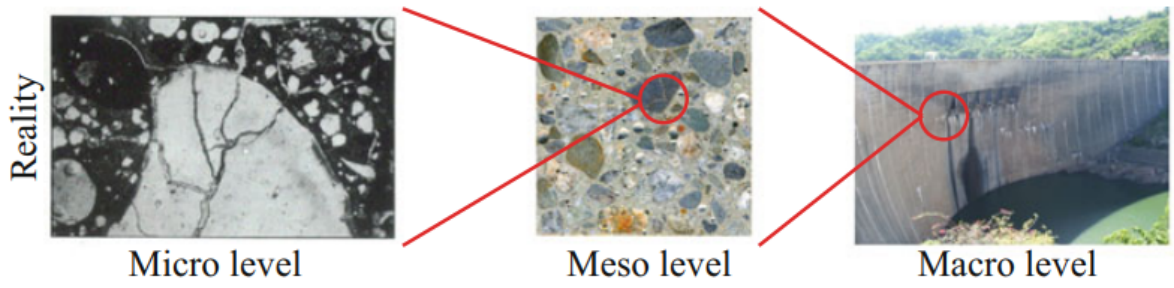

Figure 2.19: Illustration of the three categories the constitutive ASR models falls into [3]

Micro Models

Micro models are ASR models where aggregate and cement paste are separately modelled and the transport equation is used to model gel formation through the two stages of ASR. These micro-models are to detail and complex, therefore are they not relevant for structural analysis of elements affected by ASR which are on a bigger scale. However, findings and models such as the reaction extent coefficient, ξ are used in the models of bigger scale. It is important to also understand properly the phenomenon of ASR on the micro level since the meso- and macro-models are based on the knowledge gathered from the micro level [28].

Hobbs [14] proposed a model which predicts the time of cracking and for the expansion in mortar bars containing opaline silica. This model assumed the reaction from the amount of reactive aggregates and water-soluble alkali content. The prediction from the

model was compered with results from experiments which showed that its in approximate agreement. The model could correctly predict the general effect of changing water/cement ratio, aggregate/cement ratio and the cement alkali content upon the expansion of mortar containing Beltane opal. General agreement was found to exist between the observed and predicted times for cracking.

Meso Models

Meso-models are usually not so easy to define since they can fall into the category of micro-models or macro-models. But in general they can be defined as models which are focused on the aggregate, cement paste and the interfacial transition zone level.

The ASR-LDPM model by Alnagger et al. [2] came up with a model that has been able to include all the aforementioned limitations. This model called ASR-LDPM model which integrates the ASR effect into the LDPM model by Cusati et al. [9]. The LDPM model is a 3D model which simulates the mechanical interaction of coarse aggregate pieces through a system of three-dimensional polyhedral particles, each resembling (representing) a spherical coarse aggregate piece with its surrounding mortar, connected through lattice struts. This model is able to simulate the effect of material heterogeneity of the fracture process.

The ASR-LDPM model is the only available model that can predict realistic crack patterns from concrete under various conditions like free expansion, restrained expansion and various loading conditions. The model also predicts the degradation level of concrete, strength, stiffness, temperature effects on reaction kinetics and alkali content variations. This model has been made possible by a chemo-physic view the right scale and level of detail [2].

ASR-LDPM extend the LDPM model and take into account the variable alkali content in a concrete. It describes the ASR gel formation and expansion at the level of each individual aggregate pariticle. Two main processes are used to describe the evolution of ASR. Process one describes the gel formation and process two describes the water imbibition. The water imbibition results in an increase of the concrete volume. To describe the volume increase, the water imbibition is translated into inhomogeneous gel strain [2].

This model was then tested by Alnagger et al. [2] and numerical simulations of experimental

data was performed. Based on the experimental data simulations they found out that ASR-LDPM can predict accurate ASR-expansion under varying alkali content over both space time. ASR-LDPM proved that ANLP revolution highly correlate with the volume and size of cracking in the concrete. This again correlates to reduction between strength and stiffness.

Macro Models

In the macro-models the global behaviour of a ASR effected structure is emphasised where numerical model for the analysis, such as finite element method, is used. In macro-model takes into consideration the displacements, the stresses and the cracking of the structure. Some macro-models separates the reaction mechanism from the structural modelling, some models compares the kinetics with the structural modelling and some models ignores the reaction kinetics all together. Macro-models predict the long-term behaviour and the durability of concrete structures which are ASR effected [28]. Macro models used in this thesis is that of Charlwood et al. [7] and Wen [32].

Charlwood et al. [7] proposed a function, $W(\sigma)$ which describes the stress dependent expansion, as shown in 2.20. The the Charlwood function, $W(\sigma)$ is computed as such:

$$W = \frac{\varepsilon_{asr}}{\varepsilon_{asr}^{free}} \tag{2.3}$$

$$W(\sigma) = \begin{cases} 1 & if \quad \sigma \geq \sigma_L \\ 1 - \frac{log\,\sigma/\sigma_L}{log\,\sigma_u/\sigma_L} & if \quad \sigma_u \leq \sigma < \sigma_L \\ 0 & if \quad \sigma < \sigma_u \end{cases} \tag{2.4}$$

Figure 2.20 illustrates that the stress restrained expansion is the ASR expansion, ε_{asr} divided by the ASR free expasion, ε_{asr}^{free}. This ratio is called the normalized expansion, W and is dependent on the stress state of the structure. The stress $\sigma \leq \sigma_u$ means there is no expansion and $\sigma \geq \sigma_L$ means there is free expansion. These are material constant that need to be determent from experiments. These material constant are parameter that we need to implement in the subroutine when doing the structural analysis.

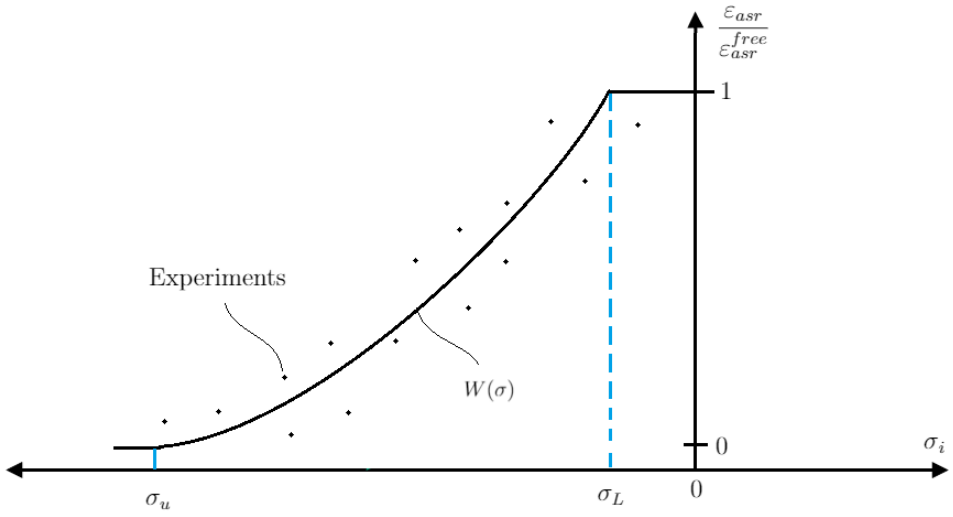

Figure 2.20: The uni-axial stress-relative expansion relationship, $W(\sigma)$ originally proposed by Charlwood et al. [7]

$W(\sigma)$ is an estimated function which is derived from numerous restrained expansion experiments. With the values from experiments can we customize the $W(\sigma)$ curve to give us an realistic development of the stress dependent ASR expansion for a concrete mixture.

Wen [32] showed that the relationship between the initial Young's modulus and the expansion may be formulated based on a simple 1D model, see figure 2.21. In this model, the ASR affected concrete is composed of healthy concrete with initial modulus of elasticity, E_0 and damaged concrete with reduced modulus of elasticity, E_{asr}.

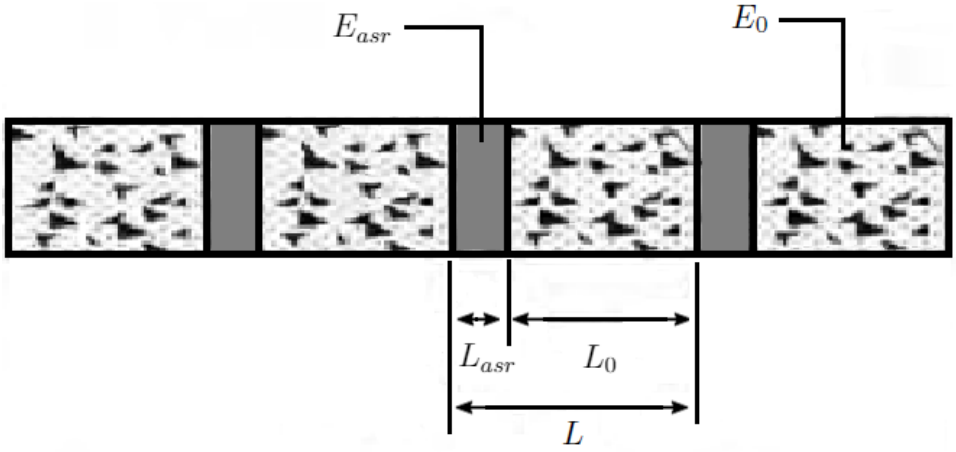

Figure 2.21: A model for the initial Young's modulus of concrete affected by ASR [32]

The concrete with initial length, L_0 expands due to ASR, $L_{asr} = \varepsilon_{asr} L_0$ so the new length of the beam becomes $L = L_0 + L_{asr}$.

2.5 The Effect of ASR on Reinforced Concrete Structures

The ASR expansion is a deformation load that occurs after a many years due to the slow developing chemical alkali silica reaction. Loads associated with direct applied deformation or loads that over time lead to deformation to the structure is called deformation loads. The deformations due to ASR expansion can be of a significant size.

When a reinforced structure is exposed to ASR expansion the deformation depends on the external loads applied and on the supports of the structure. ASR expansion is a stress dependent expansion were the magnitude and distribution of the expansion is influenced by the stresses that occurs on the structure. This means that reinforced concrete structures can be exposed to different magnitudes of ASR expansions. The ASR expansion can also be different within the same structure since some parts of the structure may have been exposed to more moisture then others. This results in the structure having an ASR gradient, κ_{asr}. Parts of the structure such as the beams can have an ASR gradient over the height of the cross section or/and in the width of the cross section. This ASR gradient can also occur due to the post tensioning effect that occurs when the concrete expands but not the reinforcement. Figure 2.22 illustrates this effect as a ASR gradient occurs over the height of the beam cross section for unrienforced and reinforced concrete beam.

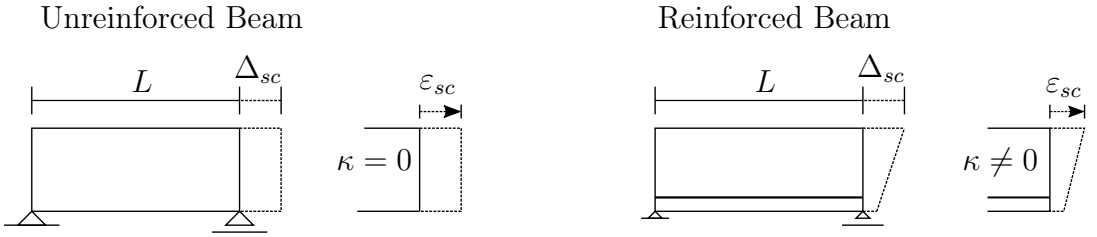

Figure 2.22: ASR expansion of an un-reinforced concrete beam and bottom reinforced concrete beam.

The uneven expansions results in tensile strain at the surface. The tensile strain can cause macro-cracking. In concrete which is unrestrained the pattern of macro-cracking formed is referred to map-cracking, since the crack pattern on the surface is similar to roads on a map. In restrained concrete which has reinforcement the macro-cracking follows the reinforcement resulting in a pattern parallel to the direction of the restraint [31].

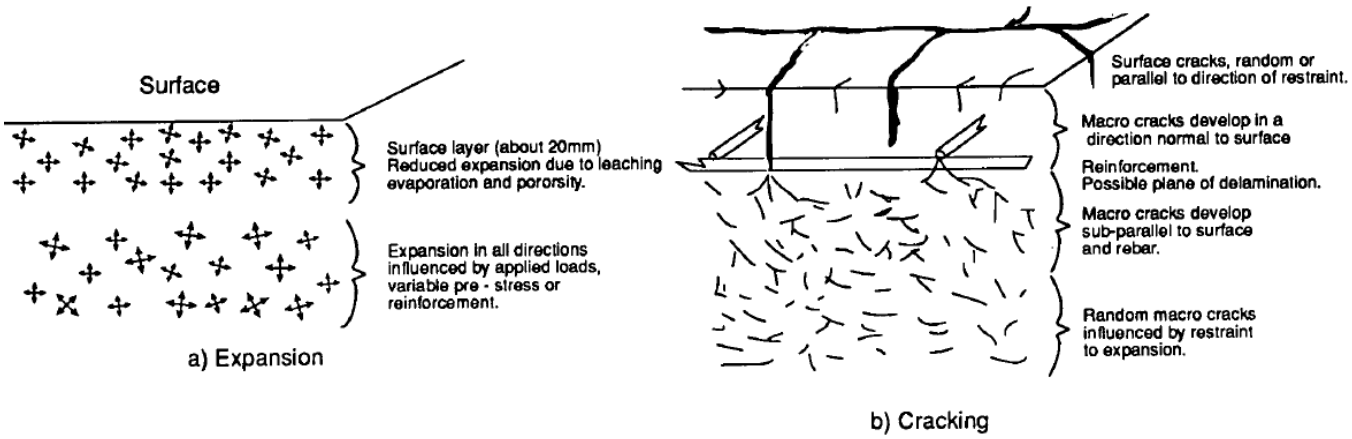

Figure 2.23: Development of cracking due to ASR [31]

The depth of macro-cracks does not usually exceed the cover and is related to the width of the macro-crack at the surface of the concrete, see figure 2.24. Observation studies from Japanese and U.K. demolished structures on sectioned members has shown that reinforcement propagates the surface cracking and that a single surface crack spreads into developing finer cracks [31].

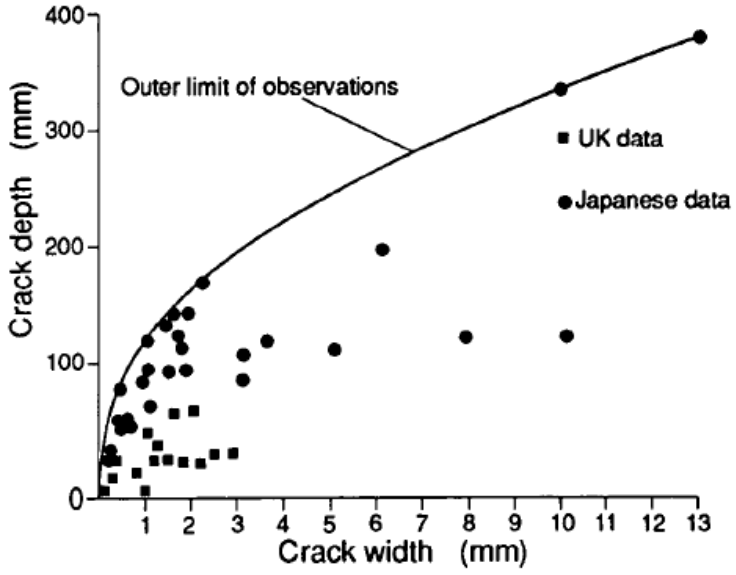

Figure 2.24: Relationship between crack depth and width in reinforced concrete [31]

The cracks has many functions in the ASR process. They act as transport network where they feed the ASR process by distributing the moisture received from the surface of the concrete. The cracks take the pressure exerted by the ASR and assist in a so called "alkali leakage" by transporting the reactive alkali to the voids and further out to the surface.

In this master thesis, Elgeseter bridge located in Trondheim, Norway, is used as a reference to show the issues regarding ASR and how ASR affects existing concrete structures.

Figure 2.25: Elgeseter bridge [21]

In 2008 the bridge was listed by the Norwegian government, meaning that the bridge must be conserved it the exact state as it is today. This gives restrictions when it comes to maintenance and repairs of the bridge.

During its lifetime the bridge has undergone changes regard its traffic pattern and different repairs and maintenance has been done. Throughout inspections it has been found that the concrete contains alkaline reactive aggregates, where ASR-reactions have influenced the durability and lifetime of the bridge.

The ASR-reaction had led to expansion of the concrete deck in the longitudinal directions of the bridge and occurrence of vertical cracks on/to the columns. Since the bridge has fixed supports at the south end, the ASR expansion was found to be enclosed to the north part where the bridge is able to move. It was found that the pointing had been closed by 17-18 cm and that the northern most pillars had gotten an inclination of approximately 200mm. since the columns were connected to the deck they were also affected by the longitudinal expansion leading to higher stresses in the columns due to the eccentricity at the top of columns. Due to this ASR-expansion the pointing had to be replaced and

the pillars in axis 7, 8 and 9 was cut at the top and recasted so that they would become vertical again.

In 2011-2012 large cracks was found on the beams. These cracks are also estimated to be a consequence due to ASR-reactions. A further expansion of the cracks on the columns can reduce the columns shear capacity and its ability to transfer shear forces. Cracks makes it also easier for chlorides to penetrate into the concrete and freeze/thaw mechanism to operate. These mechanisms will eventually reduce the capacity as it propagates corrosion of the reinforcement. Cracks and peeling of the concrete increases the ability for chlorides to penetrate into the concrete, which then will start corrosion of the reinforcement when reaching the depth of the reinforcement.

Figure 2.26: ASR consequences on Elgeseter bridge [21]

An estimated reason why the bridge has been so highly degraded over the years is due to high exposure of moisture. Tests has shown that the concrete contains a high amount of moisture which will initiate the ASR reaction leading to concrete expansion and occurrence of cracks. The influence of ASR has shown to arise only in the outer areas of the deck, where the pavement is located. Here it is estimated that the membrane has been damaged from work done to the pavement, which enables moisture to penetrate into the concrete and ASR to start. This has resulted in formation of lime on the outer sides of the beams and underneath the deck slab and their volume started to expand. As this expansion only occur to the outer parts of the bridge, the inner beams and the deck center will be exposed to strains which again influence the load actions of the structure.

Chapter 3

Structural Analysis of Reinforced Concrete Beams Affected by ASR

Oslo Metropolitan University

Engineering and Building Technology

15th of June 2020, Oslo, Norway

3 Structural Analysis of Reinforced Concrete Beams Affected by ASR

In this thesis structural analysis of reinforced concrete beams affect by ASR will be conducted. A macro model for concrete is used where the effect of ASR is modeled as induced strain and the free ASR strain, ε_{asr}^{free}, is the pre-defined field variable. Pre-defined field variable is a basic variable that is a known function of time and space. We have used pseudo time which means the time has no relevance. The free ASR strain is implemented as a pre-defined field in the FEM software Abaqus. The strain is decomposed into two parts, elastic strain and ASR strain:

$$\varepsilon = \varepsilon_{el} + \varepsilon_{asr} \tag{3.1}$$

where ε_{el} is the linear elastic strain related to the external load and/or dead load and ε_{asr} is the ASR induced strain. After the linear elastic strains are computed we need to find the stresses for the beam, which is computed as such:

$$\sigma = E\varepsilon_{el} \tag{3.2}$$

3.1 Euler-Bernoulli Beam Theory

The Euler-Bernoulli beam theory is effectively a model which provides a means to calculate the load-carrying and bending characteristics of beams. This theory is commonly referred to as "beam theory", and plays a important role in structural analysis because of its simplicity which help to analyse numerous structures in the pre-design stage to provide valuable insight into the behaviour of the structures. Other beam theories does also exist, e.g. Timoshenko beam theory, but these common that they are more complex than The Euler-Bernoulli beam theory. The beam theories are based on various assumptions and leads to different levels of accuracy [5]. The Euler-Bernoulli beam theory are based on three assumptions:

- The plane section remain plane. It is assumed that any section of the beam which was flat plane before the deformation will remain flat plane after the beam deforms.
- The plane sections remain plane also assumes that any section of a beam that was perpendicular to the neutral axis before the deformation will remain perpendicular to the neutral axis after the deformation.
- The deformed beams angels are small. It assumes that the deformations of the beam are small.

Kinematic is the description of displacement, deformation and strain. The interest in structural mechanics is to find the strain of the material because of its relation to stresses of the material. For the development of the ASR affected RC beam model, following assumption will be applied:

- Beam has plane displacements.
- The displacement of the beam follows the Euler-Bernoulli beam theory.
- Perfect bond between reinforcement and concrete which means the strain in the reinforcement is equal to the strain in concrete on the common boundary.

In the local beam coordinate system the assumptions applied will result in the following displacement field:

$$\begin{bmatrix} u \\ w \end{bmatrix} = \begin{bmatrix} \overline{u}(x) - z\frac{\partial w}{\partial x} \\ w(x) \end{bmatrix} \tag{3.3}$$

where u and w are the displacements in the local x and z direction, see figure 3.1. $\overline{u}(x) = u(x, z = 0)$ is the displacement along the x-axis [18]. The only non-zero strain is the normal strain in the x-direction. The strain at any point in the beam is given by

$$\varepsilon(x, z) = \frac{\partial u}{\partial x} = \frac{\partial \overline{u}}{\partial x} - z\frac{\partial^2 w}{\partial x^2} = \overline{\varepsilon} + \kappa z \tag{3.4}$$

where $\overline{\varepsilon}$ is the strain along the x-axis and κ is the curvature [18].

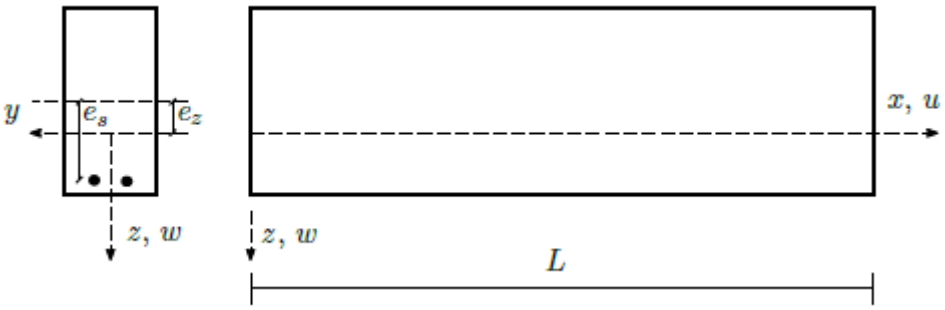

Figure 3.1: Beam geometry and coordinate system [18]

3.2 Material Models for Concrete

3.2.1 Linear Elastic ASR Damaged Model

In the analysis with short term modulus of elasticity is the concrete modeled as a linear elastic ASR damaged material. The linear elastic stress is given by

$$\sigma_c^{t+\Delta t} = E_c \varepsilon_{el}^{t+\Delta t} \tag{3.5}$$

where ε_{el} is elastic strain related to the external load or/and dead load of the beam and E_c is the modulus of elasticity for concrete. The linear elastic ASR damaged strain, ε, is therefore computed as such:

$$\varepsilon^{t+\Delta t} = \varepsilon_{el}^{t+\Delta t} + \varepsilon_{asr}^{t+\Delta t} \tag{3.6}$$

where ε_{asr} is the ASR strain from the ASR free expansion which is stress independent ($\varepsilon_{asr}^{t+} = \varepsilon_{asr}^{free}$). This gives us an linear elastic ASR damaged stress as such:

$$\sigma_c^{t+\Delta t} = E_c(\varepsilon^{t+\Delta t} - \varepsilon_{asr}^{t+\Delta t}) \tag{3.7}$$

3.2.2 Creep Model

The creep is included in the material models by calculating a long term modulus of elasticity using Eurocode 2: Design of concrete structures NS-EN 1992-1-1:2004+A1:2014+NA:2018 [12]. Eurocode 2 (EC2) calculate the final creep coefficient from which the effective modulus of elasticity of concrete, $E_{c,eff}$, is found. This model does not reduce the effective modulus of elasticity of concrete as a function of time. A more precise approach would be to use a creep model that gradually reduces the effective modulus of elasticity of concrete over its life time. However since the main focus in this thesis is to assess the influence of ASR, the effect of creep can therefore be inserted using a simplified model. The effective modulus of elasticity of concrete reduced due to creep is calculated as such:

$$E_{c,eff} = \frac{E_{cm}}{1 + \varphi(\infty, t_0)} \tag{3.8}$$

Where E_{cm} is the secant modulus of elasticity of concrete and $\varphi(\infty, t_0)$ is the final creep coefficient value. This results in an linear elastic ASR damaged stress with long term modulus of elasticity:

$$\sigma_c^{t+\Delta t} = E_{c,eff}(\varepsilon^{t+\Delta t} - \varepsilon_{asr}^{t+\Delta t}) \tag{3.9}$$

3.2.3 Stress Dependent ASR Expansion Model

The next variable that will be added to the material model to get a more detailed analysis is the stress dependency of ASR expansion. As shown in chapter 2.2.2, the ASR expansion is stress dependent. For a beam will the stresses vary with increased expansion which will influence the direction and magnitude of the ASR expansion. The stress dependent ASR strain is highly dependent on the stress history of the beam. The material model will include the stress dependency incrementally(which means a little more is added each time) until the stress dependent ASR expansion is computed [10].

The ASR expansion is computed by including the linear elastic strain, $\varepsilon_{el}^{t+\Delta t}$, the long term modulus of elasticity from creep, E_{eff}, and ASR stress dependent strain $\varepsilon_{asr}^{t+\Delta t}$:

$$\sigma_c^{t+\Delta t} = E_{c,eff}(\varepsilon_{el}^{t+\Delta t} - \varepsilon_{asr}^{t+\Delta t}) \tag{3.10}$$

Numerical method be used in the structural analysis were the stress dependent ASR is included in the ASR expansion. In the structural analysis will step two(ASR expansion) be divided in ten increments for case 1 and hundred increments for case 2. The expansions are calculated by using the stress state of the beam at every increment as illustrated in 3.2.

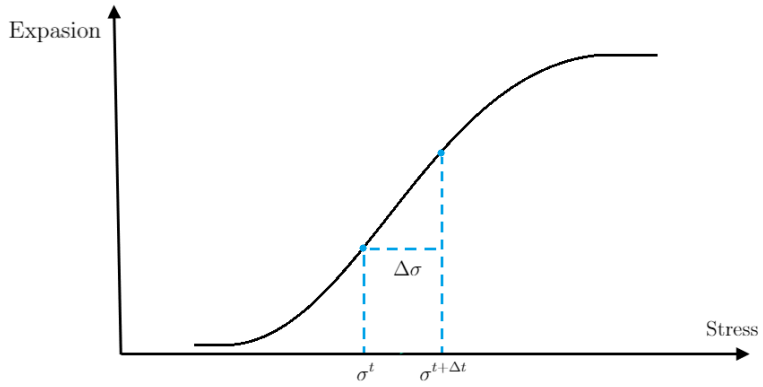

Figure 3.2: Illustration of incremental stress state included expansion

The ASR stress dependent strain was introduced by Wen [32] in his PhD-thesis. This expression computes an infinite small section of the total ASR expansion and is expressed as the derivative of the time for the expansion:

$$\begin{aligned} \dot{\varepsilon}_{asr} &= W(\sigma)\dot{\varepsilon}_{asr}^{free} \\ &\Updownarrow \\ \frac{d\varepsilon_{asr}}{dt} &= W(\sigma)\frac{d\varepsilon_{asr}^{free}}{dt} \end{aligned} \tag{3.11}$$

The calculation procedure to redo the material model from infinite small sections as the derivative of the time to incremental development is as follows:

$$\begin{aligned} \Delta\varepsilon_{asr} &= \int_t^{t+\Delta t} \frac{d\varepsilon_{asr}}{dt}dt \Rightarrow \int_t^{t+\Delta t} W(\sigma)\frac{d\varepsilon_{asr}^{free}}{dt}dt \\ &= W(\sigma)\int_t^{t+\Delta t} \frac{d\varepsilon_{asr}^{free}}{dt}dt \\ &= W(\sigma)\Delta\varepsilon_{asr}^{free} \end{aligned} \tag{3.12}$$

Where $\Delta\varepsilon_{asr}^{free}$ is the incremental free ASR strain, the $\Delta\varepsilon_{asr}$ is the incremental stress dependent strain and $W(\sigma)$ is the Charlwood function. Researchers Cope et al. [8] did

experiment where they compared the expansion from reinforced concrete beams to the free expansion of cylinder specimens which had same concrete and were stored in the same conditions. They discovered that the development of the ASR expansion for the beam is closely associated with the development of the free ASR expansion of the cylinders. Therefore, is the free ASR expansion, $\Delta\varepsilon_{asr}^{free}$ suitable parameter for the description of the expansion process which lead to the stress dependent ASR model. The ε_{asr}^{free} is a know value and so is the $\Delta\varepsilon_{asr}^{free}$ since the free expansion has a linear expansion rate as shown in 3.3.

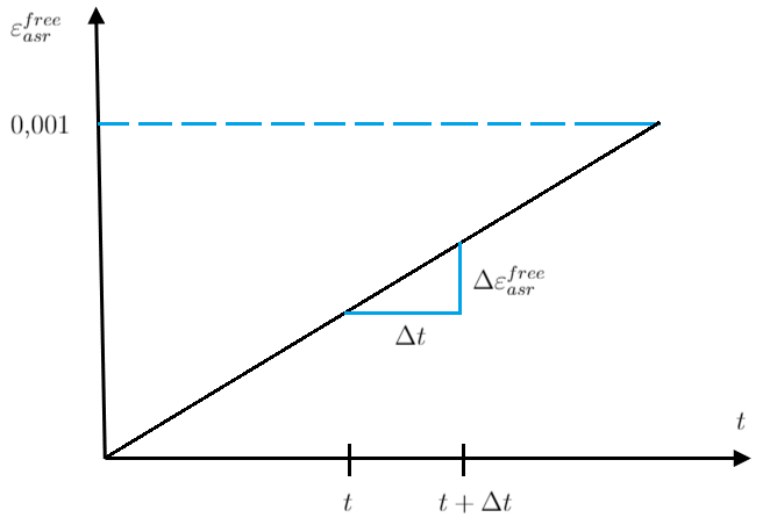

Figure 3.3: Illustration of the linear free ASR expansion

This incremental stress dependent ASR expansion $\Delta\varepsilon_{asr}$ is multiplied with the Charlwood function, $W(\sigma)$ which is the ratio of the restrained expansion to the free expansion and is referred to as the uni-axial stress-relative expansion relationship. By dividing the ASR expansion into many increments will the uni-axial stress-relative expansion relationship, $W(\sigma)$ have small differences from one increment to the next one. Therefore, can we simplify the model by assuming $W(\sigma)$ is constant. This function is originally proposed by Charlwood et al. [7]. In this thesis experiments shown by Jon and Clark [15] and Kongshaug et al. [19] are chosen so that material constants used are realistic. A graph reader has been used to extract the data from the diagram in Jon and Clark [15] research paper which is displayed on a table, see figure 3.4.

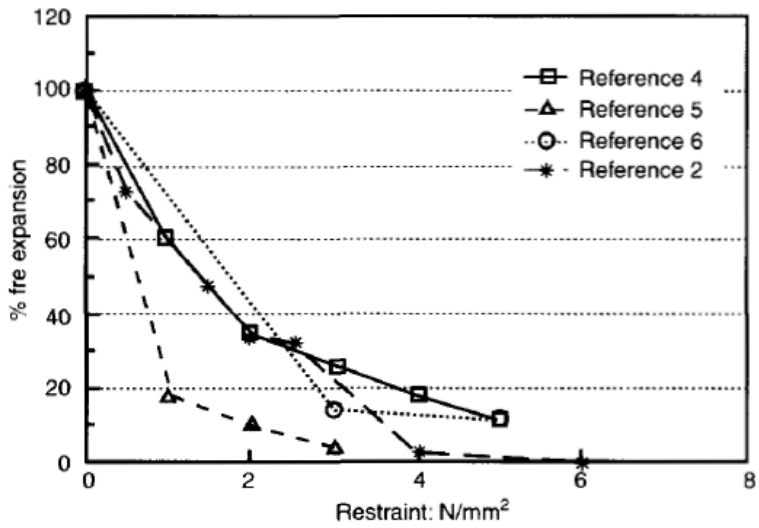

Jones & Clark (1996)

σ, N/mm^2	W, %	W, ratio
0,00	99,35	0,99
-0,46	73,64	0,74
-0,92	60,39	0,60
-0,97	18,70	0,19
-1,45	47,92	0,48
-1,94	33,12	0,33
-1,98	10,13	0,10
-2,47	32,34	0,32
-2,91	14,42	0,14
-3,00	25,71	0,26
-3,97	19,09	0,19
-4,03	3,90	0,04
-4,98	12,08	0,12
-6,00	0,78	0,01

Figure 3.4: Experimental results from Jones and Clark displayed in a table [15]

From Kongshaug et al. [19] we used a diagram showing the free volumetric strain which was extracted from specimen FC60 and the restrained (with 3 MPa in the z-direction) volumatetric strain extracted from specimen RC60. The strains where noted at 48, 83, 118 and 160 days, See figure 3.5.

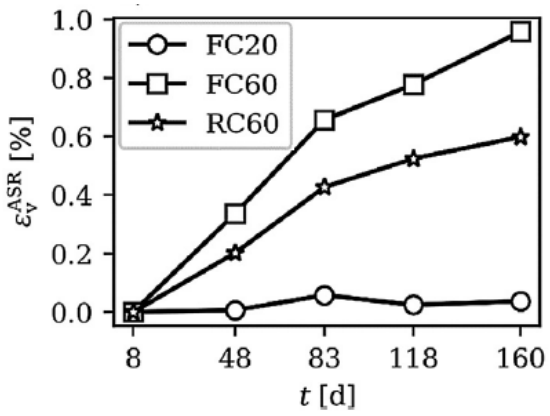

Kongshaug et al. (2020)

σ, N/mm^2	Days	ε_(asr, free), %	ε_(asr), %	W, ratio	Avrage
-3	48		0,0343		
0	48	0,3367		0,31	
-3	83		0,1120		
0	83	0,6569		0,51	0,39
-3	118		0,1168		
0	118	0,7783		0,45	
-3	160		0,0992		
0	160	0,9584		0,31	

Figure 3.5: Experimental result from Kongshaug et al. displayed in a table [19]

An curve adjustment method has been used to determent the material constants. The Charlwood function, $W(\sigma)$ has been adjusted to fit the experimental data from Jones and Clark [15] and Kongshaug et al. [19]. The material parameters, $\sigma_u = -6$ and $\sigma_L = -0,2$, was then extracted from the curve adapted Charlwood function as shown in figure 3.6.

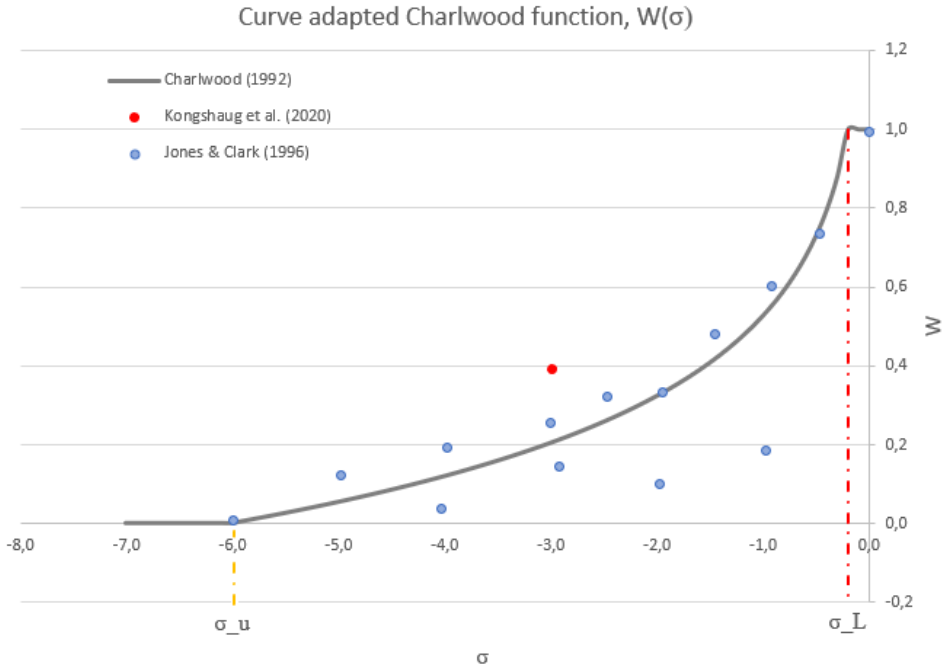

Figure 3.6: Curve adapted Charlwood function, $W(\sigma)$

The external subroutine which includes the ASR stress dependency is added to Abaqus in the structural analysis. This subroutine will calculate the stresses at end of each increment. The stress at the beginning of the time increment, σ_c^t is expressed as such:

$$\sigma_c^t = E_{c,eff}(\varepsilon^t - \varepsilon_{asr}^t) \tag{3.13}$$

where ε_{asr}^t is the ASR stress dependent strain at time t. The stress at the end of time increment is computed by adding the strain increase, $\Delta\varepsilon_{asr}$ at next increment:

$$\begin{aligned} \sigma_c^{t+\Delta t} &= E_{c,eff}(\varepsilon^{t+\Delta t} - \varepsilon_{asr}^{t+\Delta t}) \\ &\Updownarrow \\ \sigma_c^{t+\Delta t} &= E_{c,eff}(\varepsilon^{t+\Delta t} - (\varepsilon_{asr}^t + \Delta\varepsilon_{asr})) \end{aligned} \tag{3.14}$$

3.2.4 Stiffness Reduced ASR Model

In chapter 2.3.2 it is shown that the ASR expansion influences the stiffness of the structure. The modulus of elasticity of concrete is reduced with increased ASR expansion. In this material model will the reduced Young's modulus due to ASR expansion be included in the stress computation. This is done by using an external subroutine such that the analysis in Abaqus computes ASR effected stiffness, $E_c(\varepsilon_{asr}^{t+\Delta t})$ incrementally. This subroutine will include the ASR reduced stiffness and stress dependent ASR expansion incrementally. Where the stress at time of interest, σ_c^t is expressed as:

$$\sigma_c^t = E_{c,eff}(\varepsilon_{asr}^t)(\varepsilon^t - \varepsilon_{asr}^t) \tag{3.15}$$

where the long term stiffness, $E_{c,eff}$ is reduced as a function of the ASR expansion, $E_{c,eff}(\varepsilon_{asr}^t)$. The stress at next increment is computed by including the increased stress dependent ASR strain, $\Delta\varepsilon_{asr}$ and increased reduction of stiffness due to ASR, $E_{c,eff}(\Delta\varepsilon_{asr})$:

$$\begin{aligned} \sigma_c^{t+\Delta t} =& E_{c,eff}(\varepsilon_{asr}^{t+\Delta t})(\varepsilon^{t+\Delta t} - \varepsilon_{asr}^{t+\Delta t}) \\ & \Updownarrow \\ \sigma_c^{t+\Delta t} =& E_{c,eff}(\varepsilon_{asr}^t + \Delta\varepsilon_{asr})(\varepsilon^{t+\Delta t} - (\varepsilon_{asr}^t + \Delta\varepsilon_{asr})) \end{aligned} \tag{3.16}$$

The reduced stiffness due to ASR expansion function, $E_{c,eff}(\varepsilon_{asr}^{t+\Delta t})$ is obtained from Wen [32]. Wen [32] showed in his PhD-thesis that the relationship between the initial Young's modulus and the ASR expansion may be formulated based on a simple 1D model. In this model, the ASR affected concrete is composed of healthy concrete with initial modulus of elasticity, E_0 and damaged concrete with reduced modulus of elasticity, E_{asr}. The concrete with initial length, L_0 expands due to ASR, $L_{asr} = \varepsilon_{asr}L_0$ so the new length of the beam becomes $L = L_0 + L_{asr}$. The length affected by the ASR expansion is given by:

$$\begin{aligned} \varepsilon_{eld}L =& \frac{\sigma}{E_{asr}}L_{asr} + \frac{\sigma}{E_0}L_0 \\ =& \frac{\sigma}{E_{asr}}\varepsilon_{asr}L_0 + \frac{\sigma}{E_0}L_0 \end{aligned} \tag{3.17}$$

The equation is then solved with respect to the stress:

$$\begin{aligned}\sigma_c =& \frac{1}{\frac{\varepsilon_{asr}}{E_{asr}} + \frac{1}{E_0}} \varepsilon_{el} \\ =& \underbrace{(1 - \frac{\varepsilon_{asr}}{\varepsilon_{asr} + \beta^E_{asr}}) E_0}_{E_c(\varepsilon_{asr})} \varepsilon_{el}\end{aligned} \tag{3.18}$$

where $\beta^E_{asr} = E_{asr}/E_0$ is a material constant. As seen in equation 3.18 the reduced stiffness due to ASR expansion, $E_c(\varepsilon_{asr})$ has been identified. Kongshaug et al. [19] showed that the material constant, $\beta^E_{asr} = 0.0033$ was found to fit best to their experimental data when investigating the evolution of modulus of elasticity. This value for the material constant will also be used in our analysis when including the reduced stiffness due to ASR expansion material model. By including the long term modulus of elasticity, ASR stress dependent expansion and reduced stiffness due to ASR expansion the stress computation at a time of interest is as such:

$$\begin{aligned}\sigma^t_c =& E_{c,eff}(\varepsilon^t_{asr})(\varepsilon^t - \varepsilon^t_{asr}) \\ =& \frac{1}{\frac{\varepsilon^t_{asr}}{E^t_{asr}} + \frac{1}{E_{c,eff}}} (\varepsilon^t - \varepsilon^t_{asr}) \\ =& \underbrace{(1 - \frac{\varepsilon^t_{asr}}{\varepsilon^t_{asr} + \beta^E_{asr}}) E_{c,eff}}_{E_{c,eff}(\varepsilon^t_{asr})} (\varepsilon^t - \varepsilon^t_{asr})\end{aligned} \tag{3.19}$$

The stress at next increment, $\sigma^{t+\Delta t}_c$ is calculated as such:

$$\begin{aligned}\sigma^{t+\Delta t}_c =& E_{c,eff}(\varepsilon^{t+\Delta t}_{asr})(\varepsilon^{t+\Delta t} - \varepsilon^{t+\Delta t}_{asr}) \\ =& \frac{1}{\frac{\varepsilon^{t+\Delta t}_{asr}}{E^{t+\Delta t}_{asr}} + \frac{1}{E_{c,eff}}} (\varepsilon^{t+\Delta t} - \varepsilon^{t+\Delta t}_{asr}) \\ =& \underbrace{(1 - \frac{\varepsilon^{t+\Delta t}_{asr}}{\varepsilon^{t+\Delta t}_{asr} + \beta^E_{asr}}) E_{c,eff}}_{E_{c,eff}(\varepsilon^{t+\Delta t}_{asr})} (\varepsilon^{t+\Delta t} - \varepsilon^{t+\Delta t}_{asr})\end{aligned} \tag{3.20}$$

3.3 Material Model for Steel

An elastic perfectly-plastic model is often used when describing the behavior of steel, e.g when designing according to EC2 [12] using steel rebars. Under uniaxial tension the steel is elastic until it reaches the yield stress value, σ_y, after that the steel enters a plastic stage that is horizontal linear. The slope of the curve represents the stell modulus of elasticity, E_s. The stress computation of the reinforcement is modeled as such:

$$\sigma_s = E_s \varepsilon \tag{3.21}$$

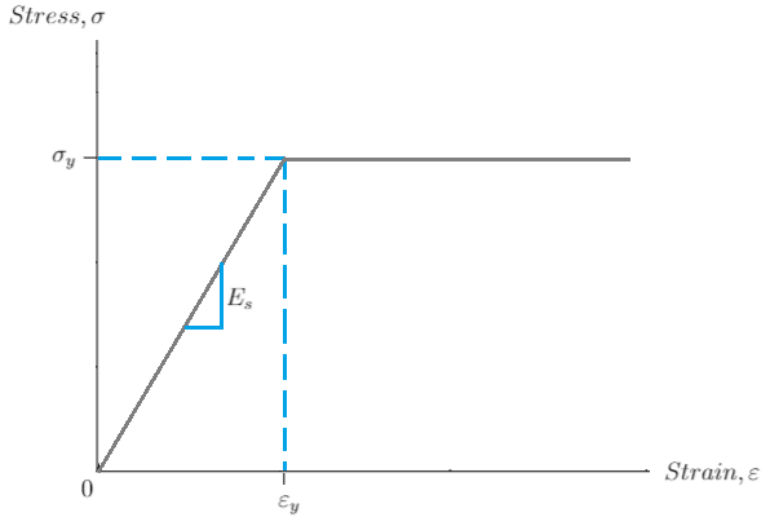

Figure 3.7: Stress-strain curve of elastic perfectly-plastic model for steel

The analysis done in this thesis are performed in stadium 1. Assuming a linear material behavior for steel in which the elastic part up until yielding is included.

3.4 Analytical Solution

To find the solution of the load action due to ASR on reinforced concrete beams, kinematics-, equilibrium- and material model (KEM) equations are used to find the solution. There is an analytical solution when assuming linear elasticity and stress independent ASR expansion. The analytical solutions were carried out in case 1, see Chapter 4.1.1 and Chapter 4.2.1, to verify the numerical model. By including the stress dependent ASR expansion and stiffness reduction due to ASR, numerical method must be used to solve the KEM equations.

3.5 Numerical Solution with Finite Element Methods in Abaqus

In this thesis we have used the finite element software Abaqus. Finite element method is a widely used to solve engineering and mathematical problems [10].

A FEM analysis calculates the displacement vector that equilibreates the internal and external forces. The structures geometry is discretized into finite elements (space). In our case the finite elements are defined as beam elements. An incremental solution procedure is used for the structural analysis.

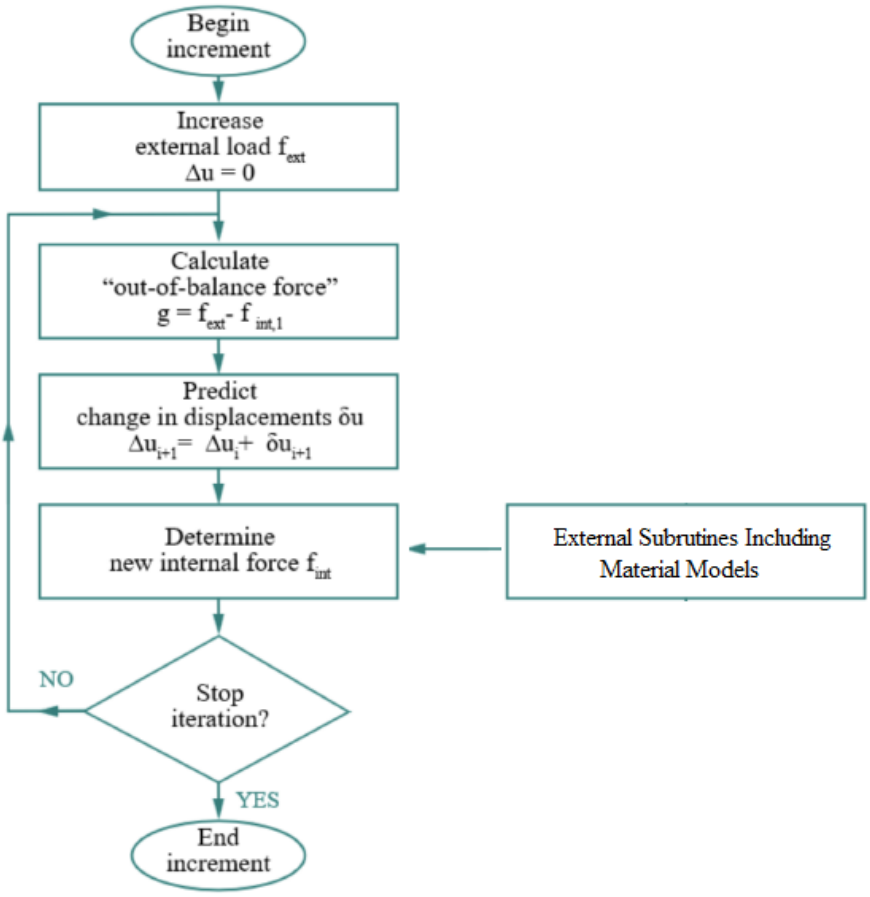

Figure 3.8: Incremental iterative solution procedure [10]

Incremental iterative solution procedure in FEM divides the time into increments. Regards to the ASR expansion in our analysis, external subroutines for the different concrete material models describing the development of the ASR is included within the FEM program. These external subroutines are included since the FEM software Abaqus, which is used in this thesis, does not have internal subroutines that describes the ASR expansion. The subroutines which includes the concrete material models used in this thesis are programmed and provided by PhD candidate Simen Sørgaard Kongshaug. The softwares Visual Studio 2020 and Parallel Studio 2020 (contains Fortran Compiler) was used to include the external subroutines to Abaqus. These softwares makes it possible for Abaqus to use the subroutines in its analysis.

In this thesis, we have investigated two methods to simulate the interaction between the reinforcement and concrete using beam finite elements. The methods will be introduced in the next sections.

Element/Kinematic-Coupling Method Using Abaqus

In Abaqus Kinematic-coupling method is used, which we have decided to name "element/kinematic-coupling method". This method uses a kinematic coupling technique where the beam is divided in two parts. The concrete is modeled as a beam element and the reinforcement is modeled as a truss element. Kinematic constraint is enforced between the degrees of freedom of the concrete and the steel element, see figure 3.10. The reinforcement is the slave element and the concrete is the master element. The parts are connected with nodes, where each slave node has a relationship with its master node, see figure 3.9.

approch.png approch.png approch.png

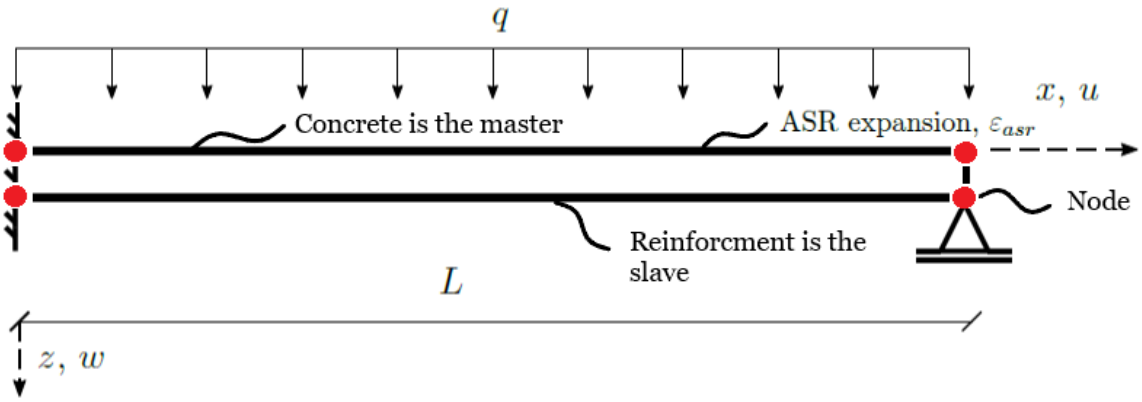

Figure 3.9: Illustration of kinematic coupling with master-slave approach

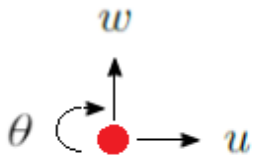

Figure 3.10: Kinematics constraint nodes with three degrees of freedom

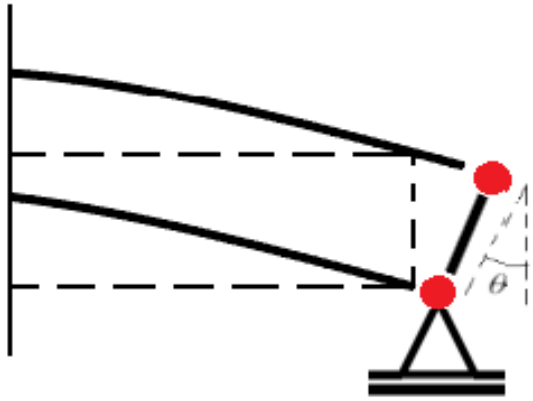

Figure 3.11: Rotation, θ, due to the ASR expansion of concrete element

Post-Processing of the Results from Element/Kinematic Coupling Method

The analysis output in Abaqus is extracted from nodes of the beam. The extracted results will contain errors at the each node. This error is known as a discretization error, and in simulation a discretization error occurs from the fact that a function (in our case the moment, shear and axial) of continuous variable is represented in the computer by a finite number of evaluations(in our case elements). The discretization error can be reduced by dividing the beam into more elements. Each concrete kinematic constraint node contains a force, F_c. The concrete force at node i, F_{ci}, is used to find the respective moment at the node, M_{ci}:

$$M_{ci} = \sum_{i} F_{ci} \cdot e_c \tag{3.22}$$

where i is the number of nodes the beam is divided into $i = 1, 2, 3...$ and A_c is the concrete cross-section area.

The element/kinematic coupling method in Abaqus will only provide moment caused by the concrete as seen in figure 3.12.

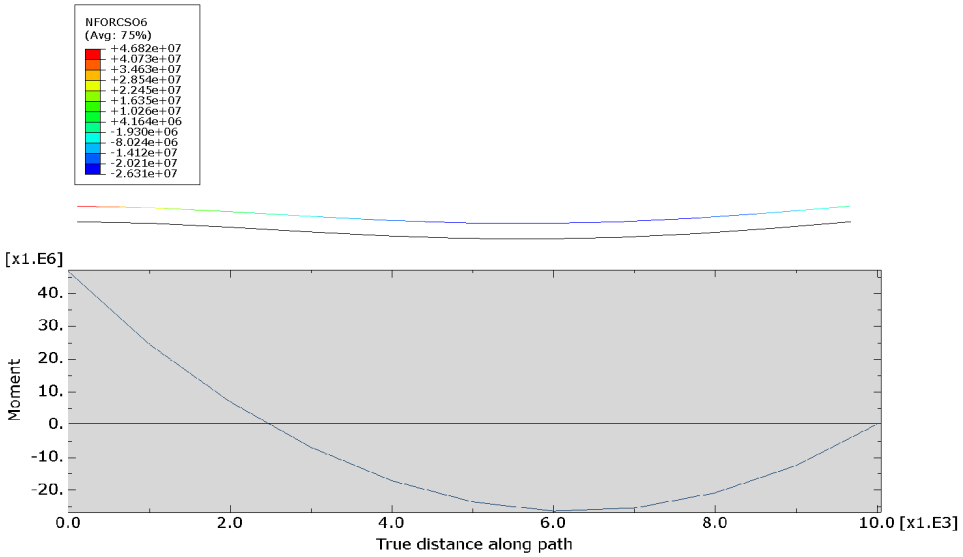

Figure 3.12: Example of a moment diagram for external load in Abaqus that only includes the concrete

This means that the moment contribution from the reinforcement needs to be added as well. Figure 3.13.

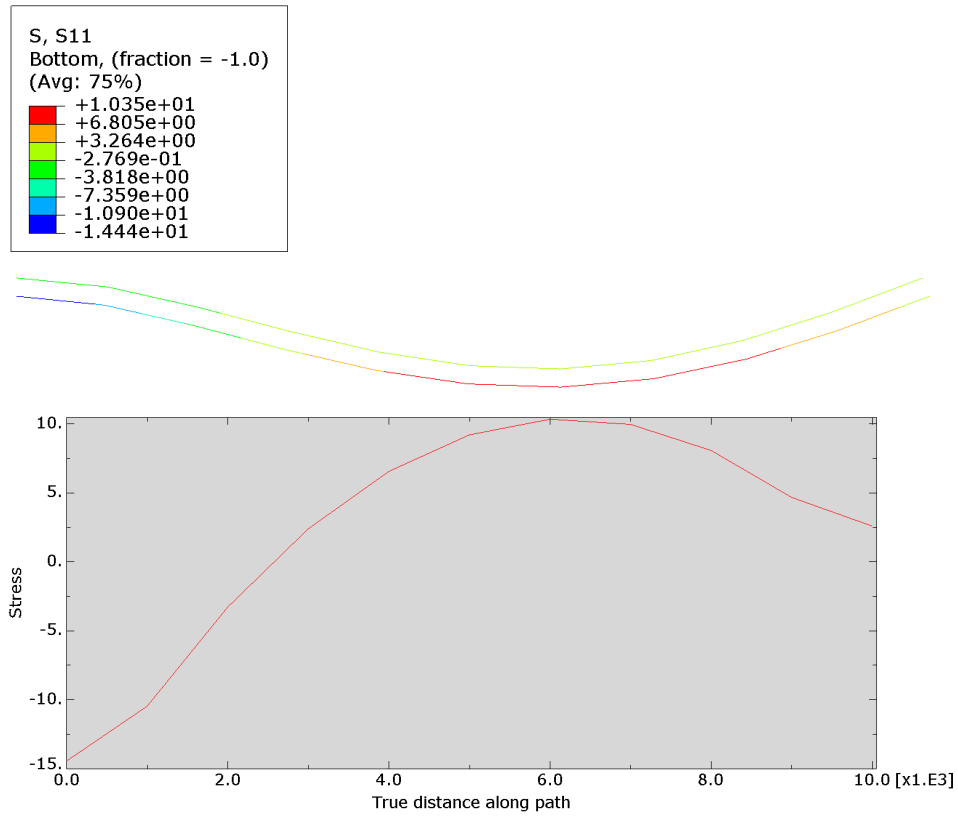

Figure 3.13: Example of a stress diagram for external load in Abaqus form the reinforcement

This is done by first extracting the steel stresses, σ_{si}, from each kinematic constraint node for the reinforcement in Abaqus and then calculating the steel forces on these nodes:

$$F_{si} = \sum_i \sigma_{si} \cdot A_{si} \tag{3.23}$$

where A_{si} is the cross section area of the reinforcement. The beam can have bottom reinforcement, top reinforcement or both top and bottom reinforcement. This means that the cross section can be different through out the beam, see figure 3.14 . Therefore will the moment contribution from the reinforcement also be different though out the beam.

$$M_{si} = \sum_i F_{si} \cdot e_s \tag{3.24}$$

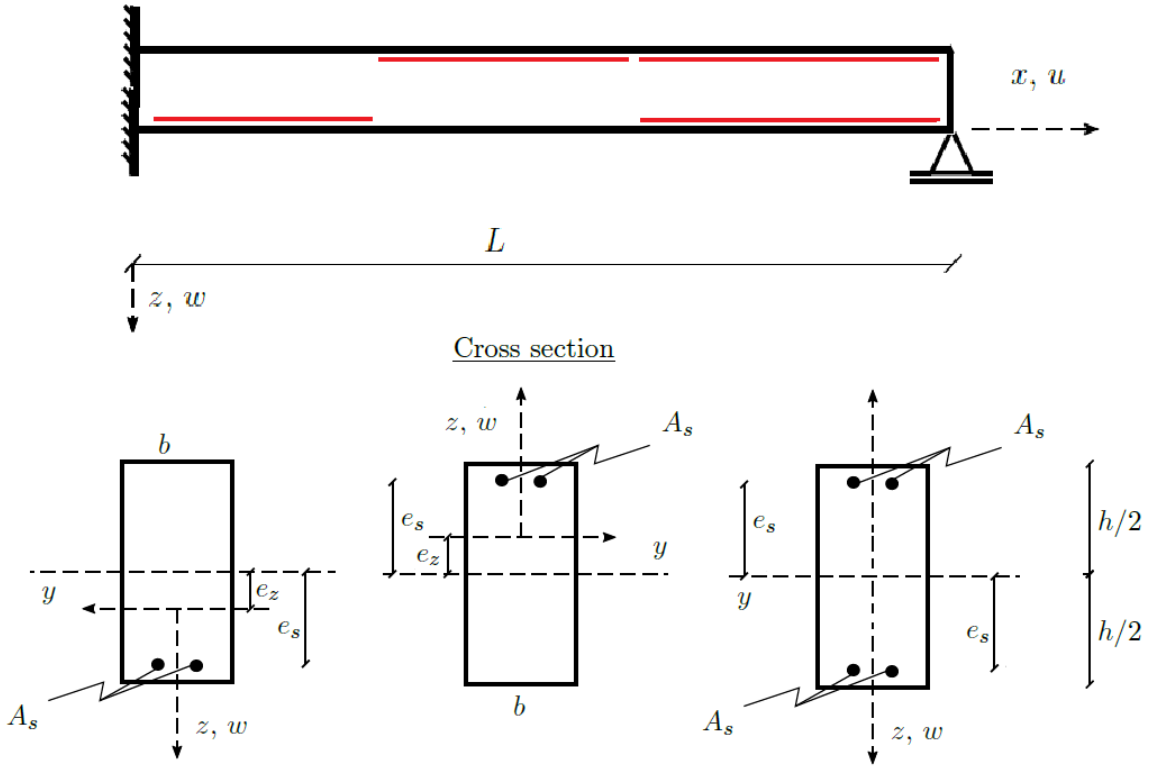

Figure 3.14: Illustration of different reinforcement throughout the beam

The total moment can then be calculated as such:

$$M_{total} = M_{concrete} + M_{reinforcement} \tag{3.25}$$

In Abaqus the dead load/external load and ASR expansion is divided into two steps. Moments are calculated for each separate step, then the results are combined to get the final results. This is expressed as such:

$$M_{total}^{combined} = M_{total}^{dead/external\ load} + M_{total}^{asr\ expansion} \tag{3.26}$$

The same will be done for the shear force without including the reinforcements stresses since it doesn't contribute to the shear force. This is expressed as such:

$$S_{total}^{combined} = S_{total}^{dead/external\ load} + S_{total}^{asr\ expansion} \tag{3.27}$$

For axial force the same process was used with the contribution from the reinforcement and is expressed as such:

$$N_{total}^{combined} = N_{total}^{dead/external\ load} + N_{total}^{asr\ expansion} \tag{3.28}$$

Rebar Method Using Abaqus

In this thesis we have investigated another numerical solution which exist in Abaqus called the rebar method. The rebar method is a alternative for the modeling of the beam, were the reinforcement element is embedded in the concrete element. In this method there is interaction between the concrete material and the steel material which means that steel follows the displacements of the concrete. This method allows for simpler and time efficient post-possessing of the output extracted from the structural analysis in Abaqus. The rebar method does the summation of concrete and steel contribution for the load actions since the reinforcement element is embedded in the concrete element [1].

3.6 Overview of Material Models used in the Structural Analysis

Six different material models is used in the structural analyses. An overview of the material models for concrete are shown in figure 3.1. For the reinforcement a elastic-perfectly plastic material model is going to be used.

The following concrete material models is used in the analyses:

- Material model 1 (MM1) include linear elastic material behaviour and short term E-modulus
- Material model 2 (MM2) include linear elastic material behaviour and long term E-modulus
- Material model 3 (MM3) include linear elastic material behaviour, long term E-modulus and stress dependent ASR expansion
- Material model 4 (MM4) include linear elastic material behaviour, long term E-modulus, stress dependent ASR expansion and reduced stiffness due to ASR
- Material model A (MMA) include linear elastic material behaviour, long term E-modulus and reduced stiffness due to ASR
- Material model B (MMB) include linear elastic material behaviour, long term E-modulus and stress dependent ASR expansion. We have changed the material constant, σ_u from $-6N/mm^2$ to $-10N/mm^2$ for the Charlwood function, $W(\sigma)$ to allow more ASR expansion.

Table 3.1: Material models for concrete and their including parameters

Material model	Linear Elastic With Short Term E-Modulus	Linear Elastic With Long Term E-Modulus	Stress Dependent ASR Expansion	Stiffness Reduction Due to ASR
MM1	✓	-	-	-
MM2	-	✓	-	-
MM3	-	✓	✓	-
MM4	-	✓	✓	✓
MMA	-	✓	-	✓
MMB	-	✓	✓	-

Chapter 4

Structural Analysis of One Span Beam and Verification of FEM Model

Oslo Metropolitan University

Engineering and Building Technology

15th of June 2020, Oslo, Norway

4 Case 1: Structural Analysis of One Span Beam and Verification of FEM Model

In case 1 a statically indeterminate beam of degree one with fixed support at the left end and roller support at the right end is to be analyzed. This beam is referred to as the one span beam. The beam is exposed to a uniformly distributed load, q, of $4N/mm$ and free ASR strain, ε_{asr}, of 0,001. The ASR expansion is set to be constant along the length of the beam. The beam is first analyzed with a uniform ASR expansion, $\kappa_{asr} = 0$ over the height (case 1A), then the beam is analyzed with a non-uniform ASR expansion, $\kappa_{asr} \neq 0$ (case 1B). This is performed to observe the effect on non-uniform ASR expansion compared to uniform ASR expansion.

The one span beam is selected due to its simple design which enable the beam to be analysed both analytically and numerically. The numerical solution is then to be compared to the analytical solution, this is done so that the numerical model can be validated. As the numerical model is valid, further numerical analysis using other material models is thus also correct. The reference beam is also selected so that the ASR's effect on a simple beam can be compared to ASR's effect on more complex beam model.

The beam is analysed in Abaqus by applying the material models as described in table 3.1. The purpose of the analysis it to determine each material models' affect on the load actions on the beam due to ASR . Then observe which material model provides the most impact to the load actions.

The analytical approach of the one span beam has been made by Simen Sørgaard Kongshaug and was given as a exercise in the course "MABY4500 - Durability and Service Life of Structures" at Oslo Metropolitan University spring 2019 [18].

Following is a description of the one span beam showing its design- and material parameters.

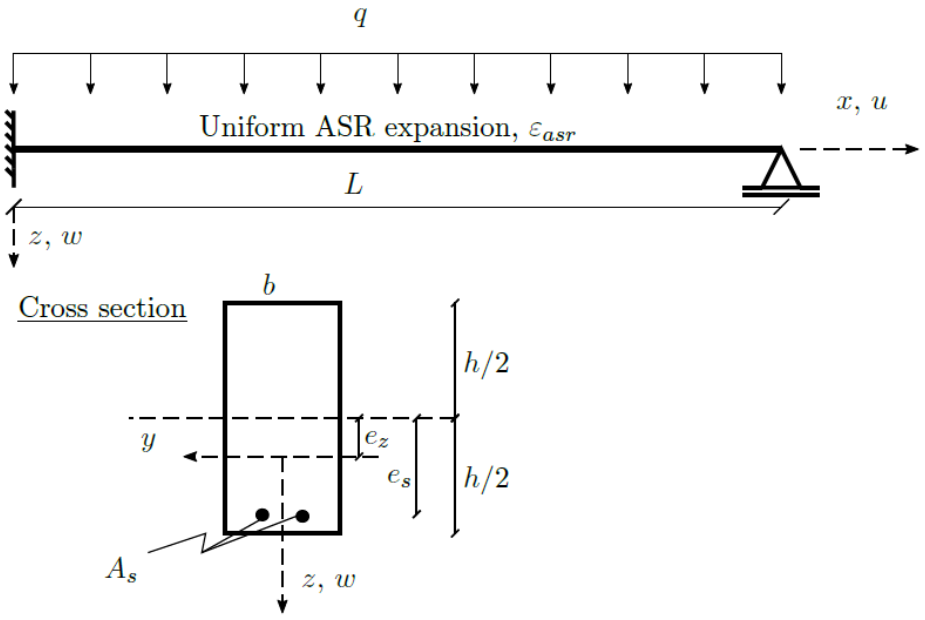

Figure 4.1: One span beam case 1. Degree one statically indeterminate continuous beam exposed to ASR expansion and uniform load [18]

The design- and material parameters shown in table 4.1 are further used in every assessment regarding case 1.

Table 4.1: Given design- and material parameters for case 1

$L[mm]$	10000
$b[mm]$	300
$h[mm^3]$	500
$e_s[mm]$	200
$A_S[mm^2]$	982
ε_{asr}	0.001
$q[N/mm]$	4
$E_c[N/mm^2]$	30000
$E_s[N/mm^2]$	200000

In the numerical analysis the effect of creep is included. The effect of creep leads to a reduced concrete modulus of elasticity. This is calculated as described in EC2, which for case 1 reads as follows:

The effective cross section thickness, h_0, is given as such:

$$h_0 = \frac{2A_c}{u} \tag{4.1}$$

where A_c is the cross section of the concrete and the u is the perimeter of the beam which is exposed to drying out in contact with the atmosphere. In case 1 these values are:

$$\begin{aligned} A_c =& b_c h_c - A_s = (500mm \cdot 300mm) - 982mm^2 \\ =& 150000mm^2 - 982mm^2 = 149018mm^2 \end{aligned} \tag{4.2}$$

The beam's perimeter is 100% exposed to the atmosphere. u is the computed as such:

$$u = 2(b_c h_c) = 2(500mm + 300mm) = 1600mm \tag{4.3}$$

The effective cross section thickness, h_0 is then:

$$h_0 = \frac{2A_c}{u} = \frac{2 \cdot 149018mm^2}{1600mm} = 186,3mm \tag{4.4}$$

Time of loading, t_0, is assumed 28 days, and cement type N is assumed. The final creep coefficient, $\varphi(\infty, t_0)$, is now found using table 3.1 in EC2. The creep coefficient then becomes $\varphi(\infty, 28) \approx 2,5$. Then the effective modulus of elasticity of concrete, $E_{c,eff}$, is calculated

$$E_{c,eff} = \frac{E_{cm}}{1 + \varphi(\infty, t_0)} = \frac{30000N/mm^2}{1 + 2,5} = 8571N/mm^2 \tag{4.5}$$

$E_{c,eff}$ is applied in the numerical analysis for every material model except the linear elastic material model with short term modulus of elasticity (MM1).

4.1 Case 1A - Reference Beam with Uniform ASR Expansion

4.1.1 Analytical Solution

Statically indeterminate beam of degree one

To find the load actions caused by the ASR expansion the calculation has been divided into the following steps:

Step 1: Find the cross section geometrical properties

The first moment of areas:

$$S_c = \int_{A_c} z dA = b \int_{z=-h/2+e_z}^{h/2-e_z} z dz = -bhe_z \tag{4.6}$$

$$S_s = \int_{A_s} z dA = (e_s - e_z)A_s \tag{4.7}$$

The position of the neutral axis is determined by equilibrium and is found using the following equation

$$E_c S_c + E_s S_s = 0 \tag{4.8}$$

If we insert the expressions for the first moment of areas (4.6)(4.7) into equation (4.8), we can find e_z:

$$e_z = \frac{E_s e_s A_s}{E_c bh + E_s A_s} = 8.4mm \tag{4.9}$$

We also need the second moment of areas:

$$I_c = \int_{A_c} z^2 dA = b \int_{z=-(h/2+e_z)}^{h/2-e_z} z^2 dz = \frac{bh^3}{12} + bhe_z^2 \tag{4.10}$$

$$I_s = \int_{A_s} z^2 dA \approx (e_s - e_z)^2 A_s \tag{4.11}$$

From the calculation of the first- and second moment of areas we get the following values:

Table 4.2: Cross sectional values

$e_z[mm]$	8.4
$S_c[mm^3]$	-1260000
$S_s[mm^3]$	188151
$I_c[mm^4]$	3135584000
$I_s[mm^4]$	36049770

Step 2: Apply the force method to find the mid support load

The problem is solved with the force method, which is illustrated in figure 4.2. The original statically indeterminate problem (degree one) is split into two statically determinate sub systems. The final solution is a linear combination of the sub systems (super position principle for linear problems). The linear combination must satisfy a kinematic constraint, which for the beam in figure 4.2 is zero vertical displacement at support B:

$$\delta_B = \delta_1 0 + X_1 \delta_1 1 = 0 \tag{4.12}$$

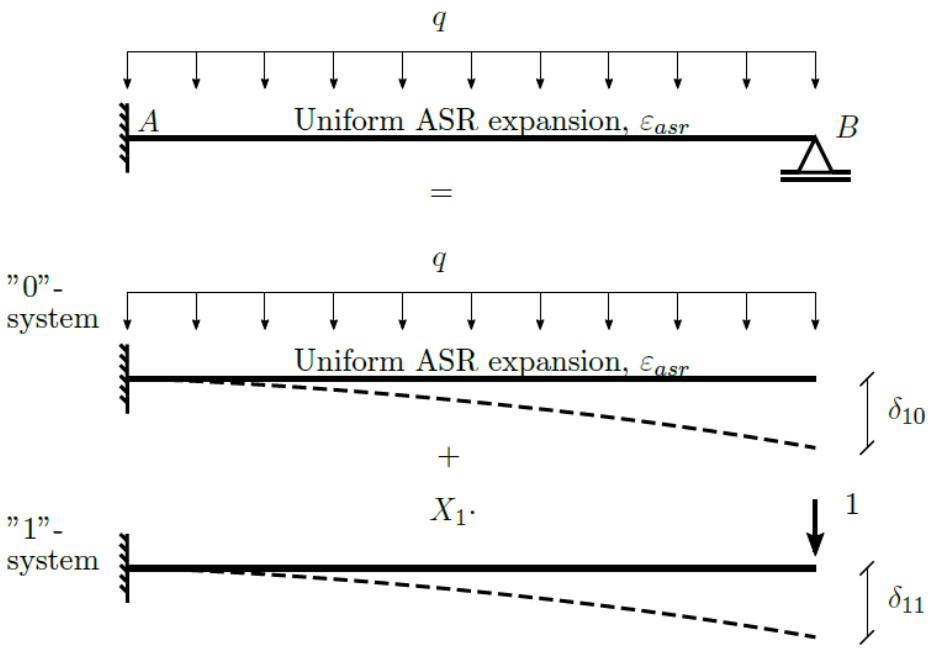

Figure 4.2: Solution with the force method [18]

The vertical displacement at the support B in the two sub systems is found by the use of the principle of virtual work (by virtual force). For this method we need the bending moments for the two sub systems. The bending moment diagrams are found by equilibrium

considerations only (statically determinate), and is given in figure 4.3.

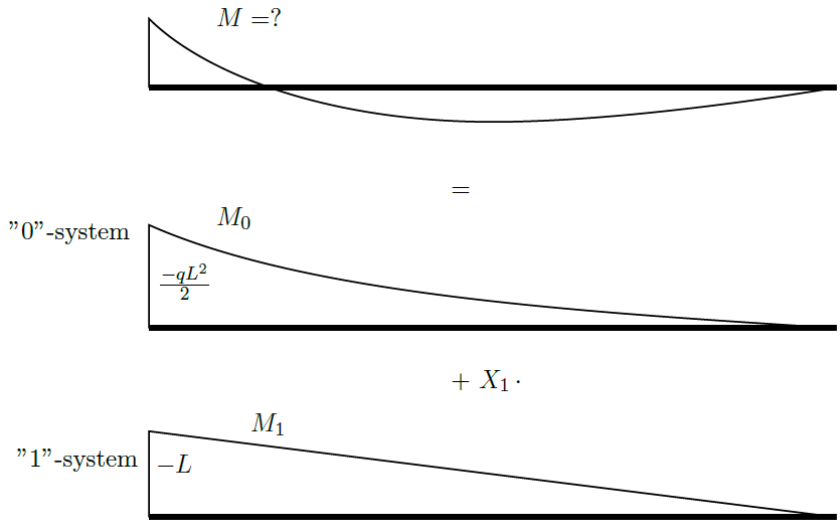

Figure 4.3: Moment diagram for the original problem (unknown) and moment diagrams for the sub systems [18]

Vertical displacement in the "0"-system:

$$1 \cdot \delta_{10} = \int_L M_1 \kappa_0 dx \tag{4.13}$$

where M_1 is the moment due to a vertical unit force at support B, which is equal to the bending moment in the "1"-system, and κ_0 is the curvature in the "0"-system, given by

$$\kappa_0 = \frac{1}{E_s I_s + E_c I_c}(M_0 + E_c S_c \varepsilon_{asr}) \tag{4.14}$$

We insert (4.14) into equation (4.13), which gives us:

$$1 \cdot \delta_{10} = \underbrace{\frac{1}{E_s I_s + E_c I_c} \int_L M_1 M_0 dx}_{From\ external\ load,\ q} + \underbrace{\frac{E_c S_c \varepsilon_{asr}}{E_s I_s + E_c I_c} \int_L M_1 dx}_{From\ ASR\ strain} \tag{4.15}$$

$$= \frac{1}{E_s I_s + E_c I_c}\left(\frac{qL^4}{8} - \frac{L^2 E_c S_c \varepsilon_{asr}}{2}\right)$$

Vertical displacement in the "1"-system:

$$1 \cdot \delta_{11} = \int_L M_1 \kappa_1 dx \tag{4.16}$$

where the curvature from the "1"-system κ_1 is given by

$$\begin{aligned} \kappa_1 &= \frac{M_1}{E_s I_s + E_c I_c} \int_L M_1 M_1 dx \\ &= \frac{1}{E_s I_s + E_c I_c} \cdot \frac{L^3}{3} \end{aligned} \tag{4.17}$$

Now we need to apply the kinematics constraint (4.12) and solve for the unknown reaction force X_1:

$$\begin{aligned} X_1 = \frac{-\delta_{10}}{\delta_{11}} &= \frac{-\frac{1}{E_s I_s + E_c I_c}\left(\frac{qL^4}{8} - \frac{L^2 E_c S_c \varepsilon_{asr}}{2}\right)}{\frac{1}{E_s I_s + E_c I_c} \cdot \frac{L^3}{3}} \\ &= -\frac{3qL}{8} + \frac{3E_c S_c \varepsilon_{asr}}{2L} \\ &= -15000N + (-5670N) = -20670N \end{aligned} \tag{4.18}$$

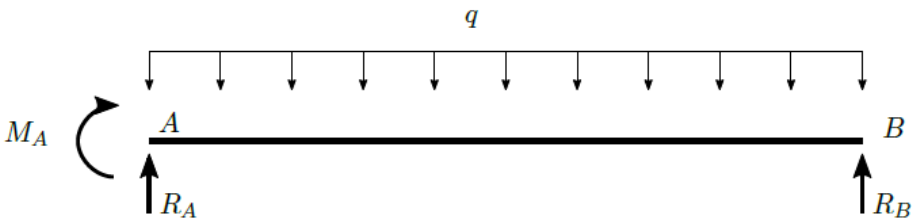

Figure 4.4: Free body diagram of the beam [18]

The free body diagram of the beam is shown in figure 4.21 (note that $R_B = -X_1 = 20670N$). The reaction forces at A are found by two equilibrium equations, i.e. the sum of moment about A is zero and the sum of vertical force is zero, which reads

$$M_A + qL\frac{L}{2} - R_B L = 0 \tag{4.19}$$

$$R_A - qL + R_B = 0 \tag{4.20}$$

The reaction forces are given in table 4.3.

Table 4.3: Reaction forces

$R_A[N]$	19330
$M_A[Nmm]$	$6.7{\cdot}10^6$
$R_B[N]$	20670

Step 3: Find the reaction forces due to ASR expansion and moment forces

From equation (4.18), we can see the reaction force at B caused by external load and the additional reaction force caused by ASR expansion. Similarly, we can find the other reaction forces due to external load and the bending moment due to ASR expansion by equilibrium, see table 4.4. Reaction forces at R_A due to ASR expansion is found by inserting R_{Basr} and neglecting the contribution from external load in equation (4.36). Vice versa when reaction forces at R_A due to external load is to be found.

Table 4.4: Reaction forces due to external load and due to ASR expansion

	Due to external load	Due to ASR expansion	Combined
$R_A[N]$	25000	-5670	19330
$M_A[Nmm]$	$-50{\cdot}10^6$	$56.7{\cdot}10^6$	$6.7{\cdot}10^6$
$R_B[N]$	15000	5670	20670

The bending moment at any position can be obtained by equilibrium and we can draw the bending moment diagram, see figure 4.5

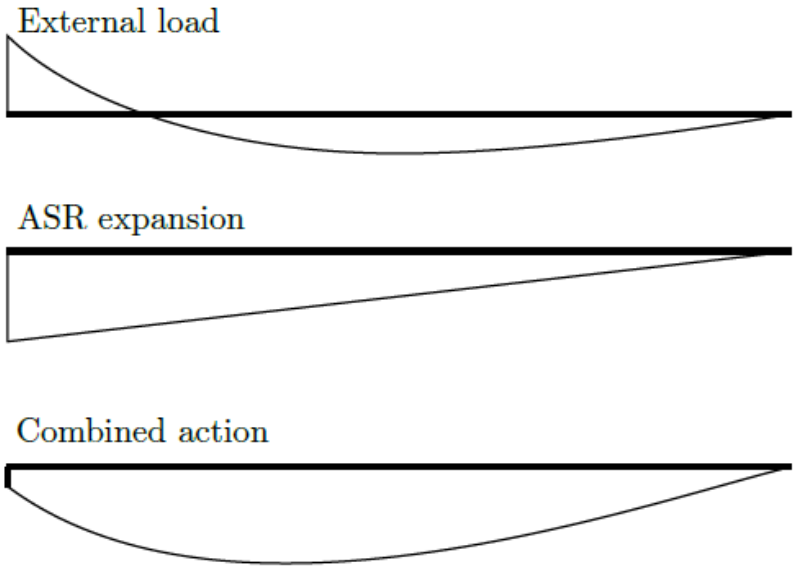

Figure 4.5: Moment diagrams

The bending moment as a function of distance from A is given by:

$$M(x) = M_A + R_A x - q\frac{x^2}{2} \tag{4.21}$$

Maximum bending moment is found where the derivative (shear force) vanish:

$$\frac{dM}{dx} = R_A - qx = 0 \quad x_{max} = \frac{R_A}{q} = 4832.5mm \tag{4.22}$$

The maximum bending moment is given by:

$$M(x_{max}) = M_A + R_A \cdot x_{max} - q\frac{x_{max}^2}{2} = 53406112.5Nmm = 53.4kNm \tag{4.23}$$

Step 4: Find the shear forces

For the given beam exposed to external loads and uniform ASR expansion, shear forces, V, is equal to the reaction forces at each supports. The shear forces can be calculated using equation 4.36, 4.37 and 4.38 where $R_A = V_A$ and $R_B = V_B$ as seen in table 4.4. The slope of the shear force diagram can be found by differentiate the bending moment function and the crossing point of the shear diagram is at the point where the moment is at its maximum. The derivative of the bending moment is a function of first degree:

$$\frac{dM}{dx} = R_A - qx \tag{4.24}$$

meaning thar the slope of of the shear diagram from V_A to V_B is linear.

Table 4.5: Reaction forces due to external load and due to ASR expansion

	Due to external load	Due to ASR expansion	Combined
$V_A = R_A[N]$	-25000	5670	-19330
$V_B = R_B[N]$	15000	5670	20670

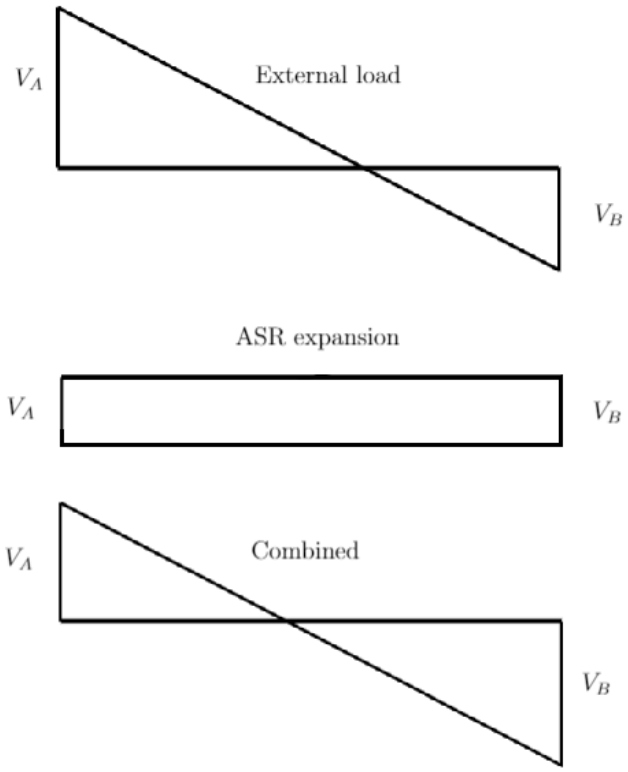

Figure 4.6: Shear diagrams

Step 5: Find the axial force

The general expression for axial force is given as follows:

$$N = \sigma A = \varepsilon E A \tag{4.25}$$

Included for ASR induced stresses, axial force can be written as follows:

$$\begin{aligned} N &= \int_A \sigma dA = \int_{A_s} \sigma_s dA + \int_{A_c} \sigma_c dA \\ &= (E_s A_s + E_c A_c)\bar{\varepsilon} + (E_s S_s + E_c S_c)\kappa - E_c(\bar{\varepsilon}_{asr} A_c + \kappa_{asr} S_c) \end{aligned} \tag{4.26}$$

The given beam is subjected to a external load, q, of $4N/mm$, and a uniform ASR expansion, ε_{asr}, of 0,001 in the longitudinal direction (x-direction).

Since the beam has roller support at the right end (at B) the beam can move freely in the x-direction. This implies that no external axial force will occur due to the external load and ASR expansion. The axial forces are found by equilibrium equation where the sum of vertical force is zero. Hence, the axial forces, N, are zero since there is no reaction forces.

$$N_A + N_B = 0 \tag{4.27}$$

Table 4.6: Axial forces due to external load and due to ASR expansion

	Due to external load	Due to ASR expansion	Combined
Axial Force, N $[N]$	0	0	0

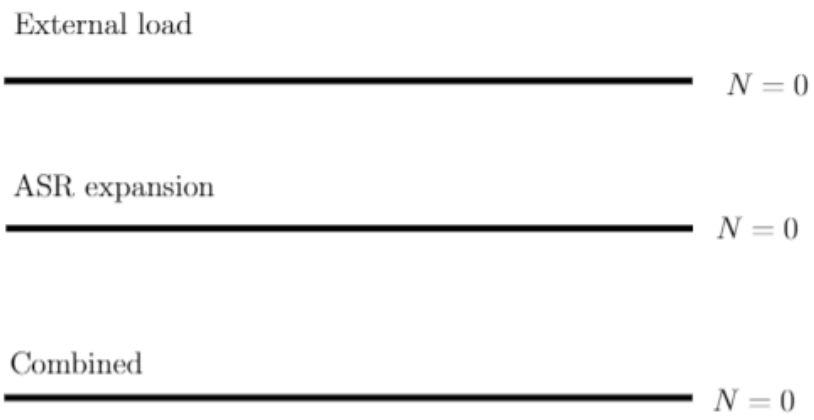

Figure 4.7: Axial force diagrams

4.1.2 Numerical Solution

Element-Coupling method in Abaqus

The beam is now to be assessed using the element-coupling method in Abaqus. Linear elastic material model (MM1) is applied. Design input values are the same as for the analytical solution and is seen in table 4.7. The beam model made in Abaqus is seen in 4.8.

Table 4.7: Input values applied in the element coupling method

$L[mm]$	10000
$b[mm]$	300
$h[mm^3]$	500
$e_s[mm]$	200
$A_S[mm^2]$	982
ε_{asr}	0.001
$q[N/mm]$	4
$E_c[N/mm^2]$	30000
$E_s[N/mm^2]$	200000

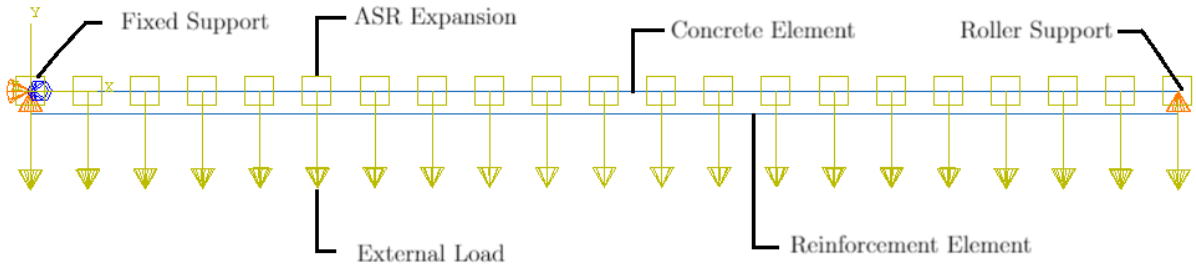

Figure 4.8: Beam model in Abaqus

From the output extracted from Abaqus moment diagrams for all the steps is shown in figure 4.9. In excel positive and negative values are defined opposite from the hand calculation, this implies that the following results, M_a, V_a and V_b, is opposite as previously shown.

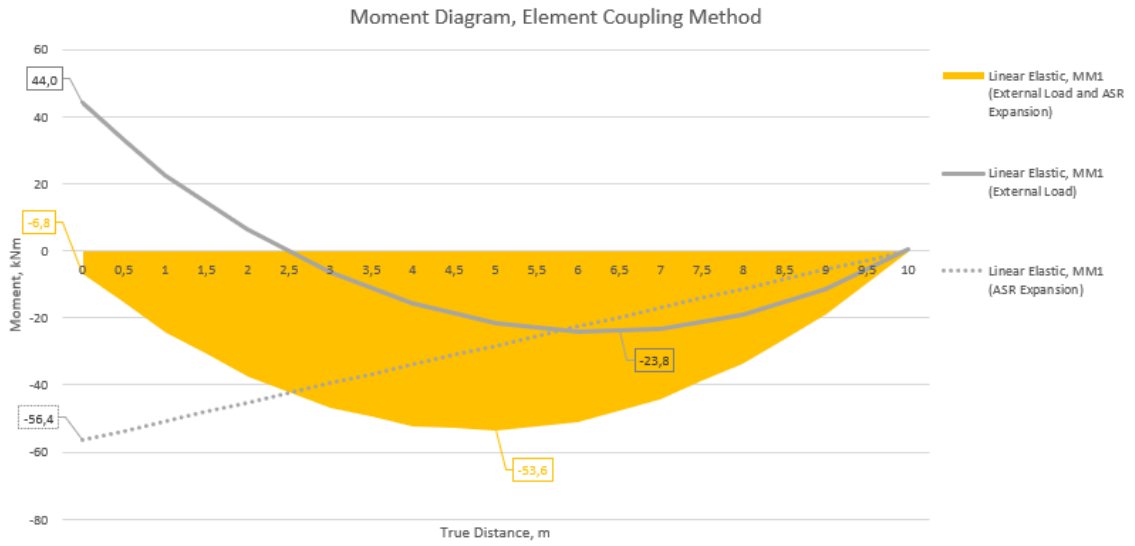

Figure 4.9: Moment diagrams for external load, ASR expansion and combined for case 1A

The longitudinal reinforcement does not contribute to the shear force. Shear force is therefore directly extracted from Abaqus without any need of including the steel contribution. Shear force diagram is shown in figure 4.10.

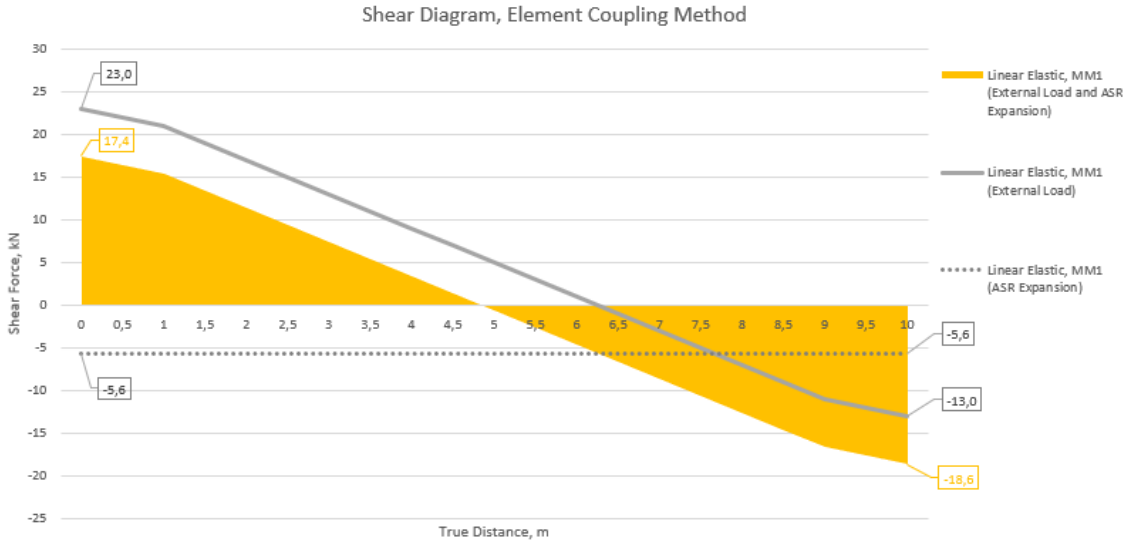

Figure 4.10: Shear diagrams for external load, ASR expansion and combined for case 1A

The axial force diagram is also directly extracted from Abaqus and is seen refAxial Diagrams Excel. Here we see that the axial force is zero, which is correct due to the roller support that does not absorb any horizontal forces.

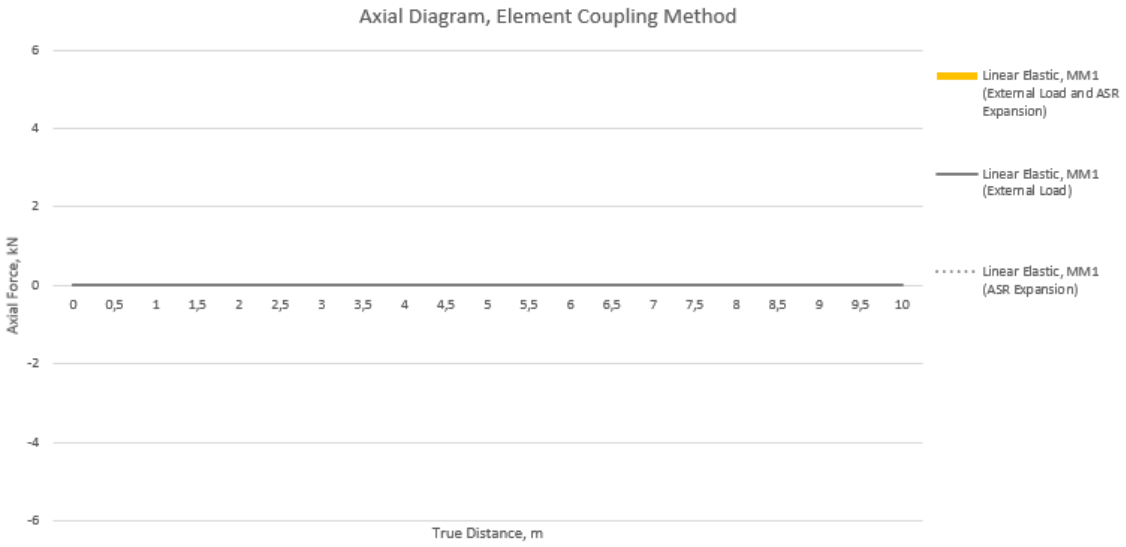

Figure 4.11: Axial diagrams for external load, ASR expansion and combined for case 1A

The deformation of the beam is shown in the figure 4.12. The uppermost picture shown the beam without any load giving zero deformation. The mid picture shows the deformation when external load is applied. As expected the stresses is zero at each support and the greatest vertical deformation, δ_y, occur where the bending moment is at its greatest (at $x = 4.8325m$). The greatest horizontal deformation, δ_x, occurs at the right end and is 9.583mm which approximately represents a strain if 0.001. The lowermost image shows the deformation of the beam including both external load and ASR expansion. Since the beam has a fixed end, and due to the contribution of reinforcement a tension force occurs which uplifts the beam and reduces the total deflection. It is also observed that the largest stresses occurs at the right end where the beam is not restrained in the x-direction due to the roller support. The left end has fixed support, giving zero deformation.

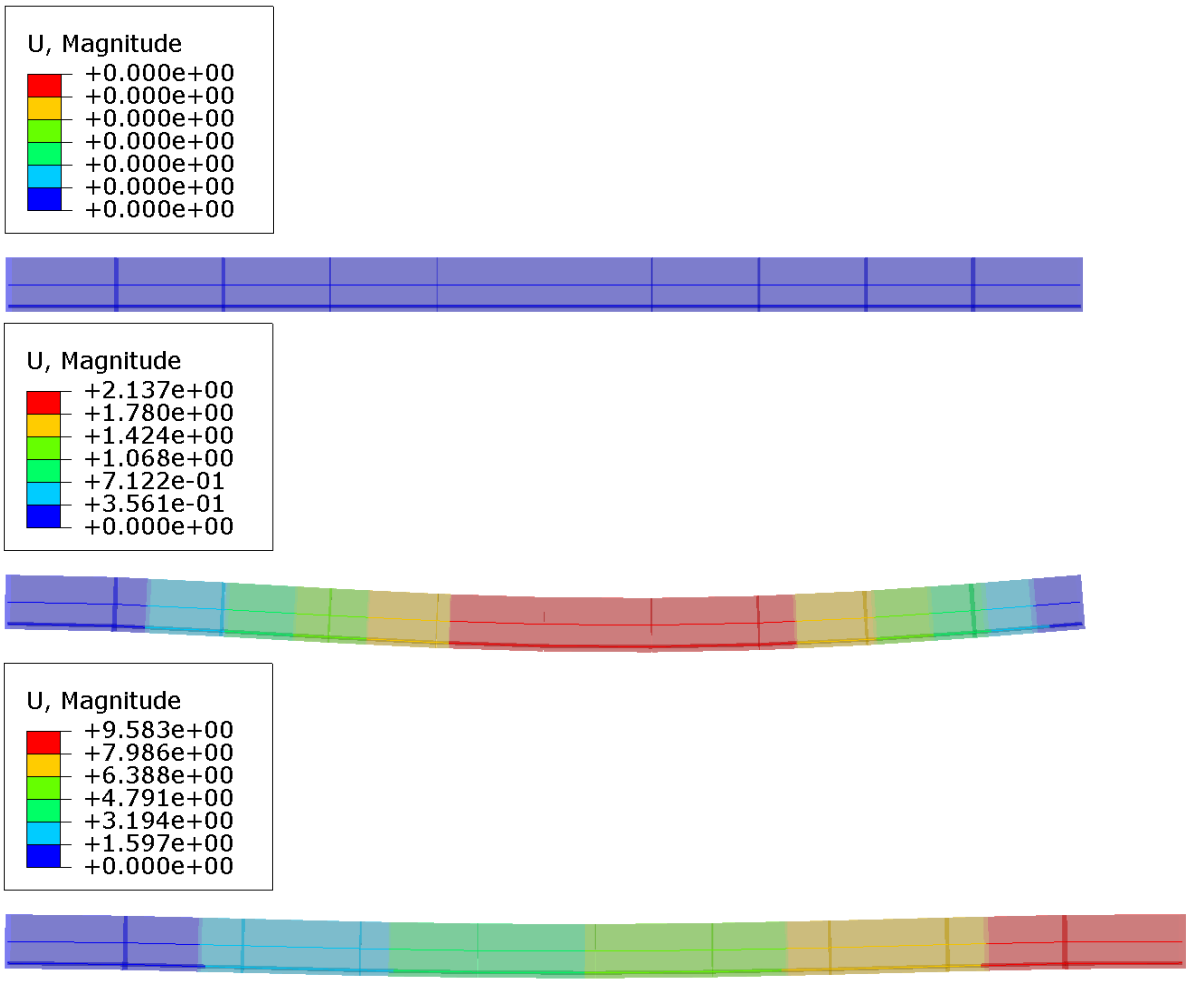

Figure 4.12: Development of deformation, results from Abaqus. Uppermost figure having no load. Mid figure exposed to external load, q, and lowermost figure exposed to external load, q, and ASR expansion

Figure 4.13 shows the stress development within the beam. It is observed that the external loads applied on the beam (mid figure) results in the concrete having approximately the same stresses throughout the beam. The reinforcement is exposed to highest stresses were the beam have the greatest deformations. When the ASR expansion is added to the analysis (lowermost figure) the concrete has increased stresses with same distribution magnitude throughout the beam. However, all of the reinforcement parts in now experiencing high stresses due to the expansion of the beam.

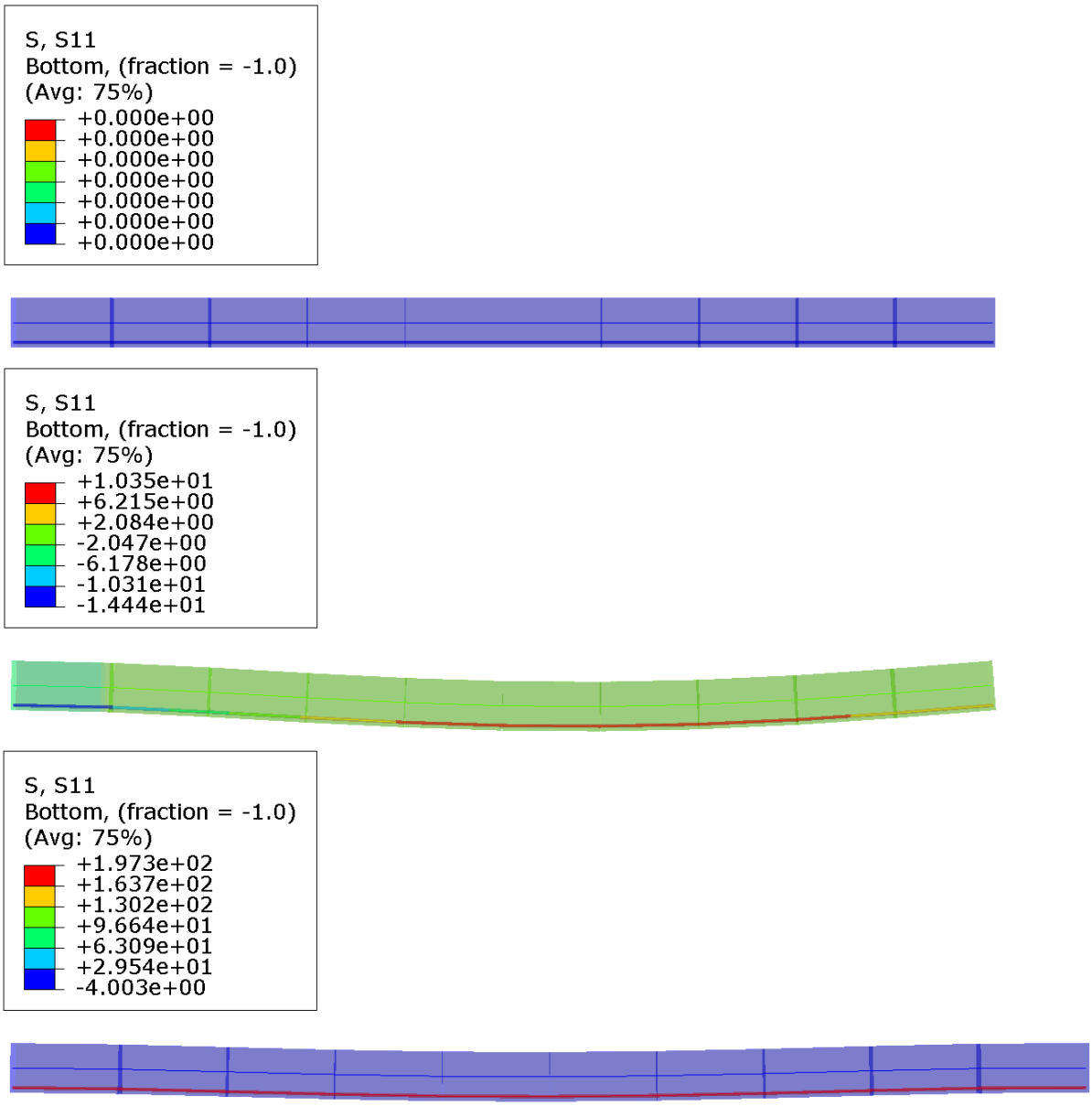

Figure 4.13: Development of stresses from the FEM analysis in Abaqus

Figure 4.14 shows the strain development within the beam. It is observed that when external load is applied, the greatest strains occur in the middle of the beam. When external and ASR expansion is applied, it is seen that greatest strain occurs in the middle, but due to ASR the strain value is now in the order of 10^{-4} compared to 10^{-5} when only external load is applied.

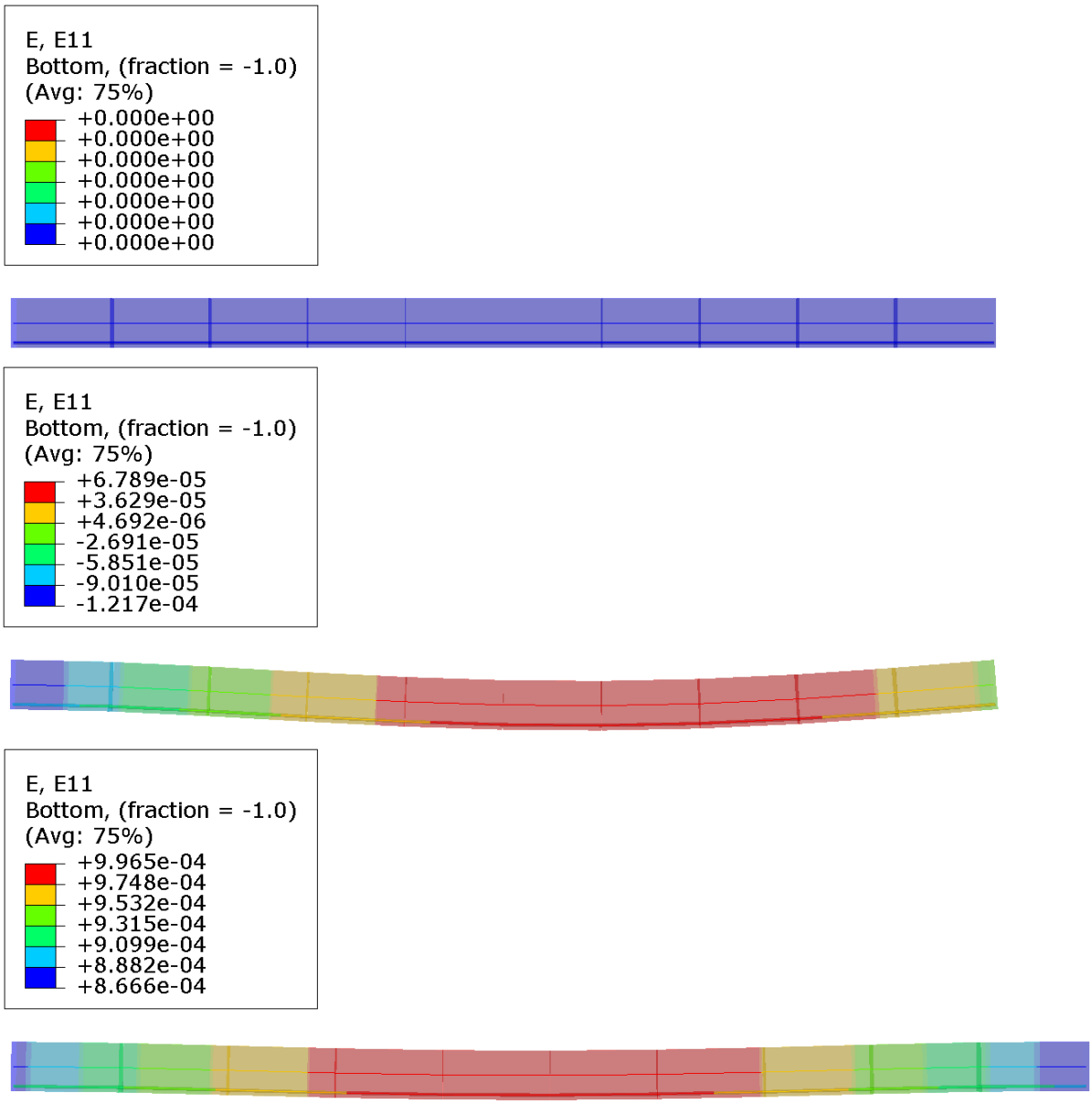

Figure 4.14: Development of strain from FEM analysis in Abaqus

Rebar Method in Abaqus

The beam is now to be assessed using the rebar method in Abaqus. Linear elastic material model (MM1) is applied. Design input values is still the same as for the analytical and element-coupling method. The model contains the same amount of element/nodes as the element-coupling model. The difference is that the rebar method does not have any master-slave structure.

Table 4.8: Input values applied in the rebar method

$L[mm]$	10000
$b[mm]$	300
$h[mm^3]$	500
$e_s[mm]$	200
$A_S[mm^2]$	982
ε_{asr}	0.001
$q[N/mm]$	4
$E_c[N/mm^2]$	30000
$E_s[N/mm^2]$	200000

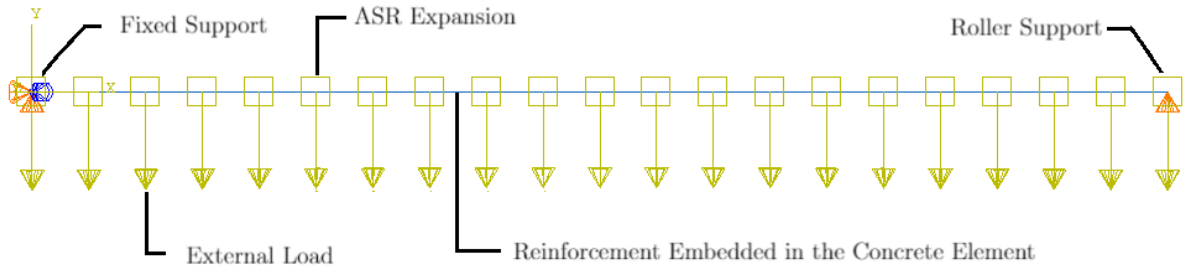

Figure 4.15: Rebar model in Abaqus

From the output extracted from the analysis done in Abaqus, moment, shear and axial diagrams for all the load cases is further shown in figure 4.16, 4.17 and 4.18.

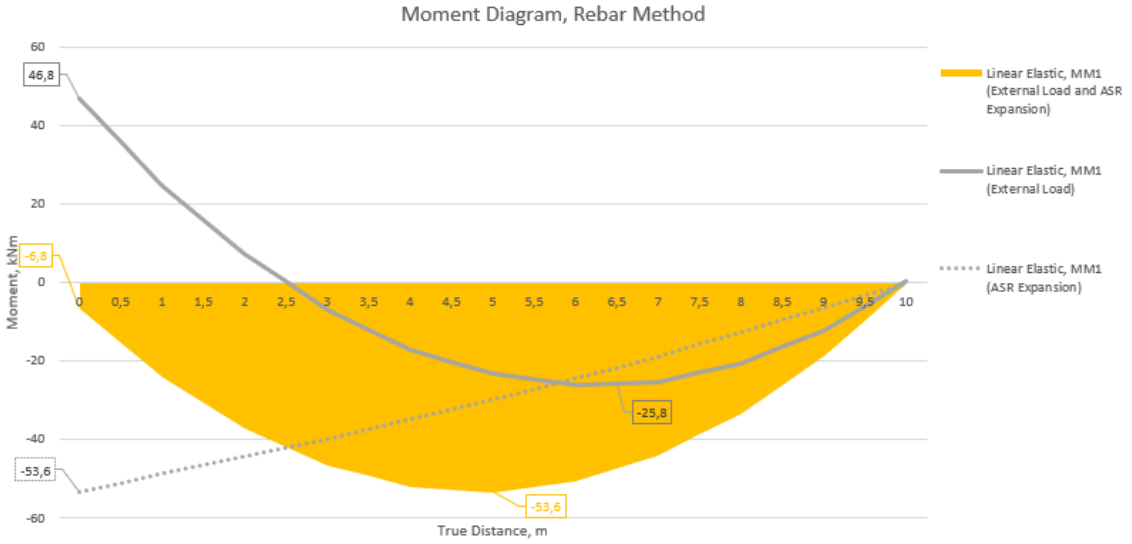

Figure 4.16: Moment diagrams for external load, ASR expansion and combined for case 1A

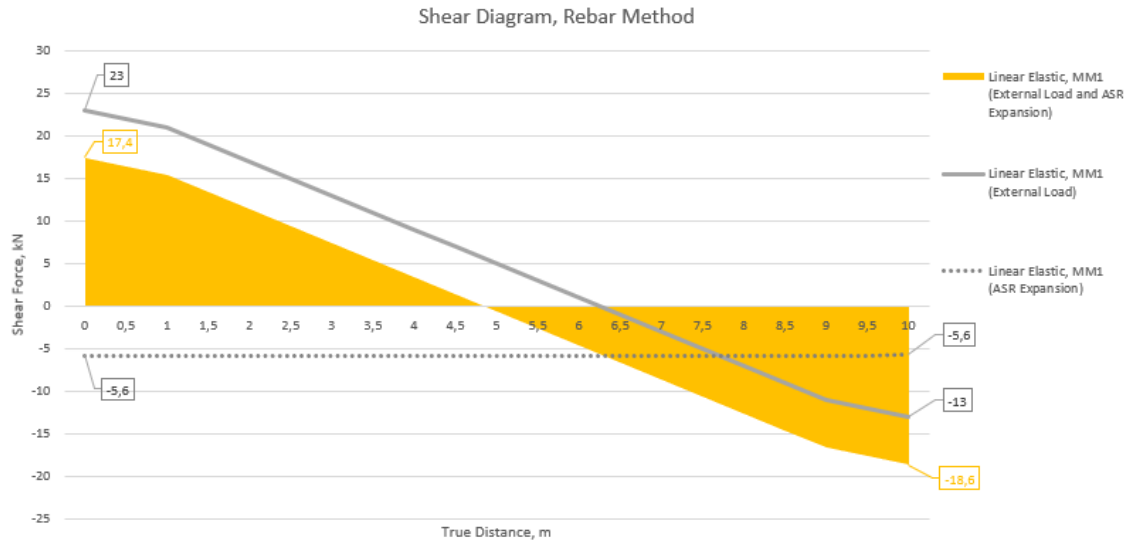

Figure 4.17: Shear diagrams for external load, ASR expansion and combined for case 1A

It is observed that the moment due to external load and moment due to ASR expansion is slightly different than observed in the element-coupling method. However, the combined moment is the same for both methods. The shear force is exactly the same as in the solution of the element-coupling method.

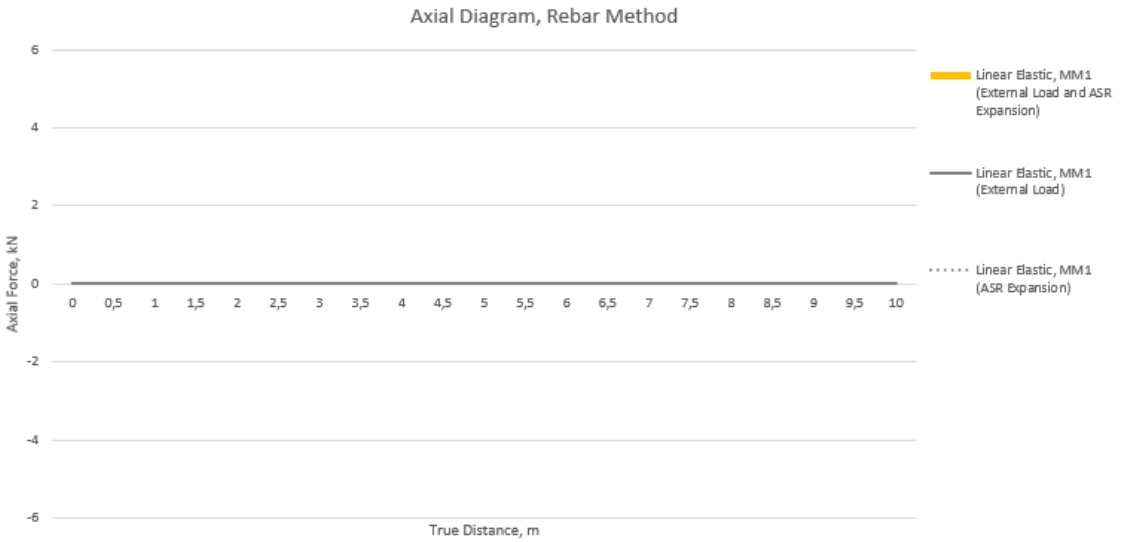

Figure 4.18: Axial diagrams for external load, ASR expansion and combined for case 1A

As seen in figure 4.18 the axial force is still zero, as predicted.

4.1.3 Verification of Numerical Solution for Case 1A

Both the element coupling method and rebar method extracts its output results from each node. At the end nodes (node 1 and 11) some of the occurring stresses are obtained by the support, meaning that the extracted end node stresses is less than in reality. This result in a discretization error on the first and the last node, shown in figure 4.19. This discretization error is a known error in FEM design and post processing of the output is needed to fix this error.

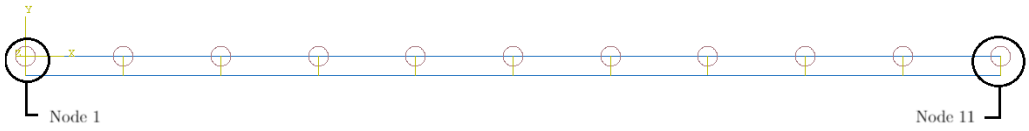

Figure 4.19: The discretization error occur at node 1 and node 11

This discretization error is recognizable on the shear diagram where the shear diagram changes gradient close to the ends. By doing a simple extrapolation of the shear diagram using every nodes except end nodes the shear force at each end of the beam would be similar to those end values calculated in the analytical solution. Since the purpose of this thesis is to compare the effect of applying different material models to an ASR affected

RC-structure, the discretization error is of less importance as this error will occur in each model making the comparison of the models valid. The discretization error is not significant. Post processing of the outputs is therefore not needed for these results. We can therefore verify that the FEM model and the use of both the element coupling method and rebar method is done correctly and the results are satisfactory compared to the analytical solution. Table 4.9 summarize the results extracted from the analytic solution, element coupling- and rebar method.

Table 4.9: Results from the analytical solution and from linear finite element method

	Analytical Solution	Element-Coupling Method	Rebar Method
$M_a(kNm)$	6.7	6.8	6.8
$M_{max}(kNm)$	53.4	53.6	53.6
$V_a(kN)$	19.3	17.4	17.4
$V_b(kN)$	20.7	18.6	18.6
$N_a(kN)$	0	0	0
$N_b(kN)$	0	0	0

As seen in table 4.9 the two numerical solutions provides exactly the same results. There are only minor differences in the values calculated in the analytical solution and calculated in the numerical solutions. The minor difference is due to decimal calculations and the discretization error in the analytical solution. It can therefore be said that the numerical methods are valid.

4.2 Case 1B - Reference Beam with Non-Uniform ASR Expansion

In this case the beam is been given a non-uniform ASR expansion. The expansion is set to be constant along the length of the beam and vary linearly over the height. The ASR is set to be twice as great at the top than at the bottom with a ASR strain $\varepsilon_{asr} = 0,001$ in the middle of the beam, at $y = h/2$. The non-uniform ASR expansion introduce a curvature, κ_{asr}, as seen in figure 4.20. The curvature is set to be linear over the height.

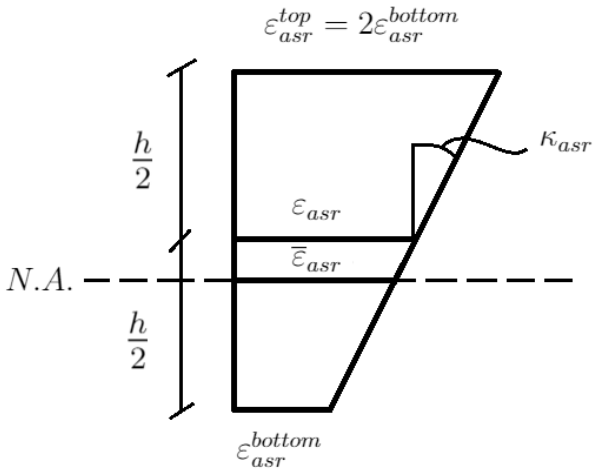

Figure 4.20: Influence of curvature over the height of the cross section

Due to the non-uniform expansion the solution is now calculated different. In this case the ASR strain at the natural axis, $\overline{\varepsilon}_{asr}$, is not the same as the ASR strain in the middle of the beam, $\varepsilon_{asr} = 0.001$. To find $\overline{\varepsilon}_{asr}$ we need to calculate κ_{asr}

$$\kappa_{asr} = \frac{\frac{2}{3} \cdot \varepsilon_{asr}}{h} = \frac{\frac{2}{3} \cdot 0.001}{500} = 1.333e^{-6} \tag{4.28}$$

We assume that this field is constant along the length of the beam and can vary linearly over the height, this gives a ASR strain expressed as such:

$$\varepsilon_{asr} = \overline{\varepsilon}_{asr} + \kappa_{asr} \cdot z \tag{4.29}$$

Where z is the distance from the mid cross section axis $(h/2)$ to the natural axis. $z =$

$e_z = 8.4mm$. To find the ASR strain at N.A. equation 4.29 is rearranged:

$$\begin{aligned}\overline{\varepsilon}_{asr} =&(\kappa_{asr} \cdot e_z) - \varepsilon_{asr} \\ =&(1.333e^{-6} \cdot 8.4) - 0.001 = 0.000988\end{aligned} \tag{4.30}$$

4.2.1 Analytical Solution

The introduction of curvature due to a non-uniform ASR expansion at the top and bottom entails that the beams load pattern will change compared to case 1a - uniform ASR expansion. Parameters used in Case 1b are the same as in Case 1a except $\overline{\varepsilon}_{asr}$ which now is 0,0009888 due to the introduction of curvature.

The contribution of introducing curvature affects the "0"-system as κ_{asr} is included in the expression of κ_0. The "0"-system then becomes:

Vertical displacement in the "0"-system:

$$1 \cdot \delta_{10} = \int_L M_1 \kappa_0 dx \tag{4.31}$$

where M_1 is the moment due to a vertical unit force at support B. M_1 is equal to the bending moment in the "1"-system, $M_1 = -L$. κ_0 is the curvature in the "0"-system given by

$$\kappa_0 = \frac{1}{E_s I_s + E_c I_c}(M_0 + E_c(S_c \overline{\varepsilon}_{asr} + I_c \kappa_{asr})) \tag{4.32}$$

where $M_0 = \frac{-qL2}{2}$, equal to the moment in the "0"-system.

We insert (4.32) into equation (4.31) which gives:

$$
\begin{aligned}
1 \cdot \delta_{10} &= \underbrace{\frac{1}{E_s I_s + E_c I_c} \int_L M_1 M_0 dx}_{From\ external\ load,\ q} + \underbrace{\frac{E_c S_c \overline{\varepsilon}_{asr}}{E_s I_s + E_c I_c} \int_L M_1 dx + \frac{E_c I_C \kappa_{asr}}{E_s I_s + E_c I_c} \int_L M_1 dx}_{From\ ASR\ strain} \\
&= \frac{1}{E_s I_s E_c I_c} \left(\frac{qL^4}{8} - \frac{L^2 E_c S_c \overline{\varepsilon}_{asr}}{2} - \frac{L^2 E_c I_c \kappa_{asr}}{2} \right)
\end{aligned}
\tag{4.33}
$$

As the "1"-system only affect the external load, q, the displacement of the "1"-system becomes the same as previous in case 1a.

Vertical displacement in the "1"-system:

$$
1 \cdot \delta_{11} = \int_L M_1 \kappa_1 dx \tag{4.34}
$$

where the curvature from the "1"-system κ_1 is given by

$$
\begin{aligned}
\kappa_1 &= \frac{M_1}{E_s I_s + E_c I_c} \int_L M_1 M_1 dx \\
&= \frac{1}{E_s I_s + E_c I_c} \cdot \frac{L^3}{3}
\end{aligned}
\tag{4.35}
$$

Now we need to apply the kinematics constraint (4.12) and solve for the unknown reaction force X_1:

$$
\begin{aligned}
X_1 = \frac{-\delta_{10}}{\delta_{11}} &= \frac{-\frac{1}{E_s I_s + E_c I_c} \left(\frac{qL^4}{8} - \frac{L^2 E_c S_c \overline{\varepsilon}_{asr} - L^2 E_c I_c \kappa_{asr}}{2} \right)}{\frac{1}{E_s I_s + E_c I_c} \cdot \frac{L^3}{3}} \\
&= -\frac{3qL}{8} + \frac{3E_c S_c \overline{\varepsilon}_{asr} + 3E_c I_c \kappa_{asr}}{2L} \\
&= -15000N + (-24368.47N) = -39368.47N
\end{aligned}
\tag{4.36}
$$

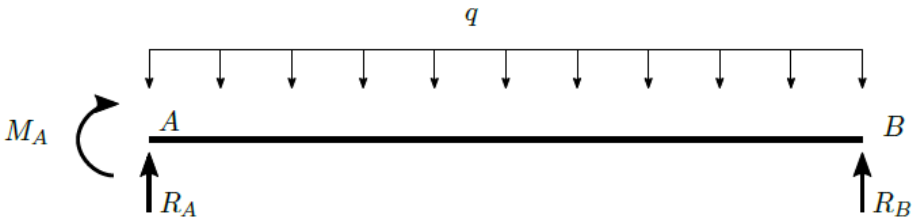

Figure 4.21: Free body diagram of the beam

The free body diagram of the beam is shown in figure 4.21 (note that $R_B = -X_1 = 39414N$). The reaction forces at A are found by two equilibrium equations, i.e. the sum of moment about A is zero and the sum of vertical force is zero, which reads

$$M_A + qL\frac{L}{2} - R_B L = 0 \tag{4.37}$$

$$R_A - qL + R_B = 0 \tag{4.38}$$

Applying the same method as done in case 1A, the forces on the beam exposed to a non-uniform ASR expansion becomes as shown in table 4.10.

Table 4.10: Analytical results case 1B

$M_A[Nmm]$	$1.94{\cdot}10^8$
$M_B[Nmm]$	0
$R_A = V_A[N]$	568
$R_B = V_B[N]$	39414
$N_A[N]$	0
$N_B[N]$	0

4.2.2 Numerical Solution

Element-Coupling Method in Abaqus

The non-uniform ASR expansion is included in Abaqus by applying the thermal expansion a free ASR strain at N.A., $\overline{\varepsilon}_{asr}$ and then applying a κ_{asr} which leads to twice as much ASR strain on top then bottom of the beam. From the output extracted from Abaqus moment, shear and axial diagrams for external load, ASR expansion and combined is shown in figure 4.23. The input data applied in Abaqus is shown in table 4.12 and the Abaqus model in is shown in figure 4.26.

Table 4.11: Values for element-coupling method

$L[mm]$	10000
$b[mm]$	300
$h[mm^3]$	500
$e_s[mm]$	200
$A_S[mm^2]$	982
$\overline{\varepsilon}_{asr}$	0.000988
$\overline{\kappa}_{asr}$	$1.333{\cdot}10^{-6}$
$q[N/mm]$	4
$E_c[N/mm^2]$	30000
$E_s[N/mm^2]$	200000

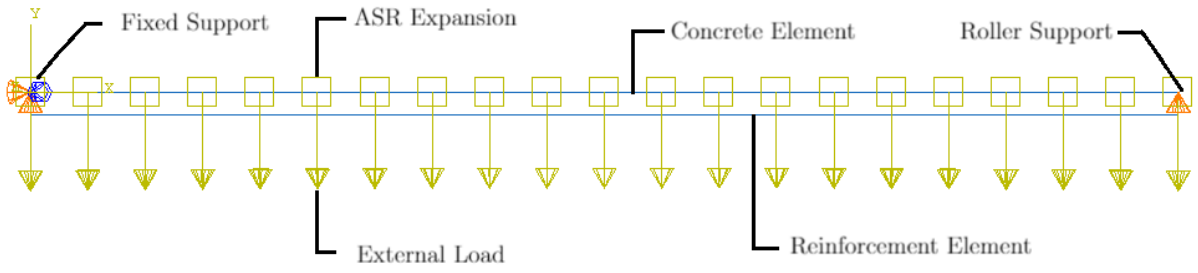

Figure 4.22: Beam model in Abaqus for case 1B

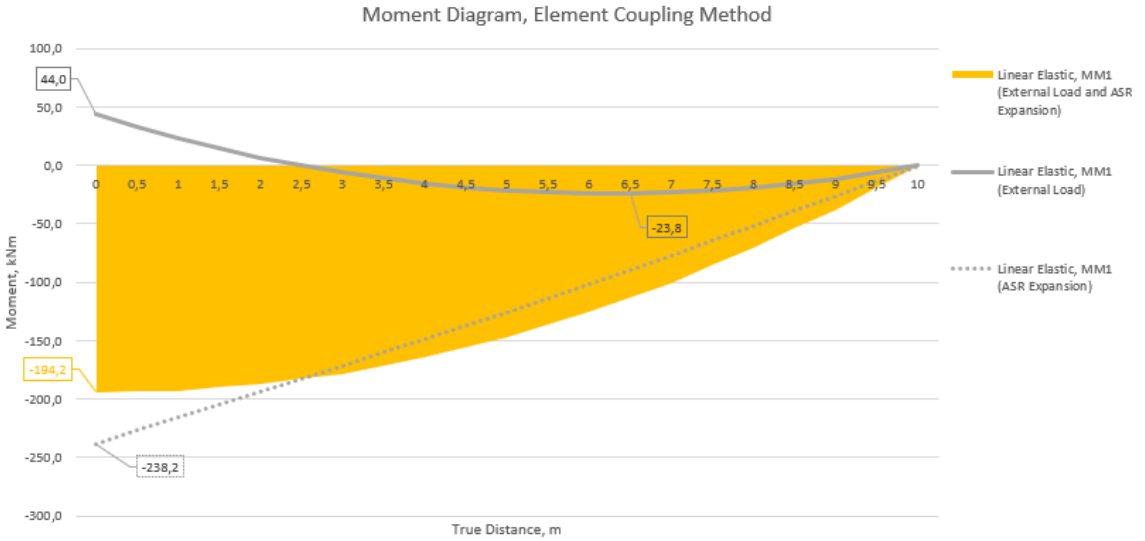

Figure 4.23: Moment diagrams for external load, ASR expansion and combined for case 1B using element coupling method with linear elastic material model (MM1)

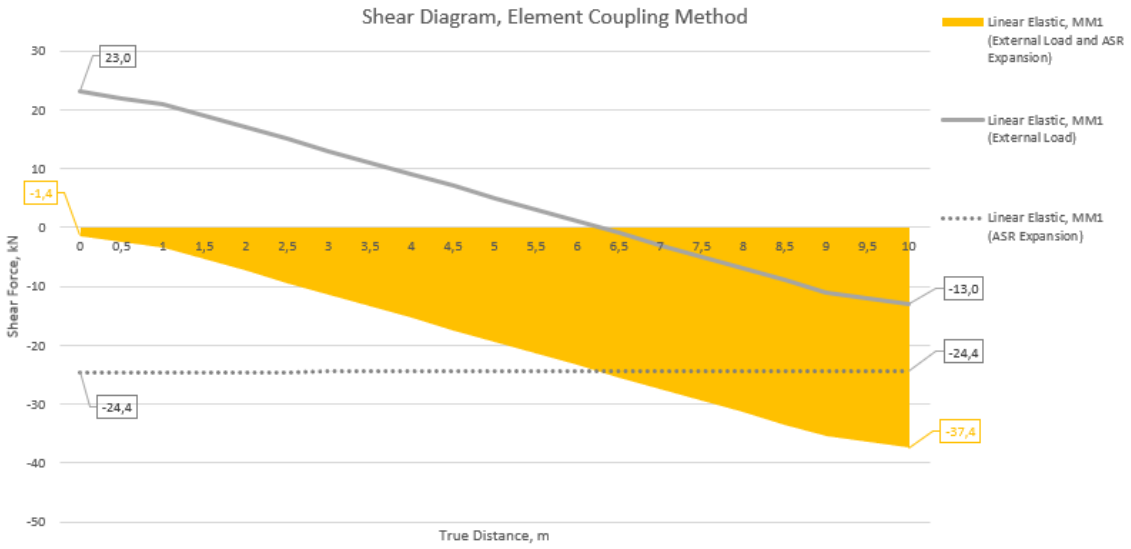

Figure 4.24: Shear diagrams for external load, ASR expansion and combined for case 1B using element coupling method with linear elastic material model (MM1)

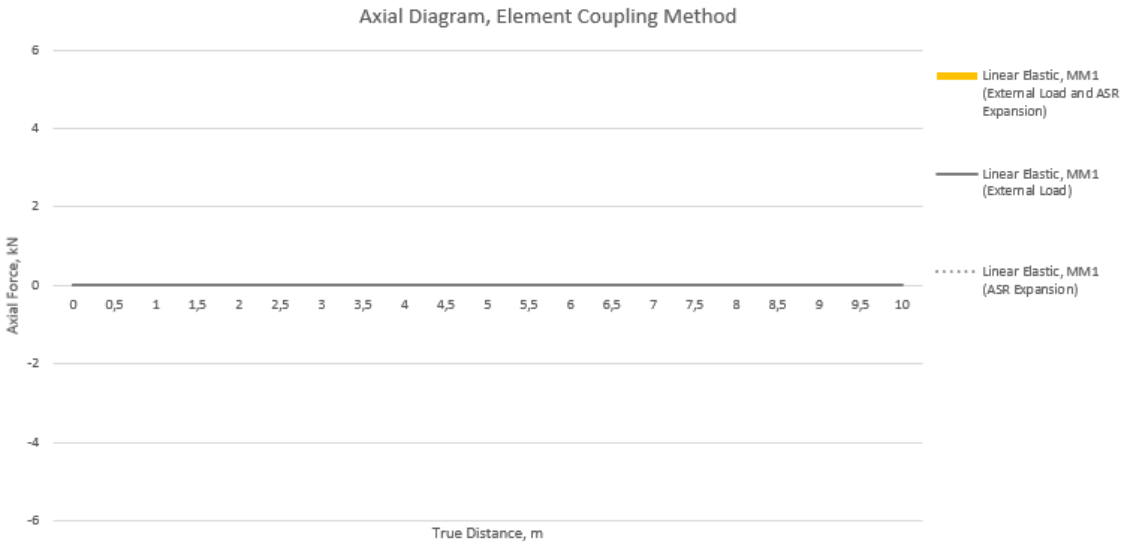

Figure 4.25: Axial diagrams for external load, ASR expansion and combined for case 1B using element coupling method with linear elastic material model (MM1)

Rebar Method in Abaqus

The beam has now been assessed in Abaqus using the rebar method. Input values are seen in table 4.12 and are the same as previously used. The Abaqus model is seen in figure 4.26.

Table 4.12: Values for rebar method

$L[mm]$	10000
$b[mm]$	300
$h[mm^3]$	500
$e_s[mm]$	200
$A_S[mm^2]$	982
$\overline{\varepsilon}_{asr}$	0.000988
$\overline{\kappa}_{asr}$	$1.333{\cdot}10^{-6}$
$q[N/mm]$	4
$E_c[N/mm^2]$	30000
$E_s[N/mm^2]$	200000

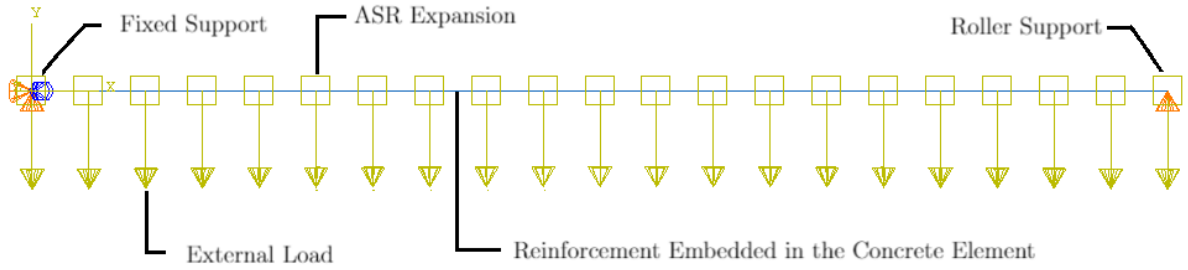

Figure 4.26: Rebar model in Abaqus for case 1B

Furthermore, moment, shear and axial axial diagrams from the analysis using linear-elastic material model (MM1) is presented:

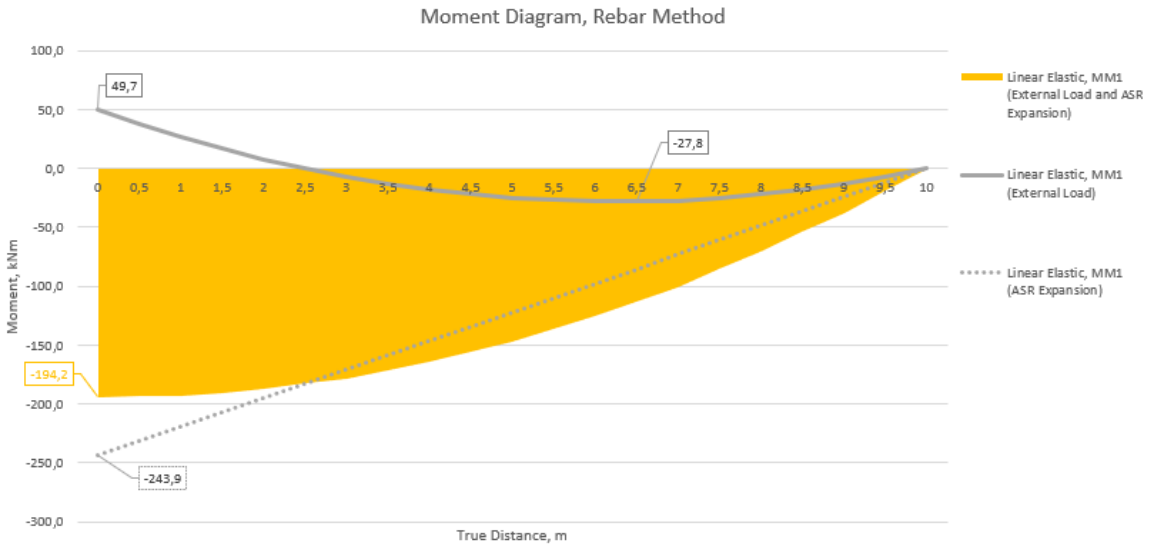

Figure 4.27: Moment diagrams for external load, ASR expansion and combined for case 1B

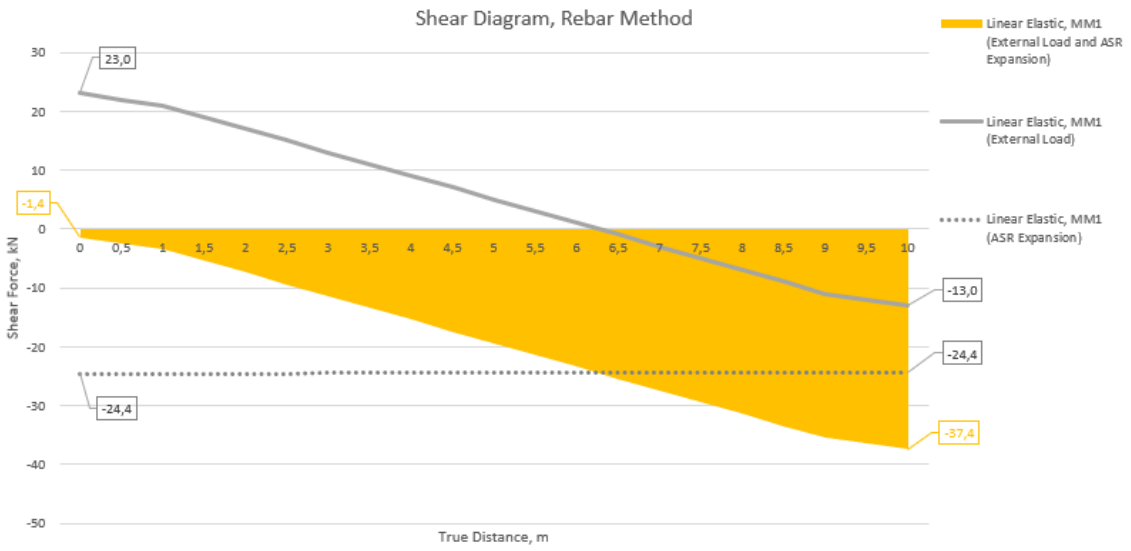

Figure 4.28: Shear diagrams for external load, ASR expansion and combined for case 1B

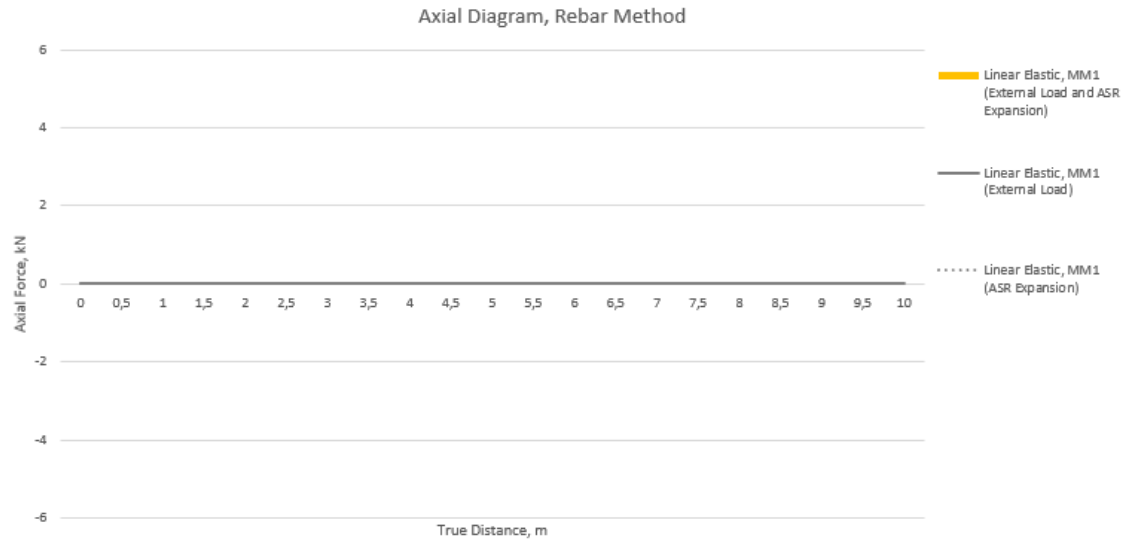

Figure 4.29: Axial diagrams for external load, ASR expansion and combined for case 1B

4.2.3 Verification of Numerical Solution for Case 1B

As seen in table 4.13 the loads calculated in Abaqus using the element-coupling and Rebar method is comparable to the loads calculated using the analytical solution. Except a minor difference in the shear force, the loads are approximately the same. The difference of shear force is likely due to discretization error in Abaqus leading to a slightly lower shear value than expected. As this discretization error is known, it can be said that the element-coupling/Rebar method with an non-uniform expansion is valid.

Table 4.13: Load results from the analytical-, element-coupling- and rebar method

	Analytical Solution	Element-Coupling Method	Rebar Method
$M_a(kNm)$	194	194.2	194.2
$M_b(kNm)$	0	0	0
$V_a(kN)$	0.568	1.4	1.4
$V_b(kN)$	39.41	37.4	37.4
$N_a(kN)$	0	0	0
$N_b(kN)$	0	0	0

It is seen in table 4.13 that the force values calculated in case 1B corresponds to the values calculated in case 1A. The bending moment is equal in the numerical models, with a moment value slightly larger than calculated using the analytical method. Shear values from the analytical solution is slightly less than the values extracted from the element coupling- and rebar method, as predicted due to the discretization error.

4.3 Summary of Results

Summary of Results for Case 1A

Results from case 1A regards every material model applied (MM1-MM4 and MMA) can be seen in Appendix B. Following is a summary of the results regards the analyses done in case 1A.

In case 1A it is observe that the ASR induced stress has the greatest impact on the moment diagram. From MM1 to MM3 maximum bending moment is decreased by 9,6kNm, from -52,9kNm to -43,3kNm, a total reduction of 18,1%. The moment at the fixed support changes from -1,4kNm to 13,8kNm from material model MM2 to MM3. It can be observed from the results that the second most impacting material model is the one which includes creep (MM2). The maximum bending moment decreases from -52,9kNm to -50,9kNm and the moment at the support decreases from -6,8kNm to -1,4kNm when the effect of creep is included in the linear elastic material model, MM1 to MM2. The change of moment from MM2 to MM3 is much greater the change from MM1 to MM2. This regards especially for the maximum bending moment. The material model with reduced stiffness due to ASR (MM4) gives the least reduction of forces when it is included. The change of moment from MM3 to MM4 are almost half the changes of moment from MM1 to MM2. From MM3 to MM4 the maximum bending moment increased from -43,3kNm to -44,8kNm and the moment at the fixed support decreases from 13,8kNm to 10,8kNm.

Figure 4.30 shows the combined moment diagram (external load and ASR) for every material model and the moment diagram from original state (only external load).

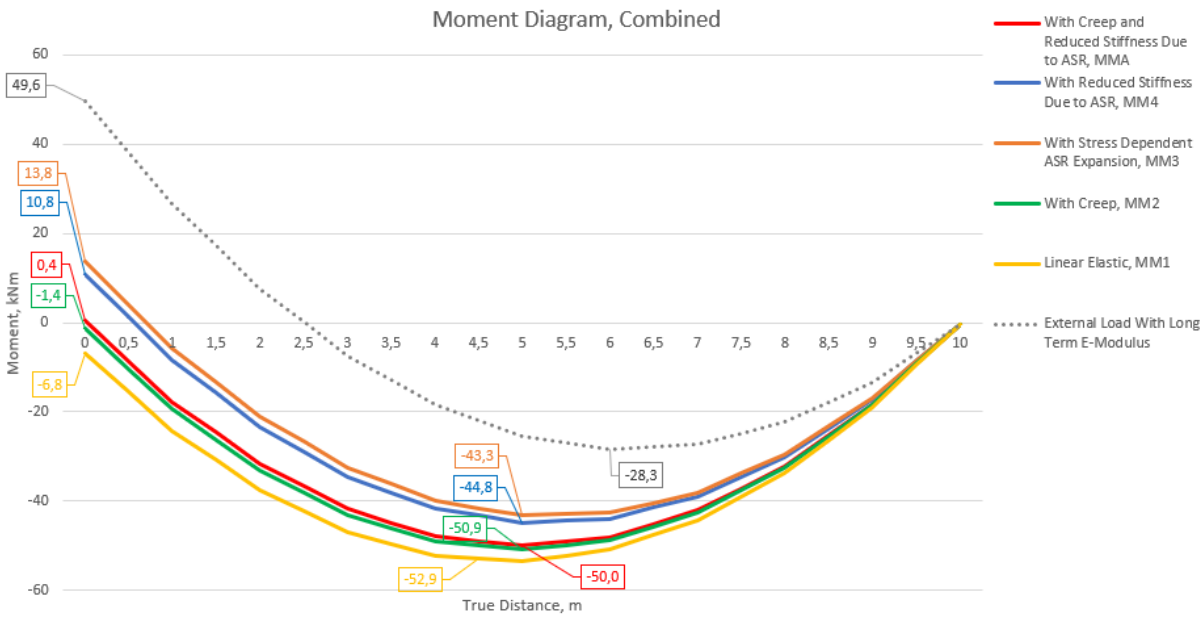

Figure 4.30: Comparison of moment diagrams case 1A

An interesting observation is that the maximum bending moment decreases by including creep (MM2) as the stiffness of the beam is reduced. But in MM4 where the stiffness is further reduced due to ASR the maximum bending moment increases. However, this increase is significantly small. In general the the differences of moment between the material models are relatively small, which has to do with the structures small size and its few constrains.

The analysis shows that material model 3, which include stress dependent ASR expansion, provides the most accurate results. As seen in figure 4.30 the moment at the fixed support when including linear elastic material behaviour and short term E-modulus (MM1) is -6,8kNm with tension at the bottom. By including the effect of creep the moment at the fixed support in MM2 becomes 1,4kNm. But when ASR induces stress in included in MM3 the moment at the fixed support is 13,8kNm giving tension at the top.

Summary of moment values are seen in table 4.14-4.16.

Table 4.14: Bending moment results

Moment (kNm)				
	At fixed support	M_{max}	Absolute difference	Support V.S M_{max}(%)
MM1	-6.8	-52.9	46.1	12.85
MM2	-1.4	-50.9	49.5	2.75
MM3	13.8	-43.3	57.1	31,9 ??
MM4	10.8	-44.8	55.6	24,1 ??

Table 4.15: Changes of maximum moment from MM1 to MM4 (kNm)

Change of M_{max} (kNm)				
	MM1	MM2	MM3	MM4
MM1	-	-2	-9.6	-8.1
MM2	2	-	-7.6	-6.1
MM3	9.6	7.6	-	1.5
MM4	8.1	6.1	-1.5	-

Table 4.16: Changes of maximum moment from MM1 to MM4 (%)

Change of M_{max} (%)				
	MM1	MM2	MM3	MM4
MM1	-	-3.8	-18.2	-15.3
MM2	3.9	-	-14.9	-12.0
MM3	22.2	17.6	-	3.5
MM4	18.1	13.6	-3.4	-

It can be observed from the shear diagram seen in figure 4.31 that the change from MM1 to MM4 is similar to change seen in the moment diagram. This is due to the relationship between moment and shear. The shear diagram shows that the shear force at the fixed support increases until MM3 and then decreases from MM3 to MM4. The Shear force in the right end has the opposite behaviour as for fixes end. This is due to the evenly distributed load, q, which provides the same development of shear force in each analysis.

Figure 4.31: Comparison of shear diagrams for case 1A

Summary of moment values are seen in table 4.17-4.19.

Table 4.17: Shear force results (kN)

	V_A	V_B	Absolute difference
MM1	17.4	-18.6	36
MM2	17.9	-18.1	36
MM3	19.4	-16.6	36
MM4	19.1	-16.9	36

Table 4.18: Change of V_A (kN)

	MM1	MM2	MM3	MM4
MM1	-	2.9	11.5	9.8
MM2	-2.8	-	8.4	6.7
MM3	-10.3	-7.7	-	-1.6
MM4	-8.9	-6.3	1.6	-

Table 4.19: Change of V_b (kN)

	MM1	MM2	MM3	MM4
MM1	-	-2.7	-10.8	-9.1
MM2	2.8	-	-8.3	-6.6
MM3	12.1	9	-	1.8
MM4	10	7.1	-1.8	-

Results from the analytical solution and linear elastic FEM analysis showed that the axial force is zero, as seen in figure 4.32. Assessment using material model 1-4 gave zero axial force as predicted which verifies that the analysis has been done correctly.

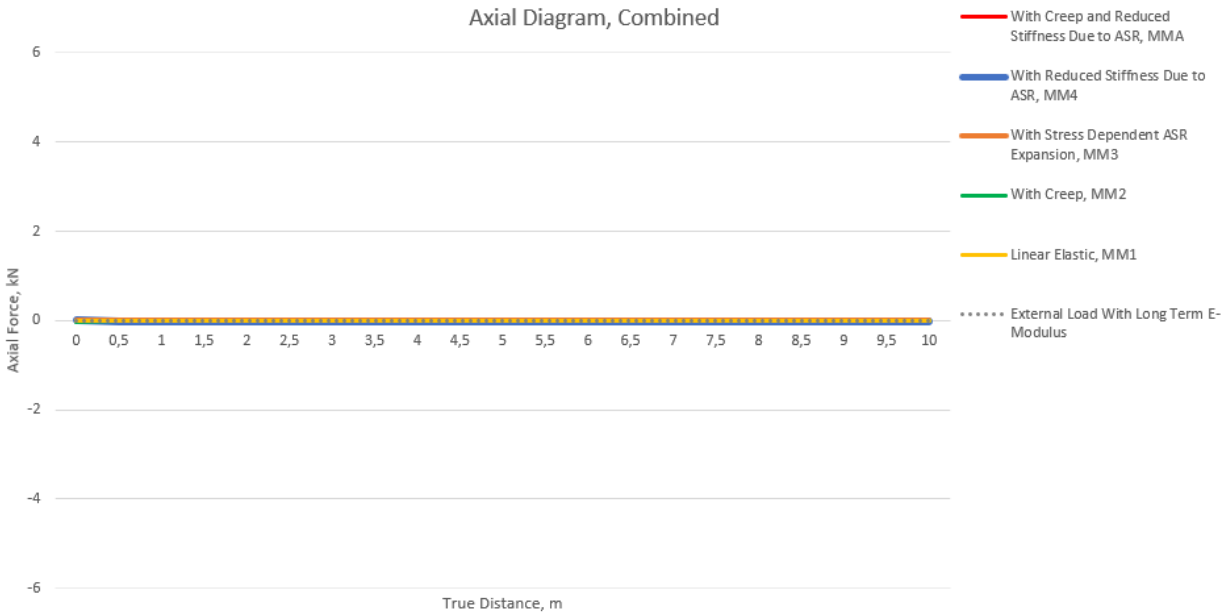

Figure 4.32: Comparison of axial diagrams for case 1A

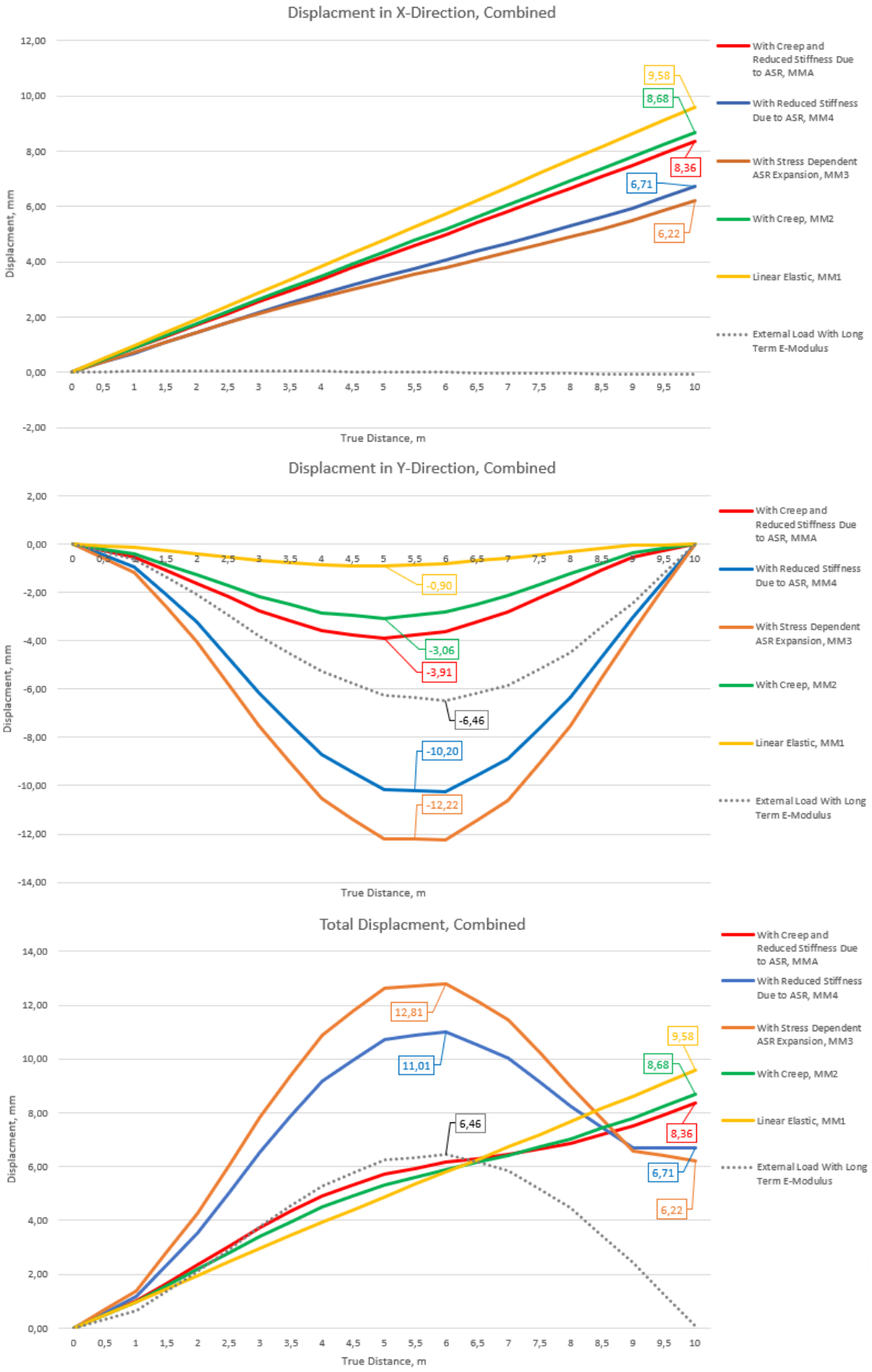

Figure 4.33: Comparison of displacements for case 1A

It is seen in figure 4.33 that the fixed support does not deform, meaning that no deflection occurs at the left end. As the right end has roller support, horizontal deformation will occur. Since the induced ASR strains are constant along the beam length, the beam will approximately increase linear over its length.

Even though the ASR strain is set to be uniform constant along the length of the beam it is seen that the ASR induced strains lead to both horizontal- and vertical deformations. It is also seen that the horizontal- and vertical deformation are interdependent. Greater vertical deflection leads to less horizontal deflection.

Total strain in x-direction is given as $\varepsilon = \varepsilon_{el} + \varepsilon_{asr}$ where $\varepsilon_{asr} = 0,001$. The ASS strain is constant in the application of every material model. ε_{el} depends on the concrete stiffness and as the E-modulus is reduced so is ε_{el}. This corresponds to the displacement observed in figure 4.33.

The horizontal deformation is gradually reduced from MM1-MM3. However, from MM3 to MM4 the horizontal deformation increases from 6.22mm to 6.71mm and the vertical deformation decreases from -12,22mm to -10.20mm. This is the same development as seen for the moment shear force.

Summary of Results for Case 1B

From the analysis of non-uniform ASR expansion, seen in figure 4.34, it is observed that when a non-uniform ASR strain is applied there is a greater difference between the material models than observed when the ASR strain is uniform.

Without ASR expansion the beam is exposed to 42.5kNm at the fixed end, (M_a). When material model 1 is applied M_a becomes 194.2kNm. A total change of 236,7kNm. The beam does also change from having tension at the top to having tension at the bottom. Depending on the structural system and placement of reinforcement, this type of changes may have a significant impact on the structural capacity. If the stress state changes to a area with less reinforcement, the capacity my be exceeded at worst leading to structural damage and failure. As material model 2-4 are applied, the moment decreases respectively. Using material model 4 the moment at A become 0.4kNm with maximum field moment of -50.0kNm. From MM1 to MM4 the moment at the fixed end is reduced by 192.8kNm. The maximum bending moment is reduced by 144.2kNm and goes from being greatest at the fixed end in case 1A to having its greatest moment value at x=4,525m in case 1B.

The greatest change of forces between the models is from MM1 to MM2 as the effect of creep is included in the material model. Including creep reduces the concrete E-modulus leading to a less stiffer concrete. As the concrete stiffness is reduced so is its capacity. Since the concrete can not withstand the same forces as previous, the remaining forces has to be obtained by the supports. Therefore as more detailed ASR material models are applied the reaction forces at the supports change.

This shows the importance of using a model that include as many parameters as possible and that the effect form each parameter must be described as deeply as possible. The more accurate and detailed model, the more precise the results become.

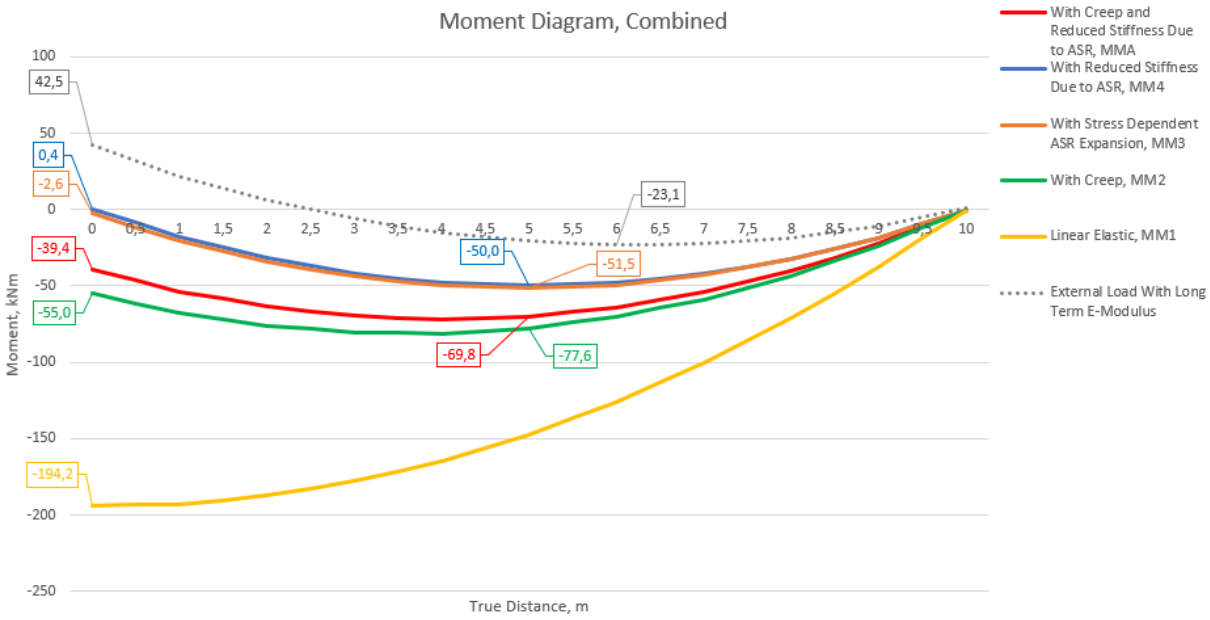

Figure 4.34: Comparison of moment diagrams for case 1B

From table 4.35 it is seen that the shear force diagram has the same development as for the moment diagram. Originally the beam is exposed to a shear force at each support of $V_a = 23kN$ and $V_b = -13kN$. By including a non-uniform ASR strain the shear force at the supports changes. The slope of the shear diagram is the same in each analysis due to uniform distributed external load, q.

The linear elastic material model with long term E-modulus (MM1) is shown to provide the greatest difference of shear force as V_a changes from 23kN to -1.4kN and V_b changes from -13kN to -37.4kN. Applying more advanced material models provides less shear force difference compared to the original state with uniformly distributed load, q. MM4 is shown to provide the least different from the original state. The greatest change of shear forces between the material models is observed from MM1 to MM2.

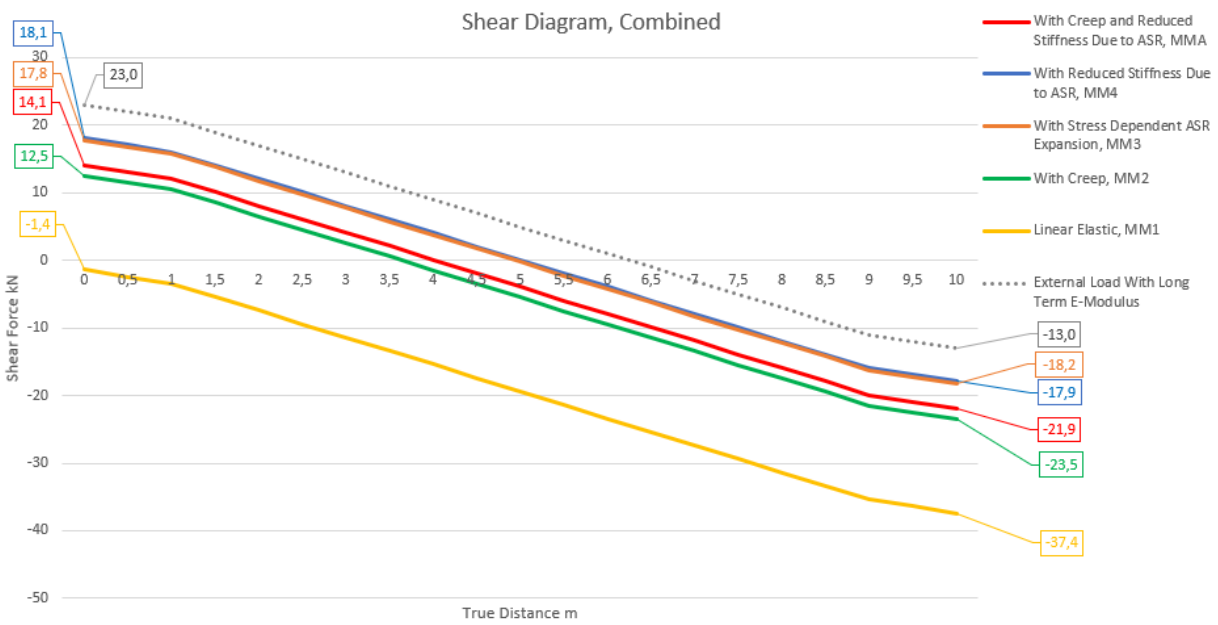

Figure 4.35: Comparison of shear diagrams for case 1B

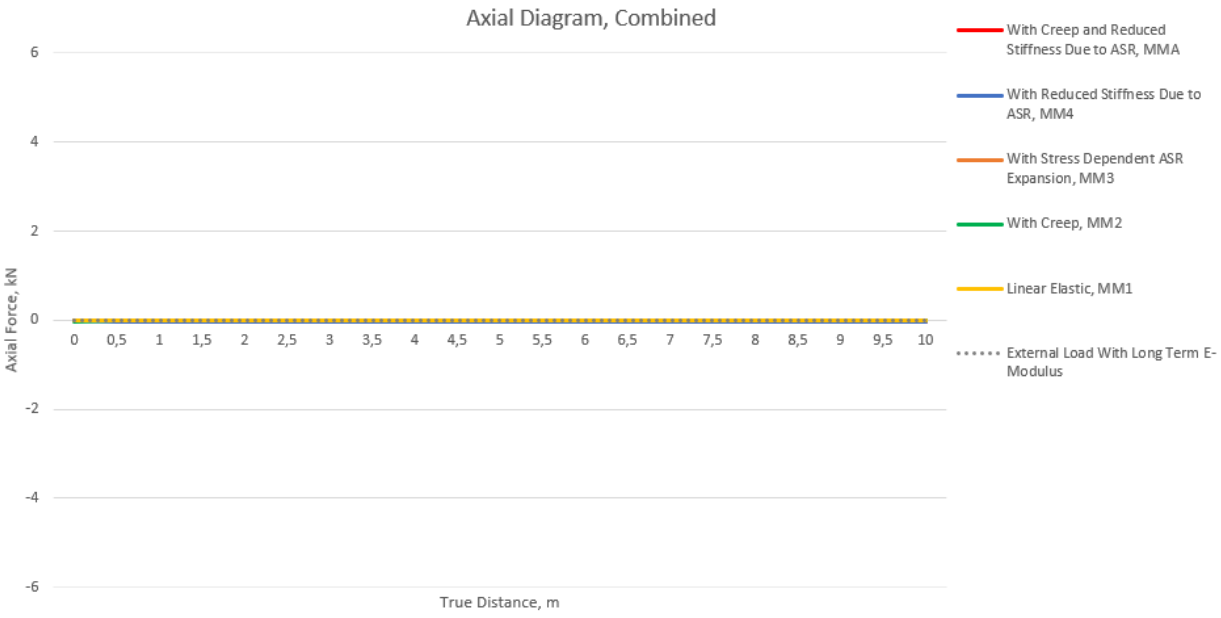

Figure 4.36: Comparison of axial diagrams for case 1B

Due to the beam's supports and the given load situation the axial force is zero, seen in figure 4.36. This is as predicted and confirmed by the equilibrium equations.

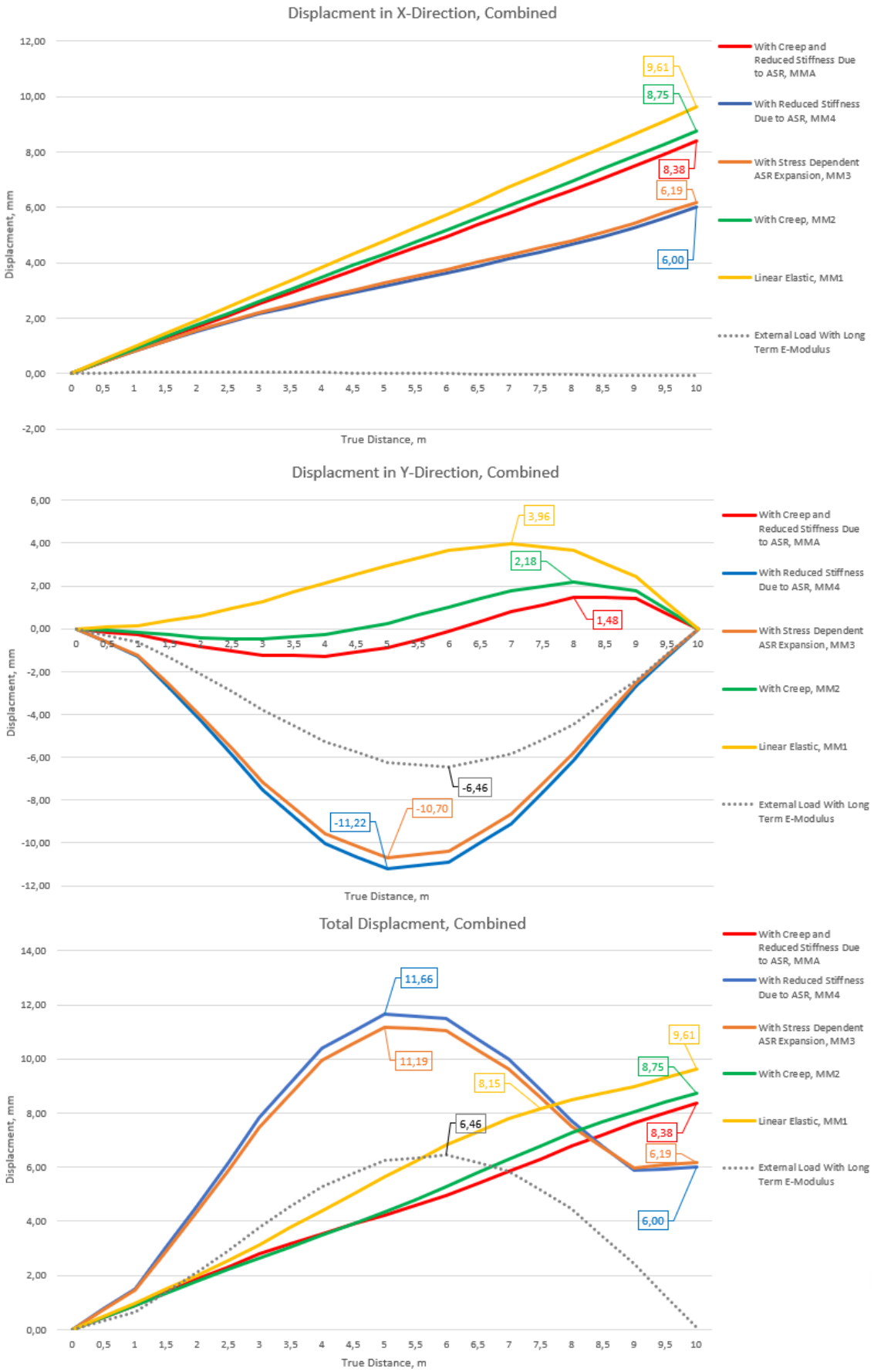

Figure 4.37: Comparison of displacements for case 1B

It is observed in figure 4.37 that the vertical deformation changes significantly from case 1A with uniform ASR strain to case 1B with non-uniform ASR expansion. The greatest differences occur for MM1, MM2 and MMA which now have a positive vertical deformation. MM3 and MM4 still experiences a negative vertical deformation. The horizontal deformation have approximately the same relationship and values in case 1B as in case 1A

Comparison of displacements between case 1A and case 1B are seen in table 4.20.

Table 4.20: Displacement form uniform and non-uniform ASR strain

	Displacement			
	Case 1A		Case 1B	
	δ_x	δ_y	δ_x	δ_y
Ext. load	0	-6.46	0	-6.46
MM1	9.58	-0.9	9.61	3.96
MM2	8.68	-3.06	8.75	2.18
MM3	6.22	-12.22	6.19	-10.7
MMA	8.36	-3.91	8.38	1.48
MM4	6.71	-10.19	6.0	-11.22

Chapter 5

Structural Analysis of Three Span Beam

Oslo Metropolitan University

Engineering and Building Technology

15th of June 2020, Oslo, Norway

5 Case 2: Structural Analysis of Three Span Beam

In case 2 Elgeseter bridge is selected as reference for the structural analysis. The beam model in this case is made to represent the last three spans of Elgester Bridge, see figure 5.1. This beam is referred to as the three span beam. As seen in figure 5.2, the reinforcement is very complex and has multiple layers of reinforcement at top and bottom. This makes it too difficult to make a exact beam model of Elgeseter bridge using the element/kinematic-coupling in Abaqus. Dr. Ing. A Aas-Jakbosen AS has performed analyses and made a model that represents the same stress-strain behavior the real three span beam would have experienced from the dead load in the linear elastic stage.

The three span beam model is indicated in figure 5.1 and consists of a three spanned T-shaped cross section beam. The model has a fixed support in the left end (support one), and has respectively roller supports at support two, three and four. The cross section is equal over the length. Span one and two has the same length and amount and placement of reinforcement. Span three differs in length and reinforcement.

The three span beam model including its parameters are provided by Dr. Ing. A Aas-Jakbosen AS [22]. Kinematic/element-coupling method is used in Abaqus for every analysis carried out in case 2. This is seen in figure 5.1-5.3.

The structural analyses of the three span beam will provide a more realistic comparison of the material models, as the analyses is done on a larger structure. Case 2 is divided into three parts:

- Case 2A: Uniform and non-uniform ASR strain, free end displacement
- Case 2B: Uniform and non-uniform ASR strain, fixed end displacement
- Case 2C: Non-uniform ASR strain, tension and compression

Case 2A include the same analyses as done in case 1. Case 2B is performed to see the effect from the different material models when a total strain, $\varepsilon = 0.001$, is set. This represents the observed strain on Elgester bridge. In case 2C axial tension and compression forces are applied to see how axial forces affects the ASR load actions.

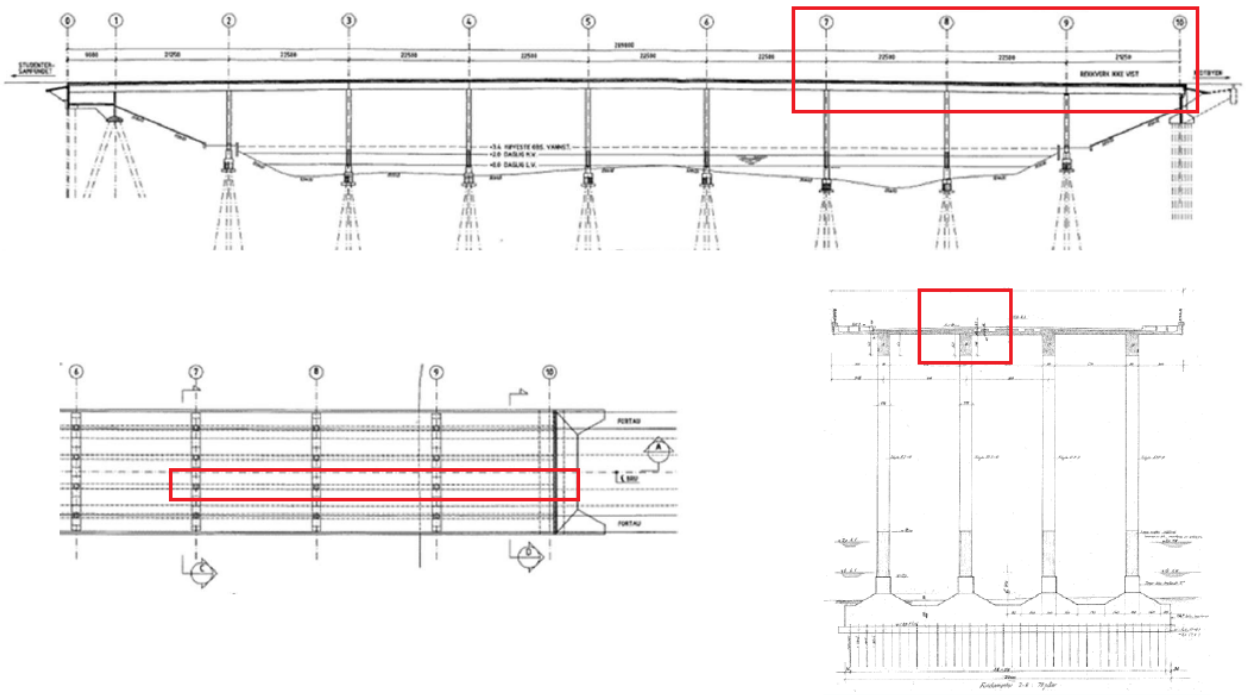

Figure 5.1: Sketch of Elgeseter bridge. The three span beam is indicated in red. Drawing provided by Dr. Ing. A Aas-Jakbosen AS [22]

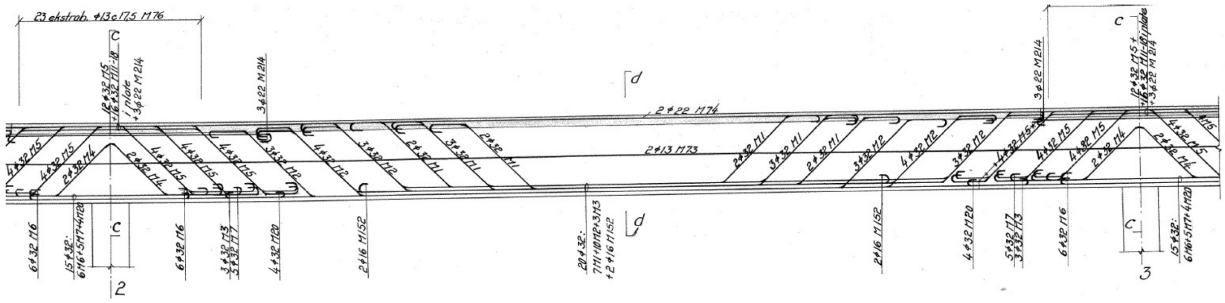

Figure 5.2: Sketch of the reinforcement in the mid beam on Elgeseter bridge [22]

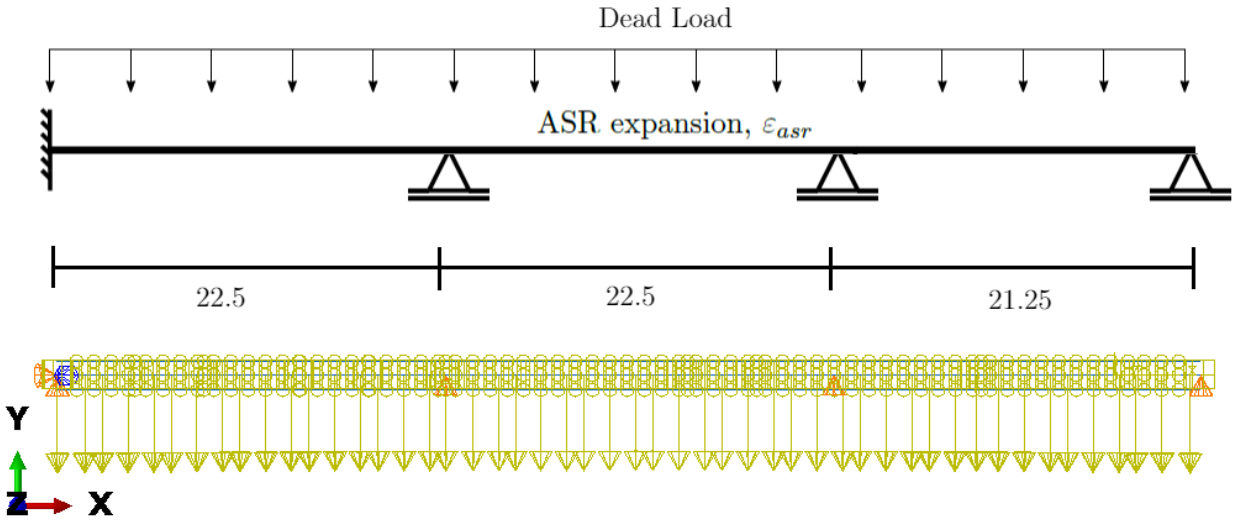

Figure 5.3: Sketch and Abaqus model of the three span beam

The 66.25m long equivalent beam is divided in elements with a length of 1m (one element is 1.25m) this leaves us with a beam as shown in figure 5.3. This beam is divided in 66 elements which gives us a satisfactory kinematic constraints throughout beam. Element/kinematic coupling is used, where the concrete element is placed in the middle with reinforcement elements on top and at the bottom.

Characteristic values is used as they provides the exact results and state of the load actions due to the induced ASR strains. Elgeseter bridge has concrete class C25 with a short term modulus of elasticity, $E_{cm} = 23312.7N/mm^2$ and long term modulus of elasticity, $E_{c,eff} = 7770.9N/mm^2$. The reinforcement used has modulus of elasticity, $E_s = 200000N/mm^2$. The structural analysis in Abaqus is done with a applied dead load of $86.67kNm$.

The three span beam is modelled using nine different cross sections, see figure 5.4. This is done to give the the equivalent beam a realistic behavior similar to the real one. Beam span one and two of the model are equal and consists of cross section 1-3. Span three consists of cross section 11-16 as seen in figure 5.4 and table 5.2 and 5.3. Cross section data is seen in table 5.5 and applied geometry in Abaqus is seen in figure 5.5.

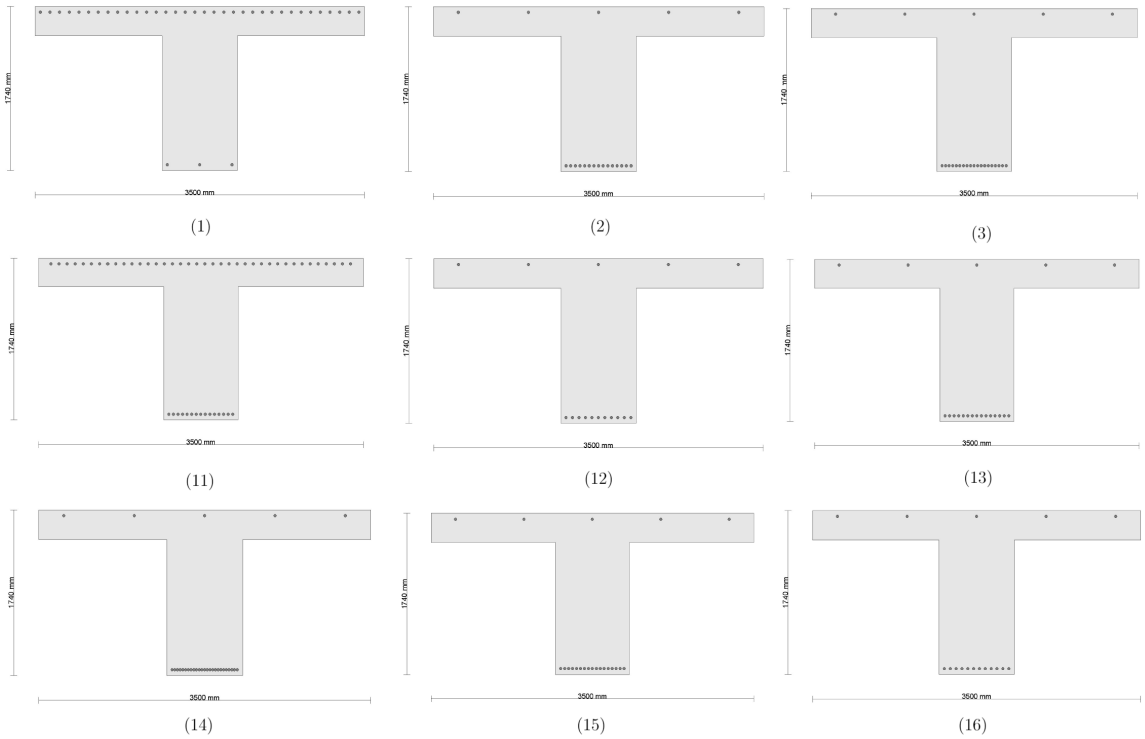

Figure 5.4: Cross sections used in the modeling of case 2 [22]

Table 5.1: Cross section data case 2 [22]

Total cross section width	3500 mm
Plate thickness	310 mm
Beam width	800 mm
Total beam height (included plate thickness)	1740 mmm

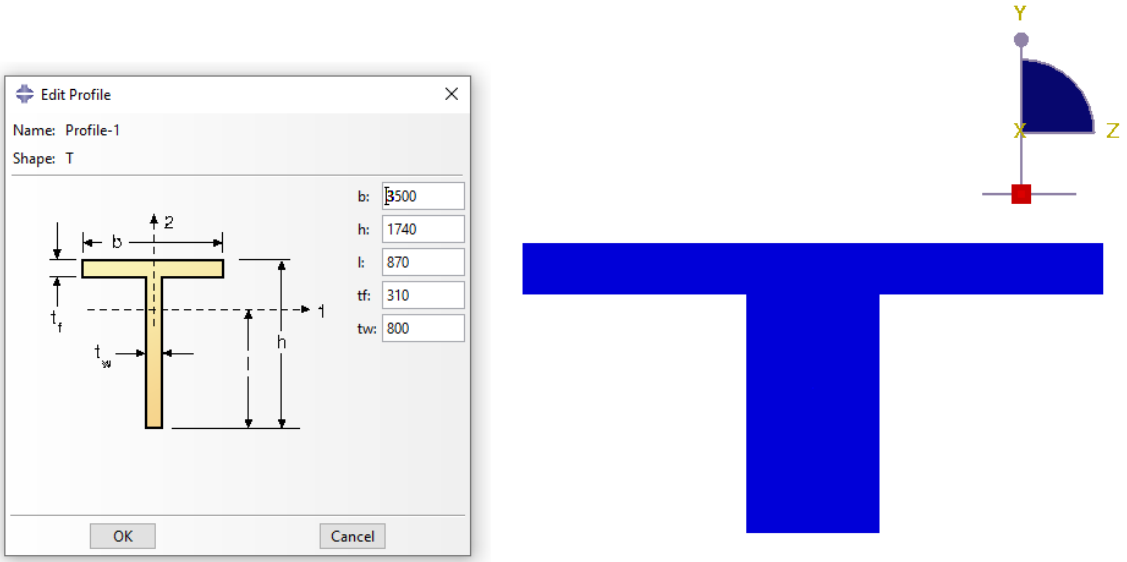

Figure 5.5: The geometry of the cross section in Abaqus

Table 5.2: Reinforcement placed in one layer at top and bottom for the first and second span (from axis to axis, 22,5m) [22]

Placement			From bottom	St.52	Bottom area	Top area
(m)	(m)	C.S	(mm)	$\phi = 32$	(mm^2)	(mm^2)
0	4.5	1	59	3	2412.7	
						27344.4
			1681	34		
4.5	8.5	2	59	15	12063.7	
						4021.2
			1681	5		
8.5	14	3	59	19	15280.7	
						4021.2
			1681	5		
14	18	2	59	15	12063.7	
						4021.2
			1681	5		
18	22.5	1	59	3	2412.7	
						27344.4
			1681	34		

- C.S=Cross Section

Table 5.3: Reinforcement placed at top and bottom for the third span (from axis to axis, 21.25m) [22]

Placement			From bottom	St.52	Bottom area	Top area
(m)	(m)	C.S	$\phi = 32$		(mm^2)	(mm^2)
0	4	11	59	15	12063,7	
						30561,4
			1681	38		
4	7	12	59	11	8846,7	
						4021,2
			1681	5		
7	8,5	13	59	15	12063,7	
						4021,2
			1681	5		
8,5	17	14	59	25	20106,2	
						4021,2
			1681	5		
17	19	15	59	17	13672,2	
						4021,2
			1681	5		
19	21,25	16	59	12	9651,0	
						4021,2
			1681	5		

Rebar Method for the Three Span Beam

The plan was to use rebar method on the equivalent beam. The benefit of using the rebar method is that the moment, shear and axial forces is directly extracted from Abaqus outputs. No summation of concrete and steel forces is needed, making this a great method to use when more advanced beams is to be analyzed. However, it turned out that the rebar method did not work when the three span beam was analysed. From the analysis done with uniform ASR expansion, it was observed that the ASR contribution was almost non existing on the last beam span (from 45m to 66,25m), see figure 5.6. Several analysis with adjustments was done to find a solution to this error, but success was not achieved. In case 1A and case 1B it was verified that the rebar method works. It seems that the rebar method in Abaqus has a weakness when the structural model gets more complex (several cross sections).

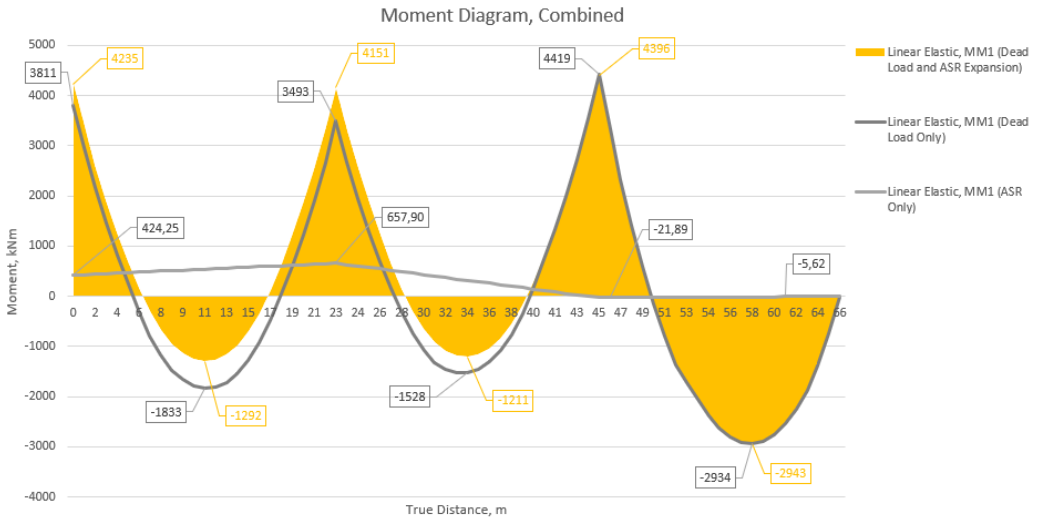

Figure 5.6: Results from rebar method on case 2A with uniform ASR expansion

Then analysis on the equivalent beam with an curvature was done, see figure 5.7 . From this analysis it was observed that the ASR contribution didn't stop at the last span. Interesting enough it seemed that the errors didn't occur when an curvature was included. We contacted Dr. Ing. A. Aas-Jakbosen AS to look closer to the results to see if there was still wrong ASR restraint forces. From their analyses they verified that there still was an error with the rebar method since the ASR contribution in our analysis had a deviation from their results of about 2000kN.

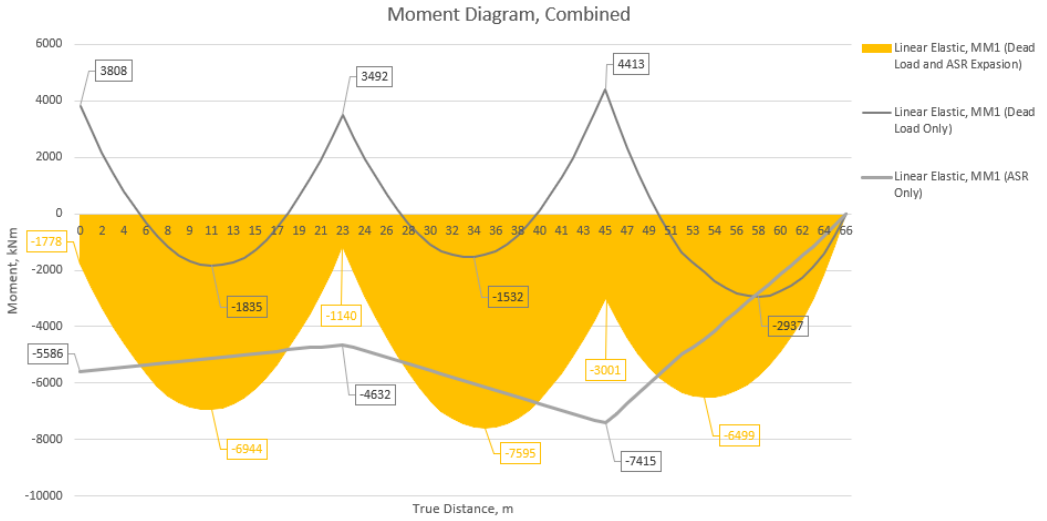

Figure 5.7: Results from rebar method on case 2A with non-uniform ASR expansion

After many attempts we concluded that the rebar method could not be used further in the analysis of case 2. Therefore, the element coupling method is further used. This rebar method error is a finding that should be taken into consideration by others when doing complex analysis of the ASR expansion in concrete structures. We assume the rebar method only works on simple ASR expansion analysis, as shown in case 1. If the rebar method weakness is verified by Abaqus, then this error should be solved to allow for more complex analysis.

5.1 Case 2A - Three Span Beam with Constant Free ASR Strain

Simulation matrix for case 2A is shown in table 5.4. The analysis includes structural analysis done with (1) only dead load, (2) dead load and a uniform ASR expansion and (3) dead load with a nonuniform ASR expansion. The uniform ASR expansion has a ASR gradient, $\kappa_{asr} = 0$, and the non-uniform ASR expansion has a gradient, $\kappa_{asr} \neq 0$, were the ASR strain on top of the beam is twice the size as the ASR strain at the bottom. These three load scenarios are assessed using every material model. In case 2A the free ASR strain is fixed, $\varepsilon_{asr} = 0.001$, meaning that the end deformation in x-direction will vary between the material models. This is due to the different material models impact on the load actions on the beam.

Table 5.4: Simulation matrix for case 2A

Case 2A					Free ASR Strain	
No.	Load	Material Model		E-module	Bottom Strain	Top Strain
1	Dead load	Lin.Elastic	MM1	Short	-	-
2	Dead load + ASR, Unifrom	Lin.Elastic	MM1	Short	0,001	0,001
3	Dead load + ASR, Gradient	Lin.Elastic	MM1	Short	0,000667	0,001333
4	Dead load	Lin.Elastic + Creep	MM2	Long	-	-
5	Dead load + ASR, Unifrom	Lin.Elastic + Creep	MM2	Long	0,001	0,001
6	Dead load + ASR, Gradient	Lin.Elastic + Creep	MM2	Long	0,000667	0,001333
7	Dead load + ASR, Unifrom	Over + Stress Dep. ASR	MM3	Long	0,001	0,001
8	Dead load + ASR, Gradient	Over + Stress Dep. ASR	MM3	Long	0,000667	0,001333
9	Dead load + ASR, Unifrom	Over + Red. ASR Stiffness	MM4	Long	0,001	0,001
10	Dead load + ASR, Gradient	Over + Red. ASR Stiffness	MM4	Long	0,000667	0,001333
11	Dead load + ASR, Unifrom	Only Red. ASR Stiffness	MMA	Long	0,001	0,001
12	Dead load + ASR, Gradient	Only Red. ASR Stiffness	MMA	Long	0,000667	0,001333

5.2 Case 2B - Three Span Beam with Equal End Displacement

In case 2B the same analysis as in case 2A is performed. However, the end deformation in x-direction is now constant fixed for all simulations. The displacement in x-direction, δ_x, is set to be 66.25mm with a deviation of $\pm 0.5mm(0.75\%)$. This means that the free ASR strain, ε_{asr}, will vary between the different material models in order to get the same fixed end deformation. The ASR gradient, κ_{asr}, will also vary for the material models with non-uniform ASR expansion. The end deformation of 66.25mm represents a total mid strain, $\varepsilon = 0.001$, which was observed on Elgeseter Bridge. Modeling plan for case 2B is seen in table 5.5.

Table 5.5: Simulation matrix for case 2B

Case 2B					Free ASR Strain		End Def.
No.	Load	Material Model		E-module	Bottom Strain	Top Strain	(mm)
1	Dead Load	Lin.Elastic	MM1	Short	-	-	-
2	Dead Load + ASR, Unifrom	Lin.Elastic	MM1	Short	a	a	66,25
3	Dead Load + ASR, Gradient	Lin.Elastic	MM1	Short	a	2a	66,25
4	Dead Load	Lin.Elastic + Creep	MM2	Long	-	-	-
5	Dead Load + ASR, Unifrom.	Lin.Elastic + Creep	MM2	Long	a	a	66,25
6	Dead Load + ASR, Gradient	Lin.Elastic + Creep	MM2	Long	a	2a	66,25
7	Dead Load + ASR, Unifrom	Over + Stress Dep. ASR	MM3	Long	a	a	66,25
8	Dead Load + ASR, Gradient	Over + Stress Dep. AS	MM3	Long	a	2a	66,25
9	Dead Load + ASR, Unifrom	Over + Red. ASR Stiffness	MM4	Long	a	a	66,25
10	Dead Load + ASR, Gradient	Over + Red. ASR Stiffness	MM4	Long	a	2a	66,25
11	Dead Load + ASR, Unifrom	Only Red. ASR Stiffness	MMA	Long	a	2a	66,25
12	Dead Load + ASR, Gradient	Only Red. ASR Stiffness	MMA	Long	a	2a	66,25

5.3 Case 2C - Three Span Beam with Axial Tension- or Compression Force

In case 2C an axial force of 5000kN is applied on the beam. The axial force is analysed both in tension and compression. This is done to include the effect of restraints caused by concrete that has not expanded to the same degree. As seen in Elgeseter bridge the outer beams were exposed to much more ASR then the inner beams. It has been observed in the earlier case analyses that the stress dependent ASR expansion, MM3, provides the most important impact to the load actions. Therefore, is it decided to include a new material model (MMB) which focuses on the change of the stress dependant ASR expansion. In MMB the Charlwood function, $W(\sigma)$, is changed by increasing the restrain material constant of the stress dependent ASR expansion, σ_u, from $-6N/mm^2$ to $-10N/mm^2$. This allows for more expansion. With this material model we want to investigate the change of material constant σ_u. In case 2C we will run analysis with only ASR gradient since it represent a more realistic ASR behaviour. The beam is still going to have an fixed end deformation of 66,25mm, with a $\pm 0.5mm(0.75\%)$ deviation, so it has similar total mid strain ($\varepsilon = 0,001$) as observed in Elgester bridge. Figure 5.8 shows the three span beam subjected to tension and compression, and table 5.6 shows the simulation matrix for case 2C.

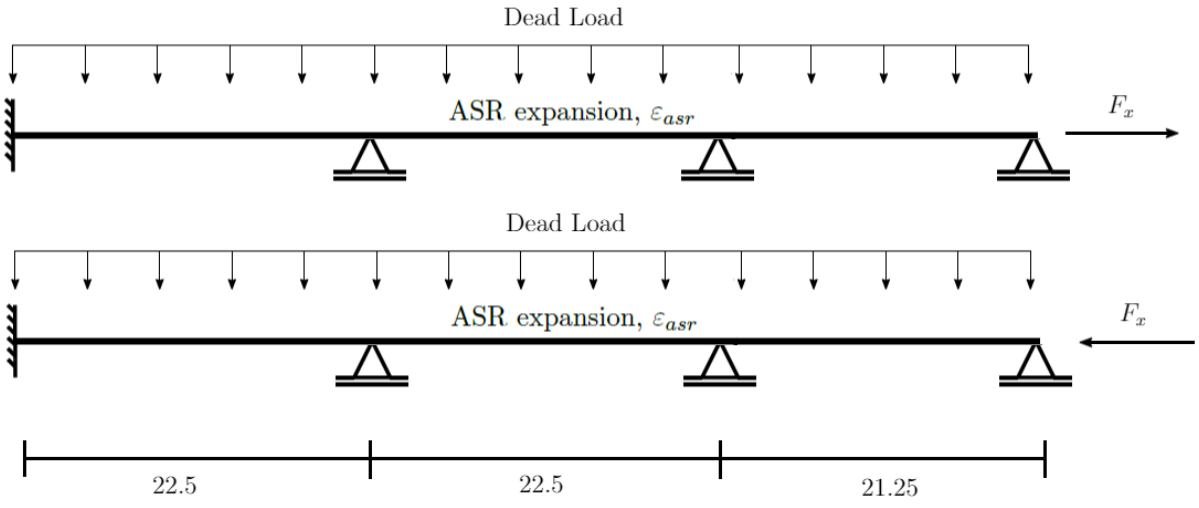

Figure 5.8: The three span bridge beam model with axial force

Table 5.6: Simulation matrix for case 2C

Case 2C					Free ASR Strain		End Def.	Axial Force
No.	Load	Material Model		E-module	Bottom Strain	Top Strain	(mm)	(kN)
1	Dead Load	Lin.Elastic + Creep	MM2	Long	-	-	-	0
2	Dead Load + ASR, Gradient	Lin.Elastic + Creep	MM2	Long	a	2a	66,25	5000
2	Dead Load + ASR, Gradient	Lin.Elastic + Creep	MM2	Long	a	2a	66,25	-5000
3	Dead Load + ASR, Gradient	Over + Stress Dep. ASR	MM3	Long	a	2a	66,25	5000
4	Dead Load + ASR, Gradient	Over + Stress Dep. ASR	MM3	Long	a	2a	66,25	-5000
5	Dead Load + ASR, Gradient	Over + Red. ASR Stiffness	MM4	Long	a	2a	66,25	5000
6	Dead Load + ASR, Gradient	Over + Red. ASR Stiffness	MM4	Long	a	2a	66,25	-5000
7	Dead Load + ASR, Gradient	Only Red. ASR Stiffness	MMA	Long	a	2a	66,25	5000
8	Dead Load + ASR, Gradient	Only Red. ASR Stiffness	MMA	Long	a	2a	66,25	-5000
9	Dead Load + ASR, Gradient	Stress Dep. ASR $\sigma_u = -10$	MMB	Long	a	2a	66,25	5000
10	Dead Load + ASR, Gradient	Stress Dep. ASR $\sigma_u = -10$	MMB	Long	a	2a	66,25	-5000

5.4 Summary of Results

Case 2A Without ASR Gradient

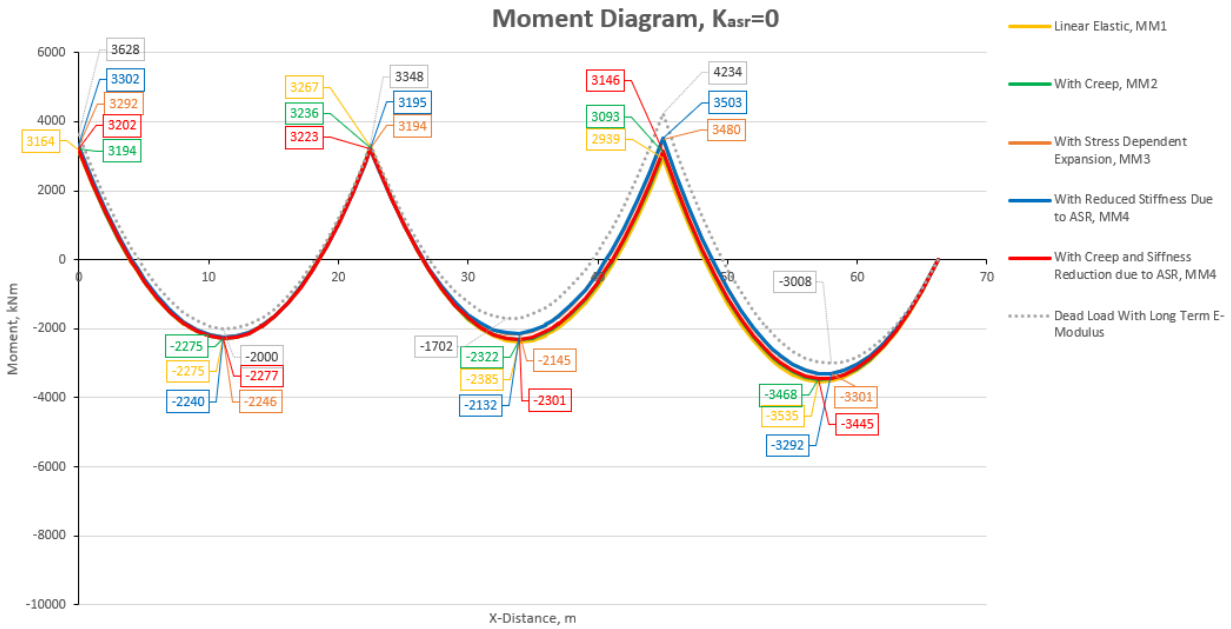

Figure 5.9: Comparison of combined moment diagrams for case 2A without ASR gradient

It is seen in figure 5.9 and 5.10 that the uniform ASR strain introduces load actions. The load actions are of a relatively small value, and have almost exactly the same values in every material model. Since the load action is of a small value, the combined moment diagram have the same path and almost the same values as for the original moment that does not include ASR.

It is seen for span 1 that the moments are approximately the same for every material model, both at the fixes support as well as the field moment. Span 3 has greater difference as MM3 and MM4 provides less moment in field, and greater moment at support 3 compared to MM1, MM2 and MMA. This difference is due to the fact that MM3 has included stress dependent expansion and MM4 has reduced stiffness due to ASR, in which they both reduces the concrete capacity compared to the other material models. And since the roller support at the right end does not obtain any moment, the moment obtained by the beam will have a greater impact in span 3 than in span 1 and 2 where the moment can be obtained by the supports.

As span 1 and 2 have the same amount and placement of reinforcement, the moment shall

have the same development for each material model. However, this is not the case as MM3 and MM4 in span 2 differs from span 1. This change is due to the moment in span 3 which affects span 2. The impact from span 3 gradually vanish, as seen in span 1 where the moment is approximately the same for every material model.

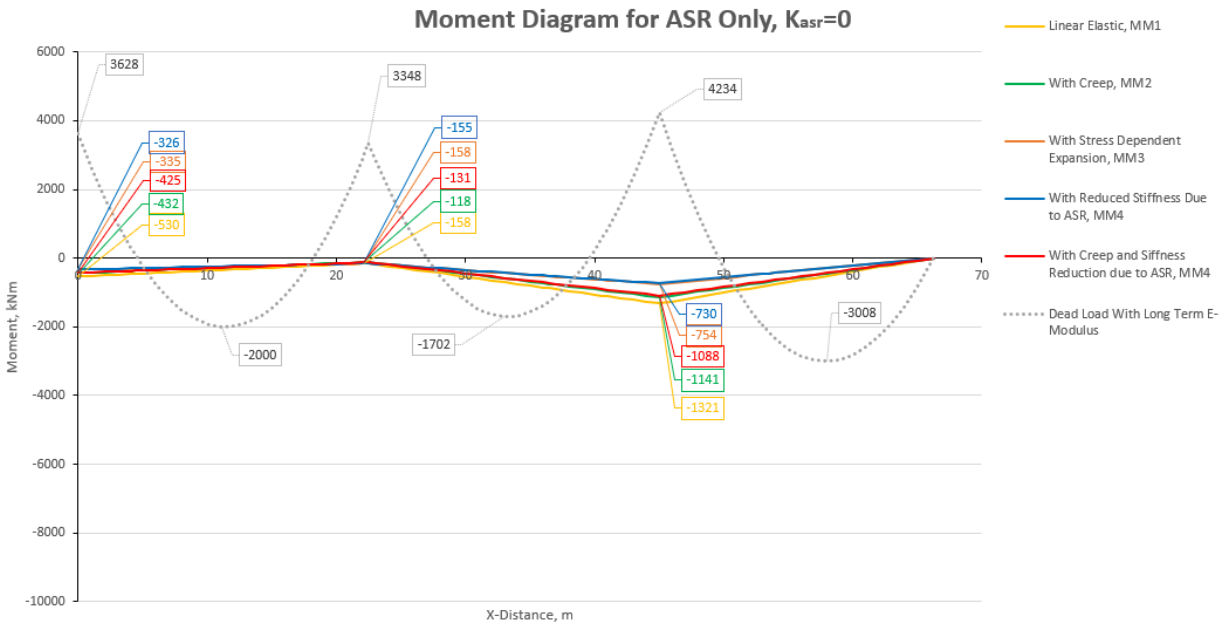

Figure 5.10: Comparison of ASR induced moments for case 2A without ASR gradient

As is seen in figure 5.10 the effect of introducing ASR induced strains to the model leads to a negative moment contribution throughout the whole beam for every material model. As for the combined moment, MM3 and MM4 provides the least negative moment due to the effect of ASR. The effect of ASR strains is greatest at support 3, and is respectively reduced at support 1 and 2. At support 3 MM3 gives a moment of -730kNm which is almost twice as small as the moment provided by MM1 with a value of -1371kNm.

As seen in figure 5.9 and 5.10, there is in general less changes to the moment when the ASR expansion is set to be uniform ($\kappa = 0$). Moment at the supports and field moments is slightly changed, but she shape and development is still the same for dead load, q, and ASR as without ASR induced strains. By bringing these sets of constrains to the analysis, no significant change of moments was observed.

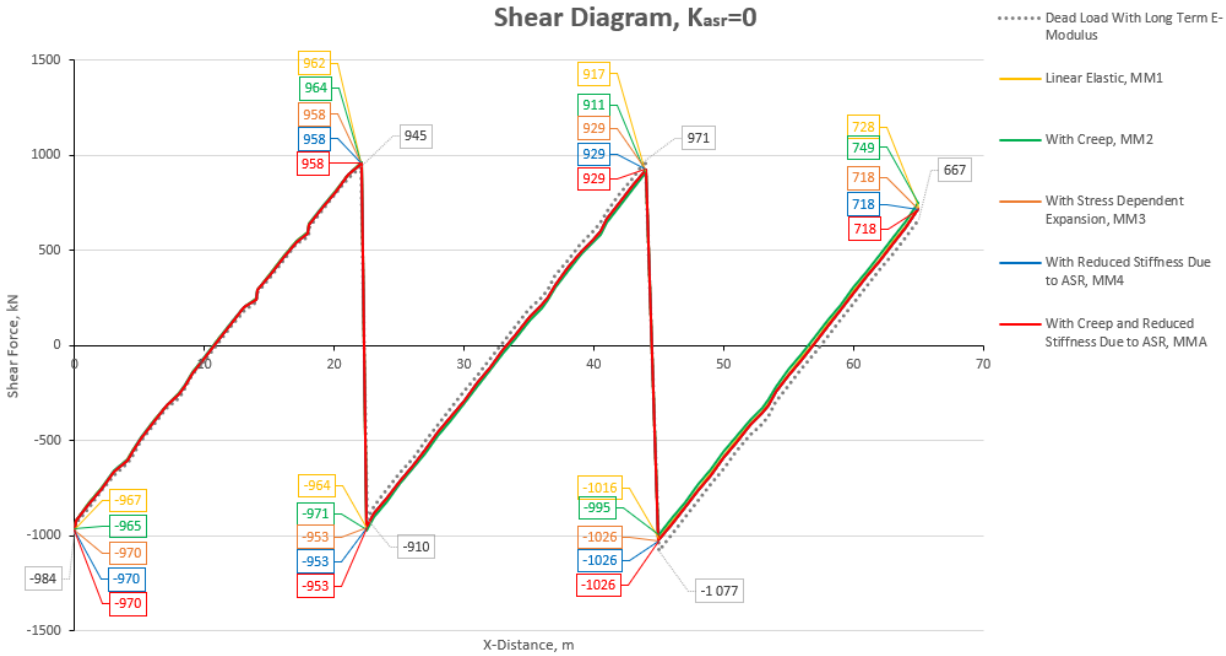

Figure 5.11: Comparison of shear diagrams for case 2A without ASR gradient

The shear diagram in figure 5.11 shows that the shear values and change throughout the beam is approximately the same. The results shows that there is no significant change of shear force by applying the different material models both compared to the original shear state as well as comparing the material models. Each material model have approximately the same shear values and development as the original state with only dead load applied.

Figure 5.12 shows that the axial force in case 2A with uniform ASR strain is zero. This is as expected.

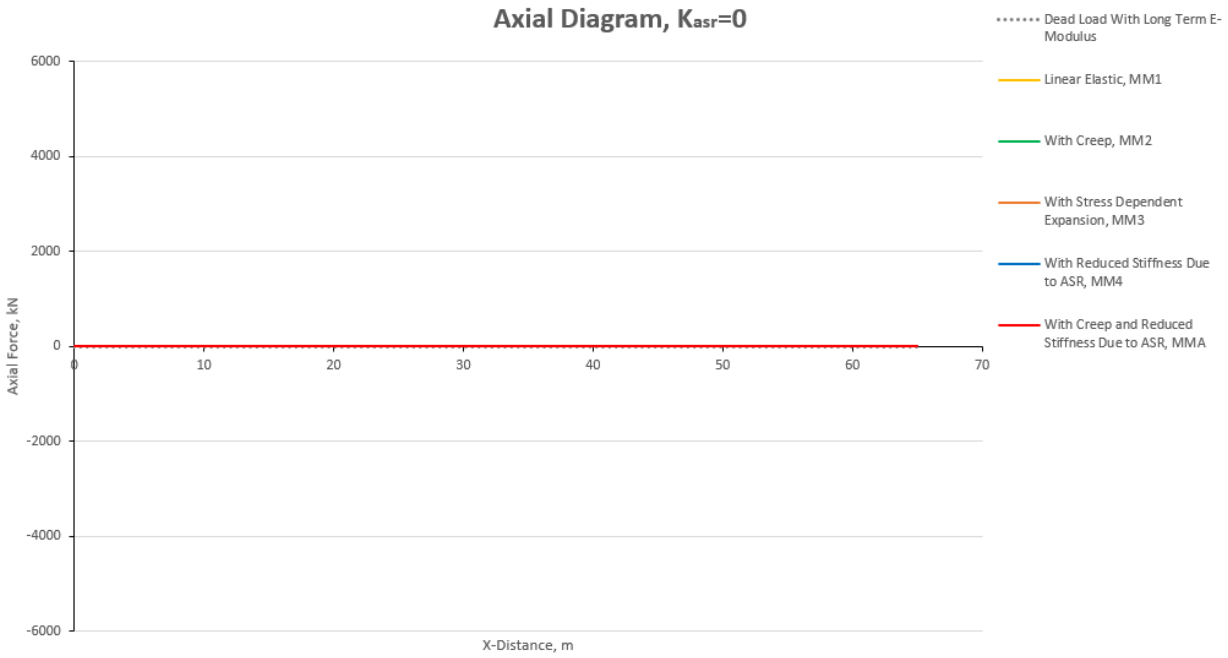

Figure 5.12: Comparison of axial diagrams for case 2A without ASR gradient

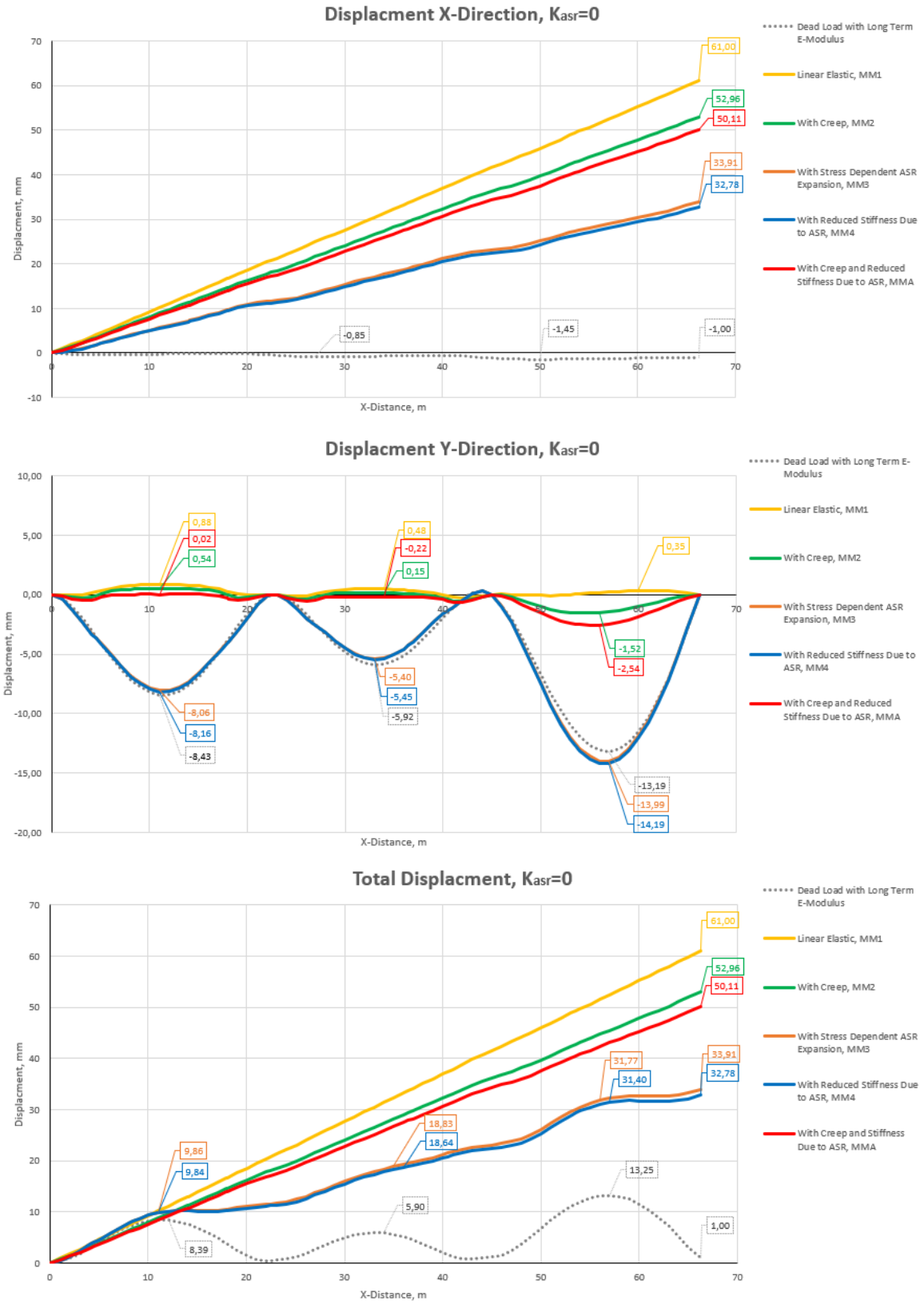

Figure 5.13: Comparison of displacements for case 2A without ASR gradient

Moment and shear results showed that there were minor differences between the forces from the material models and the original state. As seen in figure 5.13 this is not the case when displacement is assessed. The displacement results shows that there is a significant difference between the material models and differences from the original state.

Displacement in x-direction decreases gradually from MM1 to MM4. MM1 gives the largest displacement of 61cm. MM3 and MM4 results in the least displacement in x-direction with respectively displacements of $\delta_x = 32.78cm$ and $\delta_x = 33.91cm$. It is seen that the more accurate the material model is, less horizontal deformation and larger vertical deformation occurs. There is a significant difference in vertical deformations. MM1, MM2 and MMA results in almost no vertical deformation in span 1 and 2. In span 3 MM1 remains the same and MM2 and MMA gets a small negative deformation. MM3 and MM4 results in large vertical deformations. These deformations are close to those in the original state.

Table 5.7: Displacement and strains for case 2A, $\kappa = 0$

	δ_x(mm)	ε_x
MM1	61.0	0.00092
MM2	52.96	0.00080
MMA	50.11	0.00076
MM3	33.91	0.00051
MM4	32.78	0.00049

As seen in table 5.7 the total strain in x-direction, ε_x, for every material model applied is less than the set free ASR strain, $\varepsilon_{asr} = 0.001$. This is due to the ASR expansion including stiffness reduction and/or stress dependency. When the ASR expansion is stress dependent (MM3) and when the stiffness is further reduced due to ASR (MM4) the total stiffness of the concrete and its capacity is reduced giving less x-deformation compared to the other models applied. This corresponds to the fact that when the capacity is reduced (reduced stiffness) the concrete can not obtain as large forces as previous meaning that the elongation in x-direction is reduced. However, this implies that deflection in y-direction increases.

Case 2A With ASR Gradient

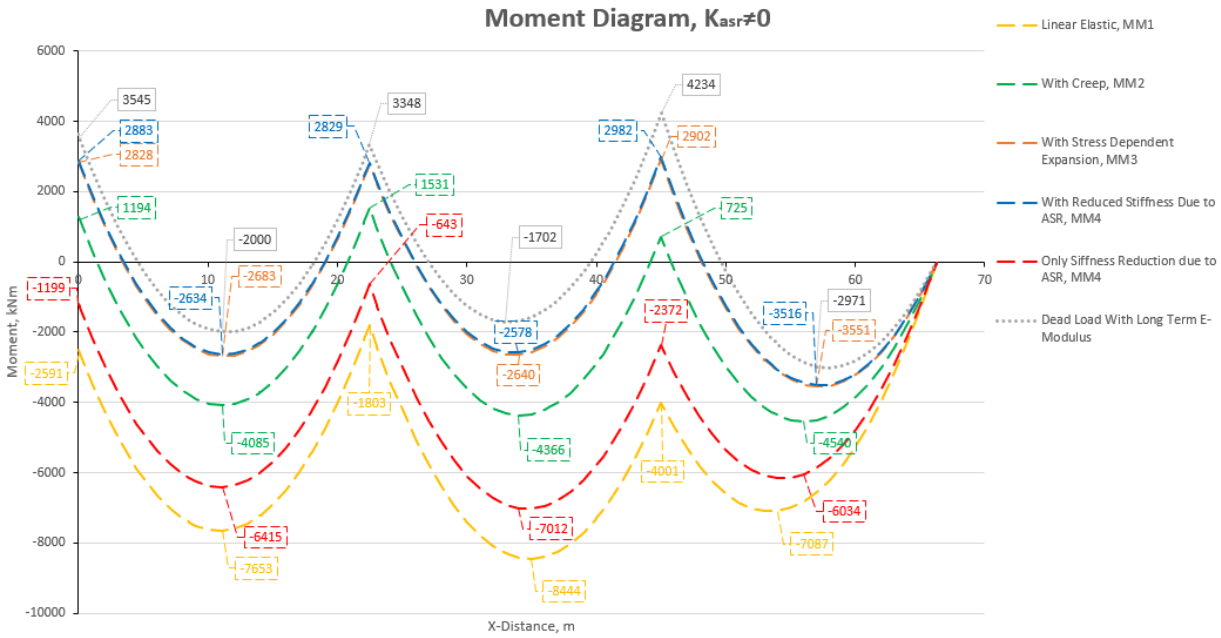

Figure 5.14: Comparison of combined moment diagrams for case 2A with ASR gradient

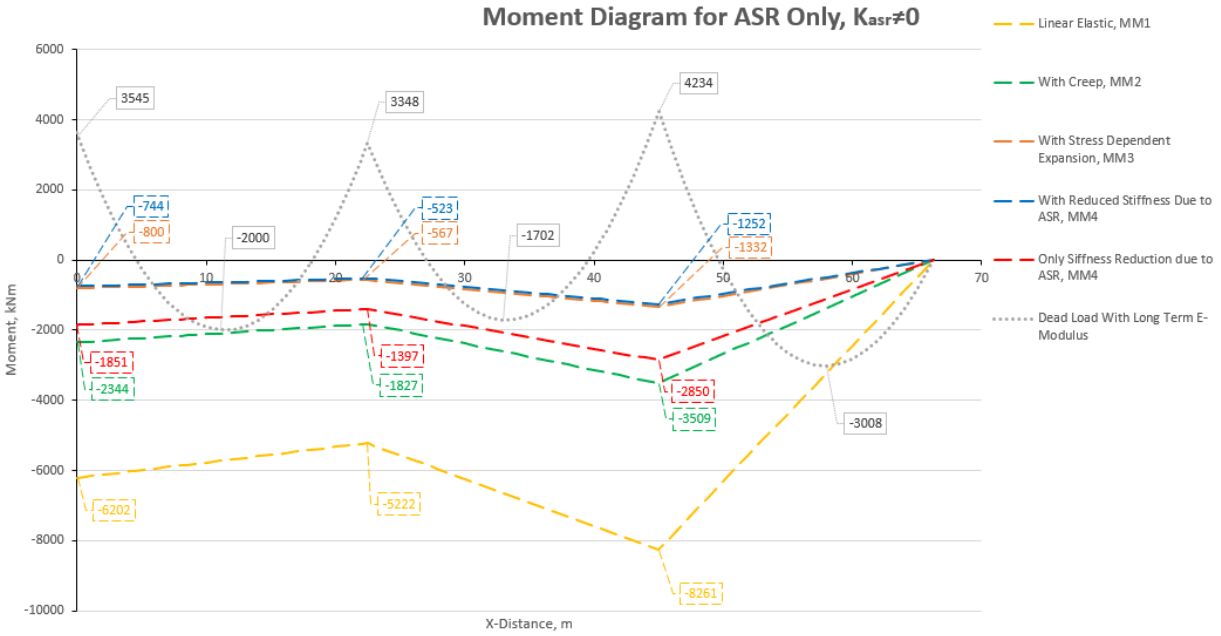

Figure 5.15: Comparison of ASR induced moments for case 2A with ASR gradient

It is seen in figure 5.14 and 5.15 that by applying a non-uniform ASR strain the ASR load actions increases for each material model compared to case 1A where the ASR strain was uniform. This implies also greater differences for the combined moments. It is seen that the combined moment for MM1 and MM2 now changes signs at the supports. The moments at the supports calculated from MM1 and MM2 have tension at the bottom part of the cross section. Where as MMA, MM3 and MM4 results in tension at the top, similar to the original state without ASR.

MM1 gives the largest ASR load action with a maximum value of -8261kNm at support 3. MM1 uses the short time E-modulus giving a mush higher E-module than in reality. MM1 is therefore not relevant as the induced ASR moment is not representative. The other material models uses the long term E-modulus, these results are therefore more representative to the reality which is reflected in ASR-moment diagram in figure 5.15

This shows the importance of using material models that describe the ASR development accurately as well as the importance of how the ASR induced strains is described over the height.

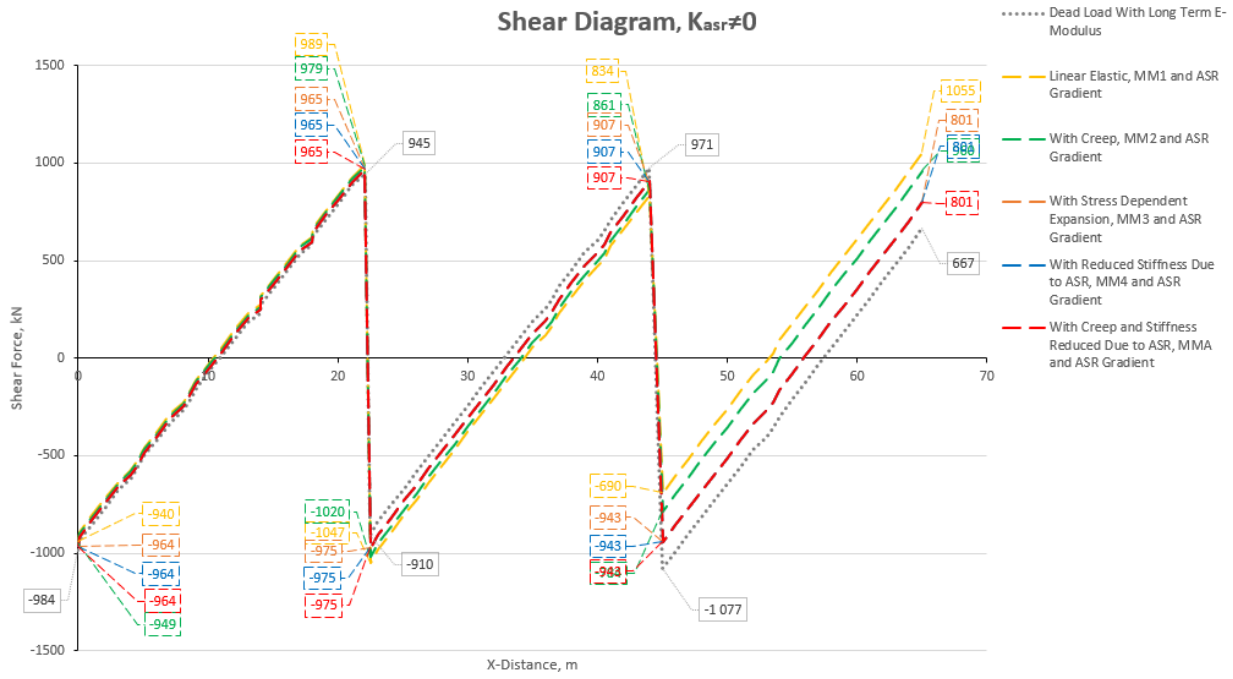

Figure 5.16: Comparison of shear diagrams for case 2A with ASR gradient

By including curvature the shear force has a change in span 3 for every material model compared to case 1A without curvature, as seen in 5.16. The shear forces at the right end increases and is reduced at support 3. This is due to the fact that the introduction of ASR redistributes the stresses thus changing the support stresses. Concrete shear capacity is a function, of amongst others, the strain state of the longitudinal reinforcement and concrete compressive strength. As the third span has a less amount of longitudinal reinforcement than span 1 and 2 larger bending moments occurs in span 3, meaning that the shear force is redistributed at the supports which respectively offsets the distribution of shear throughout the span.

Figure 5.17 shows that the axial force in case 2A with non-uniform ASR strain is zero. This is as expected.

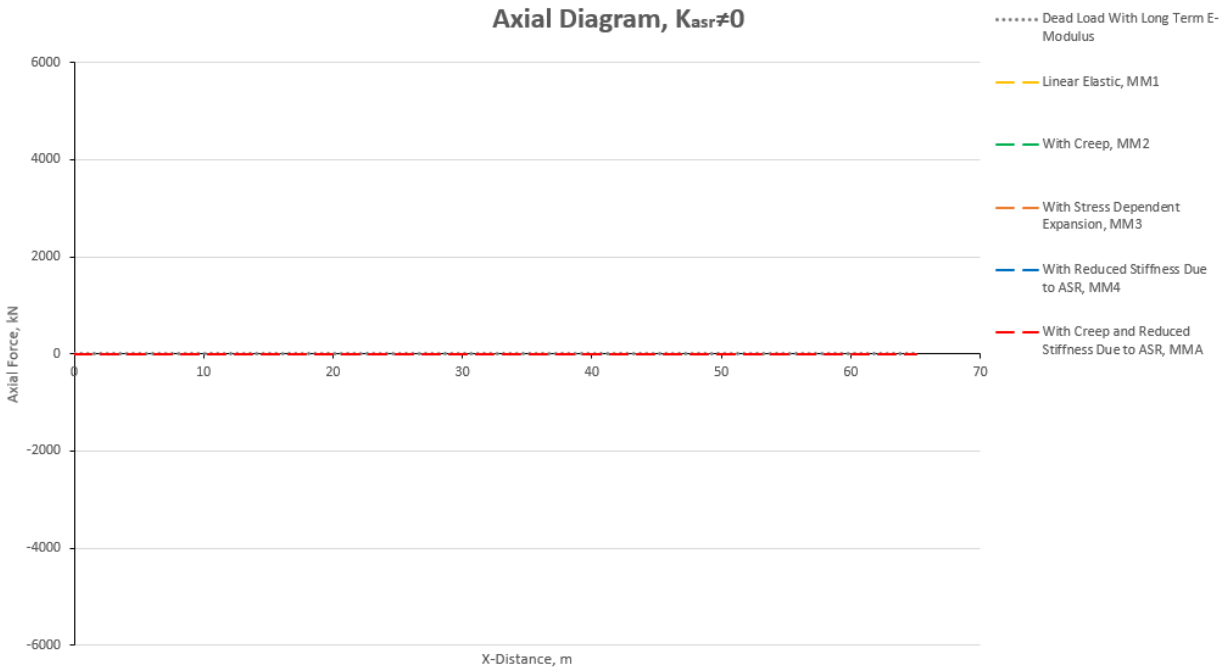

Figure 5.17: Comparison of axial diagrams for case 2A with ASR gradient

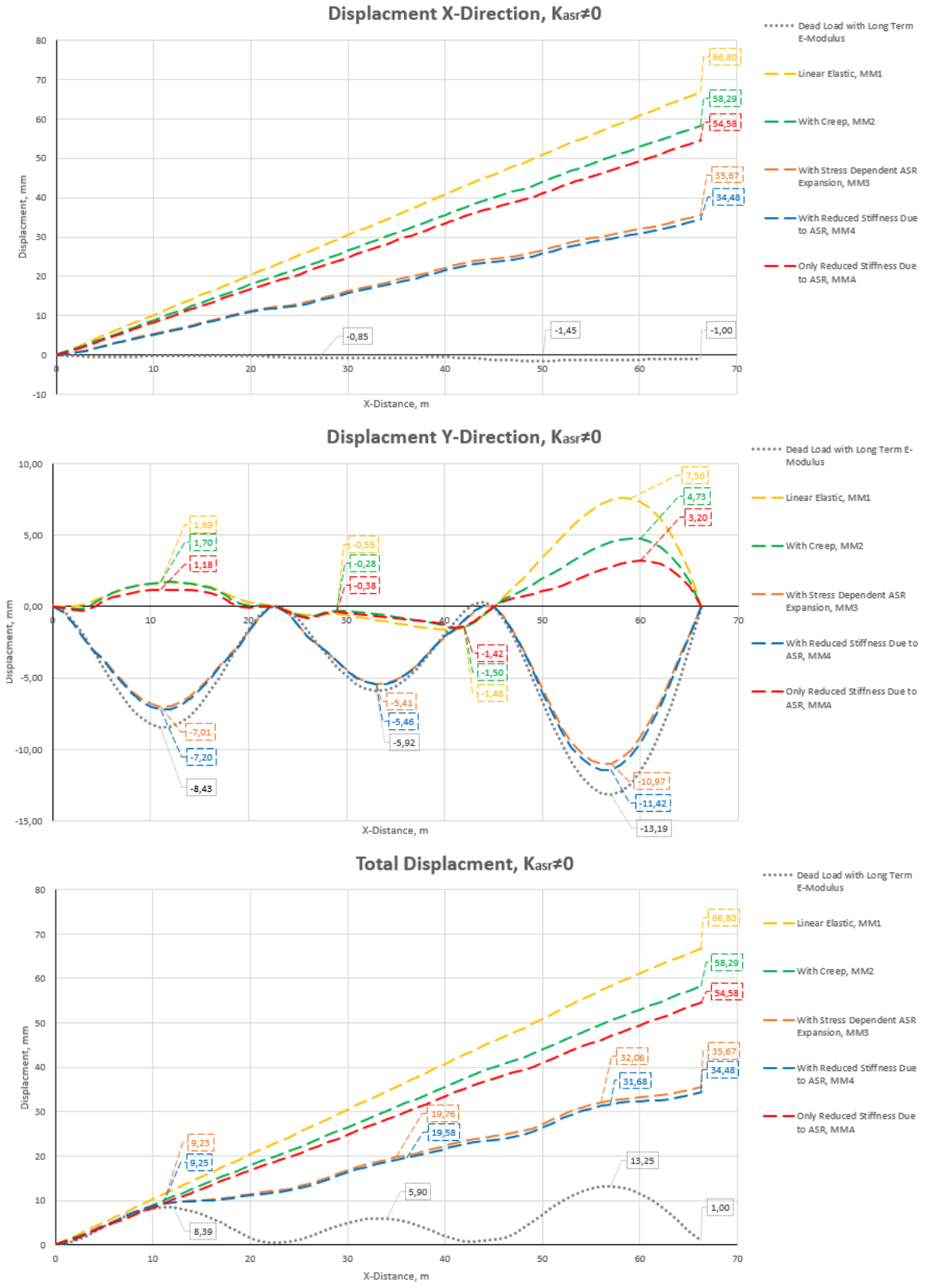

Figure 5.18: Comparison of displacements for case 2A with ASR gradient

Table 5.8: Displacement and strains case 2A, $\kappa \neq 0$

	δ_x	ε_x
MM1	66.80	0.0010
MM2	58.29	0.00088
MMA	54.58	0.00082
MM3	35.67	0.00054
MM4	34.48	0.00052

When the ASR strain is given a curvature, displacement in x-direction and total strain increases compared to without a gradient, as seen in figure 5.18 and table 5.8. It is observed that the material models have the same relationship between themselves both with and without a curvature. MM3 and MM4 gives the most accurate results, meaning that the ASR expansion at least must include stress dependent ASR expansion.

Case 2B Without ASR Gradient

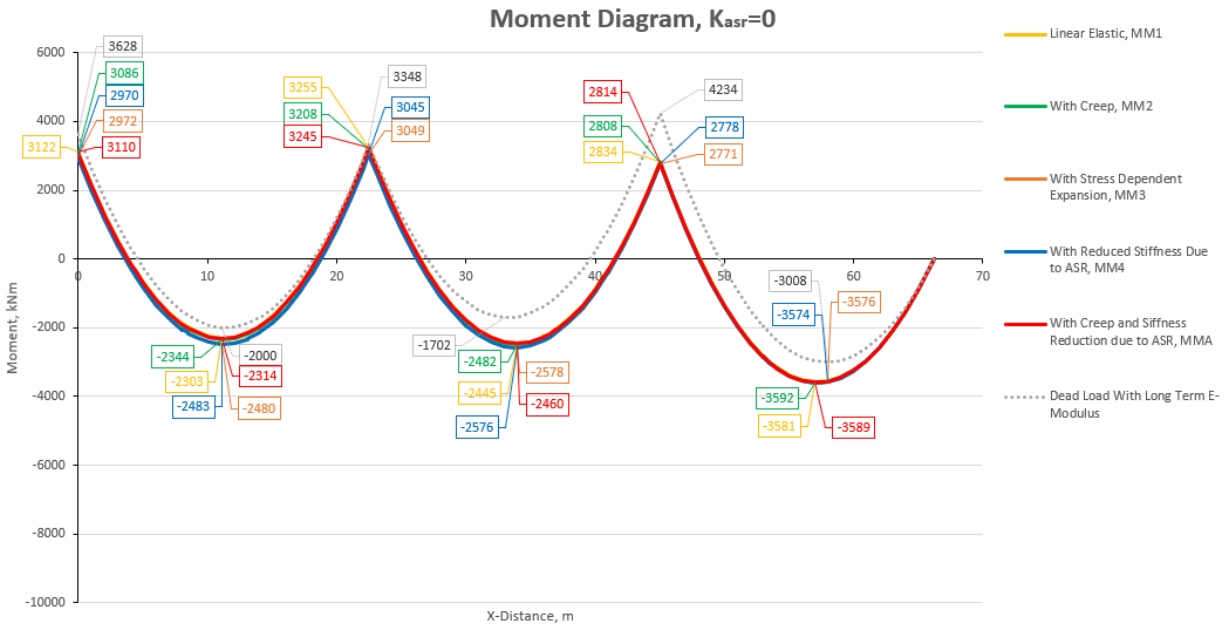

Figure 5.19: Comparison of combined moment diagrams for case 2B without ASR gradient

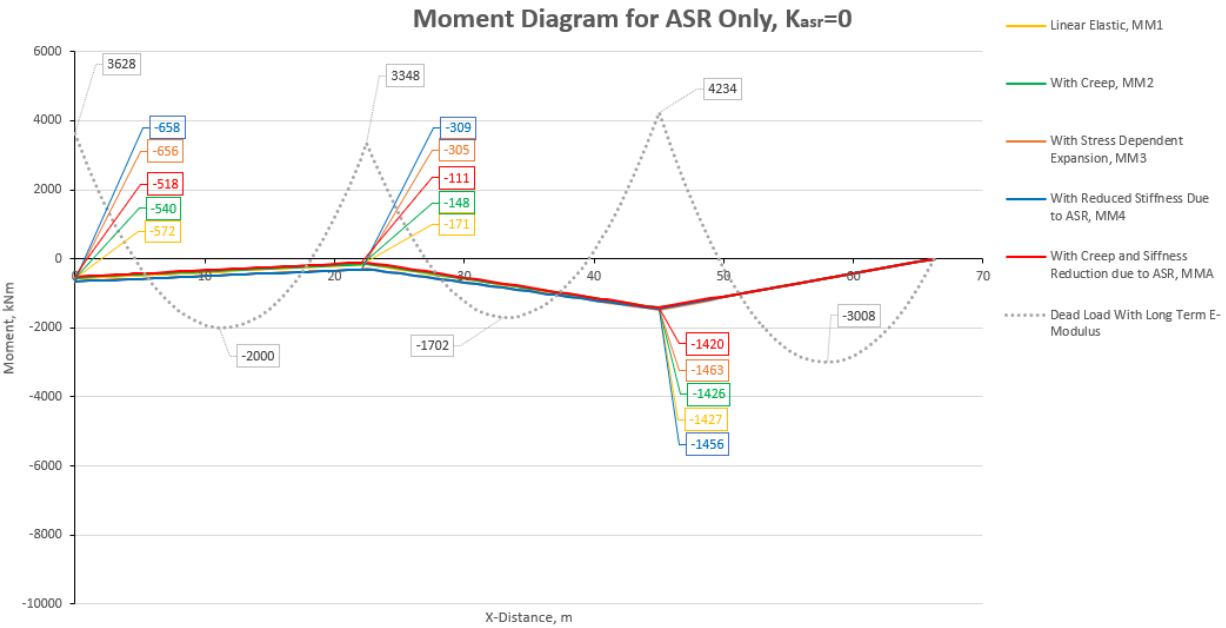

Figure 5.20: Comparison of ASR induced moments for case 2B without ASR gradient

As the material models are given the exact same end deformation and since the ASR expansion is uniform, the load action due to ASR is approximately the same in every model, seen in figure 5.24 and 5.20. The load action are negative, leading to a larger negative total moment. The biggest moment difference from the the original state is observed in span three with a increased negative moment of approximately 570kNm ($\sim 20\%$).

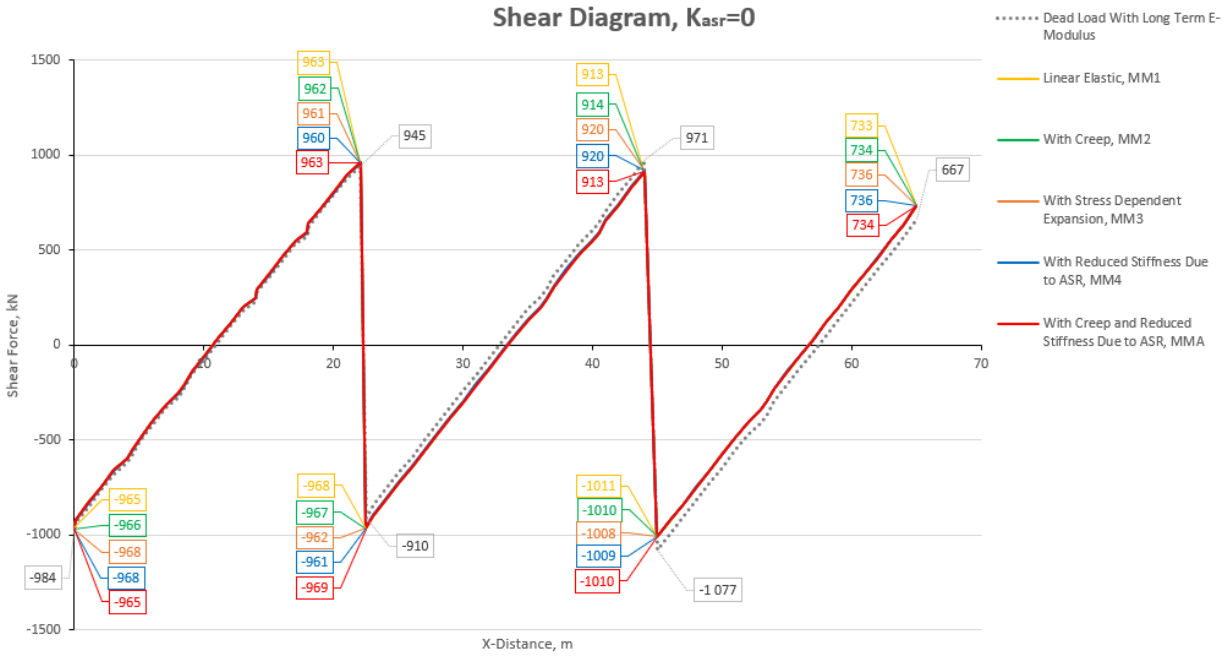

Figure 5.21: Comparison of shear diagrams for case 2B without ASR gradient

The load action due to ASR are equal for every material mode and the total moment is slightly increased. As seen in figure 5.21 this leads to minor changes in the shear force as the supports. The shear force have the same development throughout the beam as only the dead load effects development of the shear force.

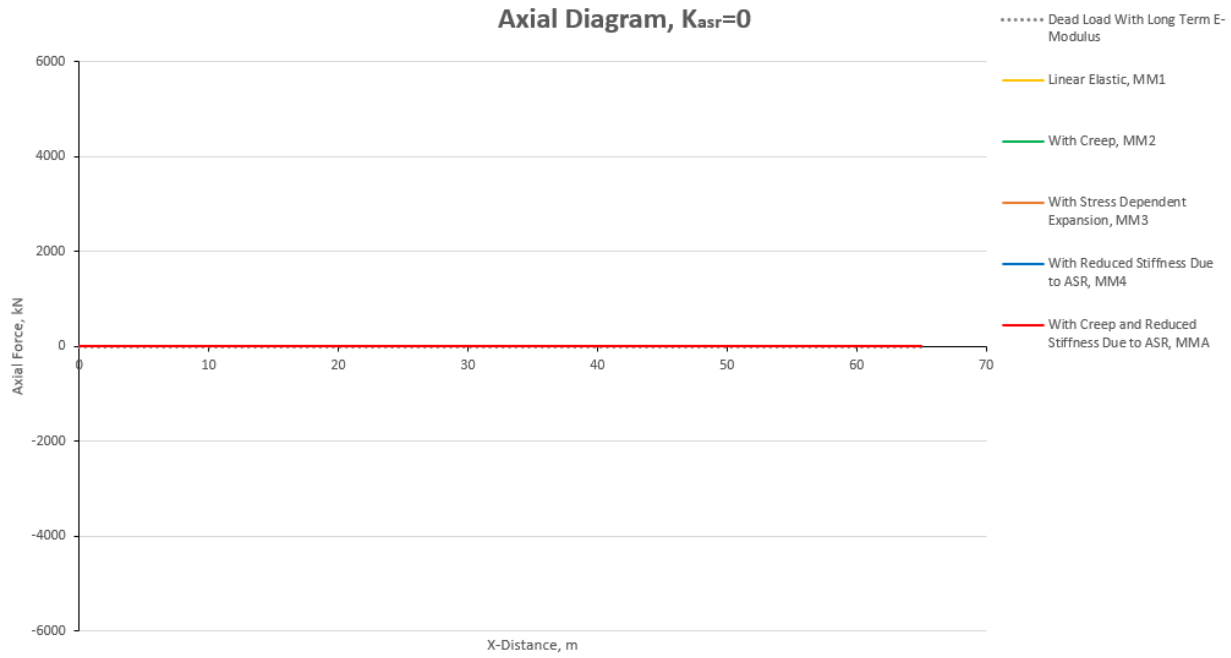

Figure 5.22: Comparison of axial diagram for case 2B without ASR gradient

Figure 5.22 shows that the axial force in case 2B with uniform ASR strain is zero. This is as expected.

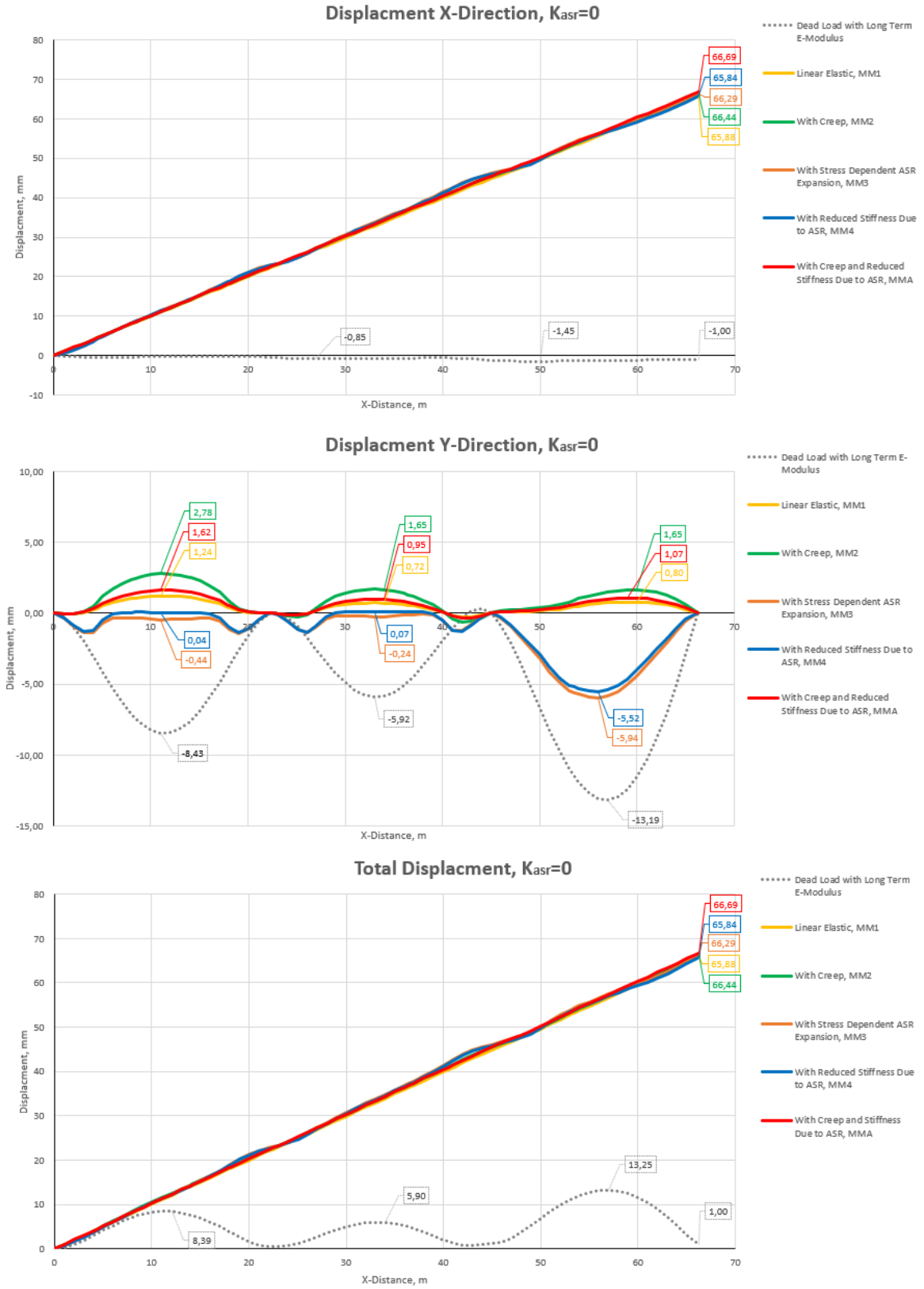

Figure 5.23: Comparison of displacements for case 2B without ASR gradient

Seen in figure 5.23, since the end deformation is fixed, each material model experience the same x-deformation. The impact and difference of y-deformation is thus due to the stiffness which depends on the material model. The including parameters in MM3 and MM4 results in negative y-deformations. MM1, MM2 and MMA results in positive y-deformations. Table 5.9 shows the occurring strains in every material model regarding case 2B with uniform ASR expansion and fixed end displacement.

Table 5.9: Displacement and strains case 2B, $\kappa = 0$

	ε	$\overline{\varepsilon}_{asr}$
MM1	0.001	0.00108
MM2	0.001	0.00125
MMA	0.001	0.0024
MM3	0.001	0.00255
MM4	0.001	0.00112

Case 2B With ASR Gradient

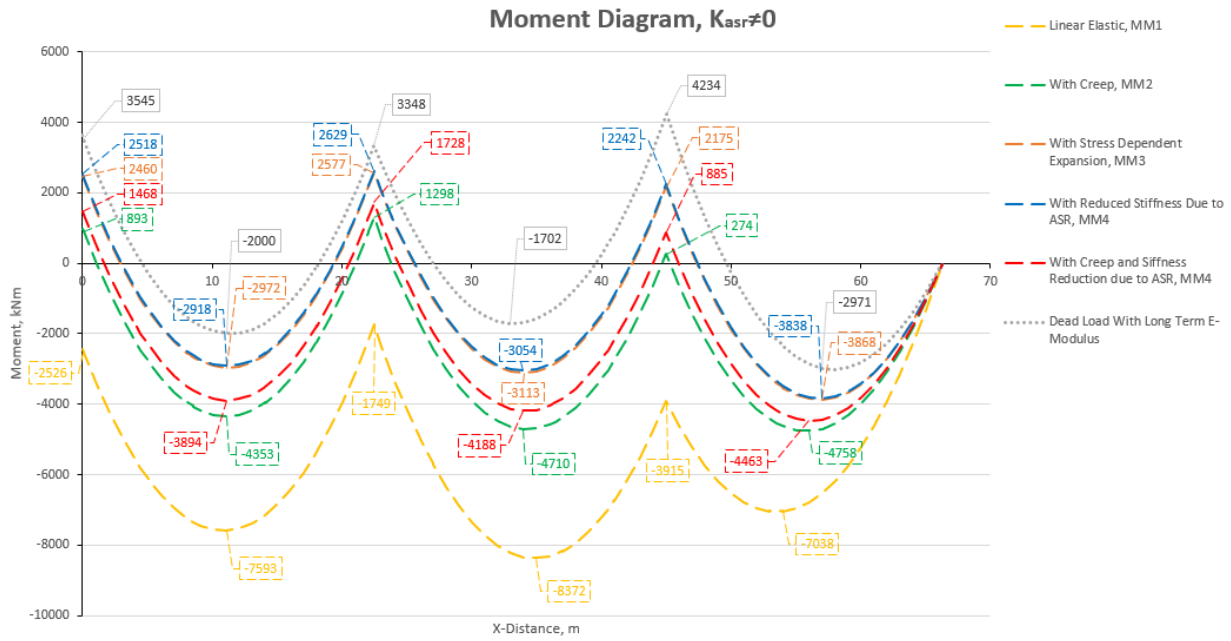

Figure 5.24: Comparison of combined moment diagrams for case 2B with ASR gradient

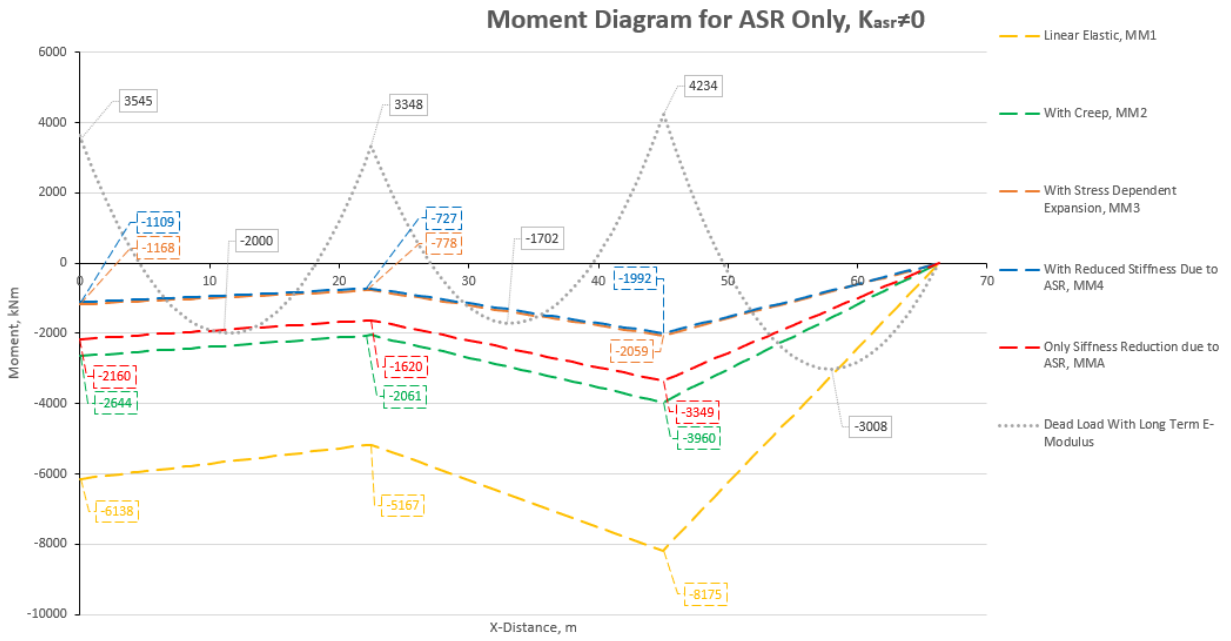

Figure 5.25: Comparison of ASR induced moments for case 2B with ASR gradient

By including a curvature to the ASR strains it is seen that the load action due to ASR increases for every material model, as seen in figure 5.24 and 5.25. There is also a much larger difference between the material models when curvature is includes compared to without a curvature. This increase and change is due to the fact that the curvature leads

to a vertical deformation. As the beam is restrained in y-direction the vertical deformation is obtained by the supports which leads to an increase of restraint moment forces.

Non-uniform expansion also entails that the more describing the material models is, the less restraint moment forces occurs, giving a more accurate result of the forces. MM3 and MM4 provides the least difference from the original state where the occurring moment at support one are reduced approximately by 1000kNm ($\sim$ 30%), and at support two reduced approximately by 700kNm ($\sim$ 20%). Support three have larger differences from the original state, where MM3 and MM4 provides a reduction of the moment by approximately 2000kNm ($\sim$ 50%).

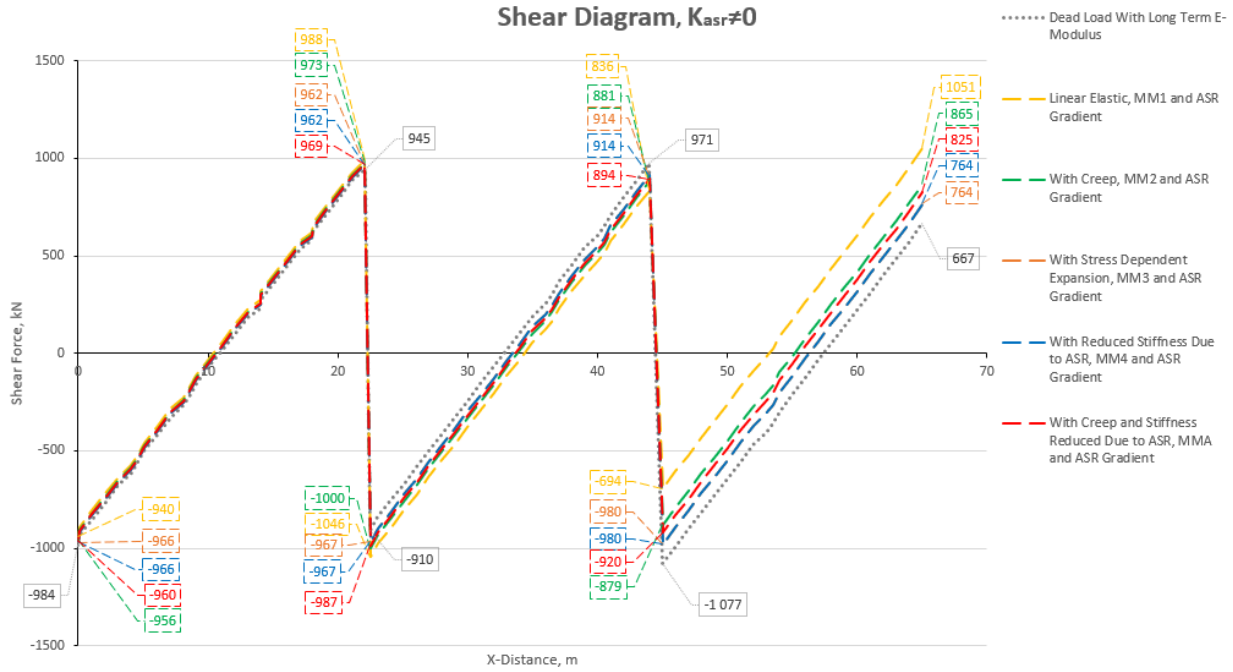

Figure 5.26: Comparison of shear diagrams for case 2B with ASR gradient

Much of the same development regards the material models seen in the moment diagrams are also seen in the shear diagram in figure 5.26. Span one and two have approximately the same shear values. In span three the shear values differs at support three and at the right end support. The difference in span three is due to relationships between moment and share, where the shear value at a given point is a result of the slope of the moment at the same point. Span three has less reinforcement than span one and two, leading to larger occurring moments in this span. This again leads to larger differences in the shear values in span three.

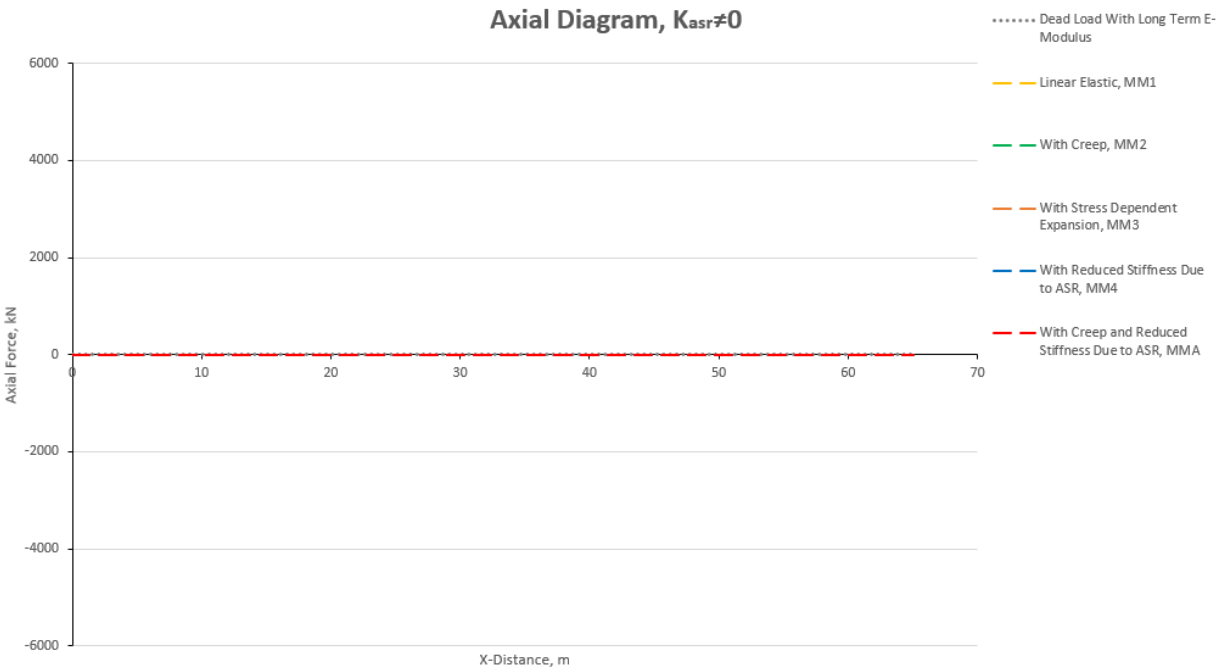

Figure 5.27: Comparison of axial diagrams case 2B with ASR gradient

Figure 5.27 shows that the axial force in case 2B with non-uniform ASR strain is zero. This is as expected.

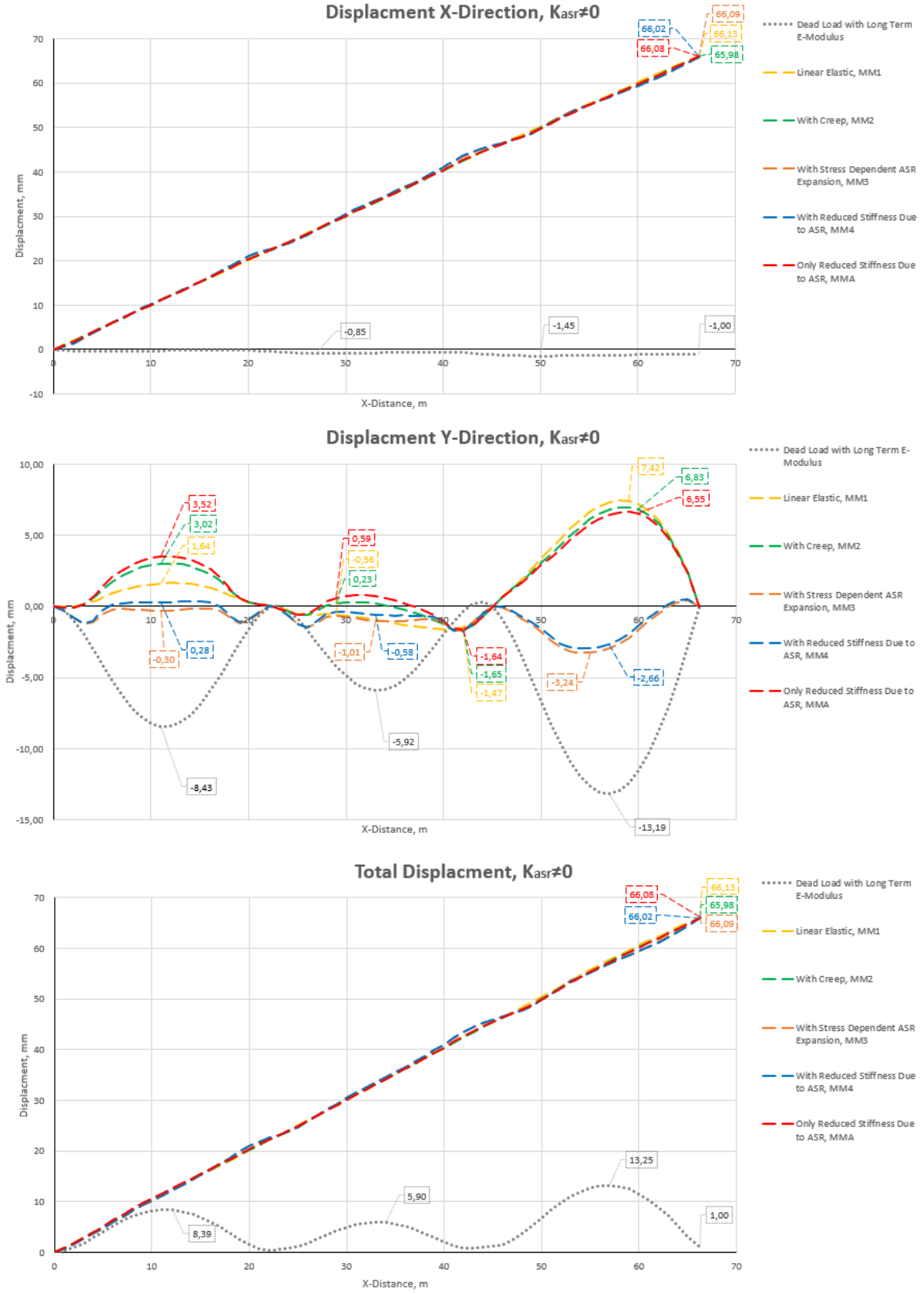

Figure 5.28: Comparison of displacements for case 2B with ASR gradient

Seen in figure 5.28 it is observed that when curvature is included deformation in y-direction increases significant. The curvature leads to vertical deformations which due to the support constraints results in larger load actions. As the end displacement is set, stresses that occur upon the set displacement limit causes the beam to deflect in the y-direction as the beam now is "restrained" in x-direction. If the beam can withstand these stresses, it causes the beam to deflect upwards as seen for MM1, MM2, MMA.

Larger y-deformations is observed for MM3 and MM4 compared to case 2A, in which the reason is due to fixed end deformation. The x-deformation is approximately twice the size in case 2B as in case 2A. MM1, MM2 and MM4 experiences approximately the same x-deformation in both case 2A and case 2B, resulting in almost the same development of y-deformations. Strains and curvature used in case 2B with non-uniform ASR expansion is seen in table 5.10.

Table 5.10: Strains and gradients for case 2B, $\kappa \neq 0$

	ε	$\overline{\varepsilon}_{asr}$	κ_{asr}
MM1	0.001	0.00099	3.79e-7
MM2	0.001	0.00113	4.32e-7
MMA	0.001	0.0022	8.42e-7
MM3	0.001	0.00235	9e-7
MM4	0.001	0.00122	4.67e-7

Case 2C with Tension

Results from each material model in case 2C can be found in Appendix B. From the results it is observe that the moment is significantly decreased due to the applied tension force. It appears that the axial tension force helps the ASR expansion which results in decreased restraint forces from ASR. The moment diagram is similar to the moment diagram seen in case 2A and case 2B without gradient. It was observed in case 2A and 2B that the gradient had great impact on the moment diagram. However, when an axial tension force is applied the ASR gradient has a significantly less impact as seen in figure 5.29 and 5.30.

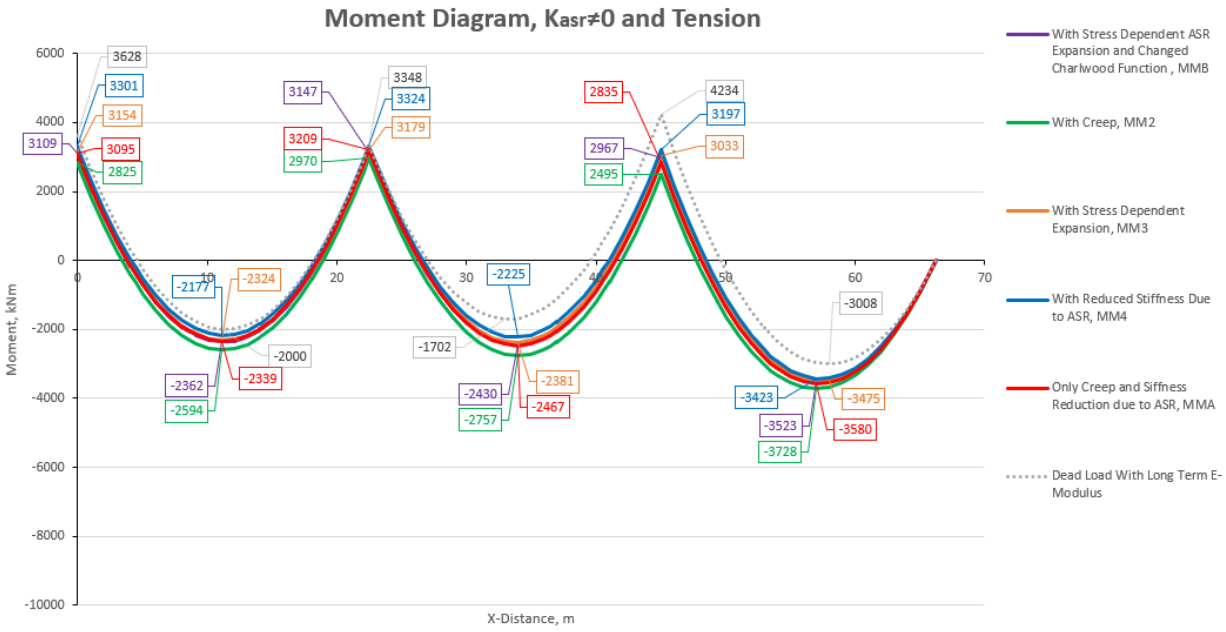

Figure 5.29: Comparison of combined moment diagrams for case 2C in tension

The most interesting observation from ASR restraint forces shown in figure 5.30 is that the reduction of stiffness due to ASR (MM4) has changed from its previous material model (MM3). In previous cases material model MM3 and MM4 had little to no difference, even when ASR gradient was applied. It seems like the axial tension force increases the stiffness reduction due to ASR. This is a important discovery since material model MM4 was observed to be not necessary in the structure assessment in the previous cases. But know it is observed that stiffness reduction due to ASR has a greater impact to the load action when tension occurs. The change in material constant σ_u to the charlwood function in the stress dependent ASR model (MMB) seems to have little impact when tension occurs. It is similar to stress dependent ASR model (MM3). Another interesting observation is

that the stress dependent ASR model (MM3) is similar to the material model with only reduced stiffness due to ASR and creep (MMA). Is seem that the stress dependent ASR expansion has less impact to the load action when axial tension forces are applied. By comparing material models MMA and MM4 we can see the impact from MM3 (200kNm) which is much smaller compared to the stress dependent ASR expansion model (MM3) showed in case 2A (1527kNm) and case 2B (1290kNm) with ASR gradient.

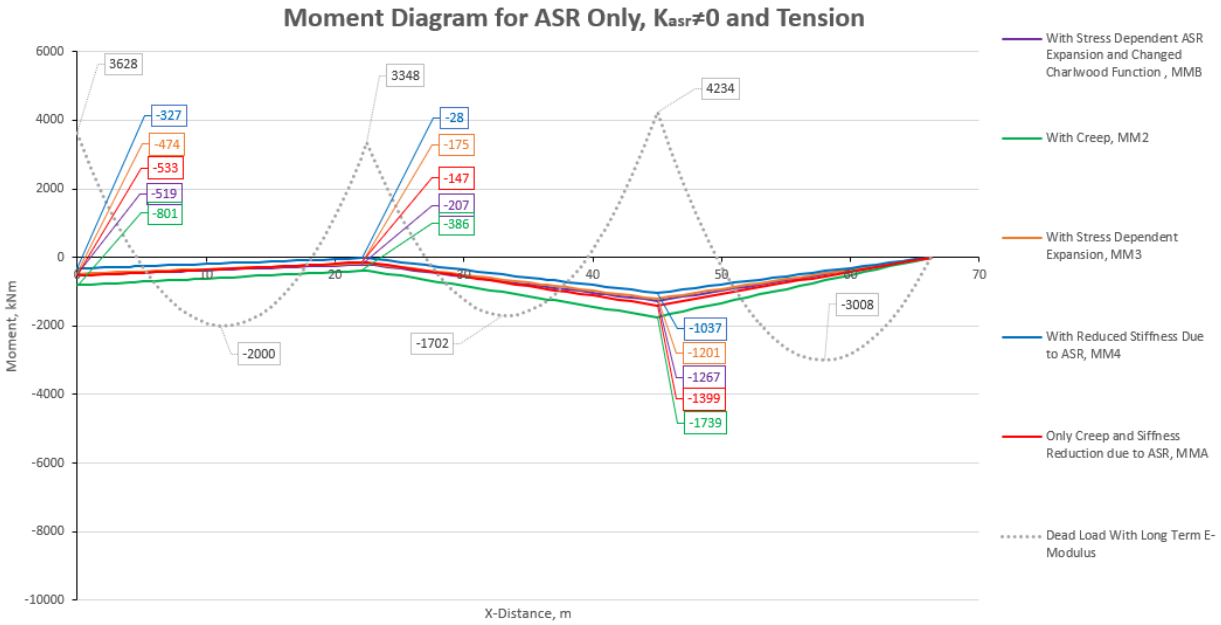

Figure 5.30: Comparison of ASR induced moments for case 2C in tension

The shear forces in case 2C seen in figure 5.31 are similar for the different material models. The axial tension force reduces the difference and the impact of the material models even if ASR gradient is applied.

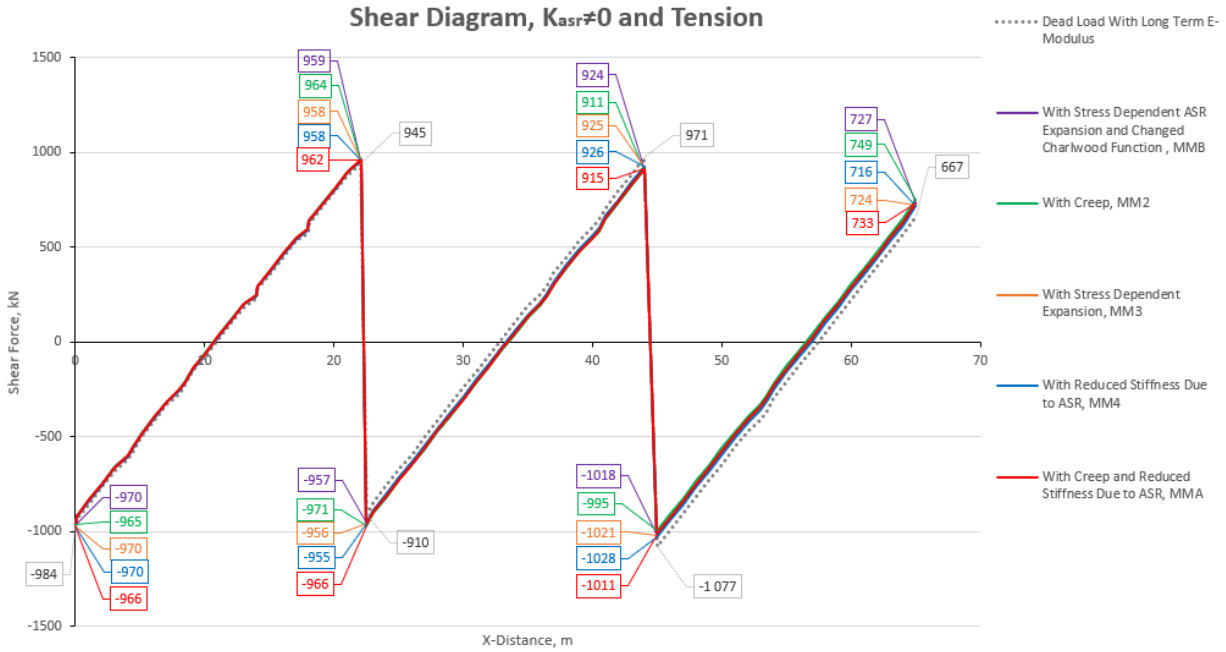

Figure 5.31: Comparison of shear diagrams for case 2C in tension

Axial force is correct as it shows the beam having 5000kN tension in figure 5.32.

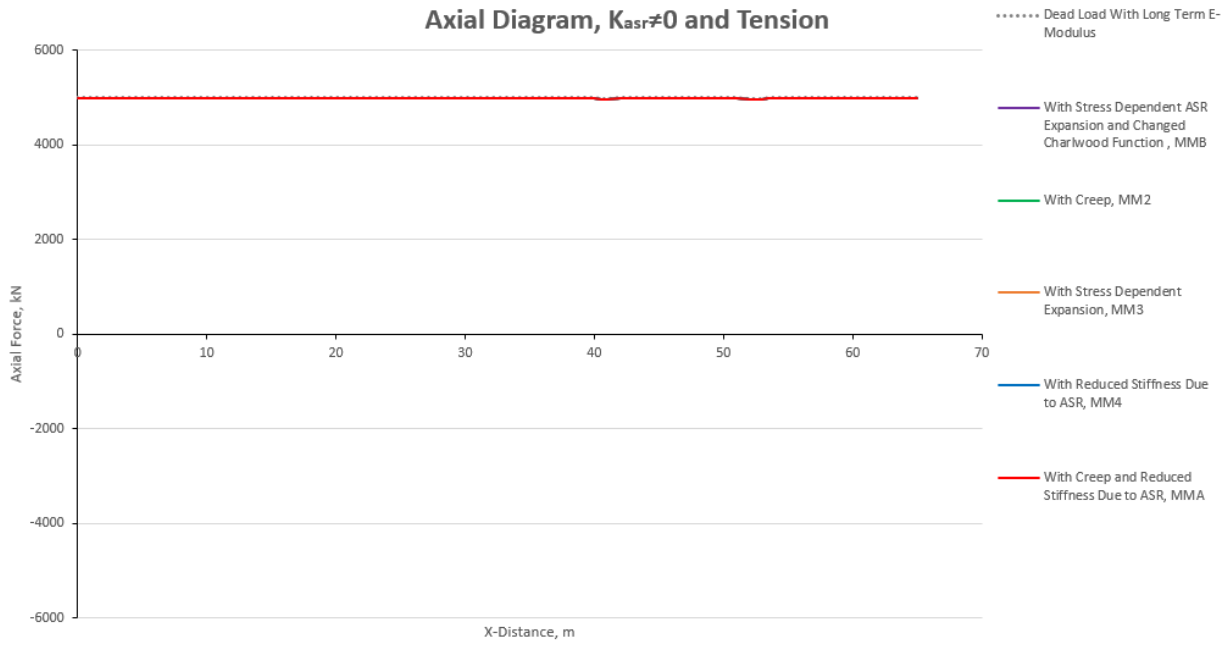

Figure 5.32: Comparison of axial diagrams for case 2C in tension

The displacement showed in figure 5.33 verifies what has been discussed earlier. The axial tension force helps the ASR expansion which leads to having less displacement in the y-direction. By applying the axial tension force the free ASR strain adjusted to get the

fixed end displacement have also been smaller, seen in table 5.11. The changes in material constant to the Charlwood function for stress dependent ASR expansion (MMB) has influence on the displacement in y-direction. This can be observed by comparing material model MM3 to MMB.

Table 5.11: Strains and gradients for case 2C, $F_x = Tension$

	ε	$\overline{\varepsilon}_{asr}$	κ_{asr}
MM2	0.001	0.00087	3.33e-7
MMA	0.001	0.00087	3.33e-7
MM3	0.001	0.001	3.83e-7
MMB	0.001	0.001	3.83e-7
MM4	0.001	0.00099	3.79e-7

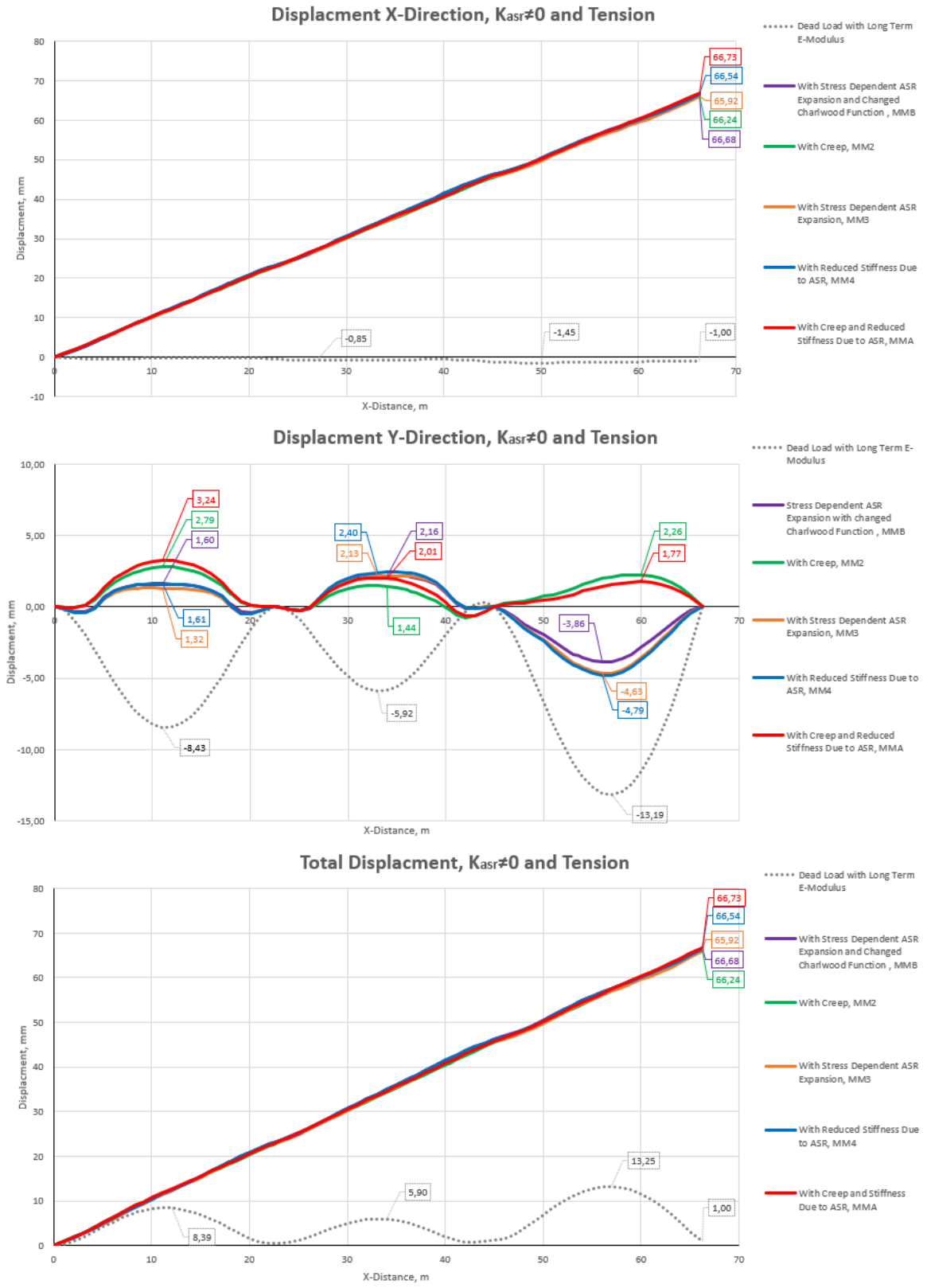

Figure 5.33: Comparison of displacements for case 2C in tension

Case 2C with Compression

As expected from the discussion of case 2C with tension axial force, the compression force will then give greater moments for the different material models, seen in figure 5.34 and 5.35. The compressive axial force makes it harder for the beam to expand because it counteracts the ASR expansion. In this analysis we can observe that the reduces stiffens due to ASR (MM4) is similar to stress dependent ASR expansion (MM3). The moment forces are reduced in the span of the beam and increased at the supports compared to moment forces from material model MM2 and MMA. The beam will have tension at the top of the supports compared to MM2and MMA where the beam has tension on the bottom and compression at the top. Material model MM3 and MM4 has the greatest impact to the moment forces. Stiffness reduction due to ASR (MM4) has no benefit when stress dependent ASR expansion is included (MM3). Reduction of stiffness due to ASR and creep (MMA) has an impact on the moment forces compered to material model MM2.

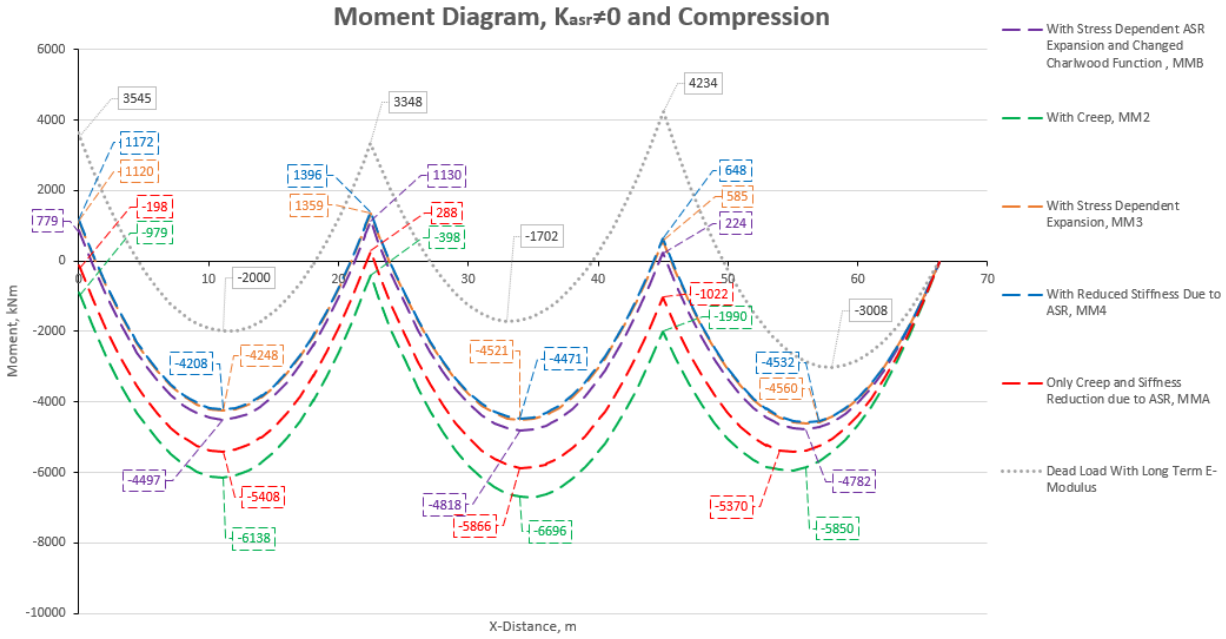

Figure 5.34: Comparison of combined moment diagrams for case 2C in compression

The most interesting observation from the results shown is that the stress dependent ASR expansion with changed charlwood function (MMB) has an increase in moment compared to MM3. As we have increased the material constant σ_u that allows the stress dependent ASR expansion more stresses increasing the moments similar. These material constant very from the concrete mixture used in the structure. Material model MM3 will influence

the action loads of the structure different for concrete structures with different concrete mixes.

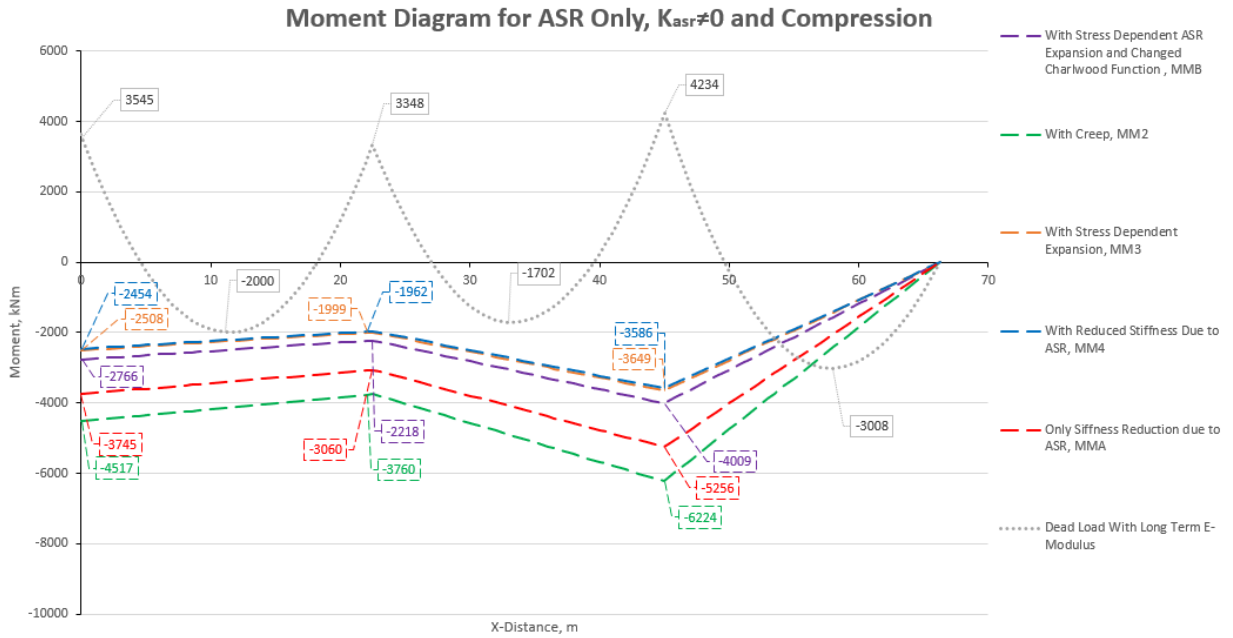

Figure 5.35: Comparison of ASR induced moments for case 2C in compression

The axial compression force also influenced the shear force as the magnitude of shear force between the material models have increased compared to case 2A and 2B with gradient, seen in figure 5.36.

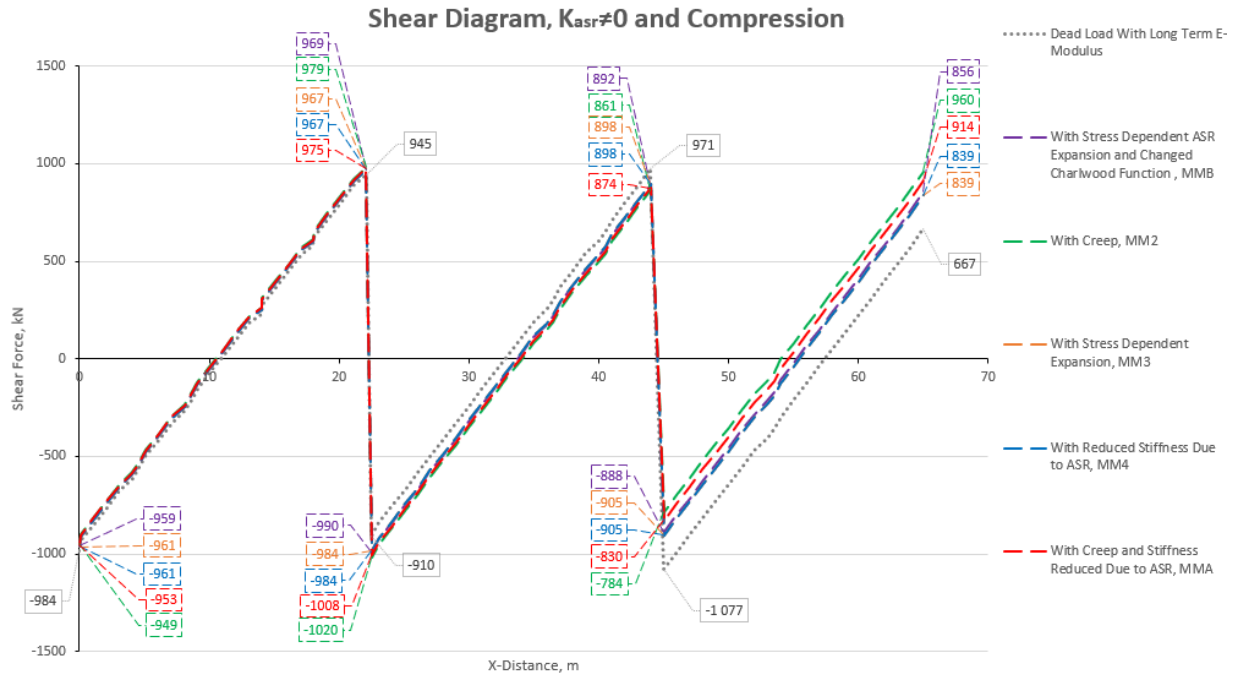

Figure 5.36: Comparison of shear diagrams for case 2C in compression

Seen in figure 5.37 the axial force is correct as it shows the beam having -5000kN compression.

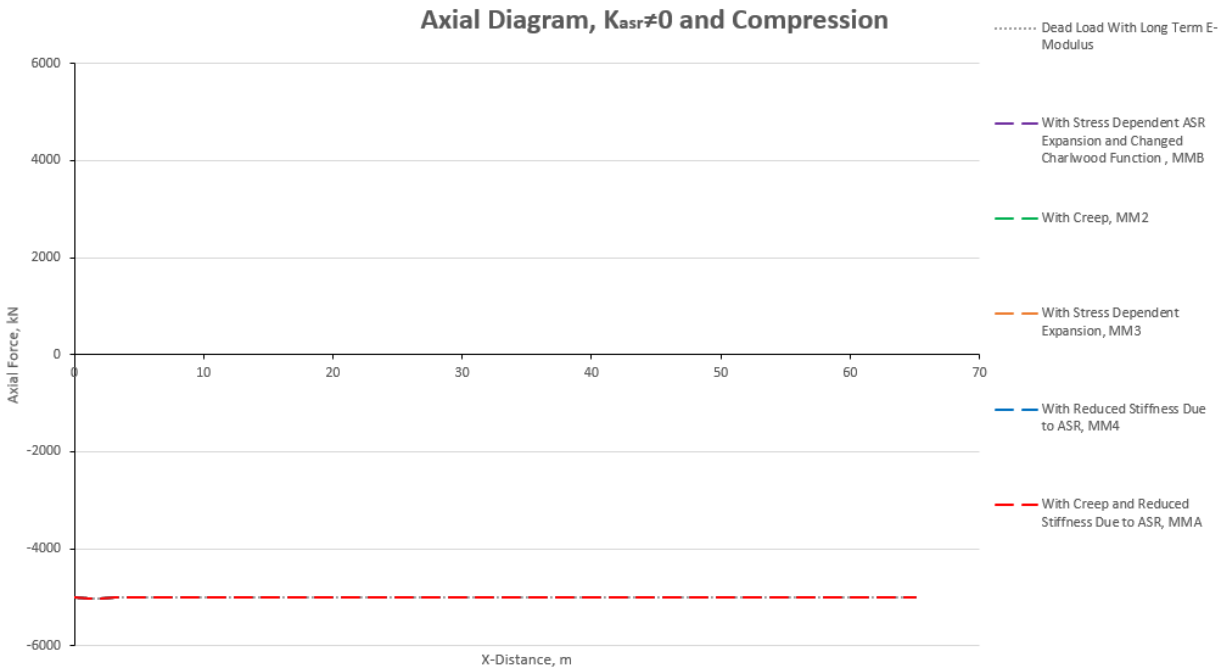

Figure 5.37: Comparison of axial diagrams for case 2C in compression

From the displacement i y-direction it can be observed that the axial compression force has increased the displacement for MM1, MM2 and MMA as expected. The most interesting observation is at the third span MM3 and MM4 has changed from having downward displacement as previously shown to now having upwards displacement. MMB has different displacement in the y-direction then material model MM3. This shows that the change of material constant in the Charlwood function has influence on the displacement also.

Displacement is seen in figure 5.38. Strain and curvature values is seen in table 5.12.

Table 5.12: Strains and gradients for case 2C, $F_x = Compression$

	ε	$\overline{\varepsilon}_{asr}$	κ_{asr}
MM2	0.001	0.0014	5.36e-7
MMA	0.001	0.00165	6.32e-7
MM3	0.001	0.0044	1.68e-6
MMB	0.001	0.00335	1.28e-6
MM4	0.001	0.0052	1.99e-6

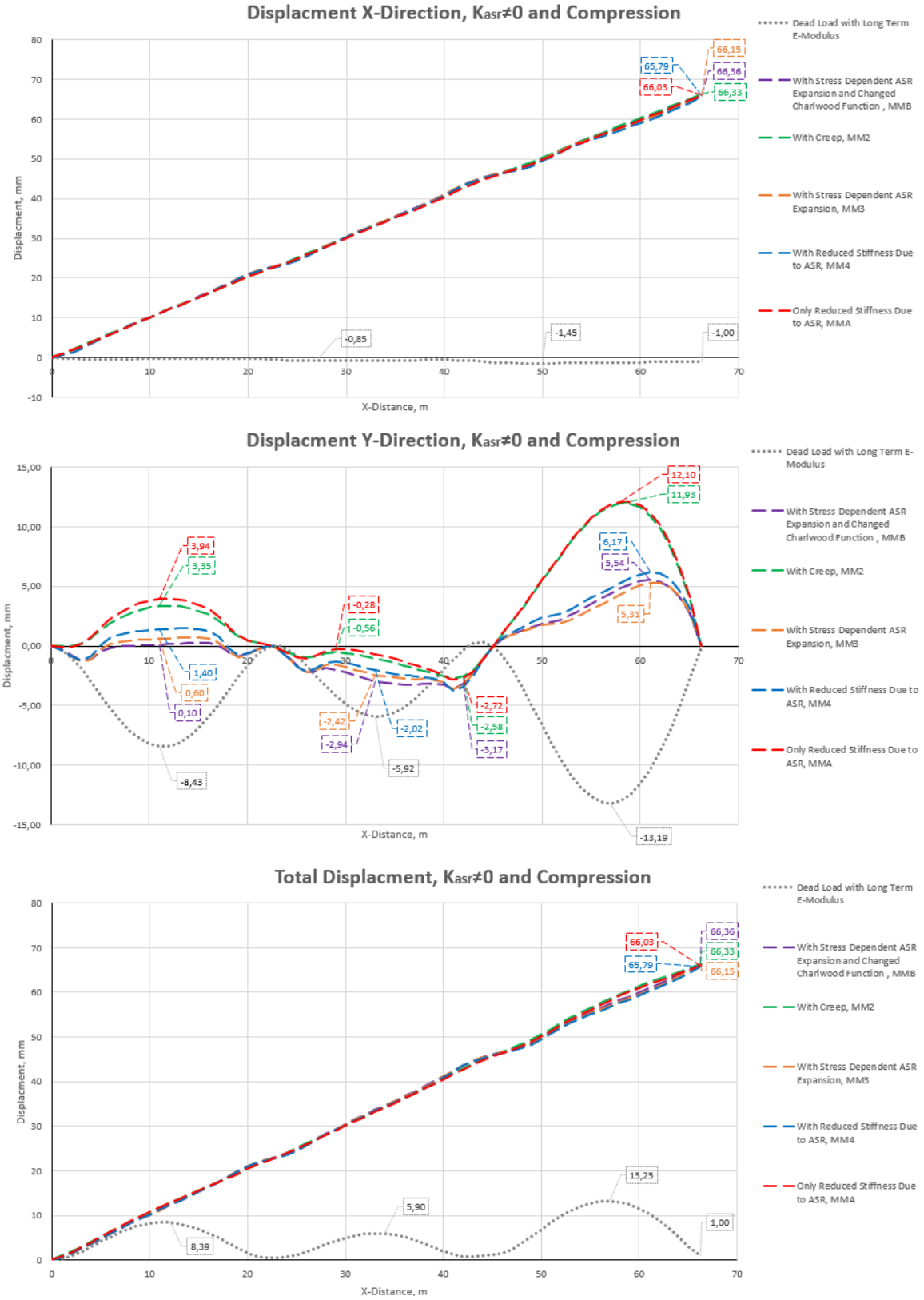

Figure 5.38: Comparison of displacements for case 2C in compression

Structural Analysis of Reinforced Concrete Beams Affected by Alkali-Silica Reaction

Chapter 6, 7 and 8

Discussion, Conclusion and Further Work

Oslo Metropolitan University

Engineering and Building Technology

15th of June 2020, Oslo, Norway

6 Discussion of Case Studies

Modeling of Reinforced Concrete Beams

The FEM software Abaqus was used to conduct the structural analyses in the case studies presented in chapter 4 and 5. The reinforced concrete beams were modeled by using beam elements for the concrete and truss elements for the reinforcement. The concrete and reinforcement were divided into multiple 1m elements dependent on the length of the beam. The reinforced concrete beams used kinematic coupling to connect the concrete element to the reinforcement elements in Abaqus.

There were challenges regarding the modeling of the beams, especially for the three span beam. Every concrete element had to manually be connected to the other reinforcement elements with kinematic coupling, every element had to be given a material property and a cross section. This was time consuming and required a lot of focus in the modeling. The model three span beam with kinematic coupling is shown in figure 6.1. The post-processing of the results also presented challenges, were we had to develop systems in excel for the calculation of the load actions and displacements. The development of the system in excel was time consuming and required many attempts before right results were calculated. Example of post-processing is shown in figure 6.2.

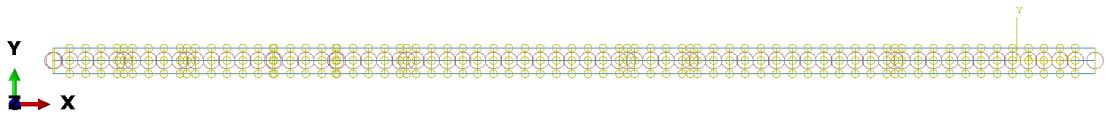

Figure 6.1: Kinematic coupling between the concrete elements and reinforcement elements in Abaqus

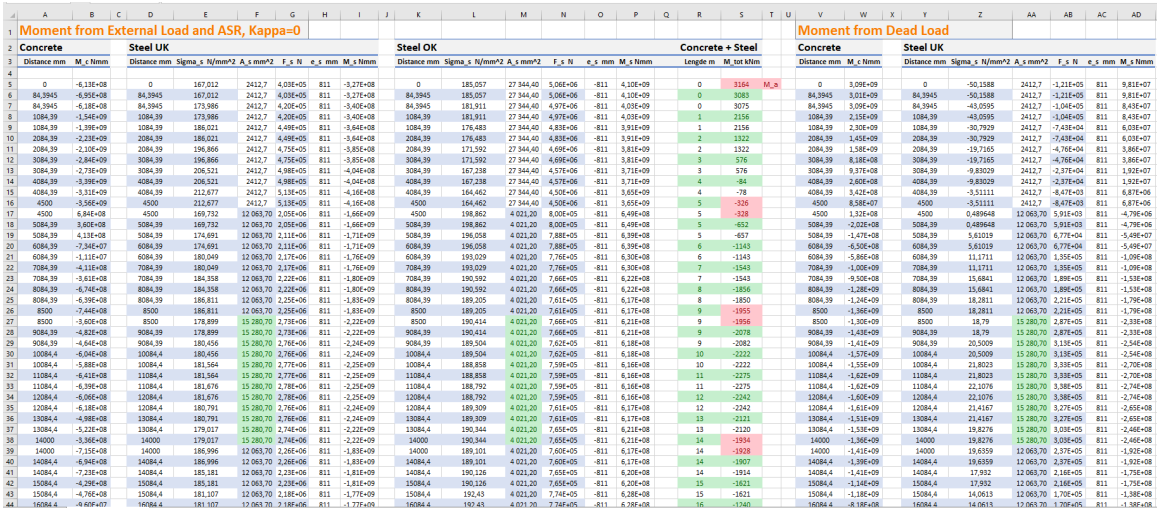

Moment from External Load and ASR, Kappa=0

Concrete		Steel UK							Steel OK							Concrete + Steel		
Distance mm	M_c Nmm	Distance mm	Sigma_s N/mm^2	A_s mm^2	F_s N	e_s mm	M_s Nmm		Distance mm	Sigma_s N/mm^2	A_s mm^2	F_s N	e_s mm	M_s Nmm		Lengde m	M_tot kNm	
0	-6,13E+08	0	167,012	2412,7	4,03E+05	811	-3,27E+08		0	185,057	27 344,40	5,06E+06	-811	4,10E+09		0	3164	M_a
84,3945	-6,95E+08	84,3945	167,012	2412,7	4,03E+05	811	-3,27E+08		84,3945	185,057	27 344,40	5,06E+06	-811	4,10E+09		0	3083	
84,3945	-6,18E+08	84,3945	173,986	2412,7	4,20E+05	811	-3,40E+08		84,3945	181,911	27 344,40	4,97E+06	-811	4,03E+09		0	3075	
1084,39	-1,54E+09	1084,39	173,986	2412,7	4,20E+05	811	-3,40E+08		1084,39	181,911	27 344,40	4,97E+06	-811	4,03E+09		1	2156	
1084,39	-1,39E+09	1084,39	186,021	2412,7	4,49E+05	811	-3,64E+08		1084,39	176,483	27 344,40	4,83E+06	-811	3,91E+09		1	2156	
2084,39	-2,23E+09	2084,39	186,021	2412,7	4,49E+05	811	-3,64E+08		2084,39	176,483	27 344,40	4,83E+06	-811	3,91E+09		2	1322	
2084,39	-2,10E+09	2084,39	196,866	2412,7	4,75E+05	811	-3,85E+08		2084,39	171,592	27 344,40	4,69E+06	-811	3,81E+09		2	1322	
3084,39	-2,84E+09	3084,39	196,866	2412,7	4,75E+05	811	-3,85E+08		3084,39	171,592	27 344,40	4,69E+06	-811	3,81E+09		3	576	
3084,39	-2,73E+09	3084,39	206,521	2412,7	4,98E+05	811	-4,04E+08		3084,39	167,238	27 344,40	4,57E+06	-811	3,71E+09		3	576	
4084,39	-3,39E+09	4084,39	206,521	2412,7	4,98E+05	811	-4,04E+08		4084,39	167,238	27 344,40	4,57E+06	-811	3,71E+09		4	-84	
4084,39	-3,31E+09	4084,39	212,677	2412,7	5,13E+05	811	-4,16E+08		4084,39	164,462	27 344,40	4,50E+06	-811	3,65E+09		4	-78	
4500	-3,56E+09	4500	212,677	2412,7	5,13E+05	811	-4,16E+08		4500	164,462	27 344,40	4,50E+06	-811	3,65E+09		5	-326	
4500	6,84E+08	4500	169,732	12 063,70	2,05E+06	811	-1,66E+09		4500	198,862	4 021,20	8,00E+05	-811	6,49E+08		5	-328	
5084,39	3,60E+08	5084,39	169,732	12 063,70	2,05E+06	811	-1,66E+09		5084,39	198,862	4 021,20	8,00E+05	-811	6,49E+08		5	-652	
5084,39	4,13E+08	5084,39	174,691	12 063,70	2,11E+06	811	-1,71E+09		5084,39	196,058	4 021,20	7,88E+05	-811	6,39E+08		5	-657	
6084,39	-7,34E+07	6084,39	174,691	12 063,70	2,11E+06	811	-1,71E+09		6084,39	196,058	4 021,20	7,88E+05	-811	6,39E+08		6	-1143	
6084,39	-1,11E+07	6084,39	180,049	12 063,70	2,17E+06	811	-1,76E+09		6084,39	193,029	4 021,20	7,76E+05	-811	6,30E+08		6	-1143	
7084,39	-4,11E+08	7084,39	180,049	12 063,70	2,17E+06	811	-1,76E+09		7084,39	193,029	4 021,20	7,76E+05	-811	6,30E+08		7	-1543	
7084,39	-3,61E+08	7084,39	184,358	12 063,70	2,22E+06	811	-1,80E+09		7084,39	190,592	4 021,20	7,66E+05	-811	6,22E+08		7	-1543	
8084,39	-6,74E+08	8084,39	184,358	12 063,70	2,22E+06	811	-1,80E+09		8084,39	190,592	4 021,20	7,66E+05	-811	6,22E+08		8	-1856	
8084,39	-6,59E+08	8084,39	186,811	12 063,70	2,25E+06	811	-1,83E+09		8084,39	189,205	4 021,20	7,61E+05	-811	6,17E+08		8	-1850	
8500	-7,44E+08	8500	186,811	12 063,70	2,25E+06	811	-1,83E+09		8500	189,205	4 021,20	7,61E+05	-811	6,17E+08		9	-1955	
8500	-3,60E+08	8500	178,899	15 280,70	2,73E+06	811	-2,22E+09		8500	190,414	4 021,20	7,66E+05	-811	6,21E+08		9	-1956	
9084,39	-6,82E+08	9084,39	178,899	15 280,70	2,73E+06	811	-2,22E+09		9084,39	190,414	4 021,20	7,66E+05	-811	6,21E+08		9	-2078	
9084,39	-4,64E+08	9084,39	180,456	15 280,70	2,76E+06	811	-2,24E+09		9084,39	189,504	4 021,20	7,62E+05	-811	6,18E+08		9	-2082	
10084,4	-6,04E+08	10084,4	180,456	15 280,70	2,76E+06	811	-2,24E+09		10084,4	189,504	4 021,20	7,62E+05	-811	6,18E+08		10	-2222	
10084,4	-5,88E+08	10084,4	181,564	15 280,70	2,77E+06	811	-2,25E+09		10084,4	188,858	4 021,20	7,59E+05	-811	6,16E+08		10	-2222	
11084,4	-6,41E+08	11084,4	181,564	15 280,70	2,77E+06	811	-2,25E+09		11084,4	188,858	4 021,20	7,59E+05	-811	6,16E+08		11	-2275	
11084,4	-6,39E+08	11084,4	181,676	15 280,70	2,78E+06	811	-2,25E+09		11084,4	188,792	4 021,20	7,59E+05	-811	6,16E+08		11	-2275	
12084,4	-6,06E+08	12084,4	181,676	15 280,70	2,78E+06	811	-2,25E+09		12084,4	188,792	4 021,20	7,59E+05	-811	6,16E+08		12	-2242	
12084,4	-6,18E+08	12084,4	180,791	15 280,70	2,76E+06	811	-2,24E+09		12084,4	189,309	4 021,20	7,61E+05	-811	6,17E+08		12	-2242	
13084,4	-4,98E+08	13084,4	180,791	15 280,70	2,76E+06	811	-2,24E+09		13084,4	189,309	4 021,20	7,61E+05	-811	6,17E+08		13	-2121	
13084,4	-5,22E+08	13084,4	179,017	15 280,70	2,74E+06	811	-2,22E+09		13084,4	190,344	4 021,20	7,65E+05	-811	6,21E+08		13	-2120	
14000	-3,36E+08	14000	179,017	15 280,70	2,74E+06	811	-2,22E+09		14000	190,344	4 021,20	7,65E+05	-811	6,21E+08		14	-1934	
14000	-7,15E+08	14000	186,996	12 063,70	2,26E+06	811	-1,83E+09		14000	189,101	4 021,20	7,60E+05	-811	6,17E+08		14	-1928	
14084,4	-6,94E+08	14084,4	186,996	12 063,70	2,26E+06	811	-1,83E+09		14084,4	189,101	4 021,20	7,60E+05	-811	6,17E+08		14	-1907	
14084,4	-7,23E+08	14084,4	185,181	12 063,70	2,23E+06	811	-1,81E+09		14084,4	190,126	4 021,20	7,65E+05	-811	6,20E+08		14	-1914	
15084,4	-4,29E+08	15084,4	185,181	12 063,70	2,23E+06	811	-1,81E+09		15084,4	190,126	4 021,20	7,65E+05	-811	6,20E+08		15	-1621	
15084,4	-4,76E+08	15084,4	181,107	12 063,70	2,18E+06	811	-1,77E+09		15084,4	192,43	4 021,20	7,74E+05	-811	6,28E+08		15	-1621	
16084,4	-9,69E+07	16084,4	181,107	12 063,70	2,18E+06	811	-1,77E+09		16084,4	192,43	4 021,20	7,74E+05	-811	6,28E+08		16	-1340	

Moment from Dead Load

Concrete			Steel UK					
Distance mm	M_c Nmm		Distance mm	Sigma_s N/mm^2	A_s mm^2	F_s N	e_s mm	M_s Nmm
0	3,09E+09		0	-50,1588	2412,7	-1,21E+05	811	9,81E+07
84,3945	3,01E+09		84,3945	-50,1588	2412,7	-1,21E+05	811	9,81E+07
84,3945	3,09E+09		84,3945	-43,0595	2412,7	-1,04E+05	811	8,43E+07
1084,39	2,15E+09		1084,39	-43,0595	2412,7	-1,04E+05	811	8,43E+07
1084,39	2,30E+09		1084,39	-30,7929	2412,7	-7,43E+04	811	6,03E+07
2084,39	1,45E+09		2084,39	-30,7929	2412,7	-7,43E+04	811	6,03E+07
2084,39	1,58E+09		2084,39	-19,7165	2412,7	-4,76E+04	811	3,86E+07
3084,39	8,18E+08		3084,39	-19,7165	2412,7	-4,76E+04	811	3,86E+07
3084,39	9,37E+08		3084,39	-9,83029	2412,7	-2,37E+04	811	1,92E+07
4084,39	2,60E+08		4084,39	-9,83029	2412,7	-2,37E+04	811	1,92E+07
4084,39	3,42E+08		4084,39	-3,51111	2412,7	-8,47E+03	811	6,87E+06
4500	8,58E+07		4500	-3,51111	2412,7	-8,47E+03	811	6,87E+06
4500	1,32E+08		4500	0,489648	12 063,70	5,91E+03	811	-4,79E+06
5084,39	-2,02E+08		5084,39	0,489648	12 063,70	5,91E+03	811	-4,79E+06
5084,39	-1,47E+08		5084,39	5,61019	12 063,70	6,77E+04	811	-5,49E+07
6084,39	-6,50E+08		6084,39	5,61019	12 063,70	6,77E+04	811	-5,49E+07
6084,39	-5,86E+08		6084,39	11,1711	12 063,70	1,35E+05	811	-1,09E+08
7084,39	-1,00E+09		7084,39	11,1711	12 063,70	1,35E+05	811	-1,09E+08
7084,39	-9,50E+08		7084,39	15,6841	12 063,70	1,89E+05	811	-1,53E+08
8084,39	-1,28E+09		8084,39	15,6841	12 063,70	1,89E+05	811	-1,53E+08
8084,39	-1,24E+09		8084,39	18,2811	12 063,70	2,21E+05	811	-1,79E+08
8500	-1,36E+09		8500	18,2811	12 063,70	2,21E+05	811	-1,79E+08
8500	-1,30E+09		8500	18,79	15 280,70	2,87E+05	811	-2,33E+08
9084,39	-1,43E+09		9084,39	18,79	15 280,70	2,87E+05	811	-2,33E+08
9084,39	-1,41E+09		9084,39	20,5009	15 280,70	3,13E+05	811	-2,54E+08
10084,4	-1,57E+09		10084,4	20,5009	15 280,70	3,13E+05	811	-2,54E+08
10084,4	-1,55E+09		10084,4	21,8023	15 280,70	3,33E+05	811	-2,70E+08
11084,4	-1,62E+09		11084,4	21,8023	15 280,70	3,33E+05	811	-2,70E+08
11084,4	-1,62E+09		11084,4	22,1076	15 280,70	3,38E+05	811	-2,74E+08
12084,4	-1,60E+09		12084,4	22,1076	15 280,70	3,38E+05	811	-2,74E+08
12084,4	-1,61E+09		12084,4	21,4167	15 280,70	3,27E+05	811	-2,65E+08
13084,4	-1,51E+09		13084,4	21,4167	15 280,70	3,27E+05	811	-2,65E+08
13084,4	-1,53E+09		13084,4	19,8276	15 280,70	3,03E+05	811	-2,46E+08
14000	-1,36E+09		14000	19,8276	15 280,70	3,03E+05	811	-2,46E+08
14000	-1,41E+09		14000	19,6359	12 063,70	2,37E+05	811	-1,92E+08
14084,4	-1,39E+09		14084,4	19,6359	12 063,70	2,37E+05	811	-1,92E+08
14084,4	-1,41E+09		14084,4	17,932	12 063,70	2,16E+05	811	-1,75E+08
15084,4	-1,14E+09		15084,4	17,932	12 063,70	2,16E+05	811	-1,75E+08
15084,4	-1,18E+09		15084,4	14,0613	12 063,70	1,70E+05	811	-1,38E+08
16084,4	-8,18E+08		16084,4	14,0613	12 063,70	1,70E+05	811	-1,38E+08

Figure 6.2: Post-processing of case 2A without ASR gradient and dead load in excel

Effect of ASR on the Load Actions

From the structural analysis it is observed that ASR induced expansion leads to load actions on the reinforced concrete beams. These load actions depends on the beam's constraints (e.g. reinforcement, span, supports, etc.), magnitude of the ASR expansion and the concrete material model used to describe the effect of ASR.

It is shown that the structural system has an impact in the development of the ASR load actions. When a beam has few constraints the load action becomes greater compared to a beam with more constraints. A beam with less constraints entails that the ASR can develop more in the structure. This difference is observed when comparing the one span beam in case 1 and the three span beam in case 2. It is observed that in case 1 the ASR induced moment has a greater difference from the moment obserwed when the beam is not affected by ASR induced expansion, as exemplified in figure 6.3.

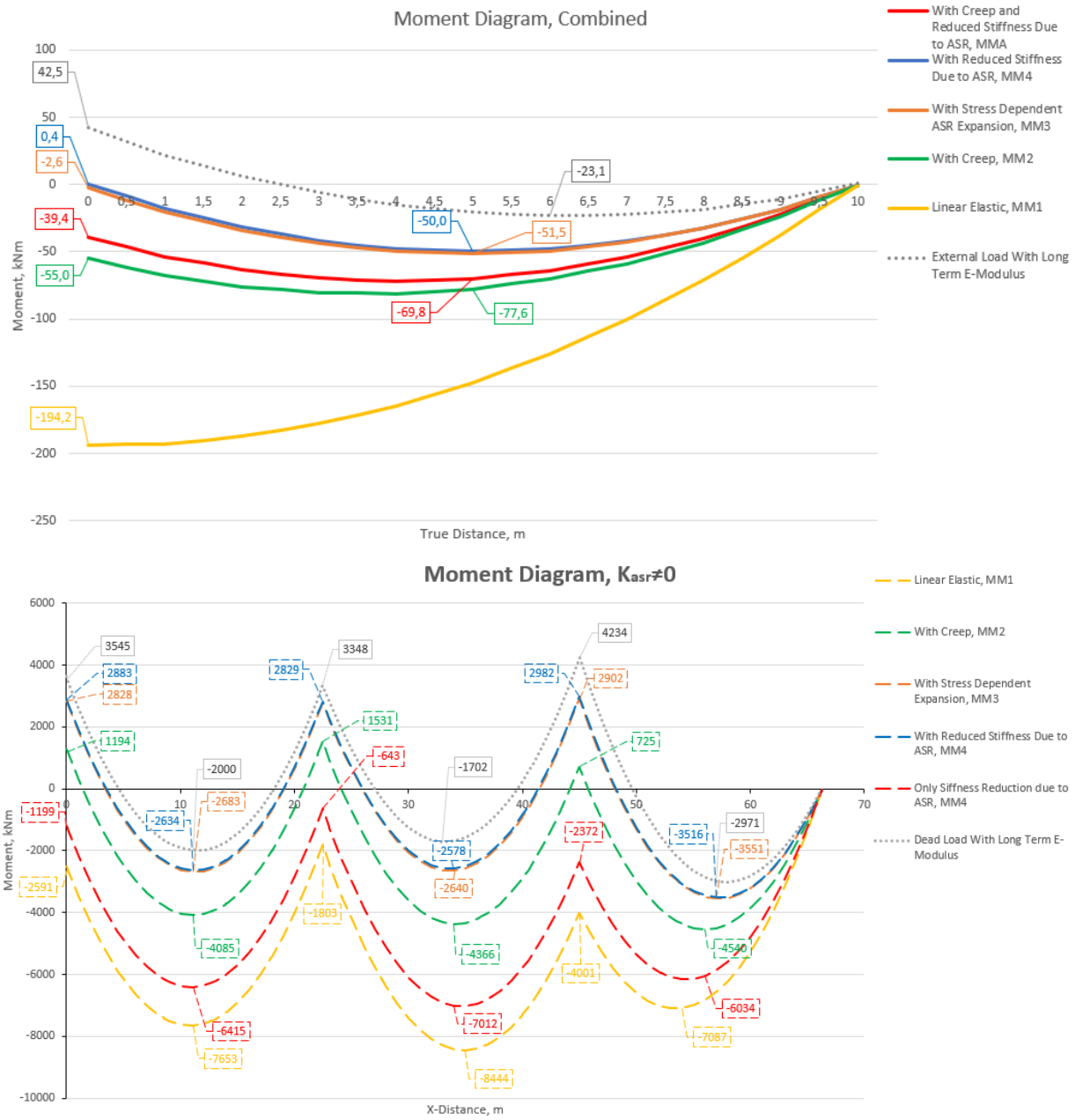

Figure 6.3: Comparison of moment diagrams for case 1B (uppermost) and case 2A with ASR gradient (lowermost)

Figure 6.3 shows the difference between the original moment (external load) and the combined moment (external load and ASR) for every material model analysed in case 1B and case 2A with gradient. It is seen that the structural system has a greater impact on development if the combined moment in case 1B than observed for case 2A with gradient.

Effect of ASR Expansion Gradient

In every analysis it is seen that the load action increases when the beam is subjected to a non-uniform ASR strain compared to a uniform ASR strain. The effect is seen in figure 6.4.

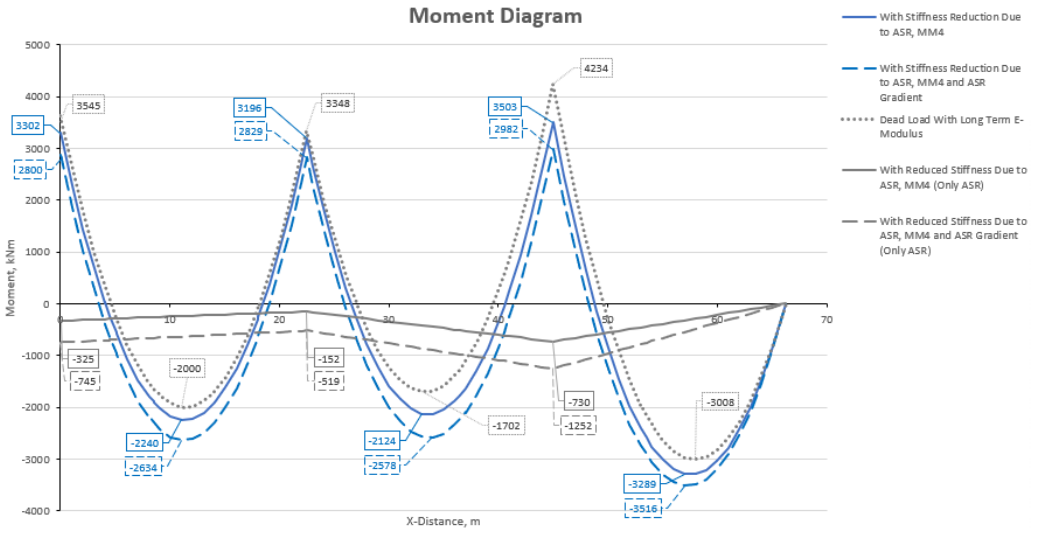

Figure 6.4: Comparison of uniform and non-uniform ASR strain for MM4 in case 2A

In the case studies a non-uniform ASR strain was introduced. This ASR strain was set to be linear over the height of the beam with twice the expansion at the top compared to the bottom of the beam. It was found that this non-uniform ASR expansion lead to vertical deformations. Since the beams was fixed in the vertical direction, an increase of load action occurred. The effect of introducing a gradient is less apparent in the three span beam than in the one span beam. This effect is seen by comparing figure 6.4 with figure 6.5. In figure 6.4 the moment has the same path, but in figure 6.5 it is seen that the moment changes from having tension at the top with uniform ASR strain applied to having tension at the bottom when a non-uniform ASR strain is applied. However, it is difficult generalize that the gradient has less impact on the three span beam than on the one span beam because there are too many differences between the cases.

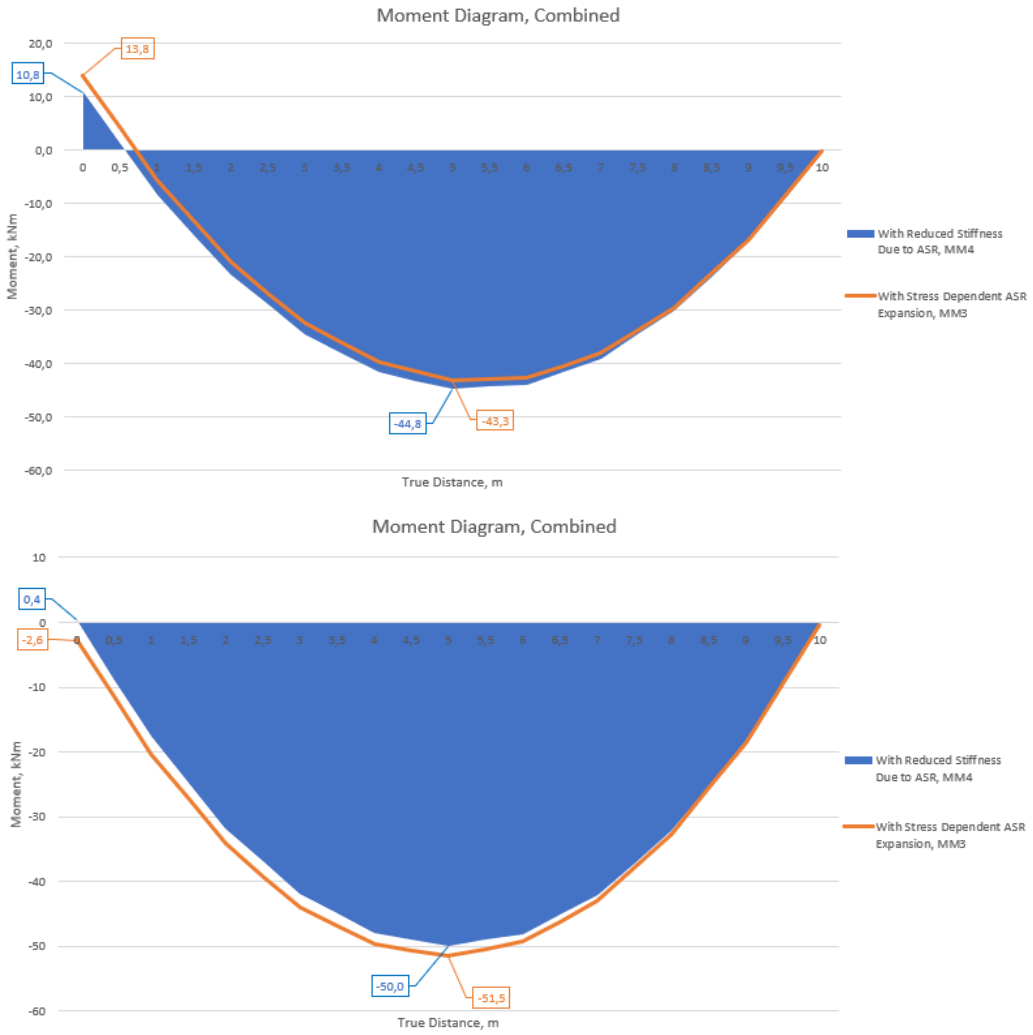

Figure 6.5: Moment diagram from MM4 in case 1A with uniform ASR strain (uppermost) and case 1B with non-uniform ASR strain (lowermost)

The development of the expansion due to a non-uniform ASR strain is also affected by the longitudinal reinforcement, where the amount and placement of the reinforcement affects the ASR expansion. For the one span beam with reinforcement at the bottom, a uniform expansion results in a post tensioning effect in the lower part of the beam, and consequently, the beam curves upwards. This post tensioning effect becomes even greater when a ASR gradient is applied with twice the ASR strain at the top than at the bottom. If the reinforcement is placed in the middle or both at the top and bottom, as for the three span beam, the post tensioning effect would not occur if the ASR strain is uniform, and if the ASR strain is non-uniform the effect is reduced.

Effect of Axial Forces

ASR can develop different within a structure, leading to some parts of the structure being more expanded than others. By applying a axial force this behaviour can be simulated.

It is seen in case 2C that the applied tension force significantly reduces the ASR load action. Since the end displacement is fixed, the introduction of tension leads to a reduced ASR strain in order for the total horizontal displacement to be 66.25mm. This would still be the case if the end deformation was free, instead of fixed, as the applied tension force would create a post tensioning effect which curves the beam increasing the vertical deformation and reducing the horizontal deformation. Since the ASR strains in 2C with tensioning are of small values, the ASR load action becomes approximately the same in every analysed material model.

The opposite behaviour is achieved when the beam is subjected to a compressive force. When the beam is subjected to compression and non-uniform ASR strain it is seen that the ASR load action increases. The compressive force significantly increases the effect of ASR gradient which leads to even larger load actions, e.g. at support 3 the moment from MM4 increases from -1992kNm in case 2B with gradient to -3586kNm in case 2C with compression. The load action increases 80%. The total field moment increases and the total moment at the supports are reduced. It is seen that the least accurate material models provide the greatest ASR load actions when compression occurs.

Load actions due to tension and compression is seen in figure 6.6. By comparing figure 6.6 and figure 6.7 the effect of introducing axial forces is seen.

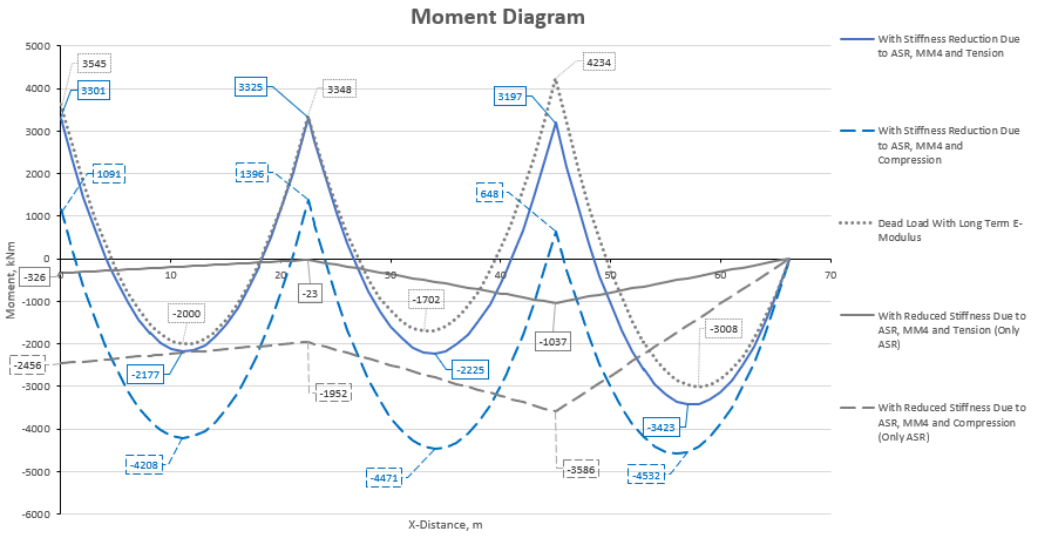

Figure 6.6: Moment diagrams from MM4 for case 2C with non-uniform ASR strain and applied tension and compressive Force

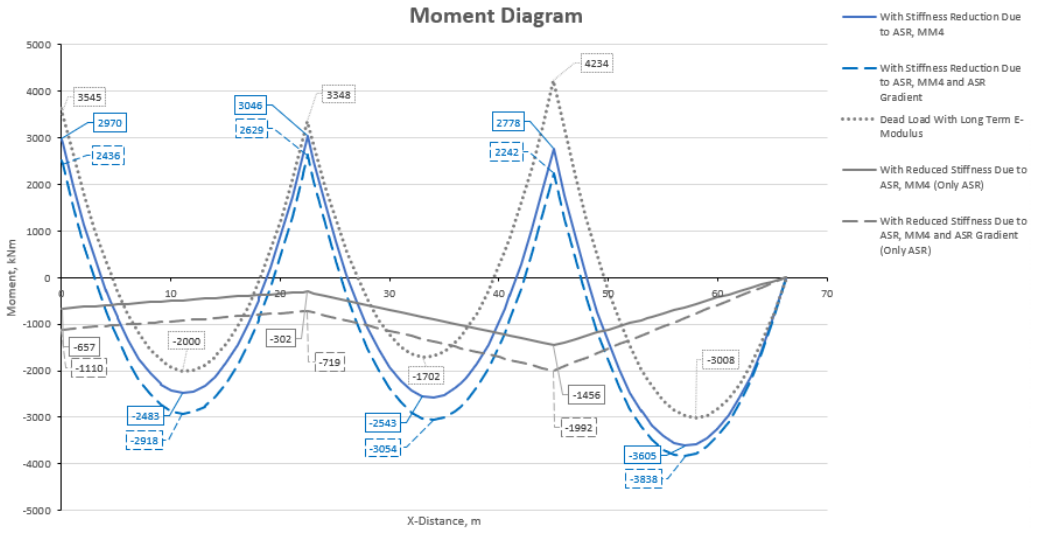

Figure 6.7: Moment diagrams from MM4 for case 2B

The Effect of Reinforcement on ASR

The longitudinal reinforcement is placed in the areas where the beam is subjected to tensile stresses. From the analysis it is shown that in some cases the load action due to ASR leads to significant changes to the total moment diagram. The result is changes of the path of the total moment and placement of tensile stresses within the cross section. In cases where the tensile stresses are relocated to areas where the beam does not have any longitudinal reinforcement, the ASR induced load actions may lead to a critical reduction of the structural capacity. It is therefore crucial that any analysis is performed using

precise material models that provides accurate results, leading to precise calculation of the load actions from then the structural assessments can be done.

The Effect of ASR Material Models on the Displacements

As exemplified in figure 6.8, when a equal ASR strain is applied in each material model the deformations differs. It is observed that when a stress dependent ASR expansion and a reduced stiffness is included in the material models, as for MM3 and MM4, the horizontal deformation decreases and the vertical deformation increases. This has proven to be valid in every analyses.

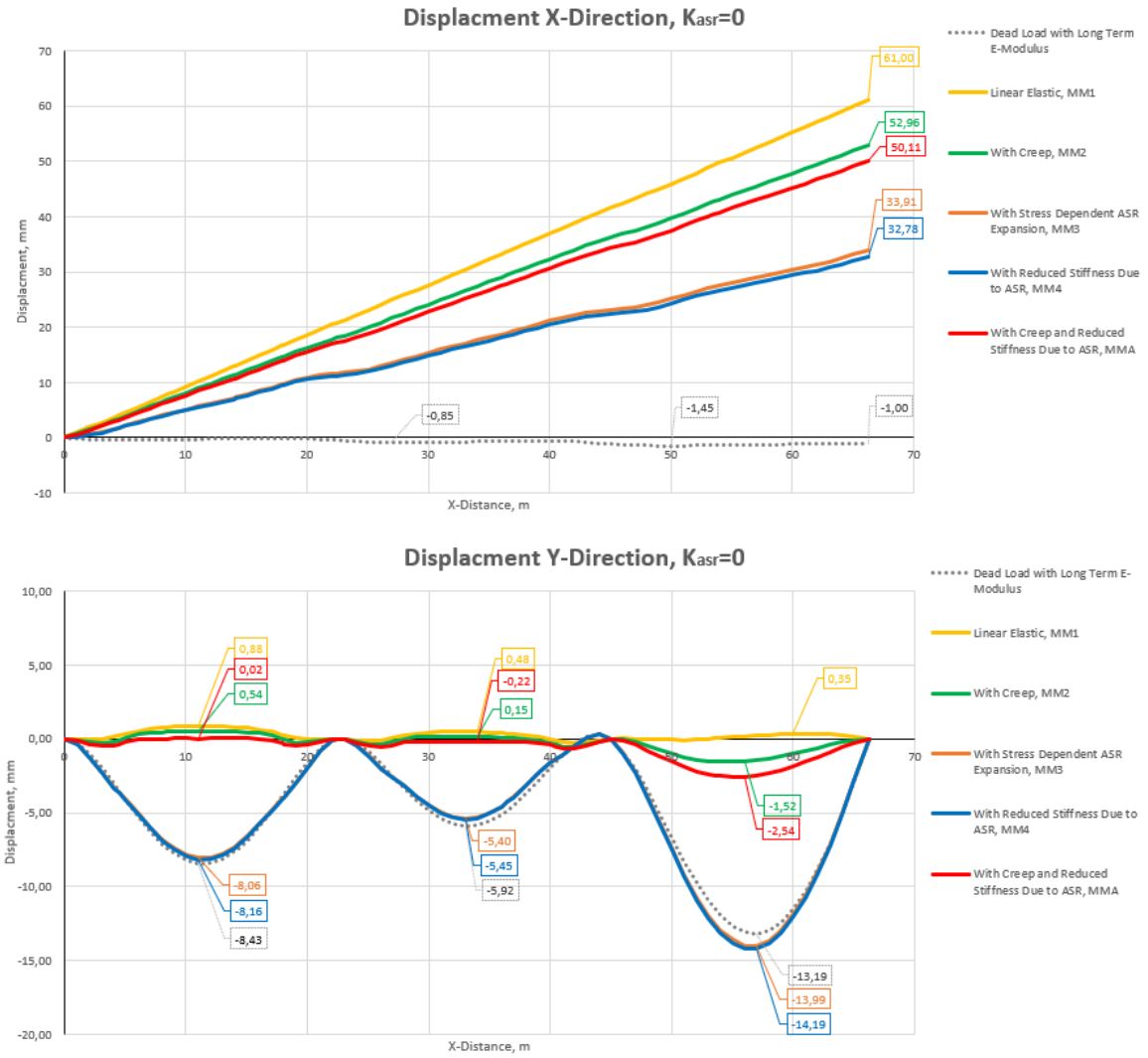

Figure 6.8: Comparison of displacements for case 2A without ASR gradient, $\varepsilon_{asr} = 0.001$

Constant end deformation implies that the ASR strain will differ in the material models. For MM3 and MM4 this leads to larger ASR strains compared to when the ASR strain is constant and the end displacement is free. As the ASR strain has increased, larger load actions occur. Meaning that the differences of load actions between the material models are reduced. However, even though the difference in load actions are reduced, MM3 and MM4 still provides less ASR load actions and therefore providing a more accurate answer. This is seen in figure 6.9. The displacement in MM3 and MM4 now is approximately twice the size as previous, the ASR strain is also increased resulting in larger load actions. This shows the importance of knowing the accurate ASR conditions on the structure, as well as the difficulties of modeling a the exact load action.

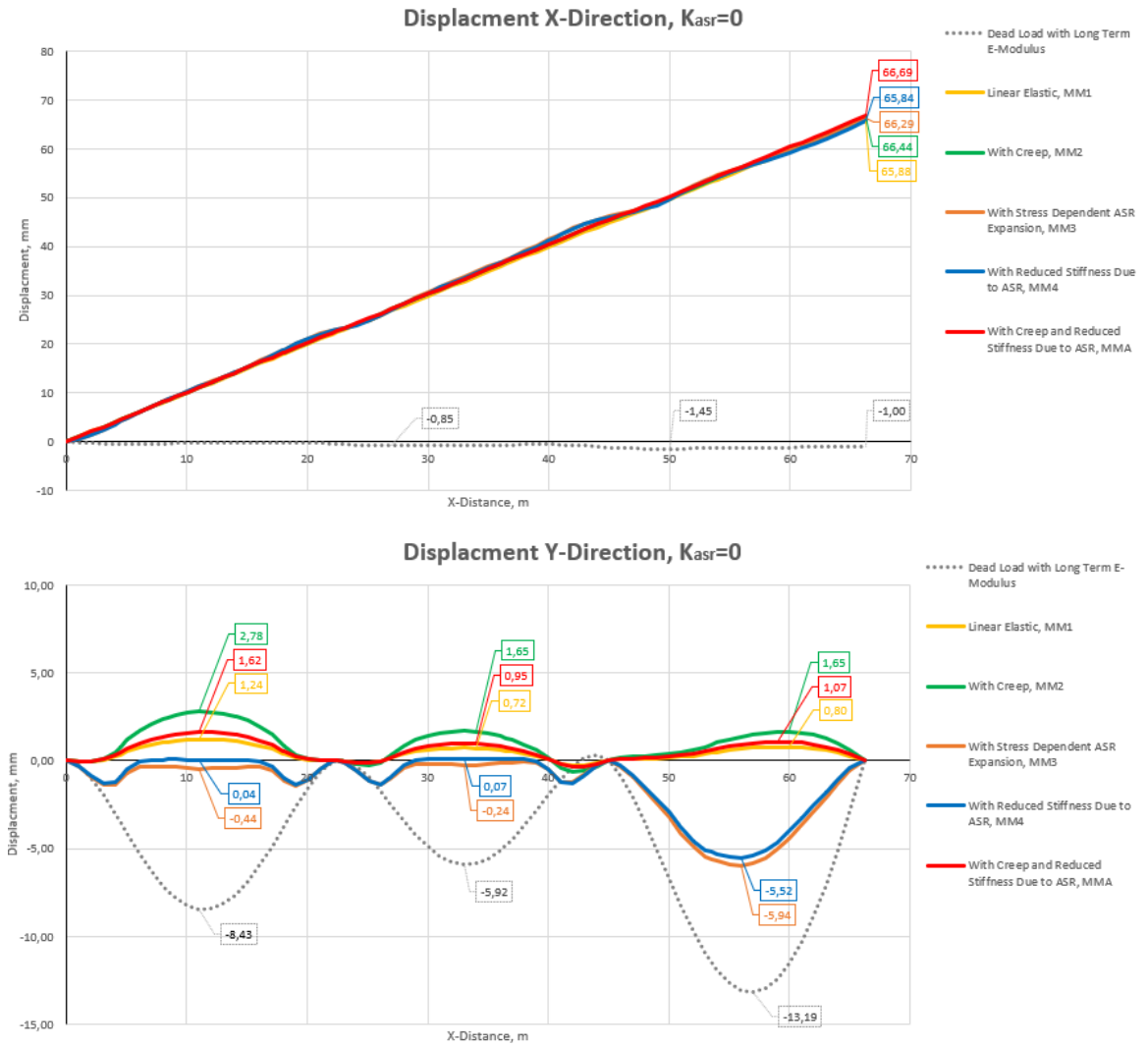

Figure 6.9: Comparison of displacements for case 2B without ASR gradient, $\varepsilon_{asr} = 0.001$

It is observed in every analysis, regardless of structural- and ASR constraints, that the most advanced material models result in the least ASR load action and a more accurate description of the effect of loads on the beam, e.g. as seen in figure 6.3. The material model should at least include a linear elastic material behavior with long term E-modulus and stress dependent ASR expansion equivalent to material model 3 (MM3) used in the analysis. More parameters can also be included in the material model, e.g. stiffness reduction due to ASR as used in MM4, but the results from the analysis has proven that the greatest effect and influence of the load action is achieved by applying MM3. The load action still decreases when more parameters are included, however further reduction is significantly less that the reduction of load action achieved by including the effect of stress dependent ASR expansion in the material model.

7 Conclusion

The following conclusion regards the structural analysis of reinforced concrete beams affected by alkali-silica reaction (ASR) can be stated:

Reinforced concrete beams can be modelled in the finite element software Abaqus using beam elements for the concrete, truss elements for the reinforcement, and a kinematic coupling to simulate the non-slip interaction. This numerical solution describes the connection between concrete and reinforcement. With this method, post processing of the output is needed in order find the internal bending moment.

The effect of ASR leads to additional load actions on the beam. Abaqus does not contain any ASR macro model that describes the effect of ASR. The ASR strains were implemented as a pre-defined field variable in Abaqus.

From the case studies it was found that the non-unifrom ASR expansion and the stress dependency of the ASR expansion had significant impact on the load actions. Stiffness reduction due to the ASR can also be included in the material model. This further reduces the load actions. However, the reduction is of a small magnitude when the stress dependency of ASR is included.

Applied ASR gradient over the height of the beam cross section has proven to increases the load actions. The ASR gradient leads to additional vertical displacement due to the support constraints which increases the load actions. An asymmetric reinforcement on the cross section of the beam causes ASR gradient. An applied tension force has shown to reduce the load actions due to ASR. An applied compressive force has shown to increase the effect of load actions due to ASR.

8 Further Work

Further work on structural analyses of reinforced concrete structures affected by ASR could include the following:

- In this thesis, the effect of material models in 1D with beam elements is studied. Further structural analyses could be performed by modeling in 3D with solid or shell elements with reinforcement embedded into the element in Abaqus.
- In the structural analyses we have included ASR gradient only on the height of the beam cross section. ASR gradient in the width of the beam cross section could be included for the ASR expansion.
- Further work could include tension stiffening and softening in the material models to model reinforced concrete more accurately.
- The rebar method, were the reinforcement element is embedded in the concrete element, was used in the modelling of reinforcement concrete beams in Abaqus. The structural analyses showed errors of the ASR restraint forces. The solution to this error could be investigated in further work since the rebar method allows for a simpler and time efficient post-processing.

References

[1] Abaqus, S. *Abaqus Analysis User's Guide: REBAR.* 2017, https://abaqus-docs.mit.edu/2017/English/SIMACAEKEYRefMap/simakey-r-rebar.htm.

[2] Alnaggar, M., Cusatis, G., and Di Luzio, G. Lattice discrete particle modeling (ldpm) of alkali silica reaction (asr) deterioration of concrete structures. *Cement and Concrete Composites 41* (2013).

[3] Andrade, C., Gulikers, J., and Polder, R. *Durability of Reinforced Concrete from Composition to Protection*, vol. Selected Papers of the 6th International RILEM PhD Workshop. Springer International Publishing, Delft, The Netherlands, 2013.

[4] Barbosa, R. A., Hansen, S. G., Hansen, K. K., Hoang, L. C., and Grelk, B. Influence of alkali-silica reaction and crack orientation on the uniaxial compressive strength of concrete cores from slab bridges. *Elsevier Ltd Construction and Building Materials* (2018).

[5] Bauchau, O. A., and Craig, J. I. *Solid Mechanics and Its Applications*, vol. SMIA, volume 163 of *Structural Analysis pp 173-221.* Springer, Dordrecht, 2009.

[6] Case, J., Chilver, L., and Ross, C. Stress-strain curves for brittle materials. *Strength of Materials and Structures (4th Edition)* (1999).

[7] Charlwood, R., Solymar, S., , and Curtis, D. A review of alkali aggregate reactions in hydroelectric plants and dams. *Proceedings of the international conference of alkali-aggregate reactions in hydroelectric plants and dams* (1992).

[8] Cope, R. J., and Slade, L. The shear capacity of reinforced concrete members subjected to alkali-silica reaction. *Structural Engineering Review* (1990).

[9] Cusatisa, G., Pelessone, D., and Mencarellia, A. Lattice discrete particle model (ldpm) for failure behavior of concrete. i: Theory. *Cement and Concrete Composites* (2011).

[10] DIANA FEA, A. Diana finite element analysis, 2019.

[11] Esposito, R., and Hendriks, M. A. N. Degradation of the mechanical properties in asr-affected concrete: overview and modeling. *Delft University of Technology, The Netherlands* (2012).

[12] European Committee for Standardization, E. Eurocode 2: Design of concrete structures - part 1-1: General rules and rules for buildings, 2018.

[13] Grimsmo, T., and Welle, K. Beregning og oppfølging av eksisterende bruer med betydelig skadeomfang. Master's thesis, NTNU - Norges teknisk-naturvitenskapelige universitet, 2017.

[14] Hobbs, D. W. The alk.a li-s.i lica reaction - a model for predicting expansion in mortar. *Cement And Concrete Association : Research And Development Division* (1981).

[15] Jones, A. E. K., and Clark, L. A. The effects of restraint on asr expansion of reinforced concrete. *British Cement Association and The University of Birmingham Magazine of Concrete Research, 1996, 48, No. 174, Mar., 1-13* (1996).

[16] Jurcut, A. C. Modelling of alkali-aggregate reaction effects in reinforced concrete structures. *Civil Engineering University of Toronto* (2015).

[17] Knutsdatter, S. M. Beregning og oppfølging av eksisterende bruer med betydelig skadeomfang. Master's thesis, NTNU - Norges teknisk-naturvitenskapelige universitet, 2018.

[18] Kongshaug, S. S. Lecture note: Structural analysis of reinforced concrete beams affected by asr. *Master course MABY4500-Durability and Service Life of Structures at Oslo Metropolitan University* (2019).

[19] Kongshaug, S. S., Oseland, O., Kanstad, T., Hendriks, M. A., Rodum, E., and Markeset, G. Experimental investigation of asr-affected concrete – the influence of uniaxial loading on the evolution of mechanical properties, expansion and damage indices. *Construction and Building Materials 245* (jun 2020).

[20] Larive, C. *Apports combinês de l'expêrimentation et de la modêlisation â la comprêhension de l'alcali-rêaction et de ses effets mêcaniques.* Laboratorie Central des ponts et Chaussêes, France, 1998.

[21] Larssen, R. M. Forsterkning og reparasjon av bruer. *Dr. Ing. A. Aas-Jakobsen* (2020).

[22] Larssen, R. M. Internal note: Elgeseter bru – ekvivalent bjelkemodell for asr-simuleringer. *Dr. Ing. A.Aas-Jakbosen AS* (2020).

[23] Liaudat, J., Carol, I., Lopez, C. M., and Saouma, V. E. Asr expansions in concrete under triaxial confinement. *Cement and Concrete Composites* (2017).

[24] Multon, S., Cyr, M., Sellier, A., Diederich, P., and Petit, L. Effects of aggregate size and alkali content on asr expansion. *Cement and Concrete Research, Elsevier* (2018).

[25] Naaman, A. Reinforced concrete. *Eco-Efficient Repair and Rehabilitation of Concrete Infrastructures, 2018 Encyclopedia of Materials: Science and Technology* (2001).

[26] Norcem. God betong er bestandig. *Norcem A.S,* (2018).

[27] Richardson, M. G. *Fundamentals of Durable Reinforced Concrete.* Spon Press London, 2002.

[28] Saouma, V., and Perotti, L. Constitutive model for alkali-aggregate reactions. *ACI Materials Journal* (2006).

[29] Stemland, H., Rodum, E., and Johansen, H. Asr – guidance for structural analysis. *Norwegian Public Roads Administration* (2016).

[30] Swamy, R. N., and Al-Asli, M. M. *Effect of alkali silica reaction on the structural behaviour of reinforced concrete beams.* ACI Structural Journal, 1989.

[31] The Institution of Structural Engineers, I. Structural effects of alkali-silica reaction: Technical guidance on the appraisal of existing structures. *SET0 Ltd* (1992).

[32] Wen, H. X. *Prediction of Structural Effects in Concrete Affected by Alkali-Aggregate Reaction.* PhD thesis, Department of Civil and Structural Engineering Faculty of Technology, 1993.

Appendix A

A1 Results from Case 1A

Reduced Stiffness Due to Creep, MM2

In MM2 the effect of creep is included, $E_c = 30000N/mm^2 \longrightarrow E_{c,eff} = 8571N/mm^2$. This analysis include a linear elastic material behaviour and the long term E-modulus, $E_{c,eff}$.

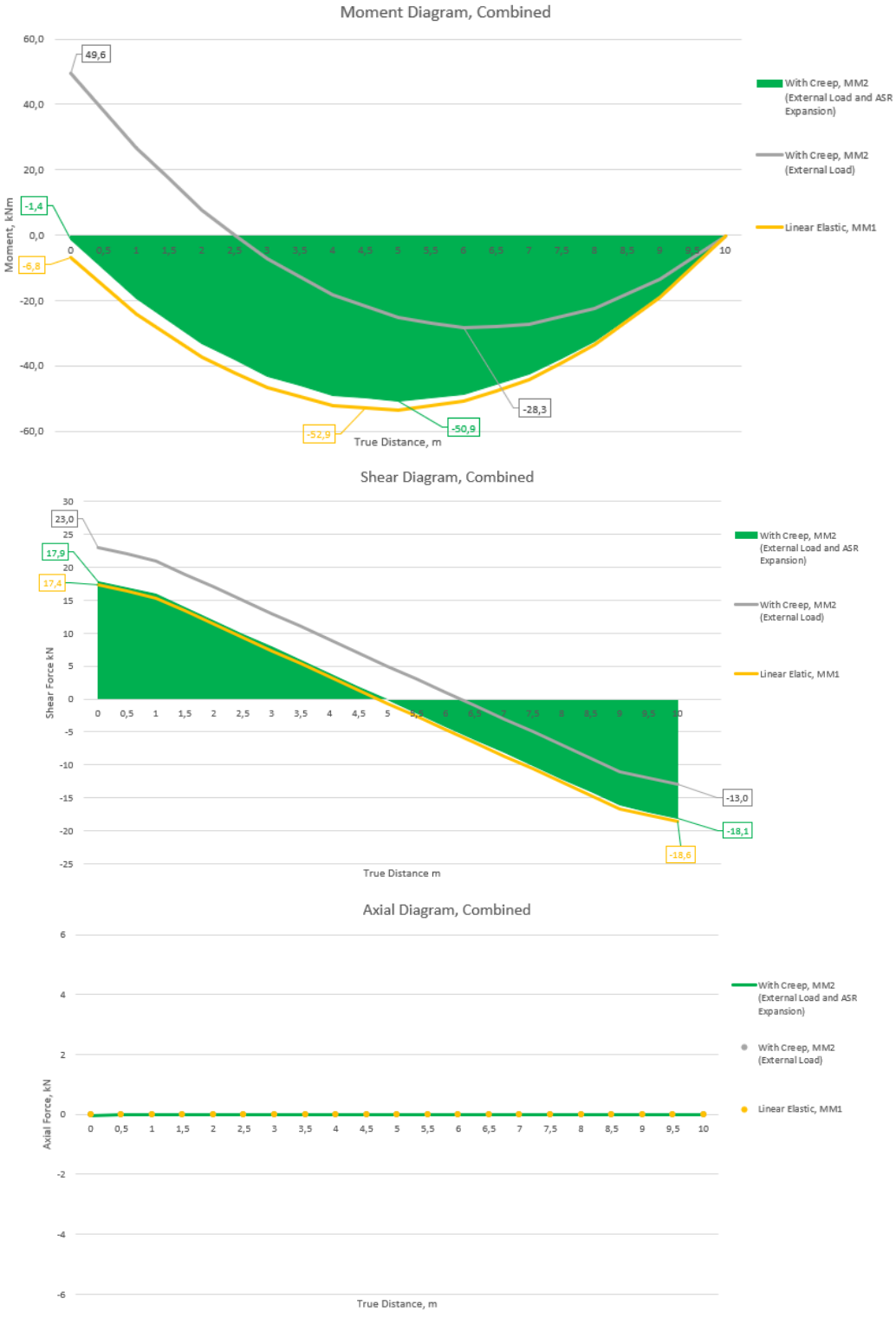

Figure A1.1: Moment-, Shear- and Axial diagram with MM2 for Case 1A

Stress Dependent ASR Expansion, MM3

In MM3 the free ASR strain is changed to stress dependent ASR strain, $\varepsilon_{asr}^{free} \longrightarrow \varepsilon_{asr}$.

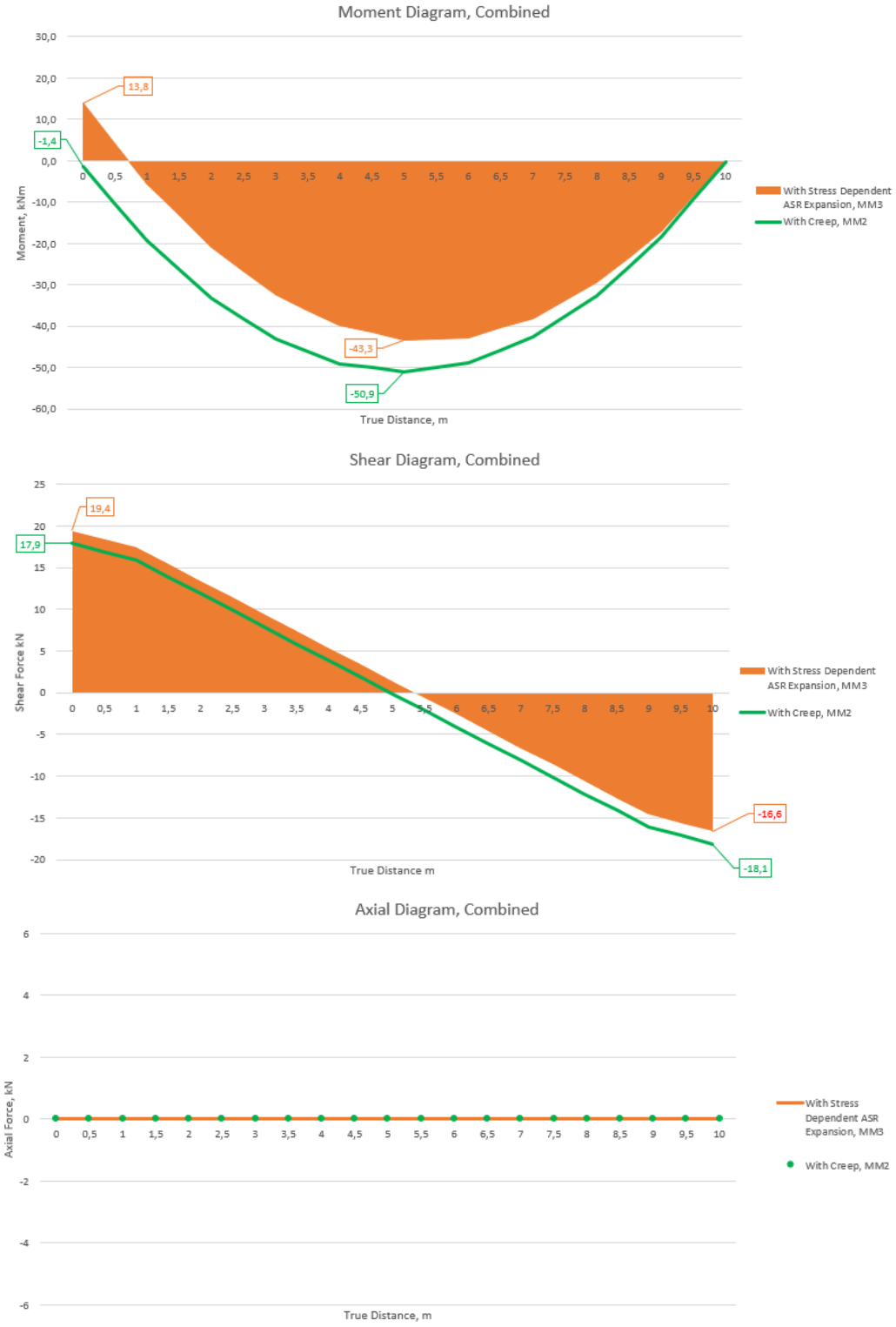

Figure A1.2: Moment-, Shear- and Axial diagram with MM3 for Case 1A

Reduced Stiffness Due to ASR, MM4

In MM4 the stiffness is reduced due to the ASR expansion, $E_{c,eff} \longrightarrow E_{c,eff}(\varepsilon_{asr})$.

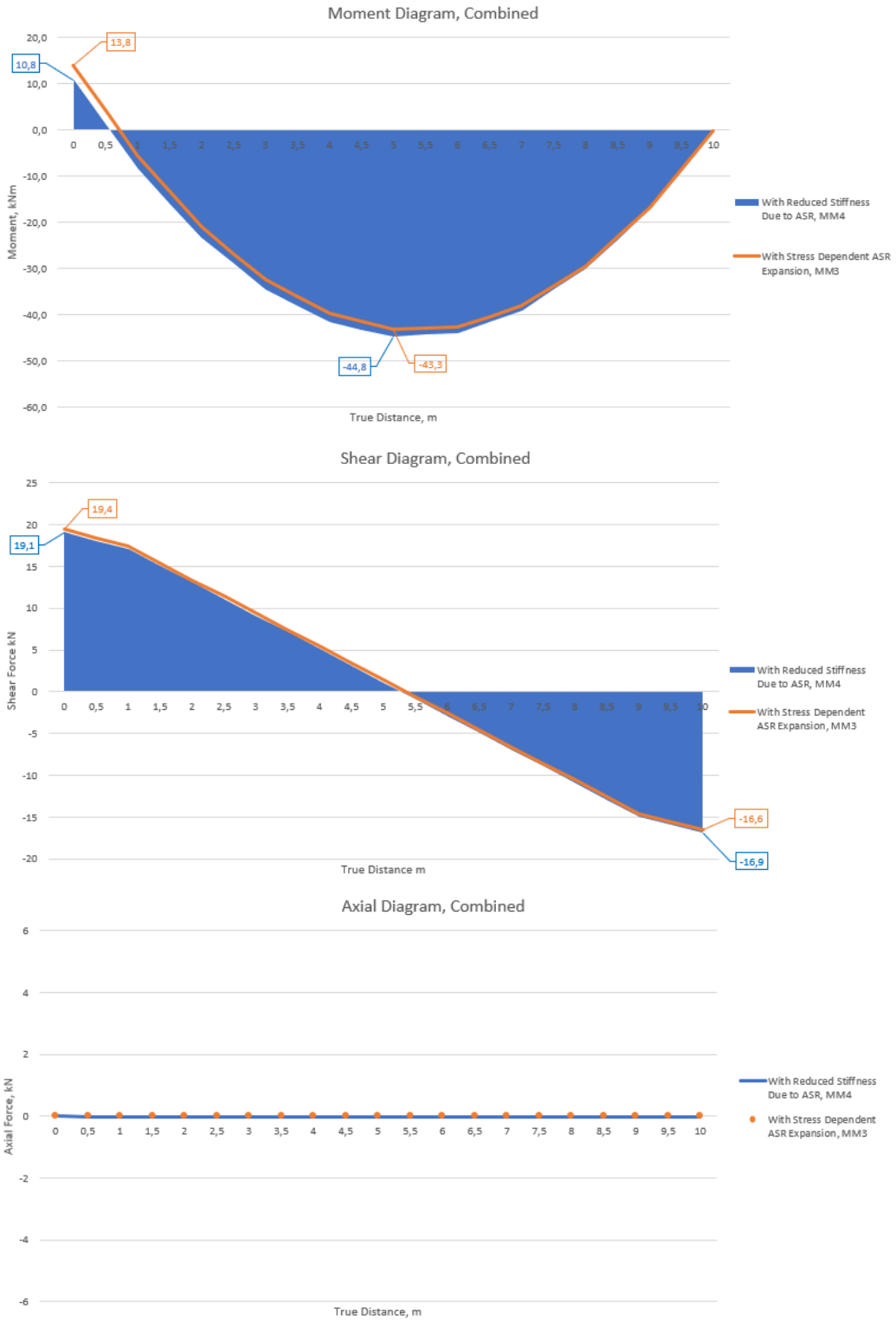

Figure A1.3: Moment-, Shear- and Axial diagram with MM4 for Case 1A

Only Reduced Stiffness Due to Creep and ASR, MMA

In MMA the beam has reduced stiffness due to creep and ASR, $E_{c,eff}(\varepsilon_{asr})$.

Figure A1.4: Moment-, Shear- and Axial diagram with MMA for Case 1A

A2 Results from Case 1B

Reduced Stiffness Due to Creep, MM2

In MM2 the only data input changed is the modulus of elasticity for concrete, $E_c = 30000N/mm^2 \longrightarrow E_{c,eff} = 8571N/mm^2$.

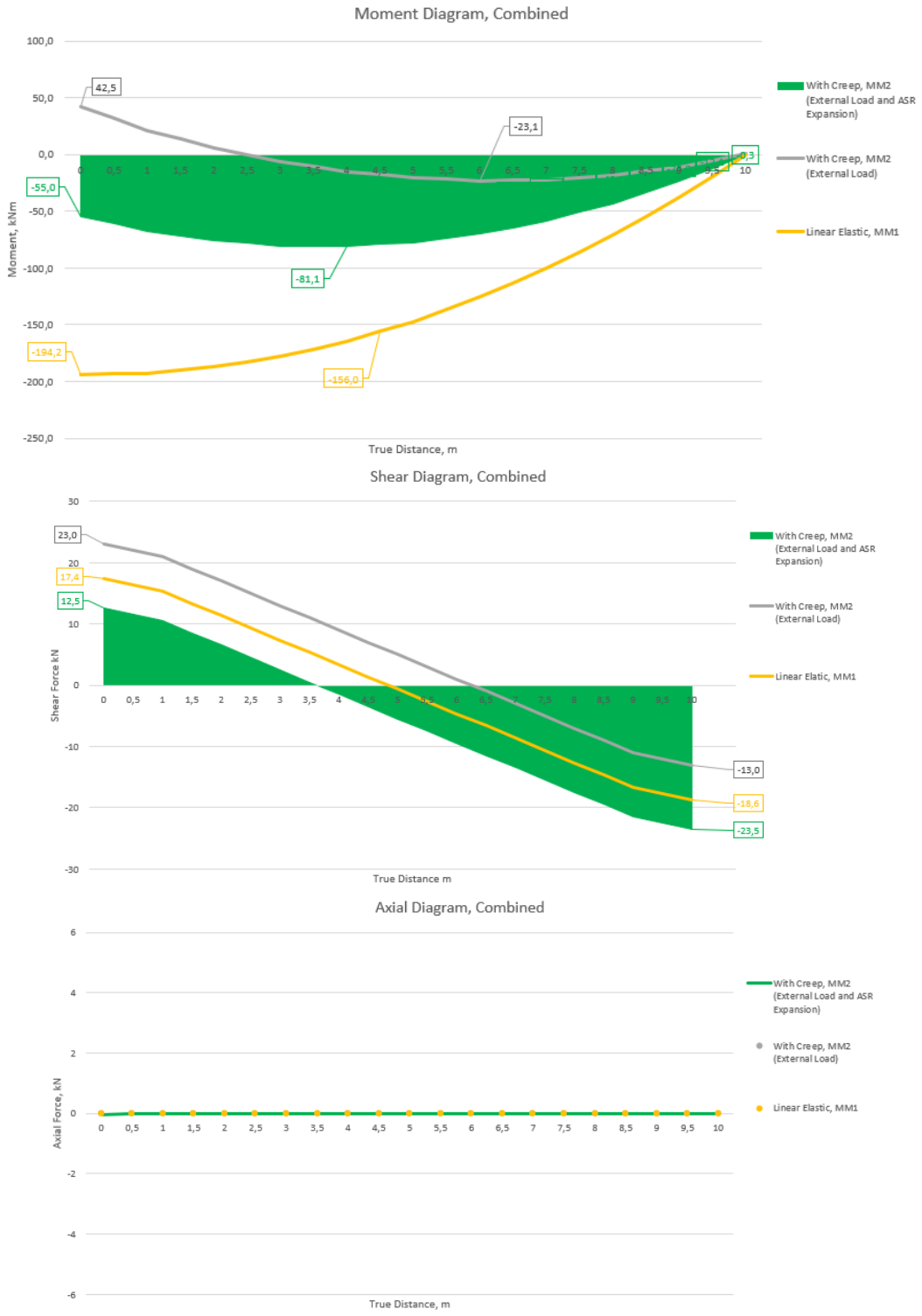

Figure A2.1: Moment-, Shear- and Axial diagram with MM2 for Case 1B

Stress Dependent ASR Expansion, MM3

In MM3 the free ASR strain is changed to stress dependent ASR strain, $\varepsilon_{asr}^{free} \longrightarrow \varepsilon_{asr}$.

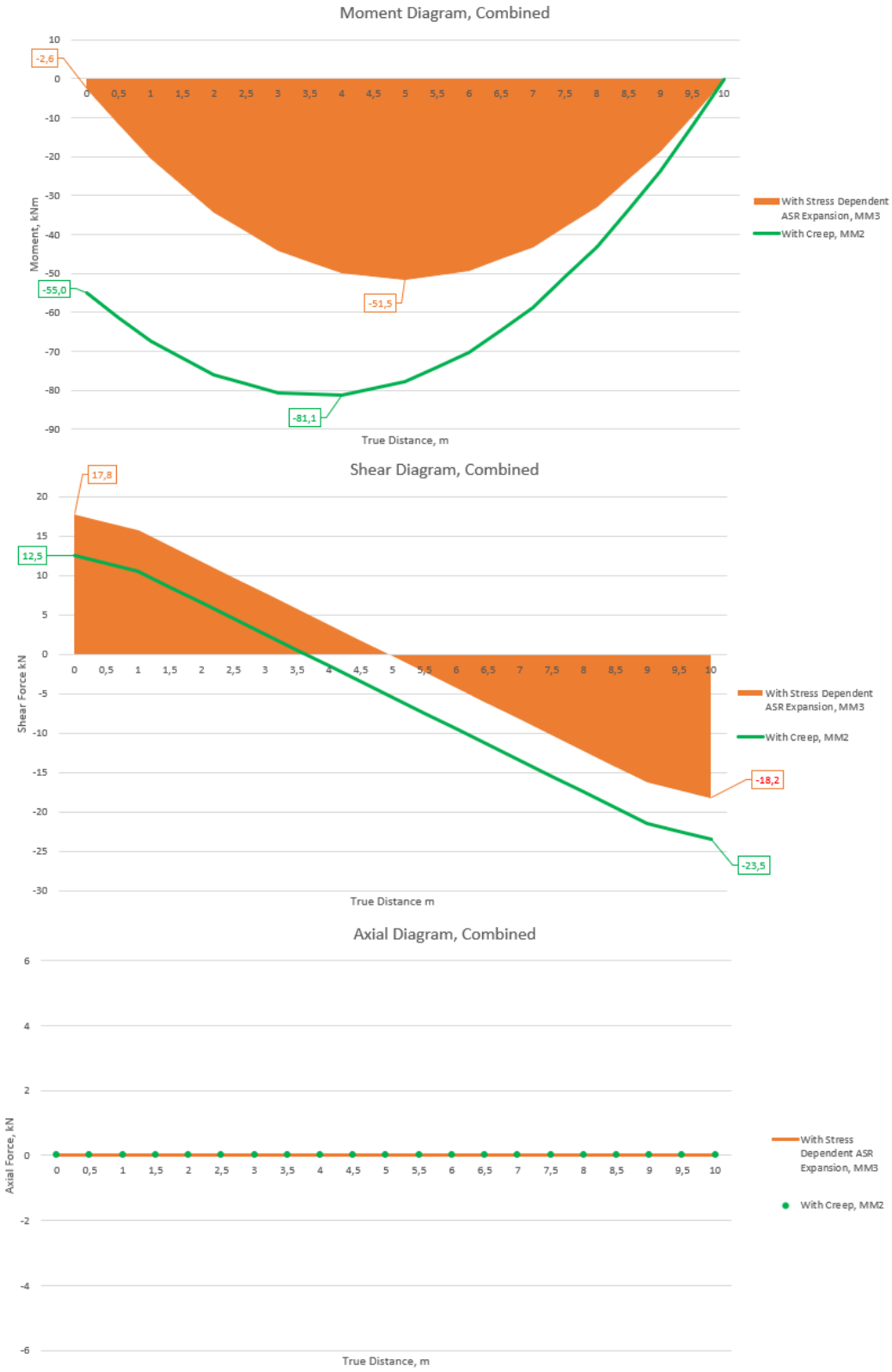

Figure A2.2: Moment-, Shear- and Axial diagram with MM2 for Case 1B

Reduced Stiffness Due to ASR, MM4

In MM4 the stiffness is reduced due to the ASR expansion, $E_{c,eff} \longrightarrow E_{c,eff}(\varepsilon_{asr})$.

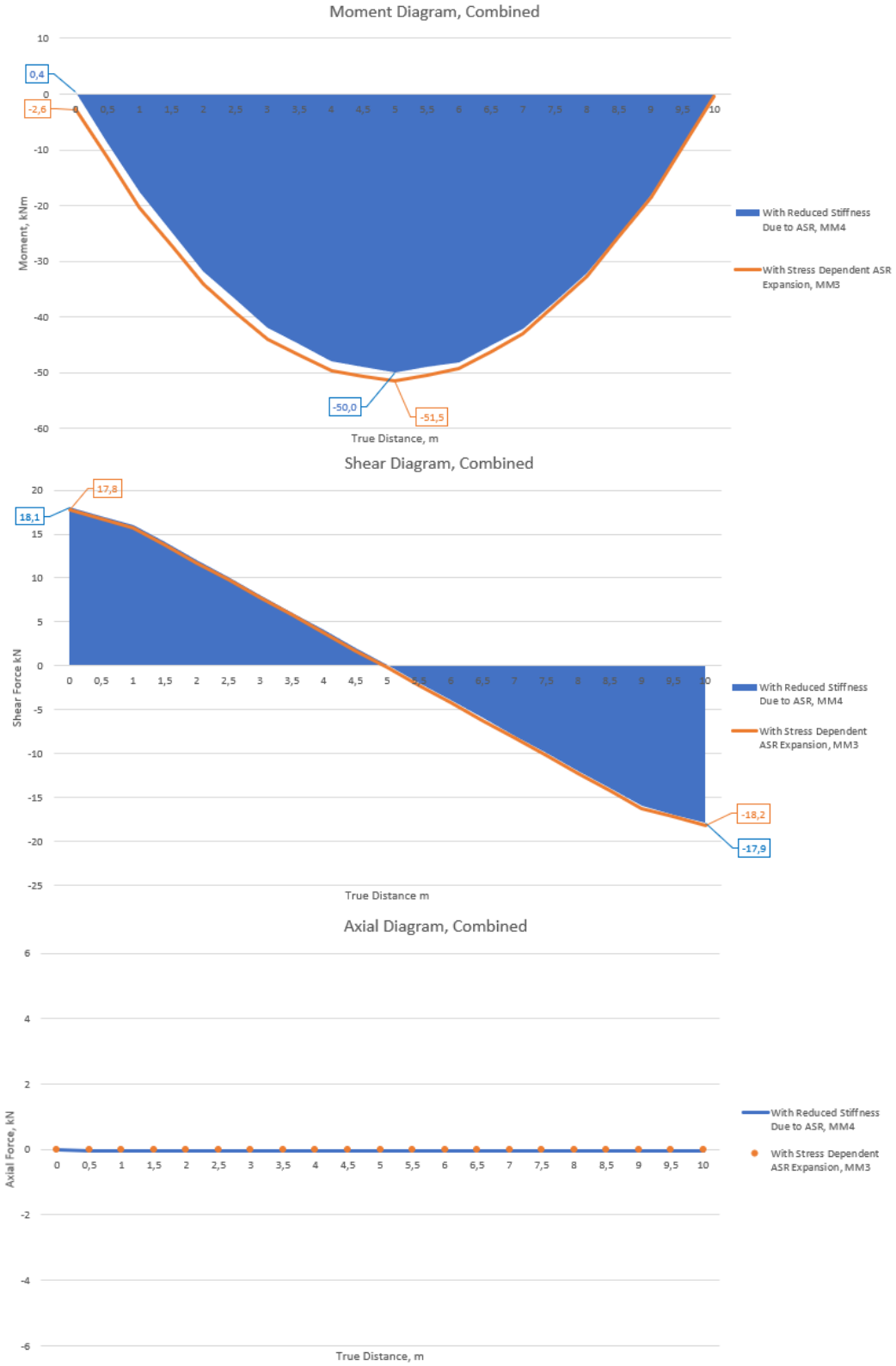

Figure A2.3: Moment-, Shear- and Axial diagram with MM4 for Case 1B

Only Reduced Stiffness Due to Creep and ASR, MMA

In MMA the beam has reduced stiffness due to creep and ASR, $E_{c,eff}(\varepsilon_{asr})$.

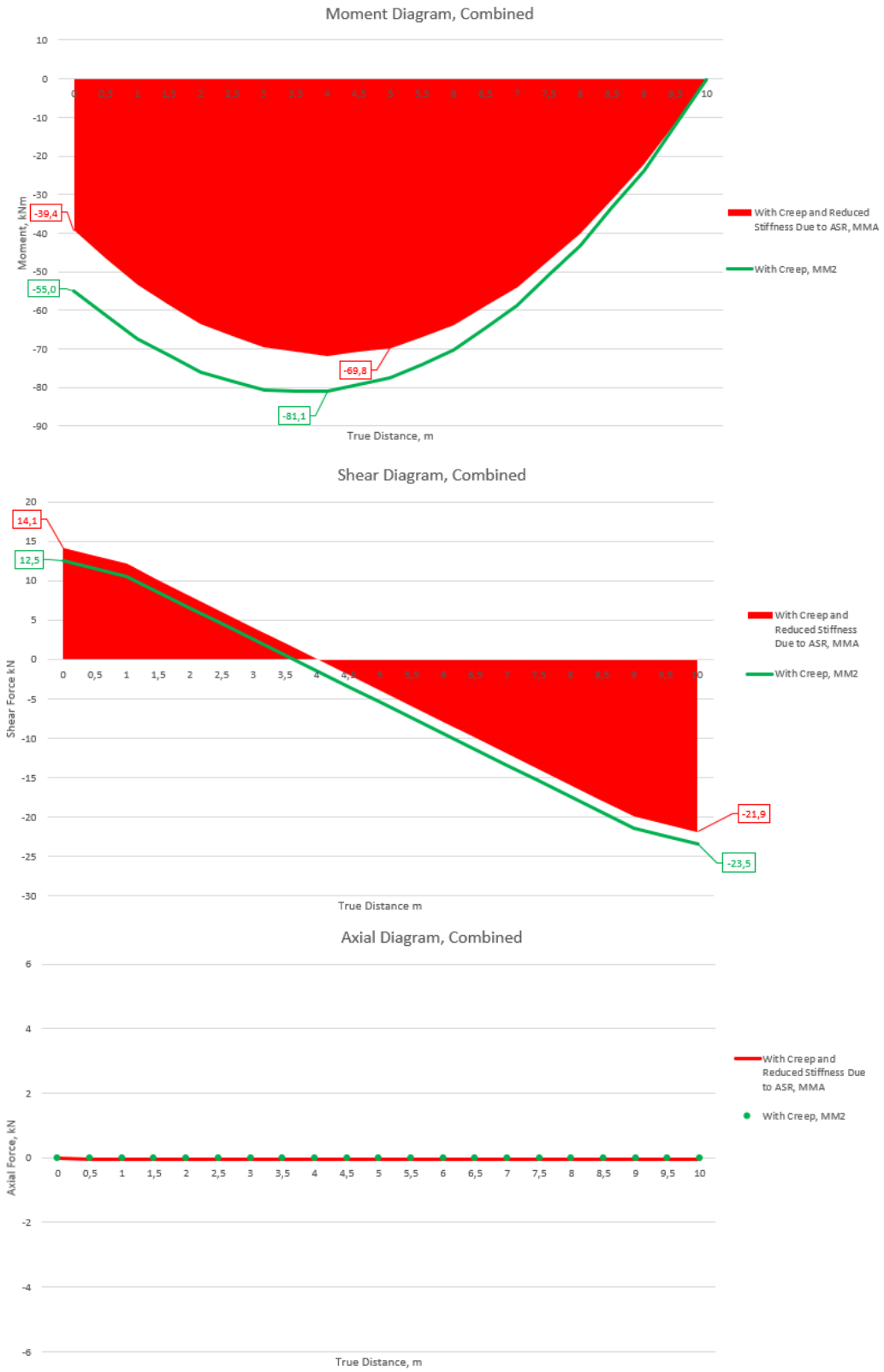

Figure A2.4: Moment-, Shear- and Axial diagram with MMA for Case 1B

A3 Results from Case 2A

Linear Elastic, MM1

In MM1 the modulus of elasticity for concrete, $E_c = 23312.7 N/mm^2$ is used.

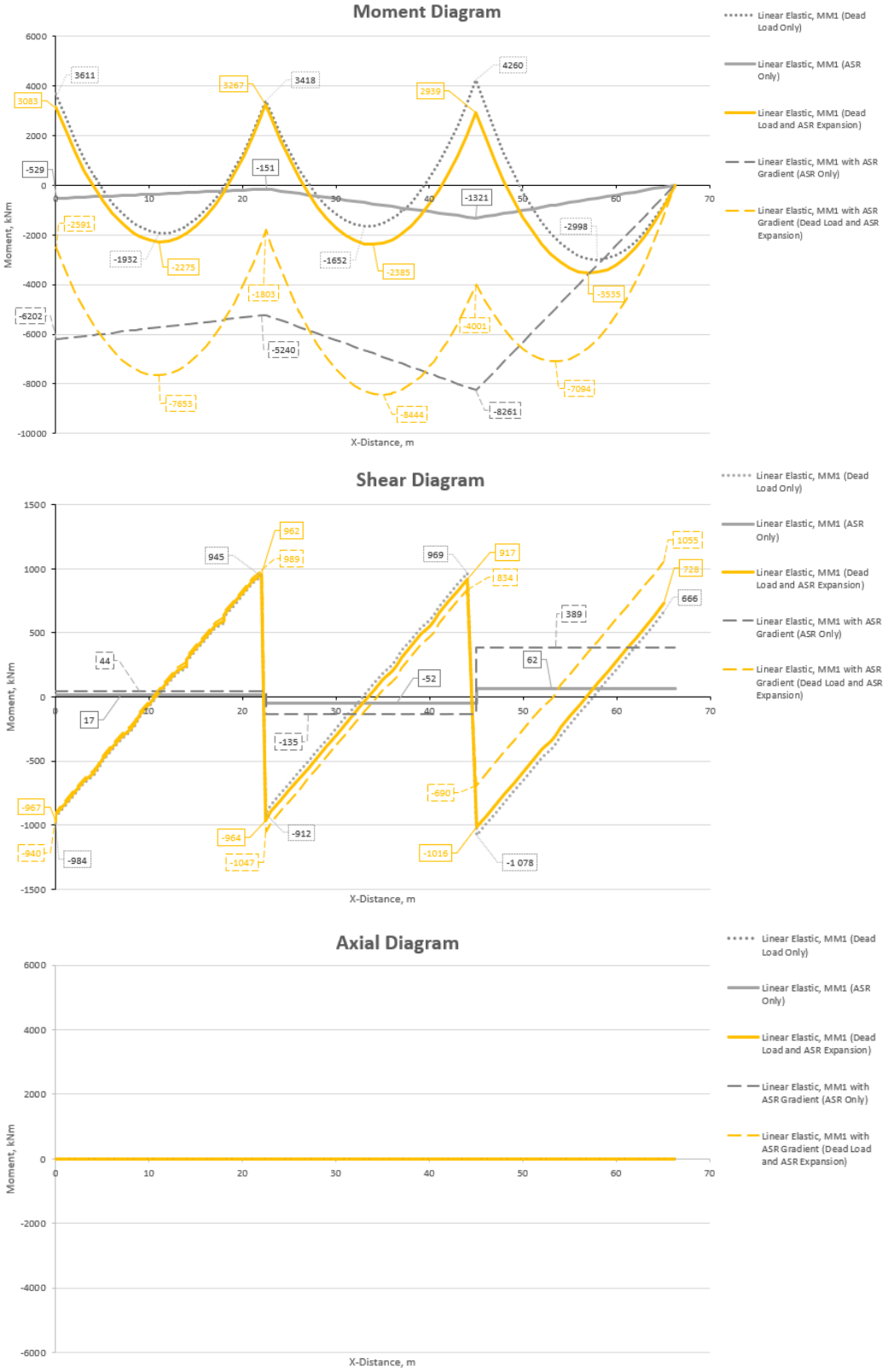

Figure A3.1: Moment-, Shear- and Axial diagram with MM1 for Case 2A

Reduced Stiffness Due to Creep, MM2

In MM2 the modulus of elasticity for concrete, $E_c = 23312.7N/mm^2$ is reduced to $E_{c,eff} = 7770.9N/mm^2$ due to the effect of creep.

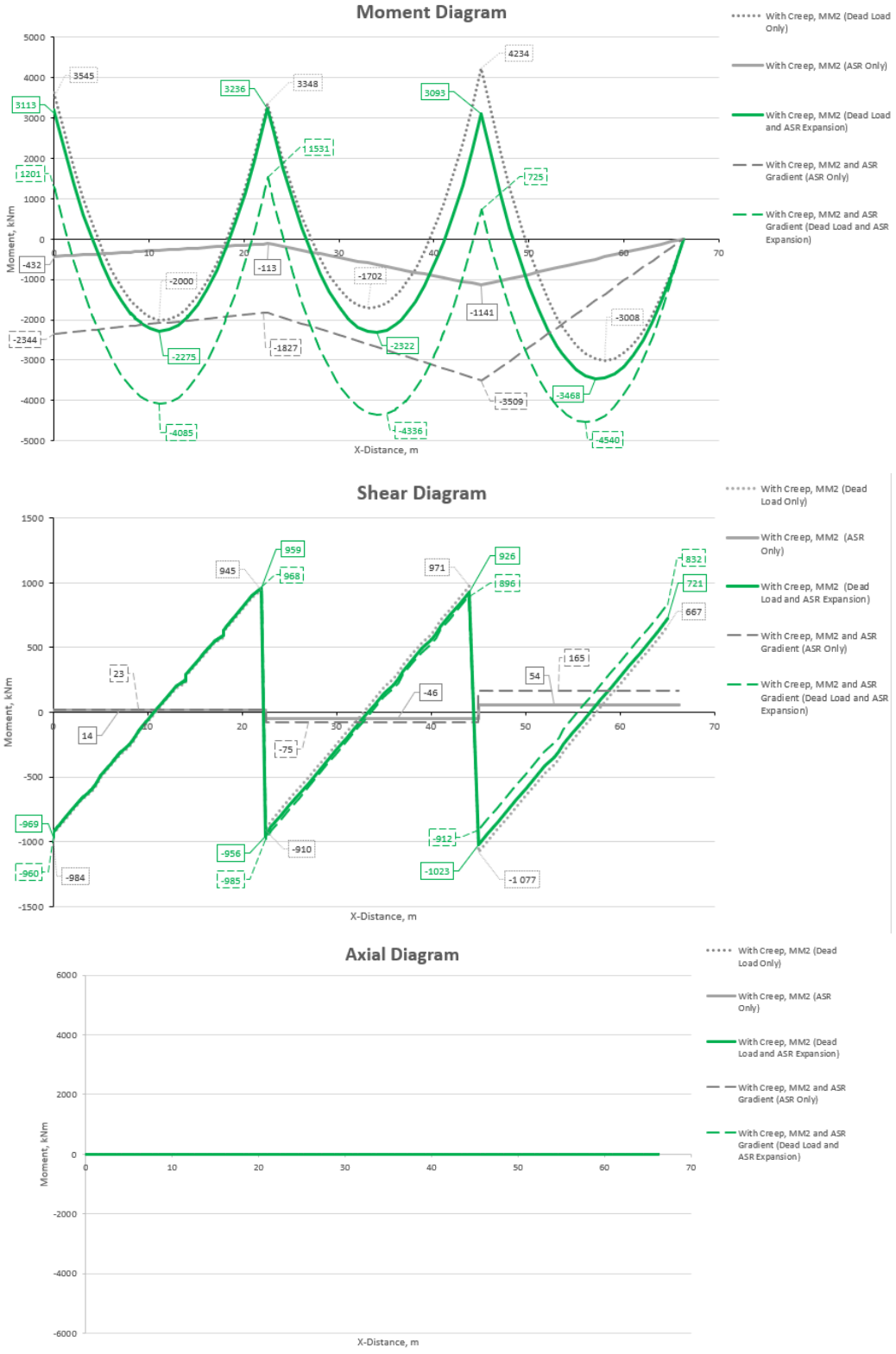

Figure A3.2: Moment-, Shear- and Axial diagram with MM2 for Case 2A

Stress Dependent ASR Expansion, MM3

In MM3 the free ASR strain is changed to stress dependent ASR strain, $\varepsilon_{asr}^{free} \longrightarrow \varepsilon_{asr}$.

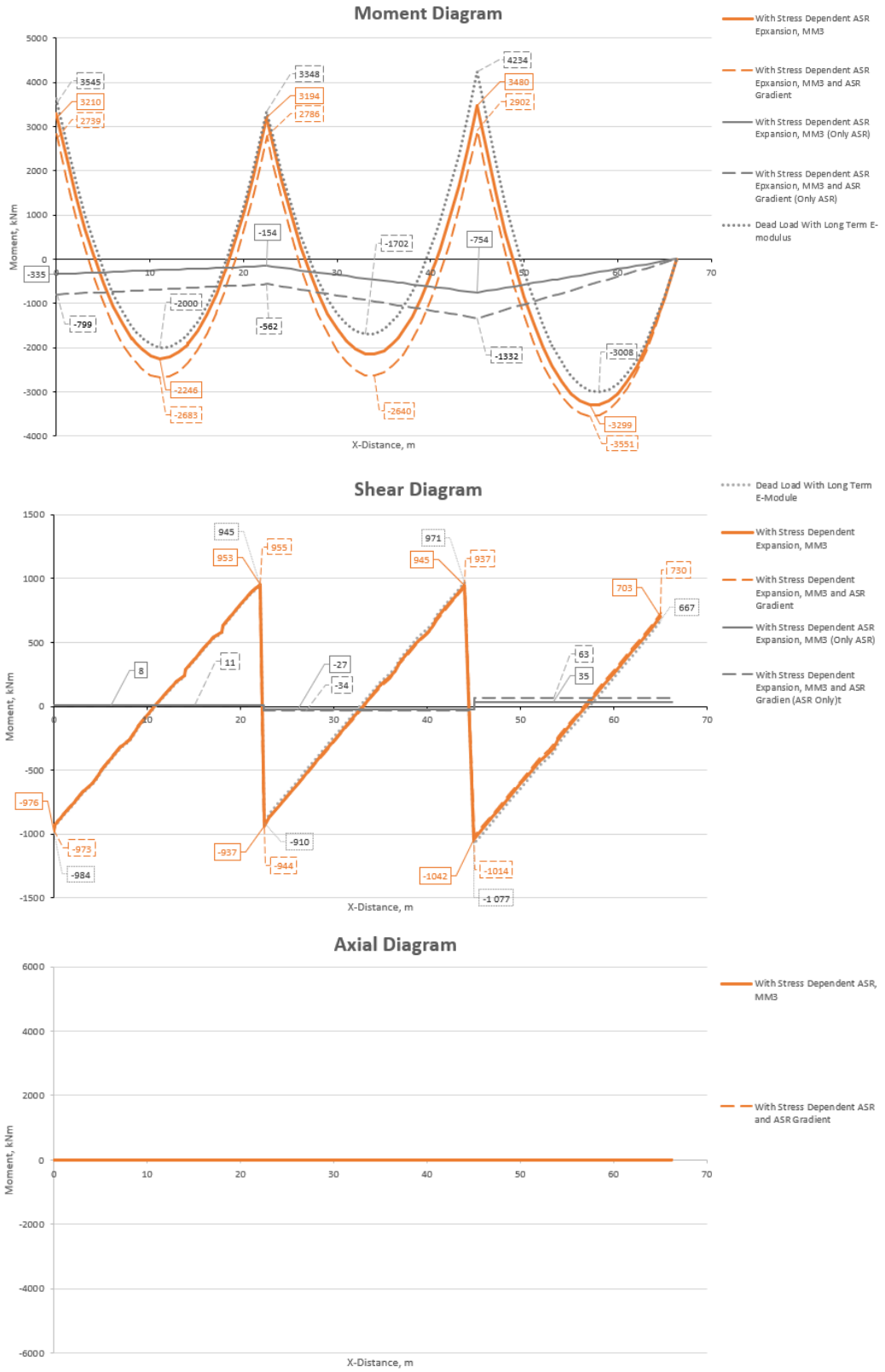

Figure A3.3: Moment-, Shear- and Axial diagram with MM3 for Case 2A

Reduced Stiffness Due to ASR, MM4

In MM4 the stiffness is reduced due to the ASR expansion, $E_{c,eff} \longrightarrow E_{c,eff}(\varepsilon_{asr})$.

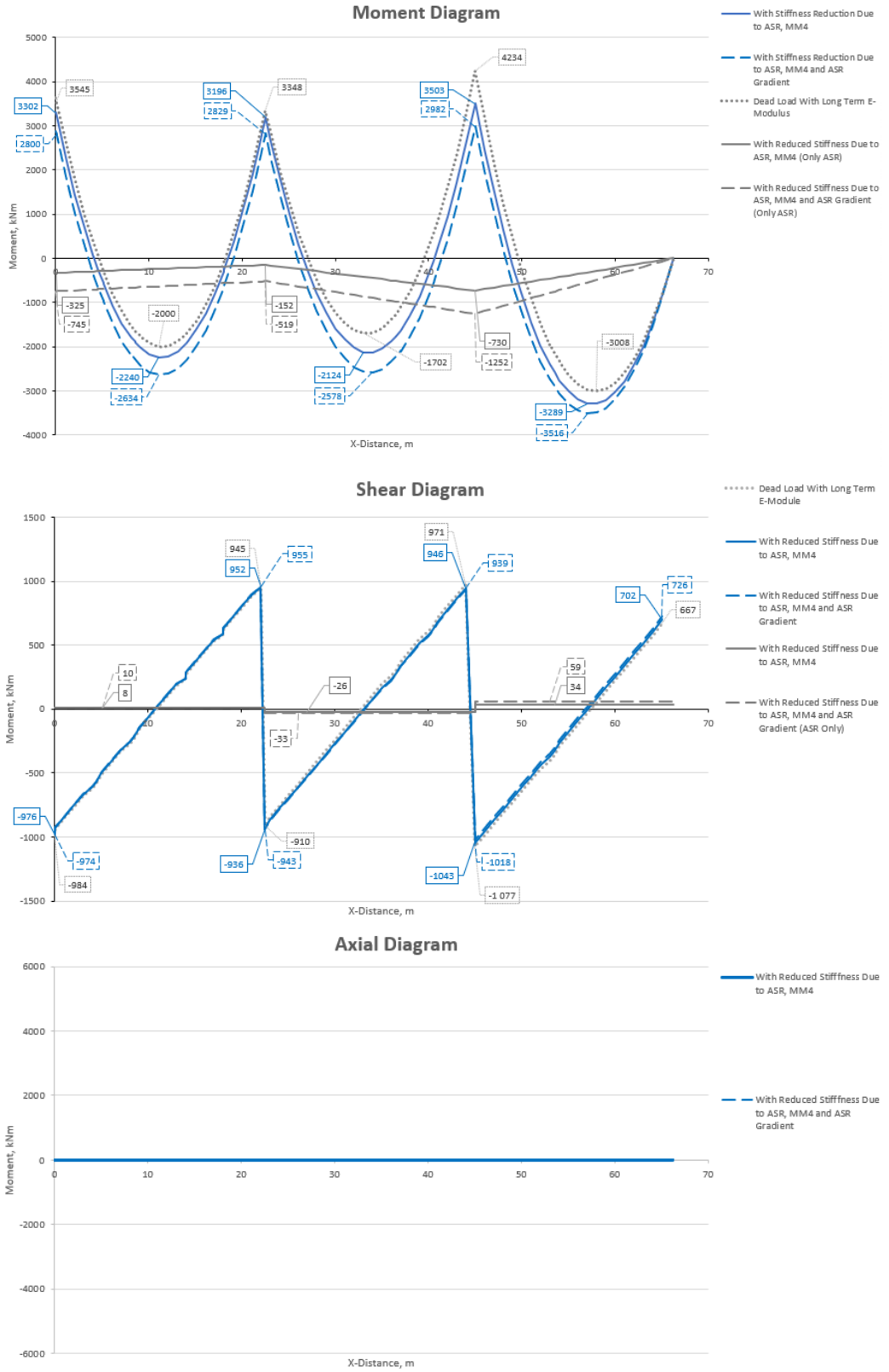

Figure A3.4: Moment-, Shear- and Axial diagram with MM4 for Case 2A

Reduced Stiffness Due to Creep and ASR, MMA

In MMA the beam has reduced stiffness due to creep and ASR, $E_{c,eff}(\varepsilon_{asr})$.

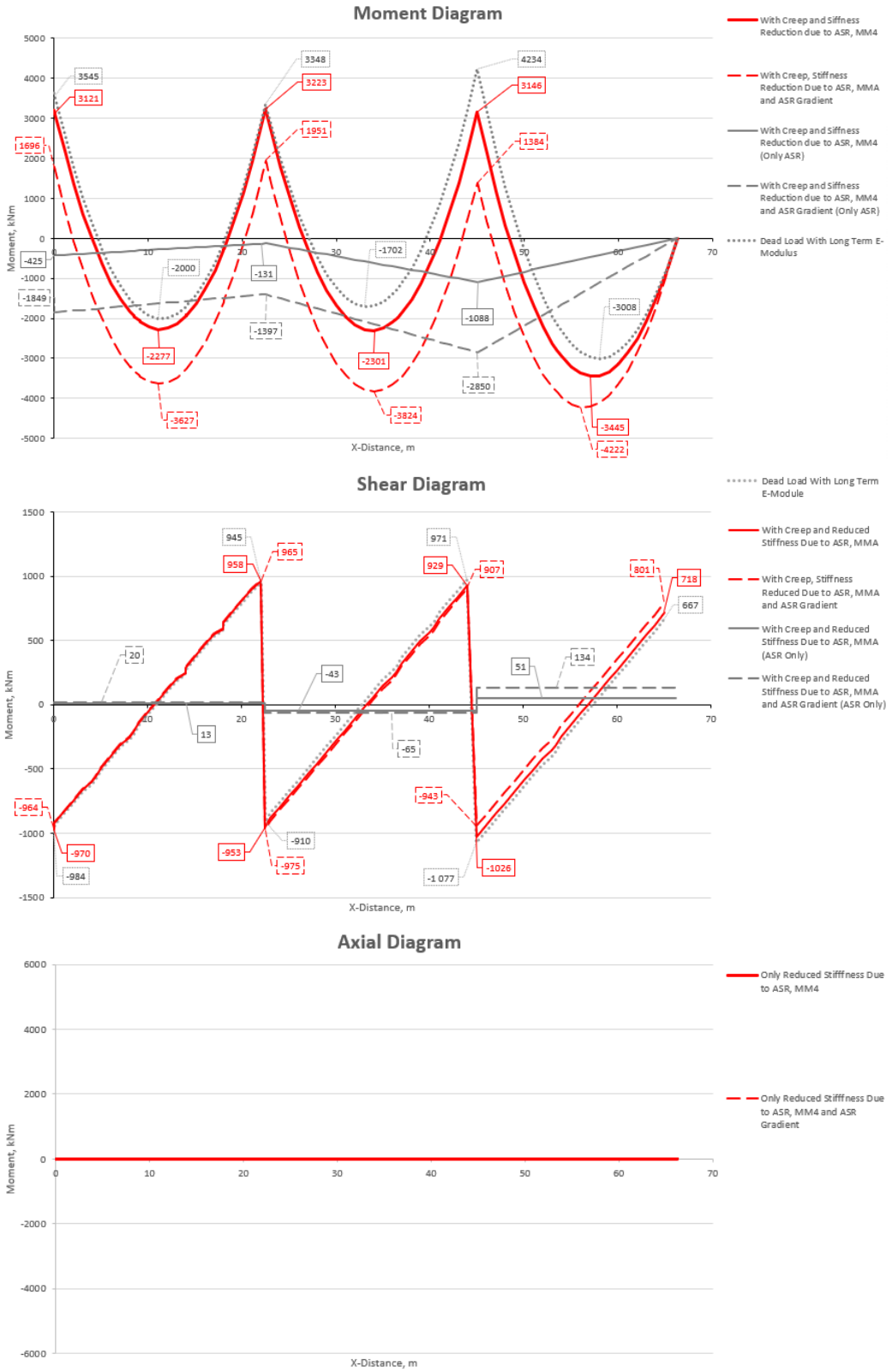

Figure A3.5: Moment-, Shear- and Axial diagram with MMA for Case 2A

A4 Results from Case 2B

Linear Elastic, MM1

In MM1 the modulus of elasticity for concrete, $E_c = 23312.7N/mm^2$ is used.

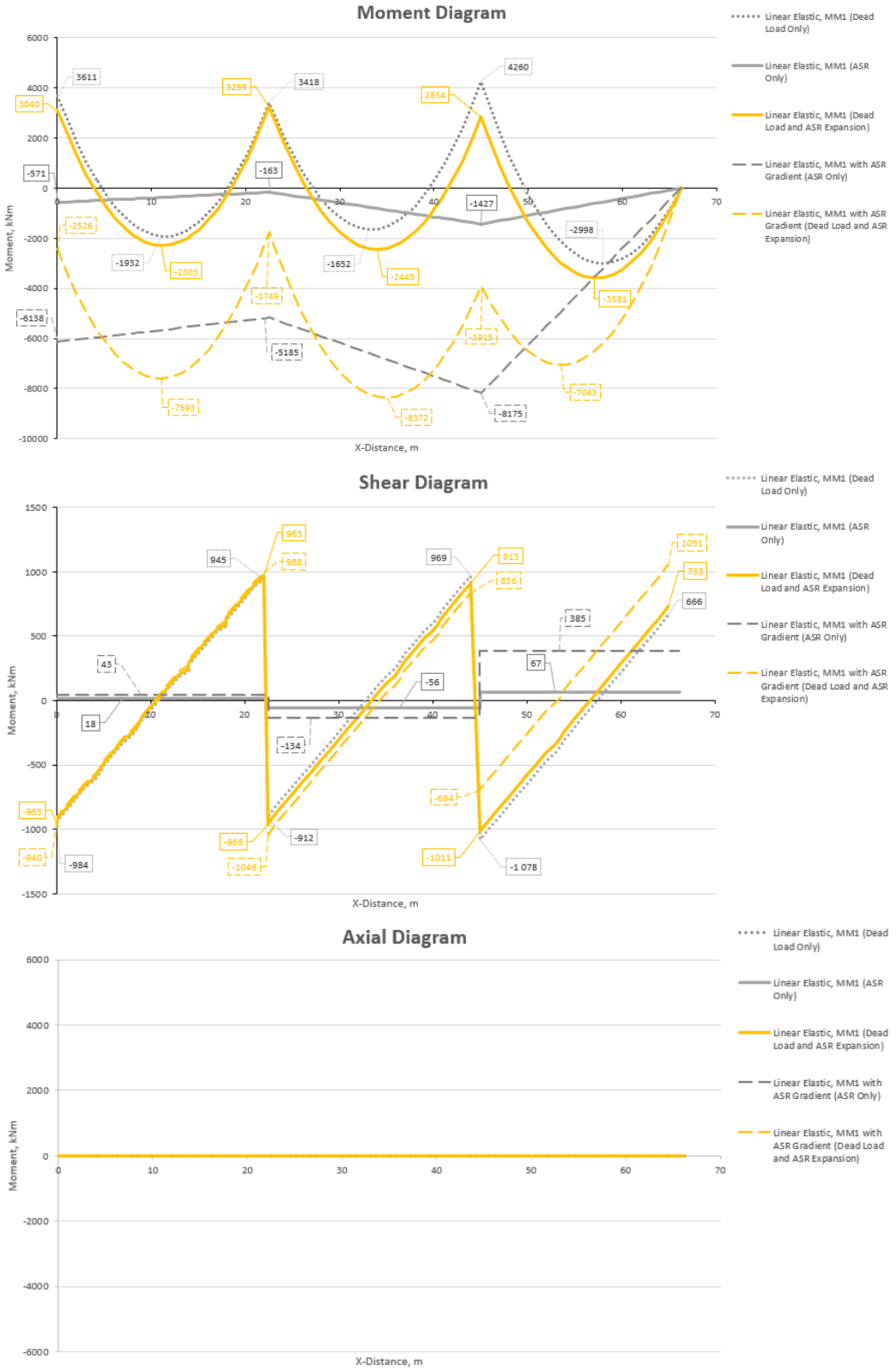

Figure A4.1: Moment-, Shear- and Axial diagram with MM1 for Case 2B

Reduced Stiffness Due to Creep, MM2

In MM2 the modulus of elasticity for concrete, $E_c = 23312.7N/mm^2$ is changed to $E_{c,eff} = 7770.9N/mm^2$ due to the effect of creep.

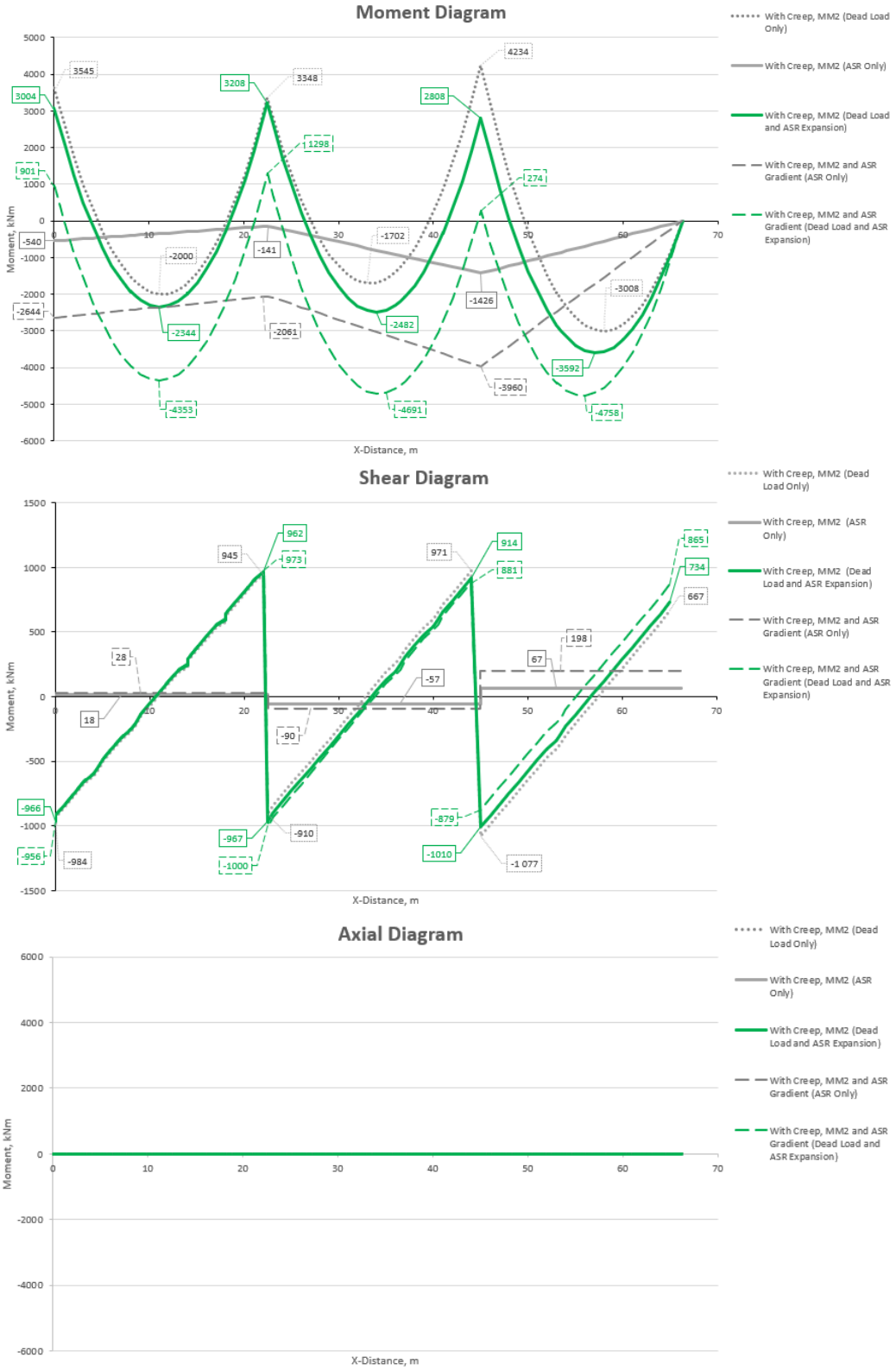

Figure A4.2: Moment-, Shear- and Axial diagram with MM2 for Case 2B

Stress Dependent ASR Expansion, MM3

In MM3 the free ASR strain is changed to stress dependent ASR strain, $\varepsilon_{asr}^{free} \longrightarrow \varepsilon_{asr}$.

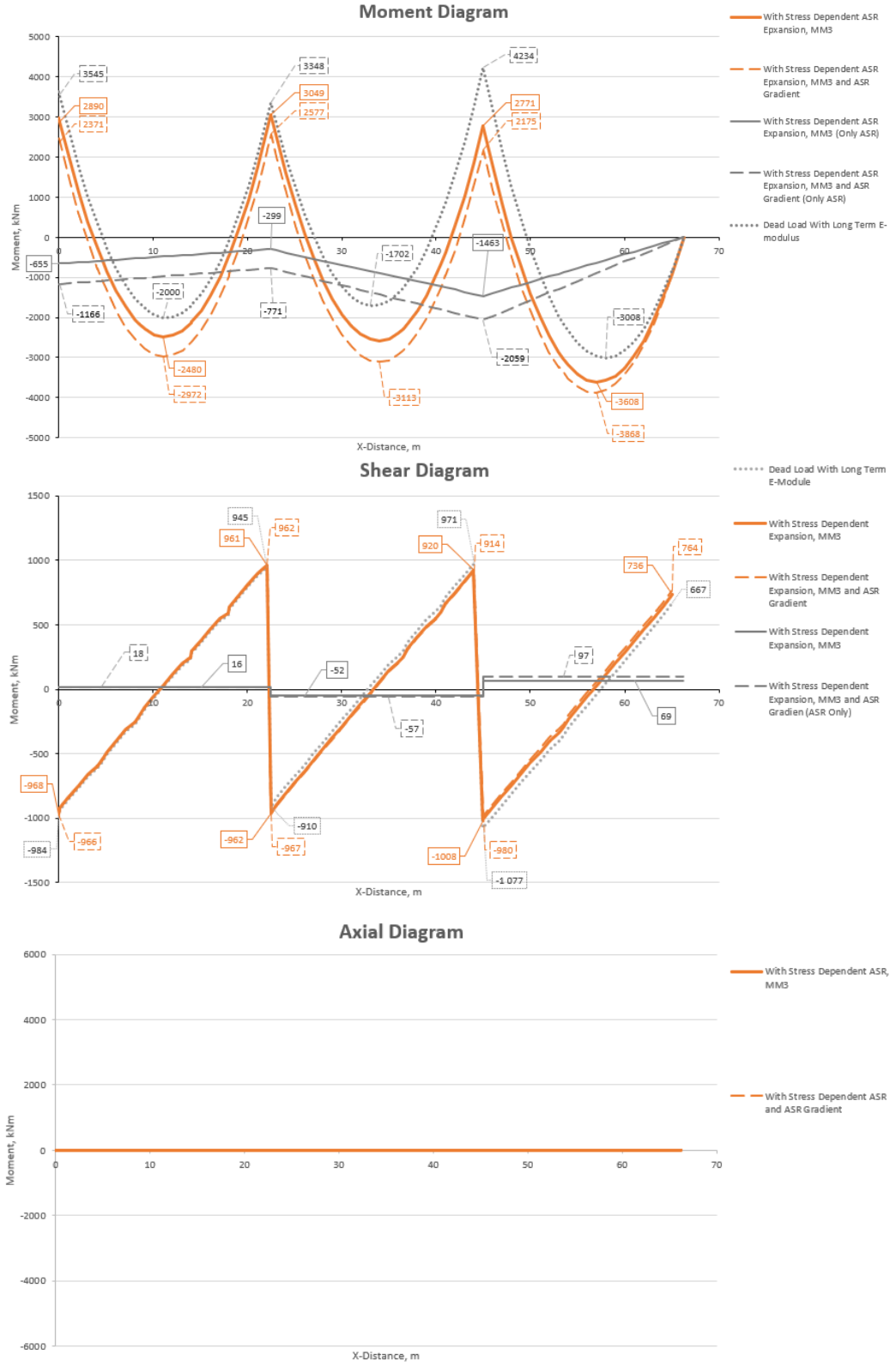

Figure A4.3: Moment-, Shear- and Axial diagram with MM3 for Case 2B

Reduced Stiffness Due to ASR, MM4

In MM4 the stiffness is reduced due to the ASR expansion, $E_{c,eff} \longrightarrow E_{c,eff}(\varepsilon_{asr})$.

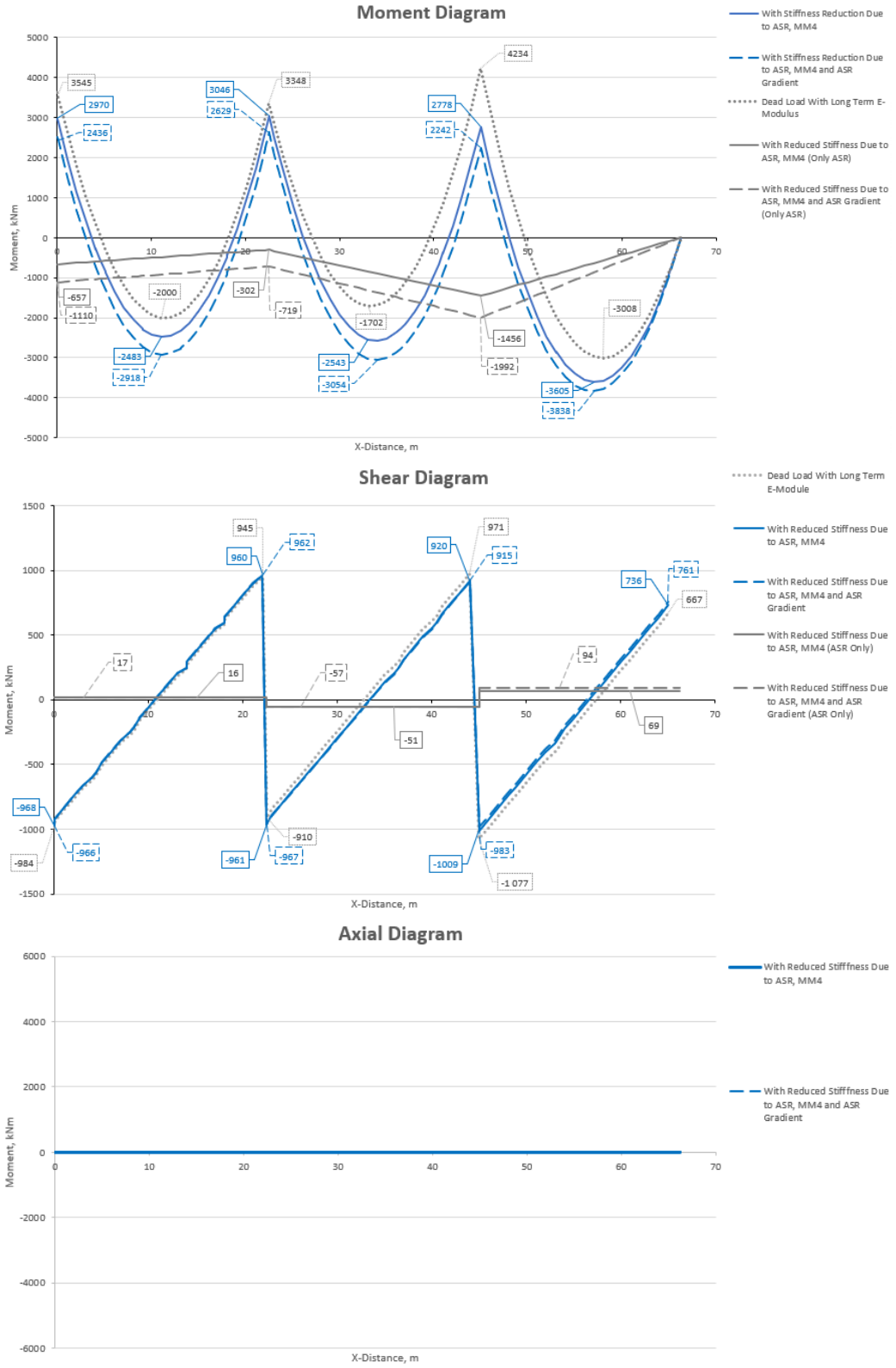

Figure A4.4: Moment-, Shear- and Axial diagram with MM4 for Case 2B

Reduced Stiffness Due to Creep and ASR, MMA

In MMA the beam has reduced stiffness due to creep and ASR, $E_{c,eff}(\varepsilon_{asr})$.

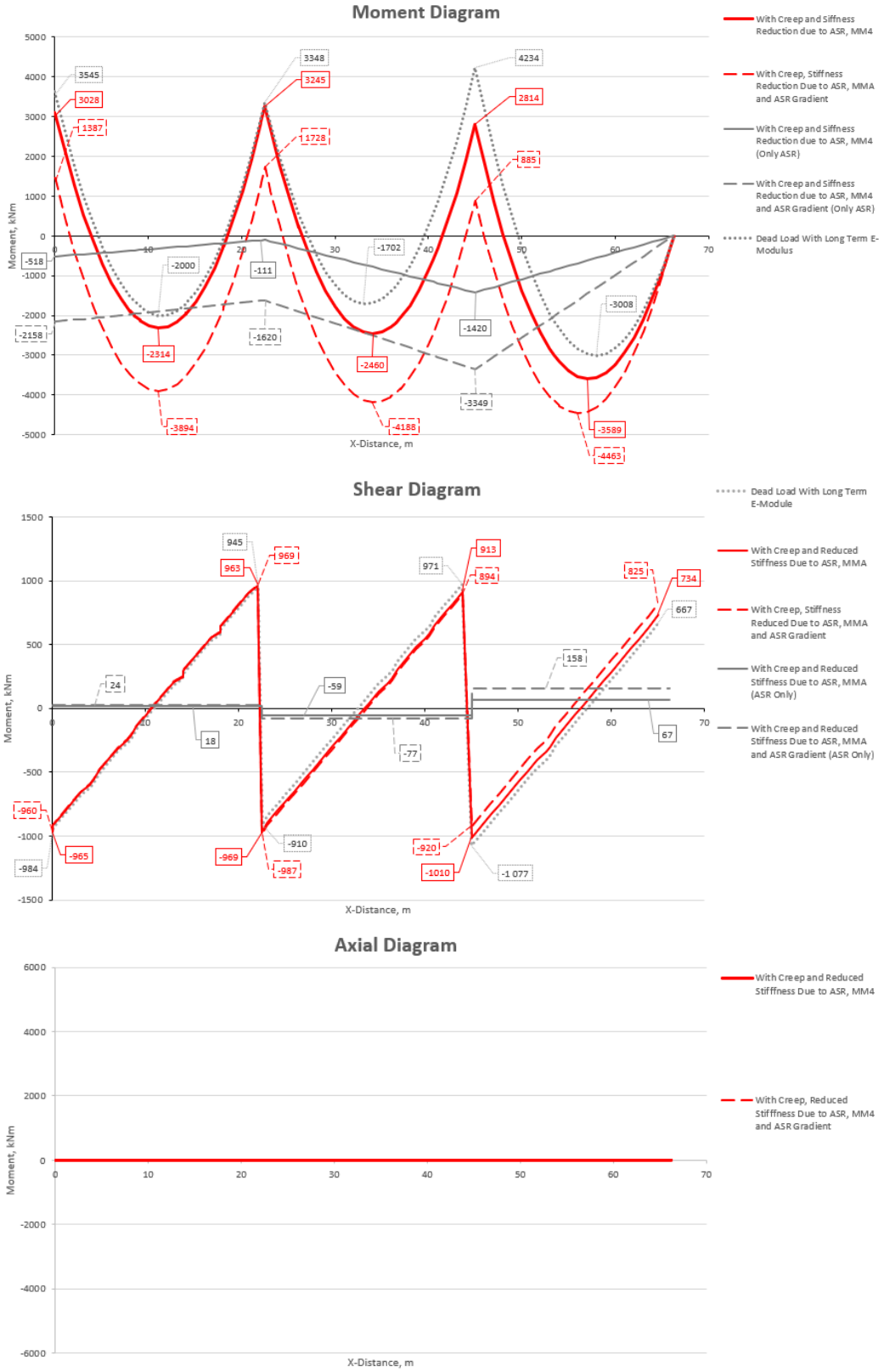

Figure A4.5: Moment-, Shear- and Axial diagram with MMA for Case 2B

A5 Results from Case 2C

Reduced Stiffness Due to Creep, MM2

In MM2 the modulus of elasticity for concrete, $E_c = 23312.7N/mm^2$ is changed to $E_{c,eff} = 7770.9N/mm^2$ due to the effect of creep.

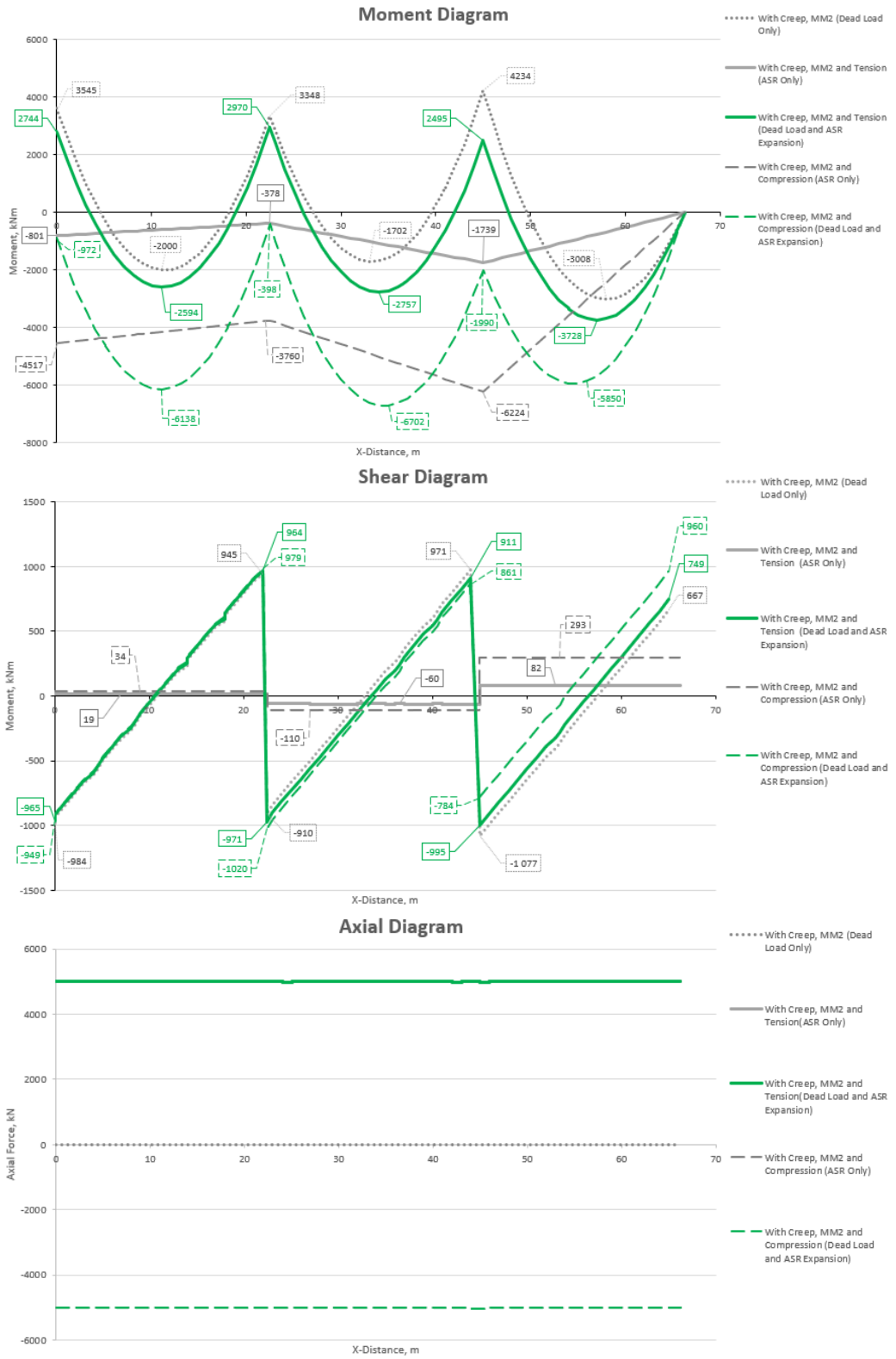

Figure A5.1: Moment-, Shear- and Axial diagram with MM2 for Case 2C

Stress Dependent ASR Expansion, MM3

In MM3 the free ASR strain is changed to stress dependent ASR strain, $\varepsilon_{asr}^{free} \longrightarrow \varepsilon_{asr}$.

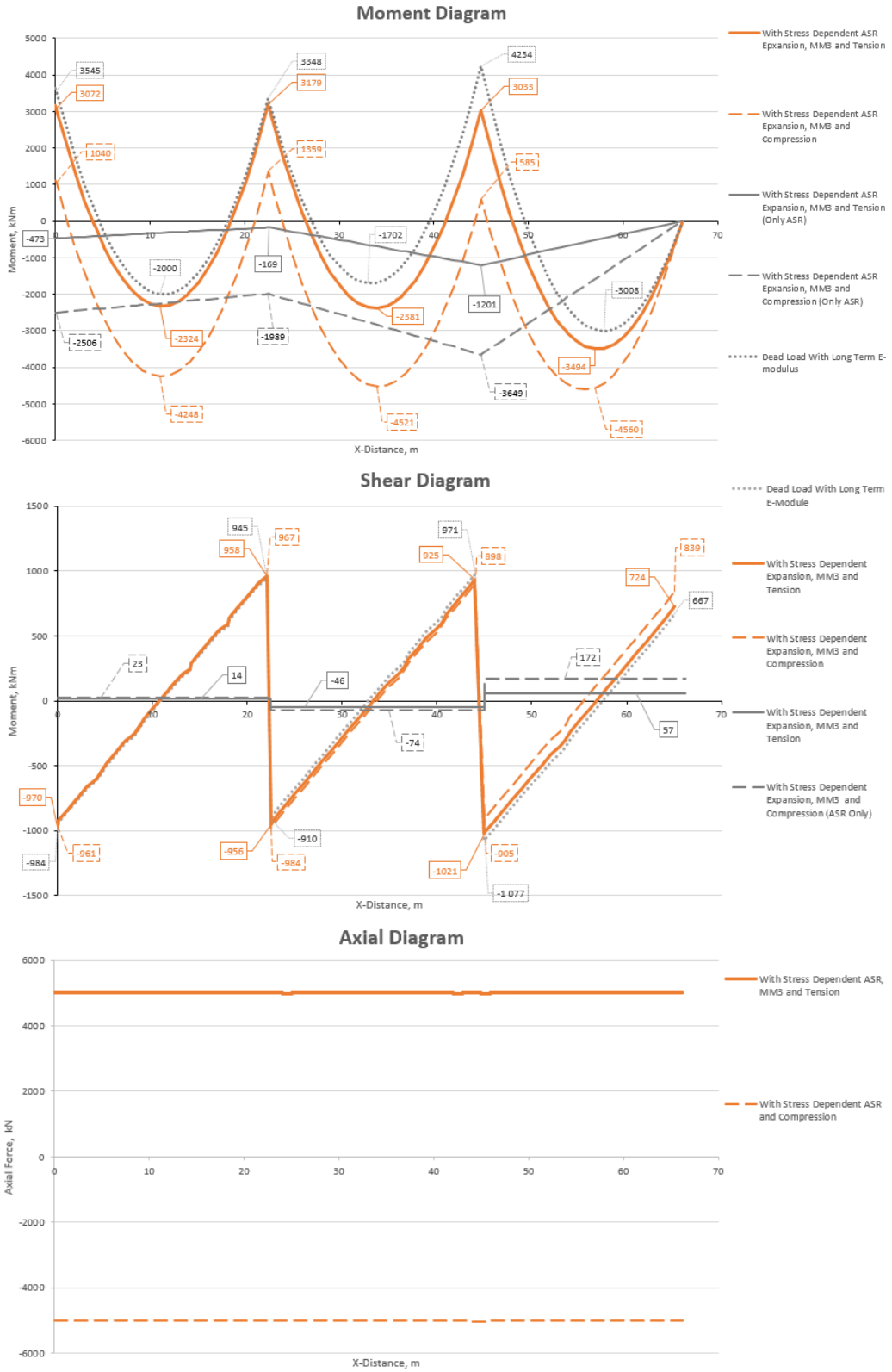

Figure A5.2: Moment-, Shear- and Axial diagram with MM3 for Case 2C

Reduced Stiffness Due to ASR, MM4

In MM4 the stiffness is reduced due to the ASR expansion, $E_{c,eff} \longrightarrow E_{c,eff}(\varepsilon_{asr})$.

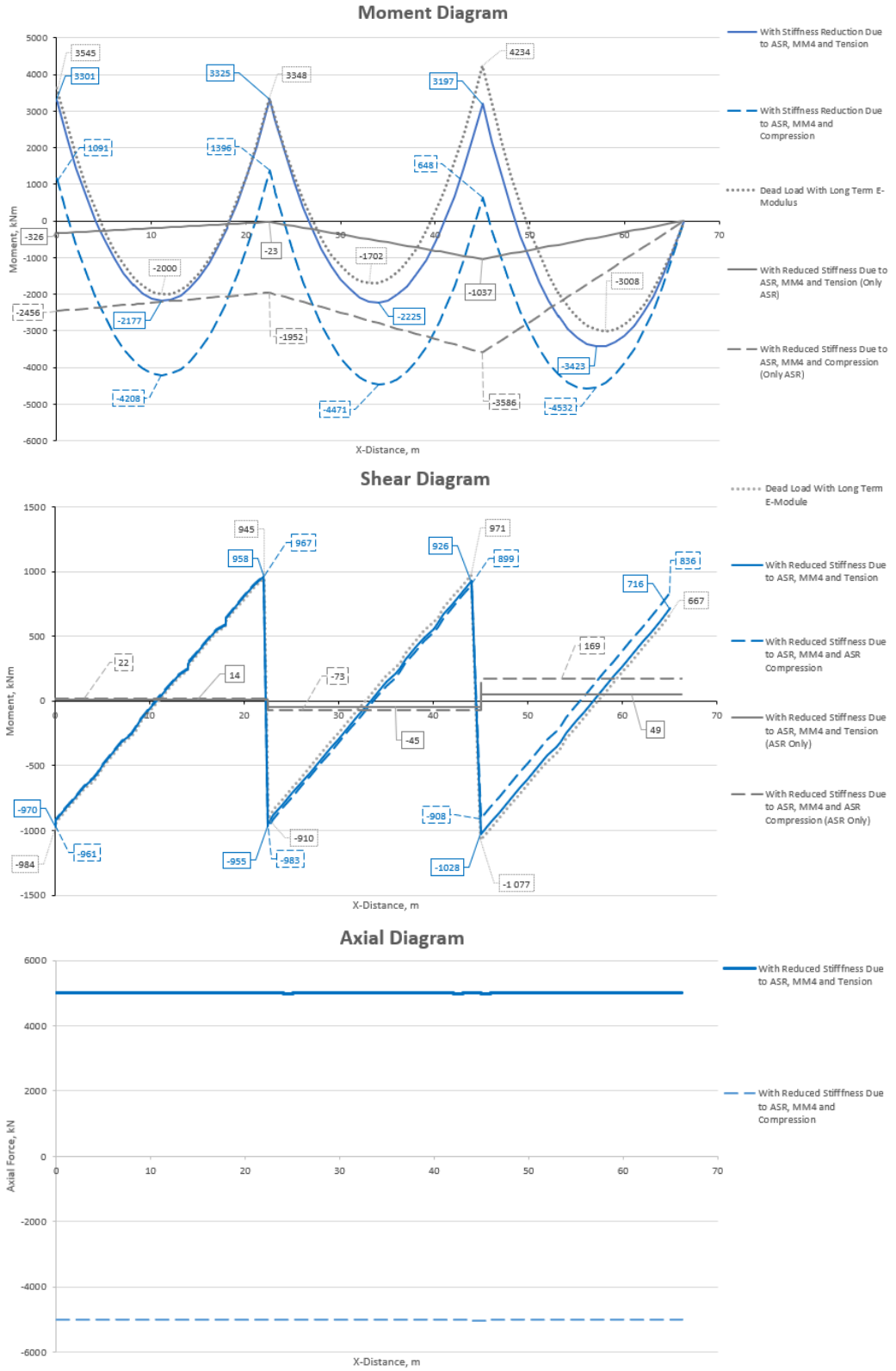

Figure A5.3: Moment-, Shear- and Axial diagram with MM4 for Case 2C

Only Reduced Stiffness Due to Creep and ASR, MMA

In MMA the beam has only reduced stiffness due to creep and ASR, $E_{c,eff}(\varepsilon_{asr})$.

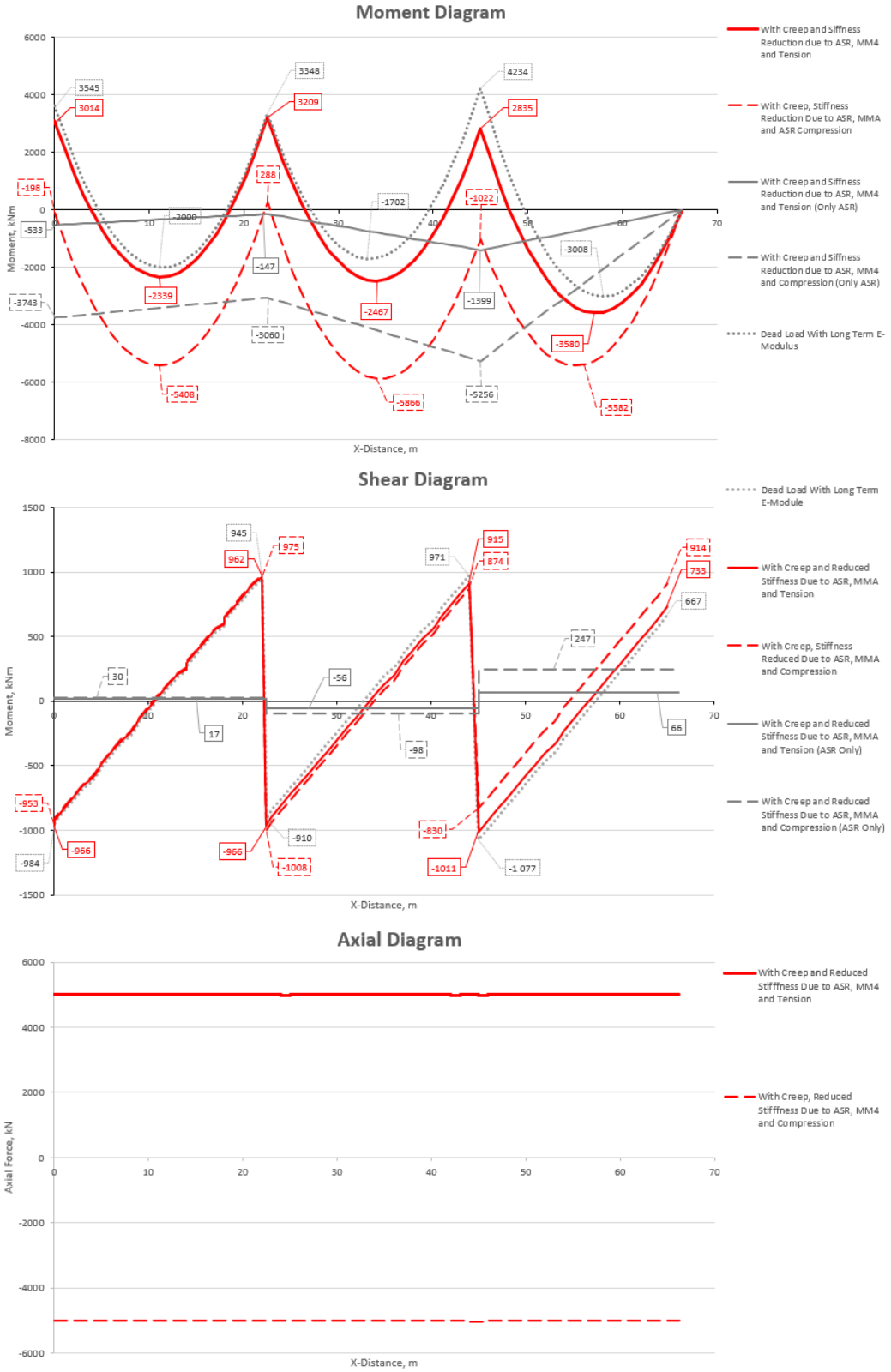

Figure A5.4: Moment-, Shear- and Axial diagram with MMA for Case 2C

Stress Dependent ASR Expansion and Changed Charlwood Function, MMB

In MMB the Charlwood function is changed by increasing the material constant of the stress dependent ASR expansion, σ_u from $-6N/mm^2$ to $-10N/mm^2$.

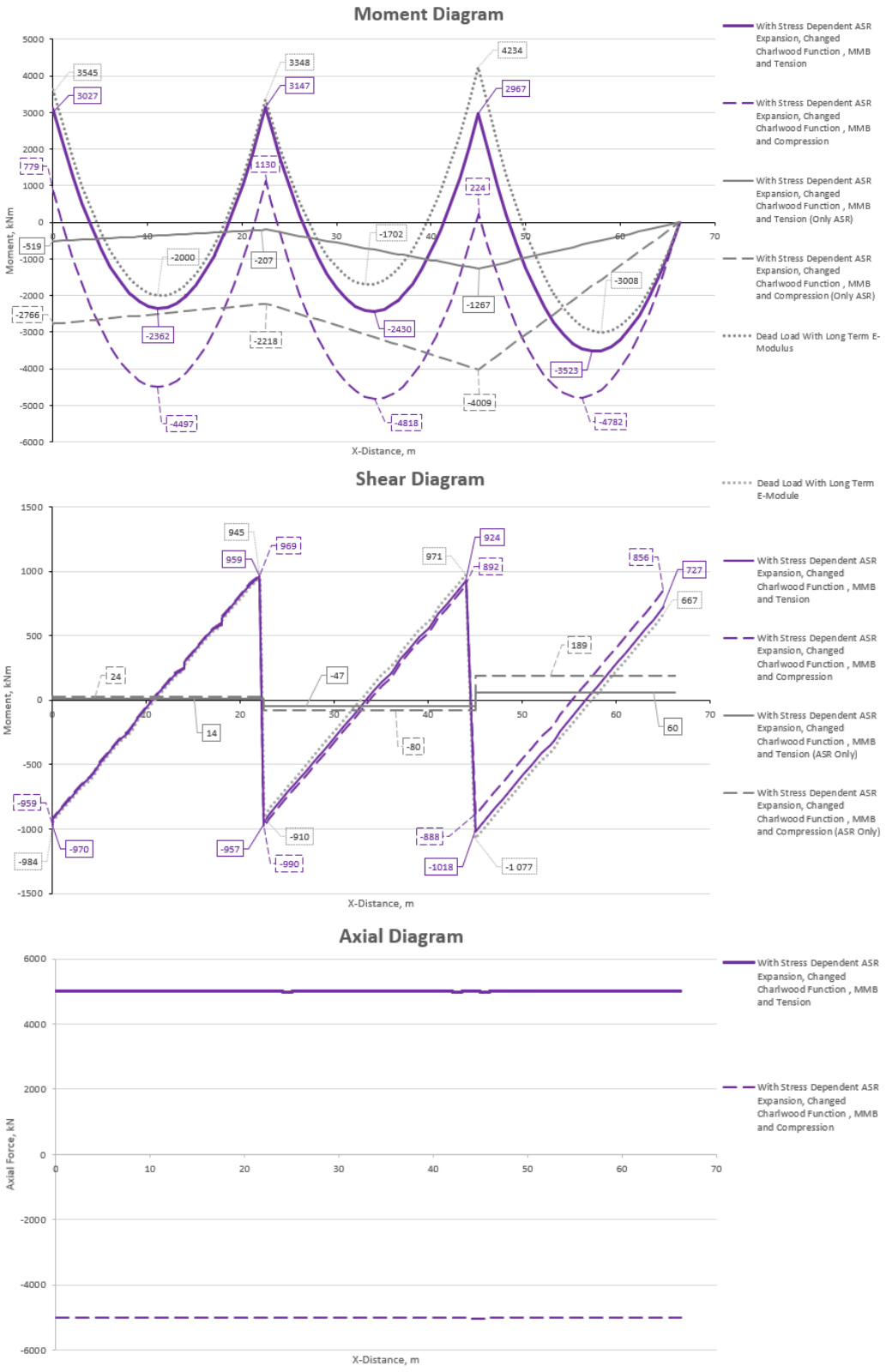

Figure A5.5: Moment-, Shear- and Axial diagram with MMB for Case 2C

Appendix B

B1 Post-Processing for Case 1

There has been done post-processing of the output for moment, shear and axial diagrams for all the material models presented in this report in case 1. We have chosen to show example of post-processing sheets from excel. The figures B1.1, B1.2 and B1.3 shows the post-processing of the moment diagrams for material model MM1 in case 1A. The same post-processing was done for all the other diagrams as well.

	A	B	C	D	E	F	G	H	I	J	K	L	M
1	Moment from External Load												
2	Concrete			Steel							Concrete + Steel		
3	Distance mm	M_c Nmm		Distance mm	Sigma_s N/mm^2	A_s mm^2	F_s N	e_s mm	M_s Nmm		Lengde m	M_tot kNm	
4													
5	0	4,68E+07		0	-14,4401	982	-14180,178	200	-2,84E+06		0	44,0	M_a
6	500	3,57E+07		500	-12,4534	982	-12229,239	200	-2,45E+06		0,5	33,3	
7	1000	2,46E+07		1000	-10,4667	982	-10278,299	200	-2,06E+06		1	22,5	
8	1500	1,58E+07		1500	-6,87173	982	-6748,0389	200	-1,35E+06		1,5	14,5	
9	2000	7,02E+06		2000	-3,27676	982	-3217,7783	200	-6,44E+05		2	6,4	
10	2500	7,30E+04		2500	-0,438665	982	-430,76903	200	-8,62E+04		2,5	0,0	
11	3000	-6,87E+06		3000	2,39943	982	2356,24026	200	4,71E+05		3	-6,4	
12	3500	-1,20E+07		3500	4,48065	982	4399,9983	200	8,80E+05		3,5	-11,1	
13	4000	-1,71E+07		4000	6,56187	982	6443,75634	200	1,29E+06		4	-15,8	
14	4500	-2,03E+07		4500	7,88621	982	7744,25822	200	1,55E+06		4,5	-18,7	
15	5000	-2,35E+07		5000	9,21055	982	9044,7601	200	1,81E+06		5	-21,7	
16	5500	-2,49E+07		5500	9,778025	982	9602,02055	200	1,92E+06		5,5	-23,0	
17	6000	-2,63E+07		6000	10,3455	982	10159,281	200	2,03E+06		6	-24,3	
18	6500	-2,58E+07		6500	10,156085	982	9973,27547	200	1,99E+06		6,5	-23,8	M_span
19	7000	-2,54E+07		7000	9,96667	982	9787,26994	200	1,96E+06		7	-23,4	
20	7500	-2,31E+07		7500	9,020385	982	8858,01807	200	1,77E+06		7,5	-21,3	
21	8000	-2,07E+07		8000	8,0741	982	7928,7662	200	1,59E+06		8	-19,2	
22	8500	-1,66E+07		8500	6,37094	982	6256,26308	200	1,25E+06		8,5	-15,3	
23	9000	-1,24E+07		9000	4,66778	982	4583,75996	200	9,17E+05		9	-11,5	
24	9500	-6,30E+06		9500	3,62698	982	3561,69436	200	7,12E+05		9,5	-5,6	
25	10000	-1,75E+05		10000	2,58618	982	2539,62876	200	5,08E+05		10	0,3	M_b
26													

Figure B1.1: Post-Processing of Moment from External Load

Moment from ASR									
Concrete		Steel						Concrete + Steel	
Distance mm	M_c Nmm	Distance mm	Sigma_s N/mm^2	A_s mm^2	F_s N	e_s mm	M_s Nmm	Lengde m	M_tot kNm	
0	-1,76E+07	0	-197,686	982	-194127,65	200	-3,88E+07	0	-56,4	M_a
500	-1,49E+07	500	-197,152	982	-193602,77	200	-3,87E+07	0,5	-53,6	
1000	-1,22E+07	1000	-196,617	982	-193077,89	200	-3,86E+07	1	-50,8	
1500	-9,57E+06	1500	-195,549	982	-192029,12	200	-3,84E+07	1,5	-48,0	
2000	-6,96E+06	2000	-194,481	982	-190980,34	200	-3,82E+07	2	-45,2	
2500	-4,35E+06	2500	-193,413	982	-189931,57	200	-3,80E+07	2,5	-42,3	
3000	-1,73E+06	3000	-192,345	982	-188882,79	200	-3,78E+07	3	-39,5	
3500	8,78E+05	3500	-191,277	982	-187834,01	200	-3,76E+07	3,5	-36,7	
4000	3,49E+06	4000	-190,209	982	-186785,24	200	-3,74E+07	4	-33,9	
4500	6,10E+06	4500	-189,141	982	-185736,46	200	-3,71E+07	4,5	-31,0	
5000	8,72E+06	5000	-188,073	982	-184687,69	200	-3,69E+07	5	-28,2	
5500	1,13E+07	5500	-187,005	982	-183638,91	200	-3,67E+07	5,5	-25,4	
6000	1,39E+07	6000	-185,937	982	-182590,13	200	-3,65E+07	6	-22,6	
6500	1,66E+07	6500	-184,869	982	-181541,36	200	-3,63E+07	6,5	-19,8	
7000	1,92E+07	7000	-183,801	982	-180492,58	200	-3,61E+07	7	-16,9	
7500	2,18E+07	7500	-182,733	982	-179443,81	200	-3,59E+07	7,5	-14,1	
8000	2,44E+07	8000	-181,665	982	-178395,03	200	-3,57E+07	8	-11,3	
8500	2,70E+07	8500	-180,597	982	-177346,25	200	-3,55E+07	8,5	-8,5	
9000	2,96E+07	9000	-179,529	982	-176297,48	200	-3,53E+07	9	-5,6	
9500	3,23E+07	9500	-178,995	982	-175773,09	200	-3,52E+07	9,5	-2,8	
10000	3,50E+07	10000	-178,461	982	-175248,7	200	-3,50E+07	10	0,0	M_b

Figure B1.2: Post-Processing of Moment from ASR Expansion

Moment from External Load and ASR

Concrete		Steel						Concrete + Steel		
Distance mm	M_c Nmm	Distance mm	Sigma_s N/mm^2	A_s mm^2	F_s N	e_s mm	M_s Nmm	Lengde m	M_tot kNm	
0	2,92E+07	0	183,245	982	179946,59	200	-3,60E+07	0	-6,8	M_a
500	2,08E+07	500	184,698	982	181373,436	200	-3,63E+07	0,5	-15,5	
1000	1,24E+07	1000	186,151	982	182800,282	200	-3,66E+07	1	-24,1	
1500	6,24E+06	1500	188,678	982	185281,796	200	-3,71E+07	1,5	-30,8	
2000	55487,1	2000	191,205	982	187763,31	200	-3,76E+07	2	-37,5	
2500	-4,27E+06	2500	192,975	982	189501,45	200	-3,79E+07	2,5	-42,2	
3000	-8,60E+06	3000	194,745	982	191239,59	200	-3,82E+07	3	-46,9	
3500	-1,11E+07	3500	195,758	982	192234,356	200	-3,84E+07	3,5	-49,5	
4000	-1,36E+07	4000	196,771	982	193229,122	200	-3,86E+07	4	-52,2	
4500	-1,42E+07	4500	197,0275	982	193481,005	200	-3,87E+07	4,5	-52,9	M_span
5000	-1,48E+07	5000	197,284	982	193732,888	200	-3,87E+07	5	-53,6	
5500	-1,36E+07	5500	196,7835	982	193241,397	200	-3,86E+07	5,5	-52,2	
6000	-1,24E+07	6000	196,283	982	192749,906	200	-3,85E+07	6	-50,9	
6500	-9,29E+06	6500	195,0255	982	191515,041	200	-3,83E+07	6,5	-47,6	
7000	-6,21E+06	7000	193,768	982	190280,176	200	-3,81E+07	7	-44,3	
7500	-1,29E+06	7500	191,7535	982	188301,937	200	-3,77E+07	7,5	-38,9	
8000	3,64E+06	8000	189,739	982	186323,698	200	-3,73E+07	8	-33,6	
8500	1,04E+07	8500	186,968	982	183602,576	200	-3,67E+07	8,5	-26,3	
9000	1,72E+07	9000	184,197	982	180881,454	200	-3,62E+07	9	-19,0	
9500	2,62E+07	9500	182,622	982	179334,804	200	-3,59E+07	9,5	-9,7	
10000	3,52E+07	10000	181,047	982	177788,154	200	-3,56E+07	10	-0,3	M_b

Figure B1.3: Post-Processing of Moment from External Load and ASR Expansion

B2 Post-Processing for Case 2

There has been done a lot post-processing of the output for moment, shear and axial diagrams for all the material models presented in this report in case 2. We have chosen to show example of post-processing sheets from excel. The figures B1.1, B1.2 and B1.3 shows parts of the post-processing of the moment diagrams for material model MM2 in case 2B. The same post-processing was done for all the other diagrams as well.

Moment from External Load and ASR, Kappa=0

Concrete		Steel UK						Steel OK						Concrete + Steel		
Distance mm	M_c Nmm	Distance mm	Sigma_s N/mm^2	A_s mm^2	F_s N	e_s mm	M_s Nmm	Distance mm	Sigma_s N/mm^2	A_s mm^2	F_s N	e_s mm	M_s Nmm	Lengde m	M_tot kNm	
0	-9,47E+08	0	159,62	2412,7	3,85E+05	811	-3,12E+08	0	195,933	27 344,40	5,36E+06	-811	4,35E+09	0	3086	M_a
84,3945	-1,03E+09	84,3945	159,62	2412,7	3,85E+05	811	-3,12E+08	84,3945	195,933	27 344,40	5,36E+06	-811	4,35E+09	0	3004	
84,3945	-8,51E+08	84,3945	177,617	2412,7	4,29E+05	811	-3,48E+08	84,3945	189,221	27 344,40	5,17E+06	-811	4,20E+09	0	2997	
1084,39	-1,77E+09	1084,39	177,617	2412,7	4,29E+05	811	-3,48E+08	1084,39	189,221	27 344,40	5,17E+06	-811	4,20E+09	1	2078	
1084,39	-1,45E+09	1084,39	208,673	2412,7	5,03E+05	811	-4,08E+08	1084,39	177,638	27 344,40	4,86E+06	-811	3,94E+09	1	2078	
2084,39	-2,28E+09	2084,39	208,673	2412,7	5,03E+05	811	-4,08E+08	2084,39	177,638	27 344,40	4,86E+06	-811	3,94E+09	2	1246	
2084,39	-2,00E+09	2084,39	236,655	2412,7	5,71E+05	811	-4,63E+08	2084,39	167,202	27 344,40	4,57E+06	-811	3,71E+09	2	1246	
3084,39	-2,74E+09	3084,39	236,655	2412,7	5,71E+05	811	-4,63E+08	3084,39	167,202	27 344,40	4,57E+06	-811	3,71E+09	3	501	
3084,39	-2,49E+09	3084,39	261,563	2412,7	6,31E+05	811	-5,12E+08	3084,39	157,912	27 344,40	4,32E+06	-811	3,50E+09	3	501	
4084,39	-3,15E+09	4084,39	261,563	2412,7	6,31E+05	811	-5,12E+08	4084,39	157,912	27 344,40	4,32E+06	-811	3,50E+09	4	-158	
4084,39	-2,98E+09	4084,39	277,441	2412,7	6,69E+05	811	-5,43E+08	4084,39	151,99	27 344,40	4,16E+06	-811	3,37E+09	4	-152	
4500	-3,23E+09	4500	277,441	2412,7	6,69E+05	811	-5,43E+08	4500	151,99	27 344,40	4,16E+06	-811	3,37E+09	5	-401	
4500	4,47E+08	4500	166,873	12 063,70	2,01E+06	811	-1,63E+09	4500	240,375	4 021,20	9,67E+05	-811	7,84E+08	5	-402	
5084,39	1,23E+08	5084,39	166,873	12 063,70	2,01E+06	811	-1,63E+09	5084,39	240,375	4 021,20	9,67E+05	-811	7,84E+08	5	-726	
5084,39	2,44E+08	5084,39	177,42	12 063,70	2,14E+06	811	-1,74E+09	5084,39	233,291	4 021,20	9,38E+05	-811	7,61E+08	5	-731	
6084,39	-2,41E+08	6084,39	177,42	12 063,70	2,14E+06	811	-1,74E+09	6084,39	233,291	4 021,20	9,38E+05	-811	7,61E+08	6	-1216	
6084,39	-1,05E+08	6084,39	188,81	12 063,70	2,28E+06	811	-1,85E+09	6084,39	225,64	4 021,20	9,07E+05	-811	7,36E+08	6	-1216	
7084,39	-5,04E+08	7084,39	188,81	12 063,70	2,28E+06	811	-1,85E+09	7084,39	225,64	4 021,20	9,07E+05	-811	7,36E+08	7	-1615	
7084,39	-3,94E+08	7084,39	197,968	12 063,70	2,39E+06	811	-1,94E+09	7084,39	219,489	4 021,20	8,83E+05	-811	7,16E+08	7	-1615	
8084,39	-7,06E+08	8084,39	197,968	12 063,70	2,39E+06	811	-1,94E+09	8084,39	219,489	4 021,20	8,83E+05	-811	7,16E+08	8	-1927	
8084,39	-6,38E+08	8084,39	203,178	12 063,70	2,45E+06	811	-1,99E+09	8084,39	215,989	4 021,20	8,69E+05	-811	7,04E+08	8	-1921	
8500	-7,42E+08	8500	203,178	12 063,70	2,45E+06	811	-1,99E+09	8500	215,989	4 021,20	8,69E+05	-811	7,04E+08	9	-2026	
8500	-4,41E+08	8500	185,401	15 280,70	2,83E+06	811	-2,30E+09	8500	218,22	4 021,20	8,78E+05	-811	7,12E+08	9	-2027	
9084,39	-5,62E+08	9084,39	185,401	15 280,70	2,83E+06	811	-2,30E+09	9084,39	218,22	4 021,20	8,78E+05	-811	7,12E+08	9	-2148	
9084,39	-5,21E+08	9084,39	188,526	15 280,70	2,88E+06	811	-2,34E+09	9084,39	215,958	4 021,20	8,68E+05	-811	7,04E+08	9	-2153	
10084,4	-6,60E+08	10084,4	188,526	15 280,70	2,88E+06	811	-2,34E+09	10084,4	215,958	4 021,20	8,68E+05	-811	7,04E+08	10	-2292	
10084,4	-6,27E+08	10084,4	190,74	15 280,70	2,91E+06	811	-2,36E+09	10084,4	214,355	4 021,20	8,62E+05	-811	6,99E+08	10	-2292	
11084,4	-6,79E+08	11084,4	190,74	15 280,70	2,91E+06	811	-2,36E+09	11084,4	214,355	4 021,20	8,62E+05	-811	6,99E+08	11	-2344	
11084,4	-6,76E+08	11084,4	190,946	15 280,70	2,92E+06	811	-2,37E+09	11084,4	214,206	4 021,20	8,61E+05	-811	6,99E+08	11	-2344	
12084,4	-6,42E+08	12084,4	190,946	15 280,70	2,92E+06	811	-2,37E+09	12084,4	214,206	4 021,20	8,61E+05	-811	6,99E+08	12	-2310	
12084,4	-6,69E+08	12084,4	189,144	15 280,70	2,89E+06	811	-2,34E+09	12084,4	215,51	4 021,20	8,67E+05	-811	7,03E+08	12	-2310	
13084,4	-5,47E+08	13084,4	189,144	15 280,70	2,89E+06	811	-2,34E+09	13084,4	215,51	4 021,20	8,67E+05	-811	7,03E+08	13	-2189	
13084,4	-5,99E+08	13084,4	185,549	15 280,70	2,84E+06	811	-2,30E+09	13084,4	218,113	4 021,20	8,77E+05	-811	7,11E+08	13	-2187	
14000	-4,12E+08	14000	185,549	15 280,70	2,84E+06	811	-2,30E+09	14000	218,113	4 021,20	8,77E+05	-811	7,11E+08	14	-2001	
14000	-7,08E+08	14000	203,449	12 063,70	2,45E+06	811	-1,99E+09	14000	215,808	4 021,20	8,68E+05	-811	7,04E+08	14	-1995	
14084,4	-6,87E+08	14084,4	203,449	12 063,70	2,45E+06	811	-1,99E+09	14084,4	215,808	4 021,20	8,68E+05	-811	7,04E+08	14	-1974	
14084,4	-7,41E+08	14084,4	199,573	12 063,70	2,41E+06	811	-1,95E+09	14084,4	218,411	4 021,20	8,78E+05	-811	7,12E+08	14	-1981	
15084,4	-4,46E+08	15084,4	199,573	12 063,70	2,41E+06	811	-1,95E+09	15084,4	218,411	4 021,20	8,78E+05	-811	7,12E+08	15	-1686	
15084,4	-5,50E+08	15084,4	190,873	12 063,70	2,30E+06	811	-1,87E+09	15084,4	224,254	4 021,20	9,02E+05	-811	7,31E+08	15	-1686	
16084,4	-1,69E+08	16084,4	190,873	12 063,70	2,30E+06	811	-1,87E+09	16084,4	224,254	4 021,20	9,02E+05	-811	7,31E+08	16	-1305	

Figure B2.1: Post-Processing of Total Moment without ASR Gradient

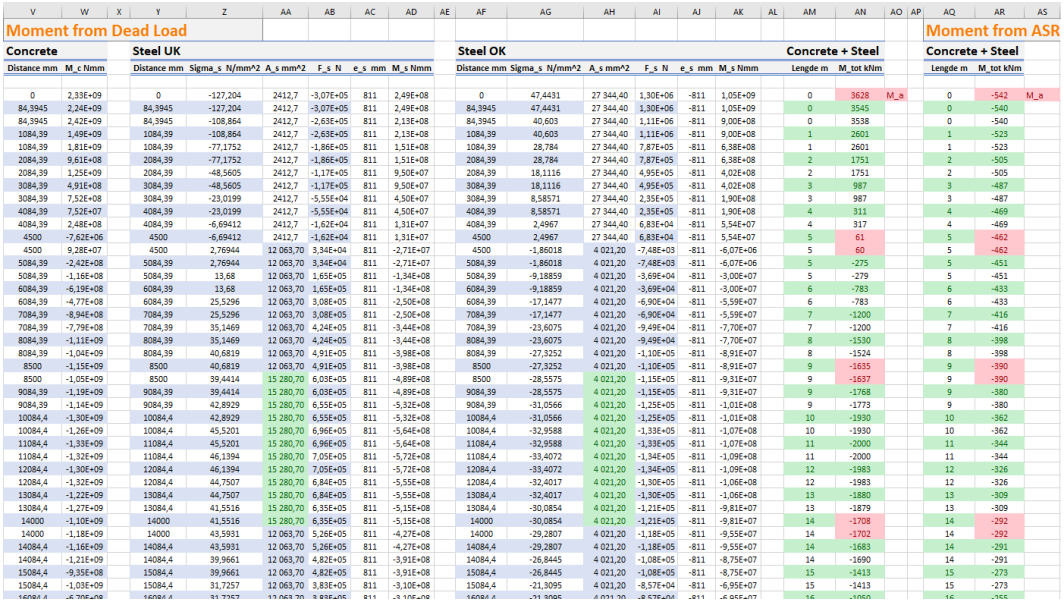

Moment from Dead Load

Concrete		Steel UK						Steel OK							Concrete + Steel			Moment from ASR		
Distance mm	M_c Nmm	Distance mm	Sigma_s N/mm^2	A_s mm^2	F_s N	e_s mm	M_s Nmm	Distance mm	Sigma_s N/mm^2	A_s mm^2	F_s N	e_s mm	M_s Nmm		Lengde m	M_tot kNm		Lengde m	M_tot kNm	
0	2,33E+09	0	-127,204	2412,7	-3,07E+05	811	2,49E+08	0	47,4431	27 344,40	1,30E+06	-811	1,05E+09		0	3628	M_s	0	-542	M_s
84,3945	2,24E+09	84,3945	-127,204	2412,7	-3,07E+05	811	2,49E+08	84,3945	47,4431	27 344,40	1,30E+06	-811	1,05E+09		0	3545		0	-540	
84,3945	2,42E+09	84,3945	-108,864	2412,7	-2,63E+05	811	2,13E+08	84,3945	40,603	27 344,40	1,11E+06	-811	9,00E+08		0	3538		0	-540	
1084,39	1,49E+09	1084,39	-108,864	2412,7	-2,63E+05	811	2,13E+08	1084,39	40,603	27 344,40	1,11E+06	-811	9,00E+08		1	2601		1	-523	
1084,39	1,81E+09	1084,39	-77,1752	2412,7	-1,86E+05	811	1,51E+08	1084,39	28,784	27 344,40	7,87E+05	-811	6,38E+08		1	2601		1	-523	
2084,39	9,61E+08	2084,39	-77,1752	2412,7	-1,86E+05	811	1,51E+08	2084,39	28,784	27 344,40	7,87E+05	-811	6,38E+08		2	1751		2	-505	
2084,39	1,25E+09	2084,39	-48,5605	2412,7	-1,17E+05	811	9,50E+07	2084,39	18,1116	27 344,40	4,95E+05	-811	4,02E+08		2	1751		2	-505	
3084,39	4,91E+08	3084,39	-48,5605	2412,7	-1,17E+05	811	9,50E+07	3084,39	18,1116	27 344,40	4,95E+05	-811	4,02E+08		3	987		3	-487	
3084,39	7,52E+08	3084,39	-23,0199	2412,7	-5,55E+04	811	4,50E+07	3084,39	8,58571	27 344,40	2,35E+05	-811	1,90E+08		3	987		3	-487	
4084,39	7,52E+07	4084,39	-23,0199	2412,7	-5,55E+04	811	4,50E+07	4084,39	8,58571	27 344,40	2,35E+05	-811	1,90E+08		4	311		4	-469	
4084,39	2,48E+08	4084,39	-6,69412	2412,7	-1,62E+04	811	1,31E+07	4084,39	2,4967	27 344,40	6,83E+04	-811	5,54E+07		4	317		4	-469	
4500	-7,62E+06	4500	-6,69412	2412,7	-1,62E+04	811	1,31E+07	4500	2,4967	27 344,40	6,83E+04	-811	5,54E+07		5	61		5	-462	
4500	9,28E+07	4500	2,76944	12 063,70	3,34E+04	811	-2,71E+07	4500	-1,86018	4 021,20	-7,48E+03	-811	-6,07E+06		5	60		5	-462	
5084,39	-2,42E+08	5084,39	2,76944	12 063,70	3,34E+04	811	-2,71E+07	5084,39	-1,86018	4 021,20	-7,48E+03	-811	-6,07E+06		5	-275		5	-451	
5084,39	-1,16E+08	5084,39	13,68	12 063,70	1,65E+05	811	-1,34E+08	5084,39	-9,18859	4 021,20	-3,69E+04	-811	-3,00E+07		5	-279		5	-451	
6084,39	-6,19E+08	6084,39	13,68	12 063,70	1,65E+05	811	-1,34E+08	6084,39	-9,18859	4 021,20	-3,69E+04	-811	-3,00E+07		6	-783		6	-433	
6084,39	-4,77E+08	6084,39	25,5296	12 063,70	3,08E+05	811	-2,50E+08	6084,39	-17,1477	4 021,20	-6,90E+04	-811	-5,59E+07		6	-783		6	-433	
7084,39	-8,94E+08	7084,39	25,5296	12 063,70	3,08E+05	811	-2,50E+08	7084,39	-17,1477	4 021,20	-6,90E+04	-811	-5,59E+07		7	-1200		7	-416	
7084,39	-7,79E+08	7084,39	35,1469	12 063,70	4,24E+05	811	-3,44E+08	7084,39	-23,6075	4 021,20	-9,49E+04	-811	-7,70E+07		7	-1200		7	-416	
8084,39	-1,11E+09	8084,39	35,1469	12 063,70	4,24E+05	811	-3,44E+08	8084,39	-23,6075	4 021,20	-9,49E+04	-811	-7,70E+07		8	-1530		8	-398	
8084,39	-1,04E+09	8084,39	40,6819	12 063,70	4,91E+05	811	-3,98E+08	8084,39	-27,3252	4 021,20	-1,10E+05	-811	-8,91E+07		8	-1524		8	-398	
8500	-1,15E+09	8500	40,6819	12 063,70	4,91E+05	811	-3,98E+08	8500	-27,3252	4 021,20	-1,10E+05	-811	-8,91E+07		9	-1635		9	-390	
8500	-1,05E+09	8500	39,4414	15 280,70	6,03E+05	811	-4,89E+08	8500	-28,5575	4 021,20	-1,15E+05	-811	-9,31E+07		9	-1637		9	-390	
9084,39	-1,19E+09	9084,39	39,4414	15 280,70	6,03E+05	811	-4,89E+08	9084,39	-28,5575	4 021,20	-1,15E+05	-811	-9,31E+07		9	-1768		9	-380	
9084,39	-1,14E+09	9084,39	42,8929	15 280,70	6,55E+05	811	-5,32E+08	9084,39	-31,0566	4 021,20	-1,25E+05	-811	-1,01E+08		9	-1773		9	-380	
10084,4	-1,30E+09	10084,4	42,8929	15 280,70	6,55E+05	811	-5,32E+08	10084,4	-31,0566	4 021,20	-1,25E+05	-811	-1,01E+08		10	-1930		10	-362	
10084,4	-1,26E+09	10084,4	45,5201	15 280,70	6,96E+05	811	-5,64E+08	10084,4	-32,9588	4 021,20	-1,33E+05	-811	-1,07E+08		10	-1930		10	-362	
11084,4	-1,33E+09	11084,4	45,5201	15 280,70	6,96E+05	811	-5,64E+08	11084,4	-32,9588	4 021,20	-1,33E+05	-811	-1,07E+08		11	-2000		11	-344	
11084,4	-1,32E+09	11084,4	46,1394	15 280,70	7,05E+05	811	-5,72E+08	11084,4	-33,4072	4 021,20	-1,34E+05	-811	-1,09E+08		11	-2000		11	-344	
12084,4	-1,30E+09	12084,4	46,1394	15 280,70	7,05E+05	811	-5,72E+08	12084,4	-33,4072	4 021,20	-1,34E+05	-811	-1,09E+08		12	-1983		12	-326	
12084,4	-1,32E+09	12084,4	44,7507	15 280,70	6,84E+05	811	-5,55E+08	12084,4	-32,4017	4 021,20	-1,30E+05	-811	-1,06E+08		12	-1983		12	-326	
13084,4	-1,22E+09	13084,4	44,7507	15 280,70	6,84E+05	811	-5,55E+08	13084,4	-32,4017	4 021,20	-1,30E+05	-811	-1,06E+08		13	-1880		13	-309	
13084,4	-1,27E+09	13084,4	41,5516	15 280,70	6,35E+05	811	-5,15E+08	13084,4	-30,0854	4 021,20	-1,21E+05	-811	-9,81E+07		13	-1879		13	-309	
14000	-1,10E+09	14000	41,5516	15 280,70	6,35E+05	811	-5,15E+08	14000	-30,0854	4 021,20	-1,21E+05	-811	-9,81E+07		14	-1708		14	-292	
14000	-1,18E+09	14000	43,5931	12 063,70	5,26E+05	811	-4,27E+08	14000	-29,2807	4 021,20	-1,18E+05	-811	-9,55E+07		14	-1702		14	-292	
14084,4	-1,16E+09	14084,4	43,5931	12 063,70	5,26E+05	811	-4,27E+08	14084,4	-29,2807	4 021,20	-1,18E+05	-811	-9,55E+07		14	-1683		14	-291	
14084,4	-1,21E+09	14084,4	39,9661	12 063,70	4,82E+05	811	-3,91E+08	14084,4	-26,8445	4 021,20	-1,08E+05	-811	-8,75E+07		14	-1690		14	-291	
15084,4	-9,35E+08	15084,4	39,9661	12 063,70	4,82E+05	811	-3,91E+08	15084,4	-26,8445	4 021,20	-1,08E+05	-811	-8,75E+07		15	-1413		15	-273	
15084,4	-1,03E+09	15084,4	31,7257	12 063,70	3,83E+05	811	-3,10E+08	15084,4	-21,3095	4 021,20	-8,57E+04	-811	-6,95E+07		15	-1413		15	-273	

Figure B2.2: Post-Processing of Moment from Dead Load and from only ASR Restraint Forces without ASR Gradient

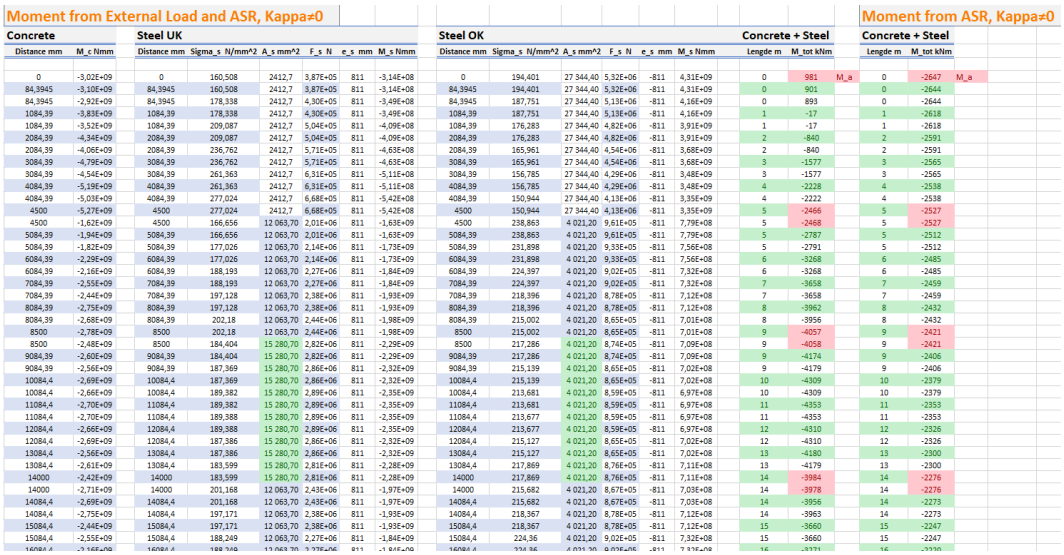

Moment from External Load and ASR, Kappa≠0

Concrete		Steel UK						Steel OK							Concrete + Steel			Moment from ASR, Kappa≠0		
Distance mm	M_c Nmm	Distance mm	Sigma_s N/mm^2	A_s mm^2	F_s N	e_s mm	M_s Nmm	Distance mm	Sigma_s N/mm^2	A_s mm^2	F_s N	e_s mm	M_s Nmm		Lengde m	M_tot kNm		Lengde m	M_tot kNm	
0	-3,02E+09	0	160,508	2412,7	3,87E+05	811	-3,14E+08	0	194,401	27 344,40	5,32E+06	-811	4,31E+09		0	981	M_a	0	-2647	M_a
84,3945	-3,10E+09	84,3945	160,508	2412,7	3,87E+05	811	-3,14E+08	84,3945	194,401	27 344,40	5,32E+06	-811	4,31E+09		0	901		0	-2644	
84,3945	-2,92E+09	84,3945	178,338	2412,7	4,30E+05	811	-3,49E+08	84,3945	187,751	27 344,40	5,13E+06	-811	4,16E+09		0	893		0	-2644	
1084,39	-3,83E+09	1084,39	178,338	2412,7	4,30E+05	811	-3,49E+08	1084,39	187,751	27 344,40	5,13E+06	-811	4,16E+09		1	-17		1	-2618	
1084,39	-3,52E+09	1084,39	209,087	2412,7	5,04E+05	811	-4,09E+08	1084,39	176,283	27 344,40	4,82E+06	-811	3,91E+09		1	-17		1	-2618	
2084,39	-4,34E+09	2084,39	209,087	2412,7	5,04E+05	811	-4,09E+08	2084,39	176,283	27 344,40	4,82E+06	-811	3,91E+09		2	-840		2	-2591	
2084,39	-4,06E+09	2084,39	236,762	2412,7	5,71E+05	811	-4,63E+08	2084,39	165,961	27 344,40	4,54E+06	-811	3,68E+09		2	-840		2	-2591	
3084,39	-4,79E+09	3084,39	236,762	2412,7	5,71E+05	811	-4,63E+08	3084,39	165,961	27 344,40	4,54E+06	-811	3,68E+09		3	-1577		3	-2565	
3084,39	-4,54E+09	3084,39	261,363	2412,7	6,31E+05	811	-5,11E+08	3084,39	156,785	27 344,40	4,29E+06	-811	3,48E+09		3	-1577		3	-2565	
4084,39	-5,19E+09	4084,39	261,363	2412,7	6,31E+05	811	-5,11E+08	4084,39	156,785	27 344,40	4,29E+06	-811	3,48E+09		4	-2228		4	-2538	
4084,39	-5,03E+09	4084,39	277,024	2412,7	6,68E+05	811	-5,42E+08	4084,39	150,944	27 344,40	4,13E+06	-811	3,35E+09		4	-2222		4	-2538	
4500	-5,27E+09	4500	277,024	2412,7	6,68E+05	811	-5,42E+08	4500	150,944	27 344,40	4,13E+06	-811	3,35E+09		5	-2466		5	-2527	
4500	-1,62E+09	4500	166,656	12 063,70	2,01E+06	811	-1,63E+09	4500	238,863	4 021,20	9,61E+05	-811	7,79E+08		5	-2468		5	-2527	
5084,39	-1,94E+09	5084,39	166,656	12 063,70	2,01E+06	811	-1,63E+09	5084,39	238,863	4 021,20	9,61E+05	-811	7,79E+08		5	-2787		5	-2512	
5084,39	-1,82E+09	5084,39	177,026	12 063,70	2,14E+06	811	-1,73E+09	5084,39	231,898	4 021,20	9,33E+05	-811	7,56E+08		5	-2791		5	-2512	
6084,39	-2,29E+09	6084,39	177,026	12 063,70	2,14E+06	811	-1,73E+09	6084,39	231,898	4 021,20	9,33E+05	-811	7,56E+08		6	-3268		6	-2485	
6084,39	-2,16E+09	6084,39	188,193	12 063,70	2,27E+06	811	-1,84E+09	6084,39	224,397	4 021,20	9,02E+05	-811	7,32E+08		6	-3268		6	-2485	
7084,39	-2,55E+09	7084,39	188,193	12 063,70	2,27E+06	811	-1,84E+09	7084,39	224,397	4 021,20	9,02E+05	-811	7,32E+08		7	-3658		7	-2459	
7084,39	-2,44E+09	7084,39	197,128	12 063,70	2,38E+06	811	-1,93E+09	7084,39	218,396	4 021,20	8,78E+05	-811	7,12E+08		7	-3658		7	-2459	
8084,39	-2,75E+09	8084,39	197,128	12 063,70	2,38E+06	811	-1,93E+09	8084,39	218,396	4 021,20	8,78E+05	-811	7,12E+08		8	-3962		8	-2432	
8084,39	-2,68E+09	8084,39	202,18	12 063,70	2,44E+06	811	-1,98E+09	8084,39	215,002	4 021,20	8,65E+05	-811	7,01E+08		8	-3956		8	-2432	
8500	-2,78E+09	8500	202,18	12 063,70	2,44E+06	811	-1,98E+09	8500	215,002	4 021,20	8,65E+05	-811	7,01E+08		9	-4057		9	-2421	
8500	-2,48E+09	8500	184,404	15 280,70	2,82E+06	811	-2,29E+09	8500	217,286	4 021,20	8,74E+05	-811	7,09E+08		9	-4058		9	-2421	
9084,39	-2,60E+09	9084,39	184,404	15 280,70	2,82E+06	811	-2,29E+09	9084,39	217,286	4 021,20	8,74E+05	-811	7,09E+08		9	-4174		9	-2406	
9084,39	-2,56E+09	9084,39	187,369	15 280,70	2,86E+06	811	-2,32E+09	9084,39	215,139	4 021,20	8,65E+05	-811	7,02E+08		9	-4179		9	-2406	
10084,4	-2,69E+09	10084,4	187,369	15 280,70	2,86E+06	811	-2,32E+09	10084,4	215,139	4 021,20	8,65E+05	-811	7,02E+08		10	-4309		10	-2379	
10084,4	-2,66E+09	10084,4	189,382	15 280,70	2,89E+06	811	-2,35E+09	10084,4	213,681	4 021,20	8,59E+05	-811	6,97E+08		10	-4309		10	-2379	
11084,4	-2,70E+09	11084,4	189,382	15 280,70	2,89E+06	811	-2,35E+09	11084,4	213,681	4 021,20	8,59E+05	-811	6,97E+08		11	-4353		11	-2353	
11084,4	-2,70E+09	11084,4	189,388	15 280,70	2,89E+06	811	-2,35E+09	11084,4	213,677	4 021,20	8,59E+05	-811	6,97E+08		11	-4353		11	-2353	
12084,4	-2,66E+09	12084,4	189,388	15 280,70	2,89E+06	811	-2,35E+09	12084,4	213,677	4 021,20	8,59E+05	-811	6,97E+08		12	-4310		12	-2326	
12084,4	-2,69E+09	12084,4	187,386	15 280,70	2,86E+06	811	-2,32E+09	12084,4	215,127	4 021,20	8,65E+05	-811	7,02E+08		12	-4310		12	-2326	
13084,4	-2,56E+09	13084,4	187,386	15 280,70	2,86E+06	811	-2,32E+09	13084,4	215,127	4 021,20	8,65E+05	-811	7,02E+08		13	-4180		13	-2300	
13084,4	-2,61E+09	13084,4	183,599	15 280,70	2,81E+06	811	-2,28E+09	13084,4	217,869	4 021,20	8,76E+05	-811	7,11E+08		13	-4179		13	-2300	
14000	-2,42E+09	14000	183,599	15 280,70	2,81E+06	811	-2,28E+09	14000	217,869	4 021,20	8,76E+05	-811	7,11E+08		14	-3984		14	-2276	
14000	-2,71E+09	14000	201,168	12 063,70	2,43E+06	811	-1,97E+09	14000	215,682	4 021,20	8,67E+05	-811	7,03E+08		14	-3978		14	-2276	
14084,4	-2,69E+09	14084,4	201,168	12 063,70	2,43E+06	811	-1,97E+09	14084,4	215,682	4 021,20	8,67E+05	-811	7,03E+08		14	-3956		14	-2273	
14084,4	-2,75E+09	14084,4	197,171	12 063,70	2,38E+06	811	-1,93E+09	14084,4	218,367	4 021,20	8,78E+05	-811	7,12E+08		14	-3963		14	-2273	
15084,4	-2,44E+09	15084,4	197,171	12 063,70	2,38E+06	811	-1,93E+09	15084,4	218,367	4 021,20	8,78E+05	-811	7,12E+08		15	-3660		15	-2247	
15084,4	-2,55E+09	15084,4	188,249	12 063,70	2,27E+06	811	-1,84E+09	15084,4	224,36	4 021,20	9,02E+05	-811	7,32E+08		15	-3660		15	-2247	

Figure B2.3: Post-Processing of Total Moment with ASR Gradient and for only ASR Restraint Forces with ASR Gradient